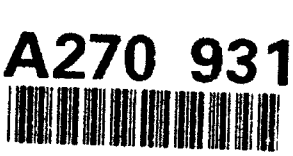

NTATION PAGE

Form Approved
OMB No. 0704-0188

1. AGENCY USE ONLY (Leave blank)	2. REPORT DATE	3. REPORT TYPE AND DATES COVERED
	8/4/93	Final Report; 20 Feb 1990 - June 30 1993

4. TITLE AND SUBTITLE

Study of Electromagnetic Wave Scattering from Characterized Rough Surfaces

5. FUNDING NUMBERS

DAAL03-90-G-0041

6. AUTHOR(S)

Kevin A. O'Donnell

7. PERFORMING ORGANIZATION NAME(S) AND ADDRESS(ES)

Professor Kevin A. O'Donnell
School of Physics
Georgia Institute of Technology
Atlanta, GA 30332-0430

8. PERFORMING ORGANIZATION REPORT NUMBER

9. SPONSORING / MONITORING AGENCY NAME(S) AND ADDRESS(ES)

U. S. Army Research Office
P. O. Box 12211
Research Triangle Park, NC 27709-2211

10. SPONSORING / MONITORING AGENCY REPORT NUMBER

ARO 27485.9-GS

11. SUPPLEMENTARY NOTES

The view, opinions and/or findings contained in this report are those of the author(s) and should not be construed as an official Department of the Army position, policy, or decision, unless so designated by other documentation.

12a. DISTRIBUTION / AVAILABILITY STATEMENT

Approved for public release; distribution unlimited.

12b. DISTRIBUTION CODE

13. ABSTRACT *(Maximum 200 words)*

In our experimental and theoretical research during our ARO grant, we have studied the optical scattering properties of rough conducting surfaces that have structure comparable to or slightly greater than the illumination wavelength. We theoretically and experimentally studied the diffuse scatter for surfaces with one-dimensional roughness, where we have seen backscattering enhancement and strong polarization effects. In the angular correlation functions associated with the scattered light, we clearly see the coherent effects that give rise to backscattering enhancement. Further experimental studies have considered backscattering enhancement from a surface with two-dimensional roughness, and we have theoretically investigated the effects of finite stylus width in the contact profilometer methods that we have used in our experiments.

14. SUBJECT TERMS

Light Scattering, Rough Surfaces, Polarization, Backscattering Enhancement

15. NUMBER OF PAGES

79

16. PRICE CODE

17. SECURITY CLASSIFICATION OF REPORT	18. SECURITY CLASSIFICATION	19. SECURITY CLASSIFICATION OF ABSTRACT	20. LIMITATION OF ABSTRACT
UNCLASSIFIED	UNCLASSIFIED	UNCLASSIFIED	UL

STUDY OF ELECTROMAGNETIC WAVE SCATTERING FROM CHARACTERIZED ROUGH SURFACES

FINAL REPORT

Author: Professor Kevin A. O'Donnell

August 4, 1993

prepared for
The U.S. Army Research Office
under Grant # DAAL03-90-G-0041

The School of Physics
Georgia Institute of Technology
Atlanta, Georgia 30332

The views, opinions, and/or findings contained in this report are those of the author and should not be construed as an official Department of the Army position, policy, or decision, unless so designated by other documentation.

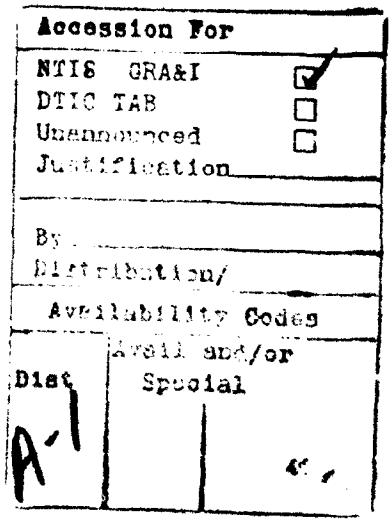

Table of Contents

1. Overview of Problem Studied 4

2. Polarization-Dependence of Light Scattered by One-Dimensional Rough Surfaces 4

3. Angular Correlation Functions in Rough Surface Scattering 6

4. Additional Research 6

5. Scientific Personnel Supported 7

6. Bibliography (Chronological) 7

7. Papers Presented at Scientific Meetings 8

8. Published Papers 10

A. "Anomalous Scattering from a Perturbed Grating" 10

B. "The Polarization-Dependence of Scattering from One-Dimensional Rough Surfaces" 13

C. "The Stokes Matrix of a One-Dimensional Perfectly Conducting Rough Surface" 19

D. "Angular Correlation Functions Of Amplitudes Scattered from a One-Dimensional, Perfectly Conducting Rough Surface" 31

E. "Angular Correlation Functions of Polarized Intensities Scattered from a One-Dimensionally Rough Surface" 42

F. "Comparisons of Theory and Experiment in Light Scattering from a Randomly Rough Surface" 52

G. "Backscattering Enhancement from an Isotropically Rough Surface" . 66

H. "Measurements of Light Scattering by a Series of Conducting Surfaces with Varying One-Dimensional Roughness" 72

I. "Effects of Finite Stylus Width in Surface Contact Profilometry" 73

1. Statement of the Problem Studied

The scattering of waves by randomly rough surfaces is a phenomenon that occurs in many fields, there have been hundreds of research papers on this subject, and many diverse theoretical and experimental investigations have been made. However, there remain many aspects of the surface scattering problem that are poorly understood and that are thus quite completely open to investigation.

In our experimental and theoretical research during our ARO grant, we have studied the optical scattering properties of rough conducting surfaces that have correlation length comparable to or slightly greater than the illumination wavelength. We have studied the diffuse and coherent scatter, as well as the angular correlation functions associated with the scattered light. We have written nine major papers for scientific journals of the highest standards, have presented five invited papers in five different countries, and have presented eleven contributed papers at other scientific conferences; all of this work has been supported exclusively by the ARO. In the following we summarize these contributions.

2. Polarization-Dependence of Light Scattered by One-Dimensional Rough Surfaces

A. Experimental Work

It is certainly true that a surface with one-dimensional (1-D) roughness will not depolarize an incident wave with p or s polarization; it was somehow concluded in previous work that the diffuse scatter from such a surface was thus specified by the mean scattered p- and s-polarized intensities I_p and I_s. We were the first to show that these intensities comprise only two of the four quantities required to describe the diffuse scatter. In Ref. 1 we showed that the multiple scattering from a 1-D rough surface may be isolated by illuminating with a +45° polarization state and detecting the mean scattered intensity with +45° polarization (hereafter called I_+). More explicitly, in Ref. 2 we showed that the diffuse scatter from a 1-D rough surface is specified by *four* unique Mueller or Stokes matrix elements, two of which are equivalent to I_p and I_s, while the other two (s_{33} and s_{34}) are quite independent of I_p and I_s. With experimental measurements, we then demonstrated the importance of all four matrix elements for a surface with Gaussian statistics and with sufficiently strong slopes to create backscattering enhancement. We showed that I_+ is related to s_{33}, and we again found that I_+ isolated the multiple scattering and hence the backscattering enhancement from the rough surface.

In some quite recent work (Ref. 8), we have investigated the effect of surface roughness on the four unique matrix elements. In addition to other results, we find unusual behavior in the coherent component of the scattered light, and we find that surprisingly smooth surfaces produce backscattering enhancement in I_+.

B. Theoretical Work

We provided the first theoretical study of the four unique matrix elements of a 1-D rough surface in Ref. 3. Using exact numerical methods for a perfect conductor, we showed results for surfaces with Gaussian statistics and roughness sufficiently strong to create backscattering enhancement. Then, with the iterated Kirchhoff method for p and s polarization, we showed that the two series generated are composed of exactly the same terms but with differing signs (this is a remarkable result that had gone unnoticed for many years). We then discussed the significance of this result on the order-by-order expressions for the four unique matrix elements, and we rigorously showed that I_+ indeed corresponds to pure double scattering. In comparisons with experimental data, the most significant differences were seen in s_{34} and were attributed to the finite conductivity of the experimental surface.

C. Comparisons of Theoretical and Experimental Work

In the previous work of others, significant differences had been seen in comparisons of theoretical and experimental results for I_p and I_s for surfaces that produce backscattering enhancement. In our recent work (Ref. 6), we showed that, for the first time, good agreement could be obtained in such comparisons. Moreover, we considered not just I_p and I_s, but all four unique matrix elements. There were two essential reasons for this success. First, our experimental surface was of much higher quality than in previous work, and secondly, we developed new numerical methods based on an impedance boundary condition that worked well for highly conductive surfaces. We also found that rather subtle properties of the experimental surface (in this case the statistics of the surface curvature) can have significant effects on the scattering properties. The good agreements obtained are impressive in view of the many subtleties of the experiments (such as surface characterization), as well as a number of assumptions made in any "exact" theoretical method.

3. Angular Correlation Functions in Rough Surface Scattering

One may ask more general questions in light scattering from a randomly rough surface. For example, at a given illumination angle, when will the amplitude scattered to some scattering angle be correlated with another amplitude for differing incident and scattering angles? What form will this correlation function take? These questions had been approached in the 1970's in work employing the Beckmann formulation in surface scattering, and such considerations had been termed the "Memory Effect" in recent years in volume scattering from disordered media.

In Ref. 4, we used the stochastic Fourier transform method due to Brown to derive a correlation condition that determines when correlations may be significant. We then employed exact numerical calculations to study the form of these correlation functions for surfaces that produce backscattering enhancement. It was found that "coherent effects" could be seen in these correlation functions. In Ref. 5, we then employed experimental methods to study the angular correlation functions of intensity. We showed that these correlations appeared to be related to the amplitude correlations by the Gaussian moment theorem. Further, we showed that the the unusual behavior arose from the coherent addition of four distinct phasors, which clearly demonstrates the coherent nature of backscattering enhancement.

The correlation functions studied in Refs. 4 and 5 appear to be quite fundamental, as the amplitude correlation functions are generalizations of the Stokes matrix elements. They also provide considerable physical insight into the scattering mechanisms occurring on any rough surface so that it is likely that they will find considerable application in future work.

4. Additional Research

In Ref. 7, we have also provided investigations of the two-dimensional nature of the backscattering enhancement from a surface with two-dimensional roughness. For the special case of normal incidence, we showed that the co- and cross-polarized scattered intensities have secondary minima and maxima at field angles surrounding the backscattering direction. These observations appear to be beyond the grasp of existing theoretical methods, but will become increasingly relevant in future theoretical work as the speed of computers continues to increase.

We have also studied the effect of stylus width in our surface characterization methods in Ref. 9. This is the fundamental experimental limitation on the resolution

achievable with the mechanical methods used throughout our work. We showed that the measure profile is highly nonlinear in the surface height and its first two derivatives. We then conducted the averaging required to obtain closed-form expressions for the first two moments of a profiled Gaussian process, and showed that the measured roughness should initially decrease with increasing stylus width. Despite the widespread application of stylus profilometry, to our knowledge this is the first time that such results have been derived.

5. Participating Scientific Personnel

Dr. Kevin A. O'Donnell, Principal Investigator
Dr. Thierry R. Michel, Postdoctoral Assistant
Dr. Min-Joong Kim, Postdoctoral Assistant
Mr. Michael E. Knotts, Graduate Student
Mr. Charles S. West, Graduate Student
Ms. Sarah J. Paukstis, Graduate Student

6. Bibliography (chronological; see attachments):

1. M.E. Knotts and K.A. O'Donnell, "Anomalous Scattering from a Perturbed Grating," Optics Letters *15*, 1485-1487 (1990).

2. K.A. O'Donnell and M.E. Knotts, "The Polarization-Dependence of Scattering from One-Dimensional Rough Surfaces," Journal of the Optical Society of America *A8*, 1126-1131 (1991).

3. T.R. Michel, M.E. Knotts, and K.A. O'Donnell, "The Stokes Matrix of a One-Dimensional Perfectly Conducting Rough Surface," Journal of the Optical Society of America *A9*, 585-596 (1992).

4. T.R. Michel and K.A. O'Donnell, "Angular Correlation Functions Of Amplitudes Scattered from a One-Dimensional, Perfectly Conducting Rough Surface," Journal of the Optical Society of America *A9*, 1374-1384 (1992).

5. M.E. Knotts, T.R. Michel, and K.A. O'Donnell, "Angular Correlation Functions of Polarized Intensities Scattered from a One-Dimensionally Rough Surface," Journal of the Optical Society of America *A9*, 1822-1831 (1992).

6. M.E. Knotts, T.R. Michel, and K.A. O'Donnell, "Comparisons of Theory and Experiment in Light Scattering from a Randomly Rough Surface," Journal of the Optical Society of America *A10*, 928-941 (1993).

7. M. E. Knotts and K. A. O'Donnell, "Backscattering Enhancement from an Isotropically Rough Surface," Optics Communications *99*, 1-6 (1993).

8. M. E. Knotts and K. A. O'Donnell, "Measurements of Light Scattering by a Series of Conducting Surfaces with Varying One-Dimensional Roughness", Journal of the Optical Society of America (Accepted July 1993; in press).

9. K. A. O'Donnell, "Effects of Finite Stylus Width in Surface Contact Profilometry," Applied Optics (accepted Feb. 1993; in press).

7. Papers Presented at Meetings
Invited:

K.A. O'Donnell and M.E. Knotts, "Scattering of Light from Randomly Rough Surfaces with Steep Slopes," presented at Modern Analysis of Scattering Phenomena, Marseille, France, September 1990.

K.A. O'Donnell and M.E. Knotts, "The Role of Polarization in Enhanced Backscattering from Rough Surfaces,"presented at the ICO Conference on Atmospheric, Volume, and Surface Scattering and Propagation, Florence, Italy, August 27-30, 1991.

K.A. O'Donnell, T.R. Michel, and M.E. Knotts, "The Polarization-Dependence of Light Scattered from Rough Surfaces," presented at the International Workshop on Light Propagation and Scattering in Dense Media and Rough Surfaces, Laredo, Spain, September 2-5, 1991.

K.A. O'Donnell, T.R. Michel, and M.E. Knotts, "Light Scattering by Conducting Surfaces with One-Dimensional Roughness", presented at International Conference on Diffractometry and Scatterometry, Warsaw, Poland, May 24-28, 1993.

K.A. O'Donnell, T.R. Michel, and M.E. Knotts, "Studies of the Coherent, Incoherent, and Angular-Correlation Scattering Properties of Conducting Surfaces with One-Dimensional Roughness," Third International Conference on Electrical Transport and Optical Properties of Inhomogeneous Media, Guanajuato, Mexico, August 9-13, 1993.

Contributed:

K.A. O'Donnell, "Backscattering Enhancement and Polarization Effects in Scattering from Rough Surfaces," presented at Progress in Electromagnetics Research Symposium, Boston, Mass., July 1989.

K.A. O'Donnell and M.J. Kim, "New Results on Wave Scattering from Random Media," presented at Army Research Office Workshop on Scattering from Surfaces, Boston University, July 1989.

M.J. Kim, K.A. O'Donnell and M.E. Knotts, "Scattering from High-Sloped 1 and 2 Dimensional Random Surfaces," presented at National Radio Science Meeting, Boulder, Colorado, January 1990.

M.E. Knotts and K.A. O'Donnell, "Backscattering of Light from Perturbed Gratings," presented at 1990 Optical Society of America Annual Meeting, Boston, November 1990.

K.A. O'Donnell and M.E Knotts, "Enhanced Backscattering and Polarimetry of Light Scattered from Rough Surfaces," presented at Progress in Electromagnetics Research Symposium, Boston, July 1991.

K.A. O'Donnell and M.E Knotts, "Polarization-Dependence of Light Scattered from Rough Surfaces with Steep Slopes," presented at SPIE Annual Meeting, San Diego, July 1991.

M.E. Knotts and K.A. O'Donnell, "Blazing Effects and Backscattering in Light Scattered from Gratings with Superposed Randomness," poster paper presented at 1991 Optical Society of America Annual Meeting, San Jose, November 1991.

M.E. Knotts, T.R. Michel, and K.A. O'Donnell, "A Comparison of Theoretical and Experimental Results for the Stokes Matrix Elements in Light Scattering from Rough Surfaces," Special Workshop on Theoretical Techniques for Scattering of Light from Surfaces, Boulder, Colorado, January 1992.

M.E. Knotts, T.R. Michel, and K.A. O'Donnell, "Comparisons of Theory and Experiment for Light Scattering from a Conducting Surface with One-Dimensional Roughness," Optical Society of America Annual Meeting, Albuquerque, September 1992.

M. E. Knotts, T. R. Michel, and K. A. O'Donnell, "Light Scattering from Conducting Surfaces with Strong One-Dimensional Roughness: Comparisons of Theory and Experiment," American Physical Society Meeting, Seattle, Washington, 22-26 March 1993.

T. R. Michel, M. E. Knotts, and K. A. O'Donnell, "Angular Correlation Functions for Light Scattered from a One-Dimensionally Rough Surface," American Physical Society Meeting, Seattle, Washington, 22-26 March 1993.

Anomalous light scattering from a perturbed grating

M. E. Knotts and K. A. O'Donnell

The School of Physics, Georgia Institute of Technology, Atlanta, Georgia 30332

Received April 24, 1990; accepted October 9, 1990

Both diffraction orders and backscattering enhancement have been observed in light scattering from a metallic diffraction grating with random groove depths. The polarization dependence of the observations is shown to be consistent with multiple-scattering models.

The scattering of electromagnetic waves from randomly rough surfaces is by no means a well-understood phenomenon. Recent measurements of light diffusely reflected from characterized rough surfaces have shown unusually enhanced backscattering toward the source of illumination.[1,2] The backscattering effects observed have been attributed to multiple scattering by surface features,[2] using arguments related to those applied to light scattering from particles.[3] There has also been considerable effort directed toward a theoretical understanding of such phenomena, though the calculations can be difficult for surfaces that produce multiple scattering. Computational methods based on the Ewald–Oseen extinction theorem[4,5] have predicted backscattering peaks similar to observations from corrugated surfaces.[6] The full-wave method[7] has also theoretically predicted unusual backscattering from deep surfaces. In most (but not all[8]) of this research it is assumed, as in the experimental observations, that the surface profile is a Gaussian random process.

In this Letter we report experimental observation of a backscattering effect from a completely different type of surface. The surfaces that we have fabricated are nearly diffraction gratings, although they have a small, deliberate, and controllable random perturbation from the ideal periodic profile. Perfect gratings have been studied in detail theoretically[9]; for such surfaces multiple scattering may occur if steep slopes are present, but the periodicity of the surface implies that the light may only be sent into the discrete directions of the grating orders. On the other hand, the perturbed gratings discussed here produce grating orders as well as diffuse scatter; it is in the latter that enhanced backscattering may be observed.

The perturbed gratings were fabricated on glass plates that had been spin coated with an 8-μm layer of Shipley 1650 photoresist. The plates were mounted on a precision x–y positioning stage, which was driven by a computer with a Newport 855 stage controller. An attenuated beam from a 10-mW He–Cd laser (Liconix 4207NB) operating at a 0.442-μm wavelength was focused to a waist of approximately 5-μm full width on the surface. The plate was scanned in a raster fashion by the computer to produce a grating of 10-μm period over a 10 mm × 10 mm area. The velocity of each line of the scan was determined by a Gaussian random-number generator in the computer, so that after development of the plate, the resulting grating structure had equally spaced Gaussian grooves with random fluctuations in groove depth.

The surface discussed here was then coated with a thin layer of vacuum-deposited gold to permit study of its reflective scattering properties. A profile of the prepared surface as measured with a diamond-stylus mechanical profilometer is shown in Fig. 1. There are clearly grooves present with a smooth Gaussian profile but with randomly varying depth. The dotted line plotted in each groove has length proportional to the reciprocal of the computer-generated random velocity, so that, assuming a linear photoresist response, this line should be equal to the groove depth. It can be seen that the agreement is generally good. From these profilometry data and the computer-generated velocities used in the exposing process, we estimate the groove width (full width at $1/e$ point of maximum depth) to be 2.4 μm, with an average groove depth of 2.5 μm and a standard deviation of 0.8 μm.

In the scattering experiments, the surface was oriented so that the incident wave vector $\mathbf{k}_i$ was orthogonal to the groove direction at all angles of incidence. It is well known that if the electric field vector $\mathbf{E}$ of the incident wave is then either parallel or orthogonal to the grooves (s or p polarization, respectively), the scattered field will have similar polarization.[4–6] Furthermore, for a corrugated surface the scattered light will remain in the plane of incidence. The quantity that we present is the normalized differential scattering cross section $\Sigma(\theta_i, \theta_s)$, defined as

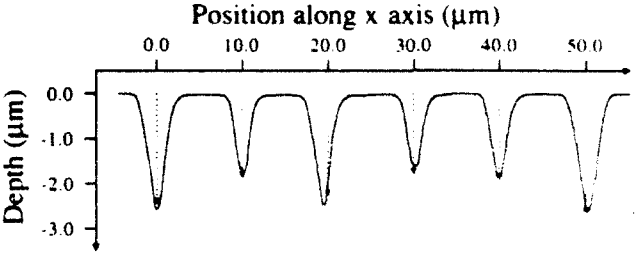

Fig. 1. Scan of a prepared random grating with a mechanical profilometer. The dotted lines have lengths proportional to the random exposure values generated by the computer.

0146-9592/90/241485-03$2.00/0

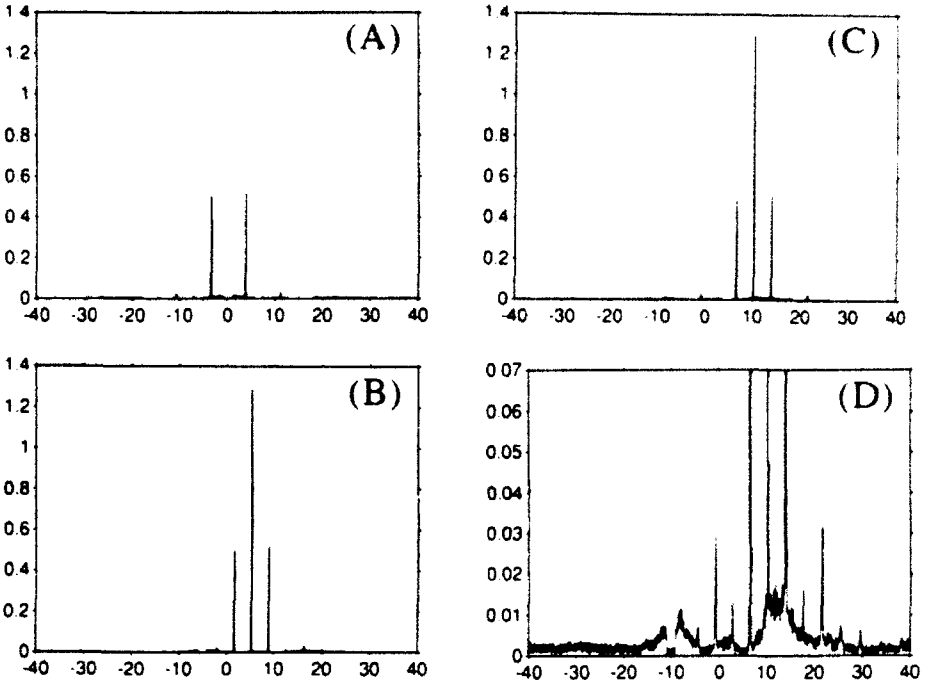

Fig. 2. s-Polarized scattering cross sections of the random grating as a function of scattering angle θ_s for angles of incidence θ_i = 0 deg (A), 5 deg (B), and 10 deg (C), (D). The strong diffraction orders move into the forward-scattering direction ($\theta_s = \theta_i$), although the broad fringes maintain a constant angle with respect to the backscattering direction ($\theta_s = -\theta_i$). The notch at the exact backscattering direction [note the missing zero order in (A)] is due to the occlusion of the detector by the source.

$$\Sigma(\theta_i, \theta_s) = \frac{1}{P_{\text{inc}}} \frac{dP(\theta_i, \theta_s)}{d\theta_s},$$

where θ_i is the angle of incidence and θ_s is the scattering angle with respect to the surface normal, P_{inc} is the incident power, and $dP(\theta_i, \theta_s)/d\theta_s$ is the scattered power per unit angle. In our experiments the expanded beam from a He–Ne laser of 0.633-μm wavelength illuminated a 6-mm-diameter area of the sample. The scattered light was then measured on an arc of radius 70 cm centered on the sample, in a manner that was discussed in more detail elsewhere.[2] Examples of scattering cross sections for this grating for s incident polarization are shown in Fig. 2. There are large zero- and first-order diffracted waves present, weak higher-order diffracted waves, and a small amount of diffuse scatter at other angles. As the angle of incidence increases, the diffraction orders move into the forward-scattering direction, as expected for an ideal grating. In contrast, the diffuse scatter exhibits a weak set of broad fringes that, as the angle of incidence increases, remain at the same angular position with respect to the source. This then appears to be a backscattering effect, although what is seen here is small compared to the diffraction orders and is perhaps not convincing.

However, we have found that a backscattering structure alone may be readily observed from this surface in a slightly different experiment. Figure 3 shows data taken with the incident field linearly polarized at +45 deg with respect to the grooves, with the scattered field resolved into parallel and orthogonal linear polarization components. The copolarized scattering [Fig. 3(A)] contains diffraction orders that, as in Fig. 2, move into the forward-scattering direction. Though it is not easily seen on the scale shown, there is also much less diffuse scatter present between the diffraction orders than in Fig. 2. The cross-polarized cross section is small [note the scale change in Fig. 3(B)] and is composed of essentially only diffuse scatter, as the dominant diffraction orders are completely extinguished near normal incidence and rise up only weakly at higher angles. Remarkably, these orthogonally polarized data have a completely different fringed structure that maintains a constant angular relationship with respect to the source, though different parts of this structure may rise or fall, depending on the angle of incidence. We thus conclude that a backscattering effect has been essentially isolated from the diffraction orders by resolving the detected polarization in this manner.

The polarization conditions employed above may seem unusual, since in previous experimental and theoretical research on enhancement from corrugated surfaces the incident polarization has been either the s or p case.[4–6] Nevertheless, the polarization conditions used in Fig. 3 are significant because they are part of the procedure necessary to measure elements of the Stokes matrix of the scatterer.[10] It is well known that, depending on the incident and detected polarization conditions, any scattering measurement corresponds to linear combinations of such matrix elements.[10] We thus conclude that the backscattering effects and grating orders of this perturbed grating necessarily reside in distinct sums of Stokes matrix elements.

Apart from these formal considerations, there is a physical manner of interpreting these data. It has been postulated that enhanced backscattering as well

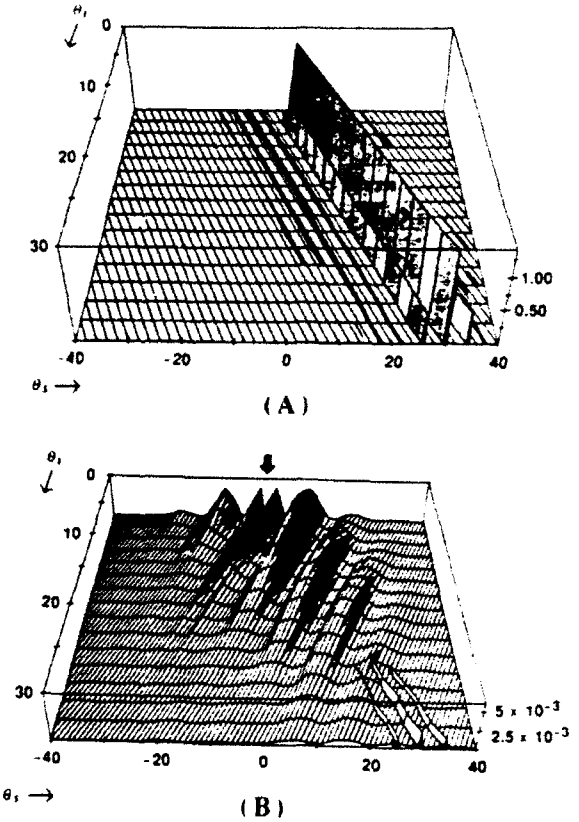

Fig. 3. Measured scattering cross sections $\Sigma(\theta_i, \theta_s)$ (vertical axis) for the random grating with incident linear polarization at +45 deg with respect to the corrugation direction; θ_i is the angle of incidence, and θ_s is the angle of scatter with respect to the surface normal. (A) and (B) are copolarized and cross-polarized scattering, respectively. The line $\theta_s = -\theta_i$ is the backscattering direction; the trough that is apparent there in (B) (heavy arrow) is due to the obstruction of the detector by the source.

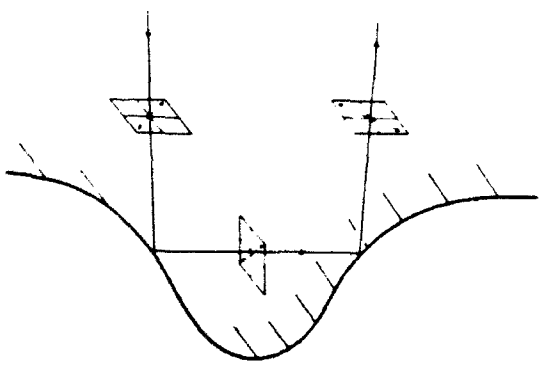

Fig. 4. Multiple scattering within a corrugation of a surface. The arrow denotes the electric field direction.

as most of the depolarization arises from multiple scattering between light paths occurring within surface valleys.[2] As shown in Fig. 4, consider an incident wave with linear polarization at 45 deg with respect to the corrugation direction. If the surface is a perfect conductor and a locally planar surface model is used, the intermediate wave sent to the other side of the valley will have the polarization shown so as to make the total electric field along the surface zero. When this is scattered at point 2, for similar reasons the light escaping from the surface will then be cross polarized with respect to the original wave. This path and its time-reversed partner are believed to give rise to backscattering enhancement[3] so that, as was found in Fig. 3(B), the enhancement should then reside largely in the cross-polarized signal. Of course this perturbed grating is not a perfect conductor, and these models are quite naïve when applied to wavelength-sized structures, yet observations of the surface field have been remarkably consistent with these arguments.[4] The approximately 11.5-deg angular period of structure in Fig. 3(B) is consistent with multiple-scattering light paths of transverse length l of 3.2 μm [through an angular diffraction width of $\arcsin(\lambda/l)$], which is reasonable for grooves as in Fig. 1. Furthermore this structure is distinct from the 3.6-deg diffraction order spacing apparent in Fig. 3(A) [as predicted for a grating of 10-μm period $\mathcal{P}$ through $\arcsin(\lambda/\mathcal{P})$].

We conclude that this perturbed grating produces enhanced backscattering in addition to the more usual diffraction orders. Although enhanced backscattering has been observed in previous research for a Gaussian surface, its interpretation in this case is by no means straightforward, as multiple-scattering paths on such a surface occur in a highly random manner. On the other hand, the perturbed grating discussed here is random enough to produce backscattering enhancement but is sufficiently regular so as to associate the observed effects with unique light paths occurring within structures on the surface. It then presents a compelling argument that multiple scattering plays an essential role in all these observations.

This research was supported by the U.S. Army Research Office.

References

1. E. R. Méndez and K. A. O'Donnell, Opt. Commun. **61**, 91 (1987).
2. K. A. O'Donnell and E. R. Méndez, J. Opt. Soc. Am. A **4**, 1194 (1987).
3. E. Akkermans, P. E. Wolf, R. Maynard, and G. Maret, J. Phys. (Paris) **49**, 77 (1988).
4. A. A. Maradudin, E. R. Méndez, and T. Michel, Opt. Lett. **14**, 151 (1989).
5. J. M. Soto-Crespo and M. Nieto-Vesperinas, J. Opt. Soc. Am. A **6**, 367 (1989).
6. A. J. Sant, J. C. Dainty, and M. J. Kim, Opt. Lett. **14**, 1183 (1989).
7. E. Bahar and M. A. Fitzwater, J. Opt. Soc. Am. A **6**, 33 (1989).
8. T. Michel, A. A. Maradudin, and E. R. Méndez, J. Opt. Soc. Am. B **6**, 2438 (1989).
9. R. Petit, ed., *Electromagnetic Theory of Gratings* (Springer-Verlag, Berlin, 1980).
10. W. S. Bickel and W. M. Bailey, Am. J. Phys. **53**, 468 (1985).

Polarization dependence of scattering from one-dimensional rough surfaces

K. A. O'Donnell and M. E. Knotts

The School of Physics, Georgia Institute of Technology, Atlanta, Georgia 30332

Received November 7, 1990; accepted January 25, 1991

The scattering of light by a one-dimensional rough surface is investigated in terms of the Stokes scattering matrix. It is shown that only four unique quantities appear in this matrix. Two of these are simply related to the *s*- and *p*-polarized scattering cross sections, although the other two quantities contain the cross correlation of electric-field amplitudes scattered by *s* and *p* incident states. Through experimental measurements with a well-characterized rough surface fabricated in photoresist, it is shown that all four unique Stokes matrix elements are significant for a surface that produces backscattering enhancement.

1. INTRODUCTION

There has recently been considerable interest in light scattering from surfaces that are randomly corrugated in only a single dimension. Enhanced backscattering has been observed in the reflective scatter from one-dimensional surfaces that have Gaussian height statistics.[1-3] These experiments have been done for comparison with theoretical predictions, as the one-dimensional surface may be approached with computationally intensive methods.[4-9] Theory and experiment have reached significant agreement regarding the form of the enhanced-backscattering structure as well as its dependence on illumination wavelength, angle of incidence, and surface correlation length.

It has been well recognized in this research that, if the incident wave is linearly polarized in a direction parallel or orthogonal to the surface corrugation (*s* or *p* polarization, respectively), a one-dimensional scatterer will produce an identically polarized scattered field. This seems to be the reason that, in all previous theoretical and experimental research, the one-dimensional rough surface has been studied only in terms of its two scattering cross sections for *s* and *p* incident polarization states. However, it has not been made at all clear in what sense these two quantities characterize the scattering properties of the surface.

In what follows we show that past research has been incomplete and that the *s* and *p* cross sections are not sufficient to describe the scattering behavior. It is shown here that complete determination of the diffuse scattering properties (i.e., those involving second-order moments of the scattered field) of a one-dimensional surface requires not two but four scattering cross sections. Indeed, two of these are effectively the *s* and *p* cross sections, but the other two quantities must be determined with an incident state that is a mixture of *s* and *p* states.

The present paper is formulated in terms of the Stokes scattering matrix. First, in Section 2 we derive the form of the Stokes matrix of a one-dimensional rough surface. Four unique elements appear in this matrix, and the procedure necessary to determine these elements is discussed in Sections 2 and 3. Experimental results are then presented in Section 4 for a one-dimensional surface that produces enhanced backscattering. All the Stokes matrix elements are measured for normal and 10° incidence so that the diffuse scattering properties have been completely specified in these cases. In particular, it is shown that the quantities neglected in previous research are highly significant for a surface that produces enhanced backscattering.

2. STOKES MATRIX OF A ONE-DIMENSIONAL ROUGH SURFACE

Consider a plane wave, as shown in Fig. 1, incident upon a one-dimensional rough surface at angle θ_i. As in previous research we assume that the incident wave vector $\mathbf{k}_i$ is orthogonal to the corrugation direction. It is well known that two conditions then follow[4-9]: First, the scattered light will remain in the plane of incidence, and one-dimensional cross sections (scattered power per unit planar angle) are thus of interest. Second, if the incident field is linearly polarized with complex amplitude E_{1i} in the plane of incidence (*p* polarization), or else is linearly polarized with complex amplitude E_{2i} in the orthogonal direction (*s* polarization), the scattered light in the far field will have the same polarization as that of the incident field.

Now, if the incident field is an arbitrary (but deterministic) polarization state, it may be considered a linear combination of *p* and *s* states. The total scattered field must then be a vector sum of the scattered fields due to the *p* and *s* components of the incident field, but these fields are orthogonal to one another and cannot then interfere. More succinctly, this condition may be written in matrix form as

$$\begin{bmatrix} E_1 \\ E_2 \end{bmatrix} = \begin{bmatrix} f_{11} & 0 \\ 0 & f_{22} \end{bmatrix} \begin{bmatrix} E_{1i} \\ E_{2i} \end{bmatrix}, \tag{1}$$

where E_1 and E_2 are the components of the scattered field. The matrix elements f_{11} and f_{22} represent the far-field scattered amplitude for incident *p* and *s* states of unit amplitude, respectively, for a particular realization of the

0740-3232/91/071126-06$05.00

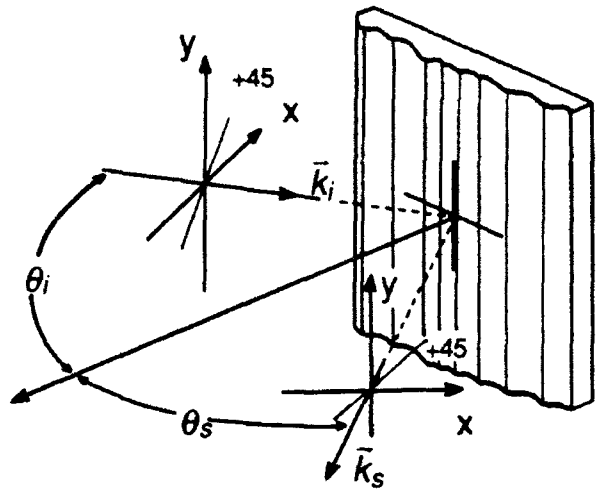

Fig. 1. Scattering of an incident wave by a one-dimensional randomly rough surface.

random surface. Further, f_{11} and f_{22} are functions of the incidence and scattering angles θ_i and θ_s (as is also the scattered field); this angular dependence will be left implicit in the quantities above. The lack of off-diagonal matrix elements is a consequence of the fact that a pure p- or s-polarized incident field will not suffer any change of polarization state.

The representation of Eq. (1) is not convenient, for the quantities that are normally of interest in studies of diffuse scatter are second-order moments of the scattered field, in which averages are taken over the ensemble of surface realizations. A natural formulation of this problem is thus in terms of Stokes vectors and matrices.[10] In this formalism the expression analogous to Eq. (1) may be readily derived with the use of well-established techniques[11,12] although the details are somewhat lengthy and will not be reproduced here. We simply state that, if the incident and scattered fields are expressed in terms of their Stokes vectors $\mathbf{V}_i$ and $\mathbf{V}_s$ the Stokes matrix $\mathbf{S}$ that relates these vectors follows from Eq. (1) as

$$\begin{bmatrix} I \\ Q \\ U \\ V \end{bmatrix} = \begin{bmatrix} s_{11} & s_{12} & 0 & 0 \\ s_{12} & s_{11} & 0 & 0 \\ 0 & 0 & s_{33} & s_{34} \\ 0 & 0 & -s_{34} & s_{33} \end{bmatrix} \begin{bmatrix} I_i \\ Q_i \\ U_i \\ V_i \end{bmatrix} \tag{2}$$

or

$$\mathbf{V} = \mathbf{S}\mathbf{V}_i, \tag{3}$$

where the elements of the Stokes vector of the scattered field $\mathbf{V}$ are given in the usual way by

$$\begin{aligned} I &= \langle |E_1|^2 \rangle + \langle |E_2|^2 \rangle, \\ Q &= \langle |E_1|^2 \rangle - \langle |E_2|^2 \rangle, \\ U &= 2\,\mathrm{Re}(\langle E_1 E_2^* \rangle), \\ V &= 2\,\mathrm{Im}(\langle E_1 E_2^* \rangle) \end{aligned} \tag{4}$$

and those of the incident field are analogously defined in terms of E_{1i} and E_{2i}. Because the matrix of Eq. (1) is diagonal, the Stokes matrix $\mathbf{S}$ contains only four unique elements, each of which appears in two places. These matrix elements are defined as

$$\begin{aligned} s_{11} &= (\langle |f_{11}|^2 \rangle + \langle |f_{22}|^2 \rangle)/2, \\ s_{12} &= (\langle |f_{11}|^2 \rangle - \langle |f_{22}|^2 \rangle)/2, \\ s_{33} &= \mathrm{Re}(\langle f_{11} f_{22}^* \rangle), \\ s_{34} &= -\,\mathrm{Im}(\langle f_{11} f_{22}^* \rangle). \end{aligned} \tag{5}$$

The angle brackets in all quantities above imply an average over the ensemble of surfaces.

Clearly, all the Stokes matrix elements may be determined theoretically from second-order moments of the quantities f_{11} and f_{22}. On the other hand, experimental determination of the Stokes matrix is not always a straightforward procedure. A general technique for measuring the Stokes matrix is given by Bickel and Bailey[13]; this involves a lengthy series of 43 measurements made with various incident and detected polarization conditions. Further, such measurements are sensitive to inevitable imperfections in polarization components, and much effort may be necessary to correct data.[14] However, for the simplified Stokes matrix of Eq. (2), it is possible to use relatively straightforward procedures to determine the entire matrix. The methods to be discussed here amount to special cases of the general technique, and the presentation will be brief; a complete discussion may be found in Ref. 13.

We consider here the effect of illuminating the scatterer with four possible incident states: (1) an s-polarized wave with Stokes vector $\mathbf{V}_s$, (2) a p-polarized wave with Stokes vector $\mathbf{V}_p$, (3) a wave that is linearly polarized at +45° ($\mathbf{V}_+$), and (4) a right-circularly polarized wave $\mathbf{V}_R$.[15] If these are assumed to have unit intensity the incident states are represented by

$$\mathbf{V}_p = \begin{bmatrix} 1 \\ 1 \\ 0 \\ 0 \end{bmatrix}, \quad \mathbf{V}_s = \begin{bmatrix} 1 \\ -1 \\ 0 \\ 0 \end{bmatrix},$$

$$\mathbf{V}_+ = \begin{bmatrix} 1 \\ 0 \\ 1 \\ 0 \end{bmatrix}, \quad \mathbf{V}_R = \begin{bmatrix} 1 \\ 0 \\ 0 \\ 1 \end{bmatrix}. \tag{6}$$

The scattered polarization state for an incident p-polarization state may be found by applying $\mathbf{V}_p$ to the Stokes matrix $\mathbf{S}$ of Eq. (2), with the result that

$$\mathbf{V} = \begin{bmatrix} s_{11} + s_{12} \\ s_{11} + s_{12} \\ 0 \\ 0 \end{bmatrix}. \tag{7}$$

This is a pure p-polarized scattered state that has, on substitution of Eqs. (5), intensity $\langle |f_{11}|^2 \rangle$. The quantity $\langle |f_{11}|^2 \rangle$ is indeed the scattering cross section for p polarization, as is to be expected. If we now apply an s-polarized state $\mathbf{V}_s$ to the matrix $\mathbf{S}$, we readily obtain the scattered polarization state as

$$\mathbf{V} = \begin{bmatrix} s_{11} - s_{12} \\ -(s_{11} - s_{12}) \\ 0 \\ 0 \end{bmatrix}. \tag{8}$$

Noting that $s_{11} - s_{12} = \langle |f_{22}|^2 \rangle$ from Eqs. (5), we conclude that the scattered field is a pure s-polarized state of intensity equal to the s cross section, which is again expected. Hence, with these two incident fields, the p and s cross sections or, equivalently, the matrix elements s_{11} and s_{12}, may be determined. However, the elements s_{33} and s_{34} do not appear in the scattered states, so it may be concluded that these elements may not be measured with either of these incident states.

On the other hand, if the +45° state $\mathbf{V}_+$ is applied to the Stokes matrix $\mathbf{S}$, the scattered field has the polarization state

$$\mathbf{V} = \begin{bmatrix} s_{11} \\ s_{12} \\ s_{33} \\ -s_{34} \end{bmatrix}. \tag{9}$$

Hence we have now brought s_{33} and s_{34} into the scattered Stokes vector, although they are in the lower two positions. Similarly, if the right-circular state $\mathbf{V}_R$ is incident, it is readily shown that the scattered polarization state is

$$\mathbf{V} = \begin{bmatrix} s_{11} \\ s_{12} \\ s_{34} \\ s_{33} \end{bmatrix}, \tag{10}$$

and again s_{33} and s_{34} have been brought into the scattered polarization state in the lower two positions. It is well known that, with suitable polarization components at the detector, any desired element of the scattered Stokes vector may be determined from two intensity measurements.[16] Thus, by using $\mathbf{V}_+$ or $\mathbf{V}_R$ as the incident wave, we find that the four Stokes vector elements are indeed the unique Stokes matrix elements, and we then conclude that the scattered field has enough information to determine the entire Stokes matrix.

At this point it is clear that there are a number of possible experimental procedures that could be used to determine the Stokes matrix elements. This situation is desirable, as it permits the experimentalist to choose the set of measurements believed to produce the most accurate results. The procedures used here are discussed in Section 3.

3. EXPERIMENTAL PROCEDURE

Experiments have been carried out to measure the Stokes matrix elements of a one-dimensional random surface that produces enhanced backscattering. This surface was fabricated as follows. First, a 50 mm × 50 mm glass plate was spin coated with three layers of Shipley 1375 photoresist. The prepared plate was exposed to eight statistically independent laser speckle patterns from a He–Cd laser operating at 0.442 μm and then was developed in Shipley 355 developer. As has been discussed in more detail elsewhere,[17,18] exposure to a large number of independent speckle patterns leads to a surface with nearly Gaussian height statistics; further, the Gaussian beam of the laser produces a height correlation function of Gaussian form. Following previous research[1-3] the optical exposing geometry was such that the speckle patterns, and therefore the surface that was made, had a correlation length of nearly 5 mm in one direction and a few micrometers in the orthogonal direction. The surface should then be an excellent approximation to a one-dimensional surface.

After fabrication the surface was coated with a layer of gold with the use of vacuum vapor deposition techniques. The surface profile was then measured with a Talystep surface profilometer with a chisel-shaped diamond stylus with 2.0 μm × 0.4 μm dimensions of the contacting face; the 0.4-μm dimension was oriented along the scanning direction so as to provide adequate resolution of the surface profile. Eight scans of the surface profile were taken from statistically independent parts of the rough surface; the data from each scan consisted of 8192 height values taken at 0.2-μm intervals along the surface. Direct statistical analysis of the data determined the standard deviation of the surface heights to be 1.95 μm and the correlation function to be an excellent approximation to a Gaussian with $1/e$ width 3.57 μm. The histogram of surface heights also provided a close fit of the desired Gaussian form (coefficient of skewness, 0.062; kurtosis, 2.79).

The scattering properties of this surface were studied with the instrument shown in Fig. 2. The source was a Jodon HN-20 He–Ne laser of 1.152-μm wavelength. A series of mirrors sent the vertically polarized laser beam over a detector and through a half-wave plate. The beam was then reflected from a final mirror, passed through a polarizer, and was incident upon the rough surface. The half-wave plate enabled the incident polarization to be oriented as desired; the polarizer that followed removed any residual ellipticity of the polarization state. The incident beam was slightly divergent so as to illuminate a 20-mm-diameter area on the surface.

An arm was mounted upon a computer-controlled rotation stage (Newport Model 495 stage with Model 855 controller) whose rotation axis was coincident with the sample. A photoconducting InSb detector was mounted upon the arm 1 m away from the sample and made measurements of the scattered intensity at all scattering

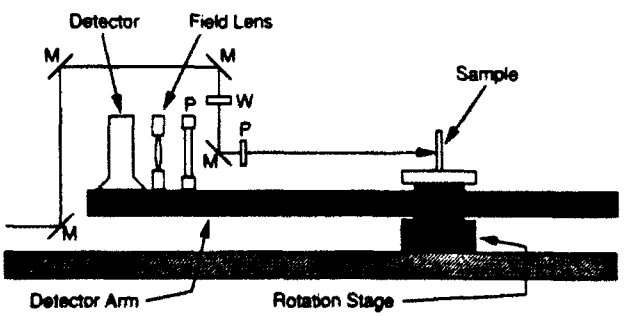

Fig. 2. Scattering instrument used in the measurements of rough surface scattering. The incident beam is brought over the detector and, after orientation of its polarization direction, is incident upon the rough surface. The detector arm may be moved out of the plane of the figure to measure the intensity at all scattering angles. M denotes a mirror, P denotes a linear polarizer, and W denotes a half-wave plate.

angles. The laser beam was modulated by a mechanical chopper, and the detector signal was processed by an Ithaco 3981 lock-in amplifier. A polarizer was mounted in front of the detector and, for reasons noted below, provisions were made for mounting a quarter-wave plate in front of the polarizer. Immediately in front of the detector, a field lens of 24.0-mm diameter imaged the rough surface onto the detector element.

Instead of using the incident states $\mathbf{V}_+$ or $\mathbf{V}_R$ to measure the Stokes matrix elements s_{11} and s_{12}, we used a method to conform to previous research.[1-3] That is, we determined the p cross section by using a p incident state, adjusting the detector polarizer in a collinear direction, and determining the scattered intensity at the detector. After measuring the s cross section in an analogous fashion, we computed the matrix elements s_{11} and s_{12} from Eqs. (5). A $+45°$ incident state $\mathbf{V}_+$ was then employed to determine the matrix elements s_{33} and s_{34}. The $\mathbf{V}_+$ state produces the scattered state of Eq. (9), and the third and fourth Stokes vector elements were found by a well-known procedure.[16] That is, we found the third element by measuring the intensity with the detector polarizer set at $+45°$ (cross polarized) and then subtracting the intensity measured at a $-45°$ setting (copolarized) to obtain s_{33}. We found the fourth Stokes vector element by recording the intensity measured with a detector sensitive to right-circular polarization and subtracting that measured with a detector sensitive to left-circular polarization. In this procedure a quarter-wave plate was mounted in front of the detector polarizer. It was oriented so that the fast and slow axes were suitably positioned at 45° with respect to the detector polarizer in the right-handed configuration; the left-handed measurement was then taken after the wave plate had been rotated by 90°.

The measurements used to determine the last Stokes vector element are difficult ones, and several errors could occur. Errors may arise from a small degree of ellipticity of the incident state, retardation errors of the wave plate itself, and misadjustments of the relative angular positions of the wave plate and detector polarizer. Considerable care has made these errors inconsequential, so that data shown have not been corrected in any manner. Laser power was also monitored during measurement procedures, although fluctuations were less than 1% and were thus insignificant.

Another concern in this experiment is the normalization of the data, for correct relative normalization is crucial in taking differences of data as is required for Stokes matrix elements. Data should ideally be normalized in the sense of a differential scattering cross section, so that the integral of the cross section over planar angle is equal to the fraction of incident power that has been scattered. Correct normalization of experimental data is quite difficult; to our knowledge, all previous measurements have, in an *ad hoc* fashion, simply normalized the scattering curve to unit area.[1-3] We have done precisely this to the s cross section, though all subsequent data have been measured correctly with respect to the height of the s cross section. For example, as will be discussed in Section 4, the p cross section has been found to correspond to a lower total scattered power.

The difficulties with normalization are rooted in a deeper problem. The surfaces fabricated are only approximately one dimensional. A significant amount of the scattered power deviates from the plane of incidence and falls outside the detector's field lens, so that data cannot be normalized from first principles. This may be traced to a small amount of residual isotropic roughness in addition to the desired one-dimensional roughness; we believe that it arises from scattering within the photoresist during surface fabrication. However, to our knowledge this problem has been present in all earlier experiments, and we also have not been able to circumvent it.

4. EXPERIMENTAL RESULTS AND DISCUSSION

The s- and p-scattering cross sections for normal incidence are shown in Fig. 3. It can be seen that these cross sections are similar and exhibit strong backscattering peaks with significant secondary maxima. There are subtle differences between the two curves; perhaps most apparent is that the s cross section falls more sharply in the range $70° < \theta_s < 90°$; this has been seen in previous experiments.[1-3] Figure 4 shows measurements made with the $+45°$ incident state $\mathbf{V}_+$. The scattered intensity resolved with the detector polarizer at $+45°$ contains

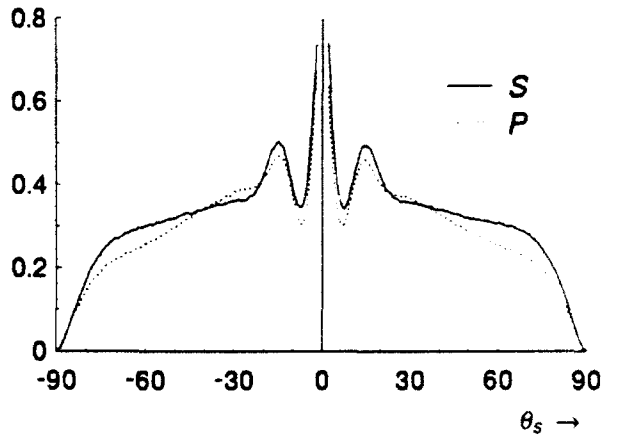

Fig. 3. Scattering cross sections for the one-dimensional surface for normally incident s- and p-polarization states.

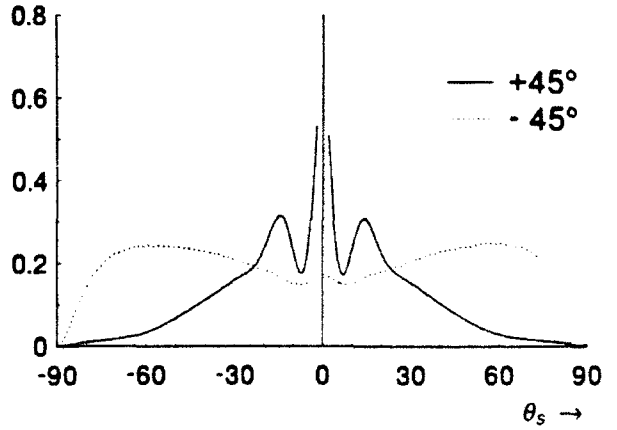

Fig. 4. Scattering cross sections for the one-dimensional surface illuminated with a normally incident wave with $+45°$ polarization. The solid curve is the scattered intensity passed by a polarizer at $+45°$ (cross polarized with respect to the source), and the dashed curve is that found with a polarizer at $-45°$ (copolarized).

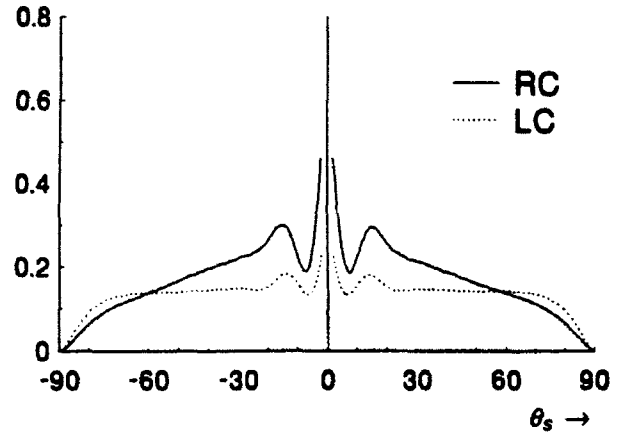

Fig. 5. Scattering cross sections for the one-dimensional surface illuminated with a normally incident wave with +45° polarization. The solid curve is the intensity in the scattered field measured with a detector sensitive to right-circular (RC) polarization, and the dashed curve is that found with a detector sensitive to left-circular (LC) polarization.

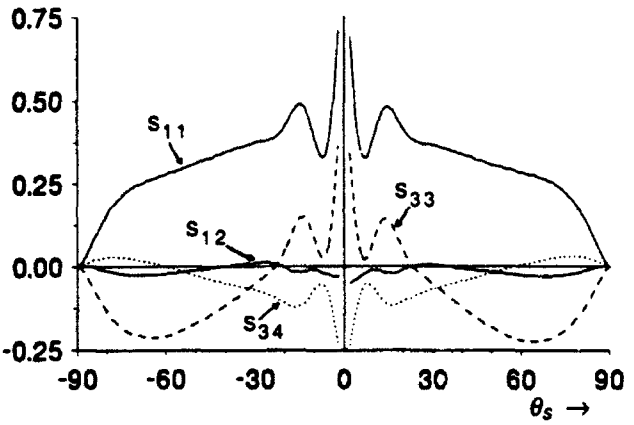

Fig. 6. The four unique elements of the Stokes matrix s_{11}, s_{12}, s_{33}, and s_{34} for the one-dimensional surface at normal incidence. They are plotted as a function of the scattering angle θ_s with respect to the surface normal.

an unusually strong backscattering structure. It is equally notable that the measurement with the detector polarizer at −45° has a significantly suppressed backscattering region, with a small peak present at $\theta_s = 0°$. Figure 5 shows data taken with the detector in right-circular- and left-circular-sensitive configurations. There is a backscattering structure present in both measurements, though there is a strong bias of the scattered field toward right-circular polarization, at least for scattering angles less than 60°.

Taking appropriate sums and differences of the measurements of Figs. 3–5 as discussed in Section 3, we obtain the full set of Stokes matrix elements as shown in Fig. 6. Clearly s_{11} is significant, but, because the p and s cross sections are similar for this surface, s_{12} remains quite small. The element s_{33} takes on the unusual form of having a large positive backscattering structure and significant negative values for $\theta_s > 23°$. In addition, s_{34} is mostly negative and also has a significant backscattering region.

There is a physical interpretation of the new information implicit in the matrix elements s_{33} and s_{34}. It has been suggested that enhanced backscattering, as well as most of the depolarization, arises from multiple scattering among light paths occurring within surface valleys.[17,18] As shown in Fig. 7, consider a single valley in the surface illuminated with an incident wave in the V_+ state. If the surface is a perfect conductor and a locally planar surface model is used, the intermediate wave sent to the other side of the valley will have the polarization shown so as to make the total electric field along the surface zero. When this is scattered at point 2, for similar reasons the light escaping from the surface will then remain polarized in the +45° direction. This path and its time-reversed partner are believed to give rise to backscattering enhancement[17,18] so that, as was seen in Fig. 4, the enhancement should reside largely in the intensity polarized at +45°. Results of other experiments have shown that enhanced backscattering may be completely isolated from ordinary scattering behavior by using precisely these polarization conditions.[19] On the other hand, measurements of the scattered intensity polarized at −45° should have contributions from single scattering from regions with weaker slopes and so should not have a significant backscattering structure. It is remarkable, however, that this measurement has the depressed levels surrounding $\theta_s = 0$ seen in Fig. 4.

It is also possible to interpret the scattering of V_+ to right-elliptical states (on average) as implied by the predominantly negative values of s_{34}. If one uses a model as in Fig. 7 and assumes that the metal is not a perfect conductor, the doubly scattered ray will be elliptically polarized because of the complex s and p reflectivities of the metal. To determine the role of these reflectivities, we have sent the V_+ state into a pair of 50 mm × 50 mm gold mirrors that, in analogy to Fig. 7, made a 90° angle with respect to each other and sent the beam back toward the source. The measured Stokes vector of the reflected beam was that of a right-elliptical state with major axis nearly along the +45° direction, in a manner qualitatively similar to the polarization states present in the backscattering region of the random surface. It is also interesting to note that, in the experiment with the pair of mirrors, the exiting polarization state is strongly dependent on the complex refractive index of the mirror; this behavior suggests that s_{33} and s_{34} may be significantly dependent on the metal of the rough surface.

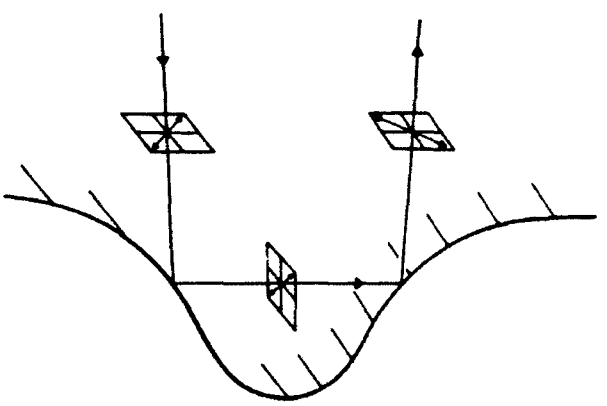

Fig. 7. Multiple scattering of the +45° incident polarization state V_+ within a valley of the random surface.

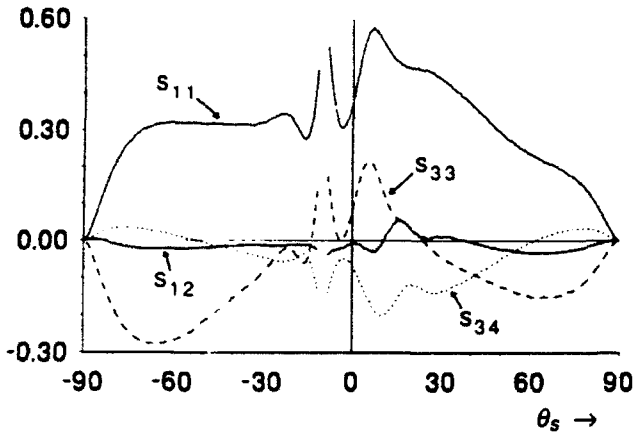

Fig. 8. The four unique elements of the Stokes matrix s_{11}, s_{12}, s_{33}, and s_{34} for the one-dimensional surface at angle of incidence $\theta_i = 10°$. The scattering angle θ_s is with respect to the surface normal; $\theta_s = -10°$ is the backscattering direction.

The properties of s_{33} and s_{34} may be interpreted in this way, and, although such models are oversimplified for a surface with wavelength-sized structures, the polarization of the field seems to obey these geometrical models. To go beyond the limitations of these arguments the Stokes matrix elements must be calculated from first principles, but these considerations are outside the scope of the present paper. For example, the angular dependence of the matrix elements implies that the $\mathbf{V}_+$ state is scattered to polarization states with, in an averaged sense, different major axis directions and handedness at various scattering angles; a full understanding of such features can be found only through rigorous calculations.

As we discussed above, all curves are normalized so that the s-scattering cross section represents a total scattered power of unity. Integration of the p cross section then provides a scattered power of 0.935. Similarly, we may find the total scattered power for the $\mathbf{V}_+$ incident state by adding the orthogonally polarized curves of Fig. 4 and integrating, providing a total scattered power of 0.969. These results are then entirely self-consistent.

Lastly, in Fig. 8 are shown plots of the four Stokes matrix elements for the same experimental parameters but with $\theta_i = 10°$. It can be seen that s_{11} has become skewed, though it still has its backscattering peak, and that s_{12} is more significant than in normal incidence. The elements s_{33} and s_{34} have also become slightly skewed, but in the backscattering region the $\mathbf{V}_+$ state is still scattered to states that are, on average, significantly right circular and in the +45° direction.

5. CONCLUSIONS

The Stokes matrix of a one-dimensional rough surface has been derived and has been found to contain four unique elements. We have presented measurements of these elements for a surface that produces backscattering enhancement. It has been found that all four elements are significant for this surface and provide important insight into the prevalent scattering mechanisms.

For the one-dimensional rough surface scattering problem, it is fortunately possible to compare theory and experiment, and both aspects of this research have benefited from this situation. However, as we have pointed out here, only one half of the relevant scattering problem has been addressed in previous research; that is, important information has been neglected in calculations, and previous experiments have not made all significant measurements. It is then only reasonable that future comparisons between theory and experiment should be based on the four unique Stokes matrix elements of the one-dimensional surface.

ACKNOWLEDGMENT

This research was supported by the U.S. Army Research Office.

REFERENCES AND NOTES

1. A. J. Sant, J. C. Dainty, and M. J. Kim, "Comparison of surface scattering between identical, randomly rough metal and dielectric diffusers," Opt. Lett. **14**, 1183–1185 (1989).
2. M. J. Kim, J. C. Dainty, A. T. Friberg, and A. J. Sant, "Experimental study of enhanced backscattering from one- and two-dimensional random rough surfaces," J. Opt. Soc. Am. A **7**, 569–577 (1990).
3. M. J. Kim, "Light scattering from characterized random rough surfaces," Ph.D. dissertation (Imperial College, London, 1989).
4. M. Nieto-Vesperinas and J. M. Soto-Crespo, "Monte Carlo simulations for scattering of electromagnetic waves from perfectly conductive random rough surfaces," Opt. Lett. **12**, 979–981 (1987).
5. J. M. Soto-Crespo and M. Nieto-Vesperinas, "Electromagnetic scattering from very rough random surfaces and deep reflection gratings," J. Opt. Soc. Am. A **6**, 367–384 (1989).
6. A. A. Maradudin, E. R. Méndez, and T. Michel, "Backscattering effects in the elastic scattering of p-polarized light from a large-amplitude random metallic grating," Opt. Lett. **14**, 151–153 (1989).
7. T. Michel, A. A. Maradudin, and E. R. Méndez, "Enhanced backscattering of light from a non-Gaussian random metal surface," J. Opt. Soc. Am. B **6**, 2438–2446 (1989).
8. T. Michel, "Enhanced backscattering of light from a randomly rough grating," Ph.D. dissertation (University of California, Irvine, Calif., 1990).
9. M. Saillard and D. Maystre, "Scattering from metallic and dielectric rough surfaces," J. Opt. Soc. Am. A **7**, 982–990 (1990).
10. See, for example, A Ishimaru, *Wave Propagation and Scattering in Random Media* (Academic, New York, 1978), Vol. 1.
11. E. L. O'Neill, *Introduction to Statistical Optics* (Addison-Wesley, Reading, Mass., 1963).
12. H. C. van de Hulst, *Light Scattering by Small Particles* (Dover, New York, 1981).
13. W. S. Bickel and W. M. Bailey, "Stokes vectors, Mueller matrices, and polarized scattered light," Am. J. Phys. **53**, 468–478 (1985).
14. D. H. Goldstein and R. A. Chipman, "Error analysis of a Mueller matrix polarimeter," J. Opt. Soc. Am. A **7**, 693–700 (1990).
15. A linearly polarized state at −45° or a left-circular state produces similar results with only sign differences in some quantities; thus they are not discussed here.
16. M. Born and E. Wolf, *Principles of Optics* (Pergamon, Oxford, 1975).
17. K. A. O'Donnell and E. R. Méndez, "Experimental study of scattering from characterized random surfaces," J. Opt. Soc. Am. A **4**, 1194–1205 (1987).
18. E. R. Méndez and K. A. O'Donnell, "Observation of depolarization and backscattering enhancement in light scattering from Gaussian random surfaces," Opt. Commun. **61**, 91–95 (1987).
19. M. E. Knotts and K. A. O'Donnell, "Anomalous scattering from a perturbed grating," Opt. Lett. **15**, 1485–1487 (1990).

a reprint from Journal of the Optical Society of America A

Stokes matrix of a one-dimensional perfectly conducting rough surface

T. R. Michel, M. E. Knotts, and K. A. O'Donnell

School of Physics, Georgia Institute of Technology, Atlanta, Georgia 30332

Received May 20, 1991; revised manuscript received October 11, 1991; accepted October 18, 1991

We study theoretically the Stokes matrix of a perfectly conducting, one-dimensional rough surface that is illuminated by a polarized light beam of finite width whose plane of incidence is perpendicular to the grooves of the surface. An exact expression for the scattered field derived from Green's second integral theorem is used to compute the angular distribution of the Stokes matrix that has eight nonzero elements, four of which are unique. Results are presented for the numerical calculation of each matrix element averaged over an ensemble of surface profiles that are realizations of a stationary, Gaussian stochastic process. All four unique matrix elements are significant, with the diagonal elements displaying enhanced backscattering and the off-diagonal elements having complicated angular dependences including structures in the retroreflection direction. With the use of a single source function evaluated through the iteration of the surface integral equation obtained from the extinction theorem for the p-polarized field, we derive an approximate expression for the Stokes matrix that indicates that multiple scattering plays an important role in the polarized scattering from a perfectly conducting rough surface that displays enhanced backscattering. The numerical calculation of each of the contributions to the Stokes matrix, taking into account single-, double-, and triple-scattering processes, enables us to assign the main features of the Stokes matrix to particular multiple-scattering processes. Experimental measurements of the matrix elements are presented for a one-dimensional Gaussian surface fabricated in gold-coated photoresist. The results are found to be reasonably consistent with the theory, although we suggest that differences in one matrix element may be due to the finite conductivity of the experimental surface.

1. INTRODUCTION

The manifestations of multiple scattering have aroused much interest in recent theoretical and experimental studies of the scattering of light from randomly rough surfaces. Enhanced backscattering has been observed in scattering from one- and two-dimensional surfaces when the height fluctuations are of the order of a wavelength and strong surface slopes are present.[1-6] Theoretical evidence that strongly suggests that the observed enhanced backscattering is intimately connected to multiple scattering has been presented.[7-10] For one-dimensional surfaces, numerical calculations have provided reasonable predictions for the angular dependence of the diffuse intensities scattered from a perfectly conducting[11,12] or penetrable[7,13,14] rough surface. A common feature of the theoretical studies of scattering from one-dimensional surfaces is that the incident electric field has been chosen to be linearly polarized either parallel or perpendicular to the grooves of the surface (s or p polarized, respectively) and, consequently, that the scattered field has the same polarization as the incident field. Although these are important cases, it has been shown[6] that the p- and the s-polarized diffuse intensities are effectively only two of a total of four unique quantities arising in the Stokes matrix of a one-dimensional rough surface. Measurements that showed that all four quantities are significant for a one-dimensional rough surface producing backscattering enhancement were reported.[6]

In the present paper we theoretically investigate the Stokes matrix of a one-dimensional, perfectly conducting rough surface. Exact expressions for the p- and the s-polarized scattering amplitudes derived from Green's second integral theorem are used to obtain the matrix, and its four unique elements are averaged over an ensemble of surface profiles that are realizations of a stationary, Gaussian stochastic process. Each Stokes matrix element is found to be significant for surface parameters that lead to enhanced backscattering. A method based on the iteration of the Kirchhoff term[15,16] in the surface integral equation satisfied by the source functions of the scattered field is used to determine the role of multiple scattering in the elements of the Stokes matrix. Experimental measurements of the matrix elements are presented for a one-dimensional Gaussian surface fabricated in gold. For the incident wavelength employed (λ = 3.392 μm), the scattering behavior is found to be comparable to that of a perfect conductor.

2. SCATTERING OF POLARIZED LIGHT FROM A PERFECTLY CONDUCTING, ONE-DIMENSIONAL ROUGH SURFACE

In this section we derive exact expressions for the elements of the Stokes matrix of a perfectly conducting, one-dimensional rough surface that is illuminated by a beam of finite width. Consider the situation shown in Fig. 1, in which a perfectly conducting half space $x_3 < \zeta(x_1)$ is separated from the vacuum above it by a randomly rough surface of equation $x_3 = \zeta(x_1)$. The surface profile function $\zeta(x_1)$ is assumed to be a single-valued stochastic pro-

0740-3232/92/040585-12$05.00

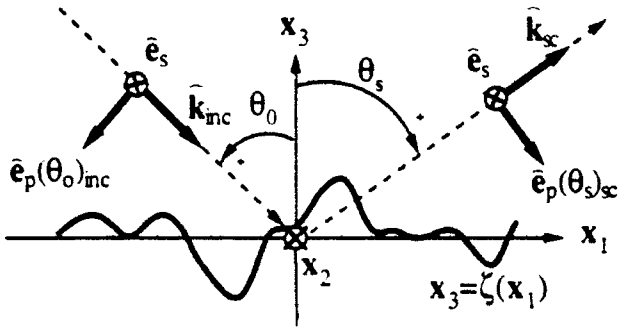

Fig. 1. Geometry of scattering by a one-dimensional rough surface. $\hat{\mathbf{k}}_{inc} = \sin\theta_0\hat{\mathbf{x}}_1 - \cos\theta_0\hat{\mathbf{x}}_3$, and $\hat{\mathbf{k}}_{sc} = \sin\theta_s\hat{\mathbf{x}}_1 + \cos\theta_s\hat{\mathbf{x}}_3$.

cess having derivatives of arbitrary order and whose ensemble average $\langle\zeta(x_1)\rangle$ vanishes. Further, the surface profile is assumed to be one dimensional in the sense that ζ is independent of x_2.

A polarized light beam whose plane of incidence is the plane x_1x_3 perpendicular to the grooves of the surface illuminates the perfect conductor from the vacuum side. Such a beam may be expressed by a Gaussian angular spectrum of incident plane waves whose wave vectors all lie in the plane of incidence. The incident electric field amplitude may be written as

$$\mathbf{E}(x_1, x_3\ \omega)_{inc} = \frac{\omega w}{2\sqrt{\pi c}}\int_{-\pi/2}^{\pi/2} d\theta\, \exp[-(\omega^2w^2/4c^2)(\theta-\theta_0)^2] \times [E_p\hat{\mathbf{e}}_p(\theta)_{inc} + E_s\hat{\mathbf{e}}_p(\theta)_{inc}]\exp[i(\omega/c)(x_1\sin\theta - x_3\cos\theta)], \quad |\theta_0| < \frac{\pi}{2}, \tag{1}$$

where

$$\hat{\mathbf{e}}_s(\theta)_{inc} = \hat{\mathbf{x}}_2, \tag{2}$$

$$\hat{\mathbf{e}}_p(\theta)_{inc} = -\hat{\mathbf{x}}_1\cos\theta - \hat{\mathbf{x}}_3\sin\theta, \tag{3}$$

c is the speed of light, and the time dependency $\exp(-i\omega t)$ is omitted. Equation (1) is an exact solution of Maxwell's equations in vacuum that, in the limit of $\omega w/2c \gg 1$, describe a Gaussian beam propagating in the direction $(\hat{\mathbf{x}}_1\sin\theta_0 - \hat{\mathbf{x}}_3\cos\theta_0)$ with transverse width $2w$ at the coordinate origin. The unit vector $\hat{\mathbf{e}}_p(\theta)_{inc}$ $[\hat{\mathbf{e}}_s(\theta)_{inc}]$ is in the direction of the electric field of a p- (s-) polarized plane wave with unit wave vector $(\hat{\mathbf{x}}_1\sin\theta - \hat{\mathbf{x}}_3\cos\theta)$. The complex amplitudes E_p and E_s determine the incident polarization state.

It follows from Maxwell's equations that Eq. (1) may also be written in the form

$$\mathbf{E}(x_1, x_3|\,\omega)_{inc} = \frac{ic}{\omega}\nabla\times[E_p\phi(x_1, x_3|\,\omega)_{inc}\hat{\mathbf{x}}_2] + E_s\phi(x_1, x_3|\,\omega)_{inc}\hat{\mathbf{x}}_2, \tag{4}$$

with

$$\phi(x_1, x_3|\,\omega)_{inc} = \frac{\omega w}{2\sqrt{\pi c}}\int_{-\pi/2}^{\pi/2} d\theta\, \exp[-(\omega^2w^2/4c^2)(\theta-\theta_0)^2] \times \exp[i(\omega/c)(x_1\sin\theta - x_3\cos\theta)], \tag{5}$$

where the p- and the s-polarized contributions to the incident electric field are clearly separated. The s-polarized electric field and the magnetic field associated with the p-polarized electric field each have a single component along $\hat{\mathbf{x}}_2$, and this component is the product of the scalar field $\phi(x_1, x_3|\,\omega)_{inc}$ with the incident amplitude E_s or E_p. For the one-dimensional problem of interest here, both the incident beam and the surface-profile function are independent of x_2. The boundary condition on the total electric field at the surface then separates into two boundary conditions, one of them containing only the p-polarized field and the other containing only the s-polarized field. Consequently, a p- (s-) polarized incident field is scattered only into a p- (s-) polarized field. The one-dimensional scattering of a p-polarized incident beam then reduces to the scattering of a scalar field satisfying a Neumann boundary condition at the rough surface. Similarly, the scattering of an s-polarized beam of light reduces to the scattering of a scalar field with a Dirichlet boundary condition at the surface. Exact expressions derived from Green's second integral theorem may then be used to calculate the scattered fields numerically; these methods have been well addressed elsewhere.[7] The p- and the s-polarized scattering amplitudes $r_p(\theta_s)$ and $r_s(\theta_s)$ may be obtained as solutions to the scattering of the incident field of Eq. (5) for the Neumann and the Dirichlet boundary conditions, respectively. These scattering amplitudes determine an exact expression for the scattered electric field in the far-field region $x_3 \to \infty$ as

$$\mathbf{E}(x_1, x_3|\,\omega)_{sc} = \frac{i}{4\pi}\int_{-\pi/2}^{\pi/2} d\theta_s \times [E_p r_p(\theta_s)\hat{\mathbf{e}}_p(\theta_s)_{sc} + E_s r_s(\theta_s)\hat{\mathbf{e}}_s(\theta_s)_{sc}] \times \exp[i(\omega/c)(x_1\sin\theta_s + x_3\cos\theta_s)], \tag{6}$$

where

$$\hat{\mathbf{e}}_s(\theta_s)_{sc} = \hat{\mathbf{x}}_2, \tag{7}$$

$$\hat{\mathbf{e}}_p(\theta_s)_{sc} = \hat{\mathbf{x}}_1\cos\theta_s - \hat{\mathbf{x}}_3\sin\theta_s. \tag{8}$$

The unit vector $\hat{\mathbf{e}}_p(\theta_s)_{sc}$ $[\hat{\mathbf{e}}_s(\theta_s)_{sc}]$ defines the direction of the electric-field vector of a p- (s-) polarized plane wave scattered in the direction $(\sin\theta_s\hat{\mathbf{x}}_1 + \cos\theta_s\hat{\mathbf{x}}_3)$.

It is convenient to define the polarization states in terms of directly measurable quantities. We thus need to compute the power present in the projection of the incident and the scattered fields on polarization states that are linear combinations of the p- and the s-polarized states described by Eqs. (2) and (3) and Eqs. (7) and (8), respectively. A useful description of polarized light in terms of these powers is that of Stokes vectors.[17] The following pairs of orthonormal vectors, defined here in the usual way,[18] are needed to compute the Stokes vectors. These pairs of unit vectors determine the linearly polarized states at $\pm45°$, as well as the right (R) and the left (L) circularly polarized states, and may be expressed as

$$\hat{\mathbf{e}}_- = \frac{1}{\sqrt{2}}(\hat{\mathbf{e}}_p + \hat{\mathbf{e}}_s), \tag{9}$$

$$\hat{\mathbf{e}}_- = \frac{1}{\sqrt{2}}(\hat{\mathbf{e}}_p - \hat{\mathbf{e}}_s), \tag{10}$$

$$\hat{\mathbf{e}}_R = \frac{1}{\sqrt{2}}(\hat{\mathbf{e}}_p - i\hat{\mathbf{e}}_s), \tag{11}$$

$$\hat{\mathbf{e}}_L = \frac{1}{\sqrt{2}}(\hat{\mathbf{e}}_p + i\hat{\mathbf{e}}_s), \tag{12}$$

where $\hat{\mathbf{e}}_\alpha$, $\alpha = p, s, +, -, R$, or L, must be replaced by $\hat{\mathbf{e}}_\alpha(\theta_0)_{inc}$ in the case of the incident field and by $\hat{\mathbf{e}}_\alpha(\theta_s)_{sc}$ in the case of the scattered field. The identities $\hat{\mathbf{e}}_\alpha\hat{\mathbf{e}}_\alpha^\dagger + \hat{\mathbf{e}}_\beta\hat{\mathbf{e}}_\beta^\dagger = \bar{\mathbf{1}}$ $[(\alpha,\beta) = (p,s), (+,-)$ or $(R,L)]$, where $\hat{\mathbf{e}}_\alpha\hat{\mathbf{e}}_\alpha^\dagger$ denotes a dyadic product and $\bar{\mathbf{1}}$ is the unit dyadic, indicate that an electric field may be completely decomposed into projections on $(\hat{\mathbf{e}}_\alpha, \hat{\mathbf{e}}_\beta)$ in the following manner: the projection of a field $\mathbf{E}(x_1, x_3|\omega)$ on $\hat{\mathbf{e}}_\gamma$ $(\gamma = \alpha$ or $\beta)$ is $\mathbf{E}_\gamma(x_1, x_3|\omega) = [\hat{\mathbf{e}}_\gamma^* \cdot \mathbf{E}(x_1, x_3|\omega)]\hat{\mathbf{e}}_\gamma$, and $\mathbf{E}(x_1, x_3|\omega) = \mathbf{E}_\alpha(x_1, x_3|\omega) + \mathbf{E}_\beta(x_1, x_3|\omega)$.

The elements of the Stokes vector $\mathbf{V} = (I, Q, U, V)$ may be expressed as[19]

$$I = P_p + P_s = P_+ + P_- = P_R + P_L, \tag{13}$$

$$Q = P_p - P_s, \tag{14}$$

$$U = P_+ - P_-, \tag{15}$$

$$V = P_R - P_L, \tag{16}$$

where, in the case of the incident field, P_α is the total power incident upon the surface that is in the projection of the incident field $\mathbf{E}_\alpha(x_1, x_3|\omega)_{inc}$. To obtain this total incident power we integrate the magnitudes of the third component of the time-averaged Poynting vector of $\mathbf{E}_\alpha(x_1, x_3|\omega)_{inc}$ on a portion of the plane $x_3 = 0$ that is such that $0 < x_2 < L_2$, where L_2 is an arbitrary length. The Stokes vector $\mathbf{V}_{inc}$ of the incident field becomes

$$\mathbf{V}_{inc} = \begin{bmatrix} I_{inc} \\ Q_{inc} \\ U_{inc} \\ V_{inc} \end{bmatrix} = \mathcal{P}_{inc} \begin{bmatrix} |E_p|^2 + |E_s|^2 \\ |E_p|^2 - |E_s|^2 \\ 2\,\Re e(E_p E_s^*) \\ 2\,\Im m(E_p E_s^*) \end{bmatrix}, \tag{17}$$

where $\mathcal{P}_{inc} \equiv L_2 c\omega/[8(2\pi)^{1/2}]$ when $\omega\omega/2c \gg 1$, as is discussed in Section 3.

The quantities P_α of interest in the calculation of the Stokes vector of the scattered field of Eq. (6) are the differential powers per unit planar angle $P_\alpha(\theta_s)_{sc}$ arising from the projection of the plane wave scattered at an angle θ_s on the polarization states $\hat{\mathbf{e}}(\theta_s)_{sc}$; $P_\alpha(\theta_s)_{sc}$ is obtained by integrating the third component of the time-averaged Poynting vectors of this projection in the domain $0 < x_2 < L_2$ of a plane in the far-field region that is parallel to the plane $x_3 = 0$. The vector $\mathbf{v}(\theta_s)_{sc}$, calculated from the scattered field through Eqs. (6) and (13)–(16), for a single realization of the rough surface, is then given by

$$\mathbf{v}(\theta_s)_{sc} = L_2 \frac{c^2}{64\pi^2\omega} \begin{bmatrix} |r_p(\theta_s)E_p|^2 + |r_s(\theta_s)E_s|^2 \\ |r_p(\theta_s)E_p|^2 - |r_s(\theta_s)E_s|^2 \\ 2\,\Re e[r_p(\theta_s)E_p r_s^*(\theta_s)E_s^*] \\ 2\,\Im m[r_p(\theta_s)E_p r_s^*(\theta_s)E_s^*] \end{bmatrix}. \tag{18}$$

With the use of the definitions [Eqs. (13)–(16)] of the elements of this vector, we may reintroduce directly measurable quantities in the following way. The total flux of the Poynting vectors $P_\alpha(\theta_s)_{sc}$ is a measure of the power per unit angle transmitted through a filter passing the field in the polarization state $\hat{\mathbf{e}}_\alpha(\theta_s)_{sc}$. This power may then be normalized by the total incident power $\mathcal{P}_{inc}(|E_p|^2 + |E_s|^2)$ to obtain the differential reflection coefficients[7] $\partial R_\alpha/\partial\theta_s$, which are the observable quantities. The vector $\mathbf{v}(\theta_s)_{sc}$ may then be related to the differential reflection coefficients as

$$\begin{bmatrix} \dfrac{\partial R_p}{\partial\theta_s} + \dfrac{\partial R_s}{\partial\theta_s} \\ \dfrac{\partial R_p}{\partial\theta_s} - \dfrac{\partial R_s}{\partial\theta_s} \\ \dfrac{\partial R_+}{\partial\theta_s} - \dfrac{\partial R_-}{\partial\theta_s} \\ \dfrac{\partial R_R}{\partial\theta_s} - \dfrac{\partial R_L}{\partial\theta_s} \end{bmatrix} = \frac{\mathbf{v}(\theta_s)_{sc}}{\mathcal{P}_{inc}(|E_p|^2 + |E_s|^2)}. \tag{19}$$

At this point a matrix $\mathbf{s}(\theta_s)$ relating the incident Stokes vector of Eq. (17) and the vector of Eq. (18) through the equation

$$\mathbf{v}(\theta_s)_{sc} = \mathbf{s}(\theta_s)\mathbf{V}_{inc} \tag{20}$$

may be calculated by using the fact that the incident amplitudes E_p and E_s are arbitrary complex constants. We find that this matrix has the form

$$\mathbf{s}(\theta_s) = \begin{bmatrix} s_{11}(\theta_s) & s_{12}(\theta_s) & 0 & 0 \\ s_{12}(\theta_s) & s_{11}(\theta_s) & 0 & 0 \\ 0 & 0 & s_{33}(\theta_s) & s_{34}(\theta_s) \\ 0 & 0 & -s_{34}(\theta_s) & s_{33}(\theta_s) \end{bmatrix}, \tag{21}$$

where

$$s_{11}(\theta_s) = C[|r_p(\theta_s)|^2 + |r_s(\theta_s)|^2], \tag{22}$$

$$s_{12}(\theta_s) = C[|r_p(\theta_s)|^2 - |r_s(\theta_s)|^2], \tag{23}$$

$$s_{33}(\theta_s) = C\{2\Re e[r_p(\theta_s)r_s^*(\theta_s)]\}, \tag{24}$$

$$s_{34}(\theta_s) = C\{-2\Im m[r_p(\theta_s)r_s^*(\theta_s)]\}, \tag{25}$$

$$C = \frac{L_2 c^2}{32(2\pi)^2\omega\mathcal{P}_{inc}}. \tag{26}$$

For each realization of the surface-profile function $\zeta(x_1)$ there is a corresponding realization of the vector $\mathbf{v}(\theta_s)_{sc}$ and of the matrix $\mathbf{s}(\theta_s)$. In this study of diffuse scattering we consider the average of the vector $\mathbf{v}(\theta_s)_{sc}$ over the ensemble of realizations of the surface-profile function

$$\mathbf{V}(\theta_s)_{sc} = \langle \mathbf{v}(\theta_s)_{sc} \rangle, \tag{27}$$

which is the scattered Stokes vector. The matrix $\mathbf{s}(\theta_s)$ averaged over the ensemble of realizations of the surface-profile function

$$\mathbf{S}(\theta_s) = \langle \mathbf{s}(\theta_s) \rangle \tag{28}$$

is the matrix enabling us to compute the scattered Stokes vector for any given incident polarization state according to

$$\mathbf{V}(\theta_s)_{sc} = \mathbf{S}(\theta_s)\mathbf{V}_{inc}; \tag{29}$$

for this reason $\mathbf{S}(\theta_s)$ is called the Stokes matrix[20] of the rough surface.

The Stokes matrix contains contributions from the coherent and the incoherent parts of the random scattered amplitudes $\langle r_\alpha(\theta_s)\rangle$ and $\Delta r_\alpha(\theta_s) = r_\alpha(\theta_s) - \langle r_\alpha(\theta_s)\rangle$, respectively. The substitution of this decomposition of the scattering amplitudes $r_\alpha(\theta_s)$ into the expression for the

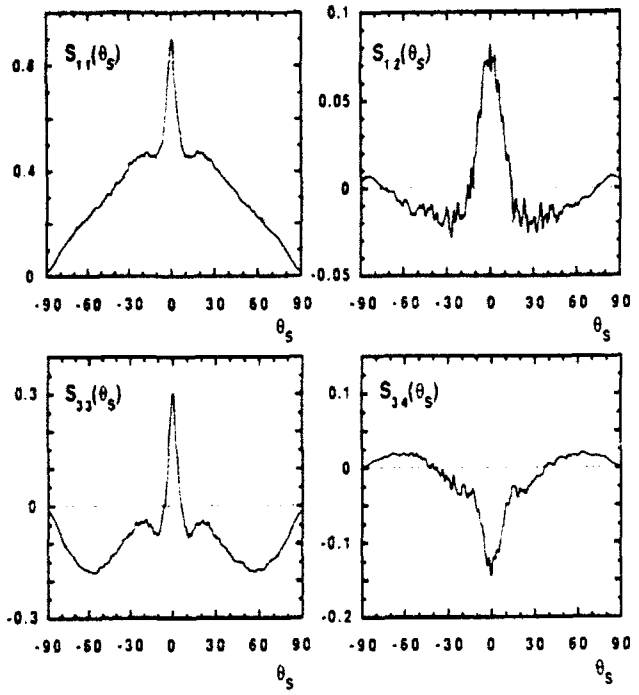

Fig. 2. The four unique elements of the Stokes matrix, $S_{11}(\theta_s)$, $S_{12}(\theta_s)$, $S_{33}(\theta_s)$, and $S_{34}(\theta_s)$, for a one-dimensional, perfectly conducting rough surface at normal incidence. $\delta/a = 0.6$, $L/g = 4$, $a/\lambda = 3$, $g/\lambda = 20$; $N_x = 600$, $N_p = 4000$.

Stokes matrix [Eq. (28)] leads to

$$\mathbf{S}(\theta_s) = \mathbf{S}(\theta_s)_{\text{coh}} + \mathbf{S}(\theta_s)_{\text{incoh}}, \tag{30}$$

where the contributions to the Stokes matrix that are due to $\langle r_\alpha(\theta_s)\rangle$ and $\Delta r_\alpha(\theta_s)$ appear in separate terms. The mean scattering amplitude $\langle r_\alpha(\theta_s)\rangle$ describes the specular part of the scattered field, and the matrix $\mathbf{S}(\theta_s)_{\text{coh}}$, which is obtained by replacing $r_\alpha(\theta_s)$ by the mean scattered amplitude in Eq. (21), is then the specular or the coherent part of the Stokes matrix. The matrix $\mathbf{S}(\theta_s)_{\text{incoh}}$, calculated from Eq. (28) by using the fluctuating part of the scattering amplitude instead of the full amplitude, is the incoherent part of the Stokes matrix. Finally, the differential reflection coefficient $\partial R_\alpha/\partial\theta_s$ averaged over the ensemble of realizations of the surface profile may be calculated by replacing $\mathbf{v}(\theta_s)_{\text{sc}}$ by the scattered Stokes vector in Eq. (19). The quantity obtained is the differential scattered power per unit planar angle θ_s, $I_\alpha(\theta_s)$ that is due to the projection of the scattered field on the polarization state $\hat{\mathbf{e}}_\alpha$, normalized by the incident power and averaged over the ensemble of realizations of the surface profile. The experimental procedure to measure the cross section $I_\alpha(\theta_s)$ is described in Section 5.

3. NUMERICAL RESULTS

The Stokes matrix has been calculated for a surface-profile function assumed to be a stationary, Gaussian stochastic process characterized by the properties $\langle\zeta(x_1)\rangle = 0$ and $\langle\zeta(x_1)\zeta(x_1')\rangle = \delta^2 \exp[-(x_1 - x_1')^2/a^2]$, where δ^2 is the variance of $\zeta(x_1)$ and a is the transverse correlation length of the surface. Each realization of the surface profile $\zeta(x_1)$ was computed at $N_x = 600$ equally spaced abscissas, and the scattering amplitudes $r_p(\theta_s)$ and $r_s(\theta_s)$ were calculated as a function of the scattering angle by the method described in Section 2. The incident beam used in the computation may be obtained from Eqs. (4) and (5) through an approximate integration valid in the limit $\omega w/2c \gg 1$. The incident-scalar field of Eq. (5) may be approximated by[21]

$$\begin{aligned}\phi(x_1, x_3|\omega)_{\text{inc}} = \exp\{&i(\omega/c)(x_1 \sin\theta_0 - x_3\cos\theta_0)\\ &\times [1 + W(x_1, x_3)]\}\\ &\times \exp[-(x_1\cos\theta_0 + x_3\sin\theta_0)^2/w^2],\end{aligned} \tag{31}$$

where

$$W(x_1, x_3) = \frac{c^2}{w^2\omega^2}\left\{\left[\frac{2}{w^2}(x_1\cos\theta_0 + x_3\sin\theta_0)^2\right] - 1\right\}. \tag{32}$$

This analytic expression is simpler to evaluate numerically and is sufficiently accurate. The Stokes vector of the incident beam of Eqs. (4) and (31) is given by Eq. (17), where, for this approximation, $\mathcal{P}_{\text{inc}}$ is given by

$$\mathcal{P}_{\text{inc}} = L_2\frac{cw}{8(2\pi)^{1/2}}\left[1 - \frac{c^2}{2\omega^2 w^2}(1 + 2\tan^2\theta_0)\right]. \tag{33}$$

The 1/e half-width of the illuminated portion of the surface is denoted by g, and it is related to the 1/e half-width w of the incoming beam by $g = w\cos\theta_0$. N_p independent realizations of the surface profile were used to obtain estimates of the elements of the Stokes matrix. Each element of the matrix of Eq. (21) was arithmetically averaged over this finite ensemble. For the parameters discussed below, it was found that the coherent part of the Stokes matrix elements was negligible. All the results presented are for $\mathbf{S}(\theta_s)_{\text{incoh}}$, which was indistinguishable from $\mathbf{S}(\theta_s)$, hence we refer to all the results simply as Stokes matrix elements.

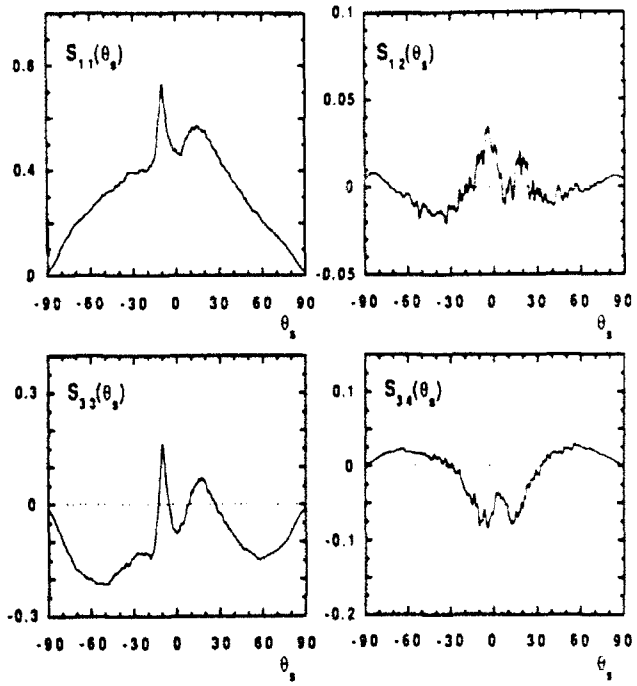

Fig. 3. The four unique elements of the Stokes matrix $S_{11}(\theta_s)$, $S_{12}(\theta_s)$, $S_{33}(\theta_s)$, and $S_{34}(\theta_s)$ for the same parameters as in Fig. 2 but with $\theta_0 = 10°$.

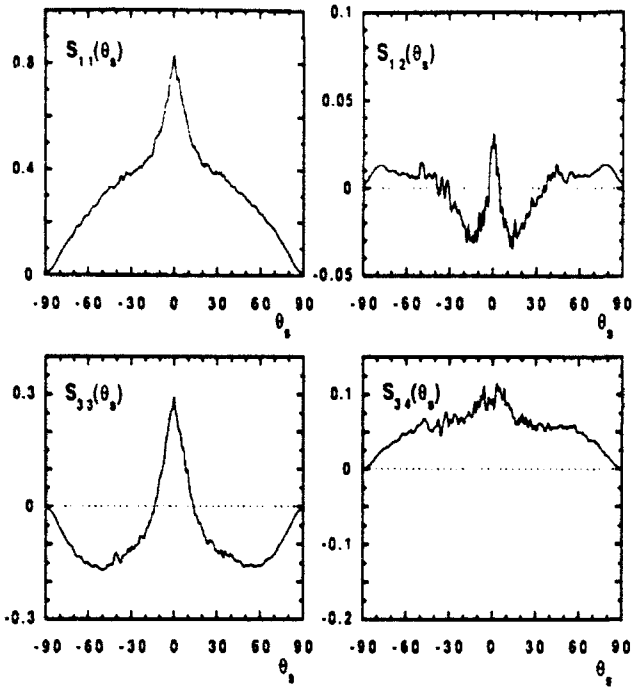

Fig. 4. The four unique elements of the Stokes matrix, $S_{11}(\theta_s)$, $S_{12}(\theta_s)$, $S_{33}(\theta_s)$, and $S_{34}(\theta_s)$, for a one-dimensional, perfectly conducting rough surface at normal incidence. $\delta/a = 0.6$, $L/g = 4$, $a = \lambda$, $g/\lambda = 20$; $N_s = 600$, $N_p = 4000$.

The ratio δ/a was 0.6, and thus the standard deviation of the surface slope $\langle \zeta'^2(x_1) \rangle^{1/2} = \sqrt{2}\,\delta/a$ was 0.8485. The length L of the surface was such that $L/g = 4$, and the illuminated width g was such that $g/\lambda = 20$. The angle of incidence θ_0 is measured counterclockwise from $\hat{\mathbf{x}}_3$, and the scattering angle θ_s is measured clockwise from $\hat{\mathbf{x}}_3$; all the angles in the figures are in degrees. The total scattered power always matched the incident power to within 0.5%. Averages were obtained over $N_p = 4000$ surface profiles.

In Fig. 2 we show the Stokes matrix elements $S_{11}(\theta_s)$, $S_{12}(\theta_s)$, $S_{33}(\theta_s)$, and $S_{34}(\theta_s)$ calculated for the case $\theta_0 = 0°$ and $a/\lambda = 3$. First, strong peaks at $\theta_s = 0°$ are observed in the angular distribution of $S_{11}(\theta_s)$, and $S_{33}(\theta_s)$. The enhanced backscattering peak observed in $S_{11}(\theta_s)$, as well as the secondary maxima on both sides of the peak, is related through Eq. (19) to that found in previous studies[7] of the s- and the p-polarized differential reflection coefficients for surfaces with comparable parameters. The peak and the secondary maxima observed in the angular distribution of $S_{33}(\theta_s)$ are similar to those observed in $S_{11}(\theta_s)$. The off-diagonal elements of the Stokes matrix are smaller than the diagonal elements, but they have clearly risen out of the statistical noise. The element $S_{12}(\theta_s)$ displays a peak at $\theta_s = 0°$, while $S_{34}(\theta_s)$ has a minimum at this angle. In Fig. 3 we present results with the same parameters as in Fig. 2 but with $\theta_0 = 10°$. The angular distributions of the diagonal elements of the Stokes matrix display a peak in the retroreflection direction $\theta_s = -\theta_0$. The amplitudes of these peaks relative to the magnitude of the background at θ_s near $-\theta_0$ is smaller than at normal incidence. A broad structure near the retroreflection direction is observed in the off-diagonal elements, and other extrema, located near an angle at which the diagonal elements have a maximum, are also observed.

The four unique matrix elements of $\mathbf{S}(\theta_s)$ calculated in the case $a = \lambda$ are shown in Figs. 4 and 5 for normal incidence and $\theta_0 = 10°$, respectively. Enhanced backscattering is clearly observed in the two diagonal elements for both angles of incidence. The width of this peak at its base is approximately three times larger in the case $a/\lambda = 1$ than in the case $a/\lambda = 3$, as would be expected from the multiple-scattering interpretation of this effect.[7,13,14] It is again found that the off-diagonal elements of the Stokes matrix are smaller than the diagonal elements. The element $S_{12}(\theta_s)$ has a peak in the retroreflection direction for both angles of incidence. The element $S_{34}(\theta_s)$ is positive at all the scattering angles, and the form of the curve is significantly different from the case $a/\lambda = 3$.

4. DISCUSSION

For any incident polarization state, the Stokes matrix determines the Stokes vector of the light scattered from the surface and may thus determine the intensity passed by an arbitrary polarization component. One illustrative example of this property follows. Consider an incident beam in a linear polarization state at +45°, such that $(E_p, E_s) = (1/\sqrt{2})(1,1)$ in Eq. (4). The scattered Stokes vector obtained from Eq. (29) is

$$\mathbf{V}(\theta_s)_{sc} = \mathcal{P}_{inc} \begin{bmatrix} S_{11}(\theta_s) \\ S_{12}(\theta_s) \\ S_{33}(\theta_s) \\ -S_{34}(\theta_s) \end{bmatrix}. \tag{34}$$

Substituting $\mathbf{V}(\theta_s)_{sc}$ into Eq. (19), we may express the power passed by a linear polarizer at ±45° in terms of the Stokes matrix elements as

$$I_{\pm}(\theta_s) = (1/2)[S_{11}(\theta_s) \pm S_{33}(\theta_s)]. \tag{35}$$

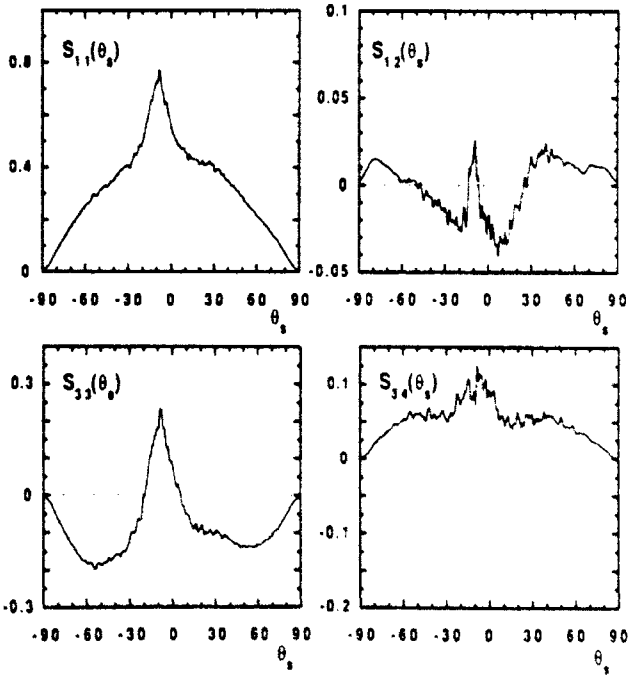

Fig. 5. The four unique elements of the Stokes matrix, $S_{11}(\theta_s)$, $S_{12}(\theta_s)$, $S_{33}(\theta_s)$, and $S_{34}(\theta_s)$, for the same parameters as in Fig. 4 but with $\theta_0 = 10°$.

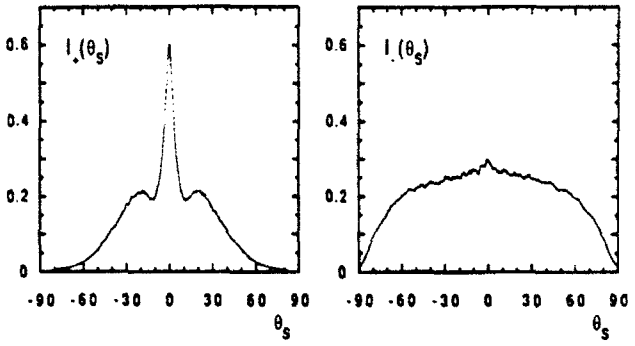

Fig. 6. Scattered powers $I_+(\theta_s)$ and $I_-(\theta_s)$ for a +45° linearly polarized field incident at normal incidence upon a one-dimensional, perfectly conducting rough surface. $\delta/a = 0.6$, $L/g = 4$, $a/\lambda = 3$, $g/\lambda = 20$; $N_x = 600$, $N_p = 4000$.

These quantities are shown in Fig. 6 as calculated from the Stokes matrix elements of Fig. 2. $I_+(\theta_s)$ displays a strong enhanced backscattering peak with well-defined secondary maxima on both sides, while $I_-(\theta_s)$ has a small backscattering peak and a strong background. These observations have a physical interpretation that supports the multiple-scattering interpretation of enhanced backscattering[14] as occurring from the coherent interference of the retroreflected waves arising from pairs of time-reversed multiple-scattering paths. In the geometric optics limit, a wave linearly polarized at ±45° that is once reflected from the perfectly conducting surface escapes with polarization state ∓45°. Consequently, if we assume that the correlation of the scattering amplitudes resulting from multiple-scattering processes of different multiplicities is negligible, $I_-(\theta_s)$ is entirely due to scattering processes in which the incident wave is reflected an odd number of times, while the $I_+(\theta_s)$ is produced by processes including even numbers of reflections. Finally, one expects the multiple-scattering contributions to $I_\pm(\theta_s)$ to decrease in magnitude as the number of reflections increases. The strong enhanced backscattering present in $I_+(\theta_s)$ is thus presumably dominated by double-scattering processes, while the strong background present in $I_-(\theta_s)$ is due to single scattering, although the small amount of enhanced backscattering present in $I_-(\theta_s)$ is then due to triple scattering. It is also worth noting that the results displayed in Figs. 2 and 3 are similar to experimental measurements that were reported recently (see Fig. 4 of Ref. 6).

The Stokes vectors of Eq. (34) obtained from the Stokes matrix elements displayed in Figs. 2–5 can also be used to calculate the mean powers scattered into s-, p-, R-, and L-polarized states. Equivalently, we may consider the angular distributions of

$$S_{12}(\theta_s) = \tfrac{1}{2}[I_p(\theta_s) - I_s(\theta_s)], \tag{36}$$

$$S_{34}(\theta_s) = \tfrac{1}{2}[I_L(\theta_s) - I_R(\theta_s)]. \tag{37}$$

These Stokes matrix elements have complicated angular dependences, including peaks in the retroreflection direction and sign changes. In the case $a = \lambda$, for example, an incident beam in a +45° polarization state preferentially scatters into p-polarized states in the retroreflection direction and at high scattering angles, but at intermediate scattering angles the surface more efficiently scatters s-polarized light. For the same ratio a/λ, the scattered polarization state is left handed and elliptical at all scattering angles. In the case $a/\lambda = 3$, the light is also preferentially p polarized at high scattering angles and around the retroreflection direction, although over a larger range of scattering angles than in the case $a = \lambda$. Figures 2 and 3 also show that the handedness of the elliptically polarized scattered light changes in this case: it is left handed at high scattering angles and right handed at scattering angles close to the retroreflection direction.

To clarify the origin of these features we carried out calculations displaying the effect of multiple scattering on the matrix of Eq. (21). Methods based on the iteration of the Kirchhoff term in the integral equation of the second kind satisfied by the source functions of the scattered field may be used to demonstrate explicitly the role of multiple scattering. In particular, it may be shown[7,15,16] that the scattering amplitudes $r_p(\theta_s)$ and $r_s(\theta_s)$ may be written in the form of the series

$$r_\alpha(\theta_s) = r_\alpha^{(1)}(\theta_s) + r_\alpha^{(2)}(\theta_s) + r_\alpha^{(3)}(\theta_s) + \ldots, \qquad \alpha = p, s, \tag{38}$$

where $r_\alpha^{(n)}(\theta_s)$ $(n > 0)$ is the scattering amplitude computed from the contribution to the source function calculated through $(n-1)$ iterations of the surface integral equation derived from the extinction theorem for the α-polarized field. The scattering amplitude $r_\alpha^{(1)}(\theta_s)$ arises from the Kirchhoff approximation, and the nth term $r_\alpha^{(n)}(\theta_s)$ of the series is the contribution to the scattering amplitude $r_\alpha(\theta_s)$ that is due to n successive interactions of the field with the rough surface.

We show in Appendix A that there is a fundamental relationship between these two series for s and p polarizations. In particular, it is shown that

$$r_s^{(n)}(\theta_s) = (-1)^n r_p^{(n)}(\theta_s), \qquad n > 0, \tag{39}$$

so that the two series are composed of the same terms with only sign differences in terms of odd order. The matrix elements of Eqs. (22)–(25) may then be calculated in terms of $r_p^{(n)}(\theta_s)$, only with the results that

$$s_{11}(\theta_s) \equiv 2C\{|r_p^{(1)}(\theta_s)|^2 + |r_p^{(2)}(\theta_s)|^2 + |r_p^{(3)}(\theta_s)|^2 + 2\,\mathrm{Re}[r_p^{(1)}(\theta_s) r_p^{(3)*}(\theta_s)]\}, \tag{40}$$

$$s_{12}(\theta_s) \equiv 4C\{\mathrm{Re}[r_p^{(1)*}(\theta_s) r_p^{(2)}(\theta_s)] + \mathrm{Re}[r_p^{(2)}(\theta_s) r_p^{(3)*}(\theta_s)]\}, \tag{41}$$

$$s_{33}(\theta_s) \equiv 2C\{-|r_p^{(1)}(\theta_s)|^2 + |r_p^{(2)}(\theta_s)|^2 - |r_p^{(3)}(\theta_s)|^2 - 2\,\mathrm{Re}[r_p^{(1)}(\theta_s) r_p^{(3)*}(\theta_s)]\}, \tag{42}$$

$$s_{34}(\theta_s) \equiv 4C\{\mathrm{Im}[r_p^{(1)*}(\theta_s) r_p^{(2)}(\theta_s)] + \mathrm{Im}[r_p^{(2)}(\theta_s) r_p^{(3)*}(\theta_s)]\}, \tag{43}$$

where we have truncated series of Eq. (38) to include only the first three terms so that the multiple-scattering processes of multiplicities of at most three have all been included.

These results provide a direct physical interpretation of the exact calculations discussed above. For example, for an incident polarization state at +45°, we may again determine the power transmitted with a linear polarizer in the scattered field at ±45° from Eqs. (35) and relations (40)

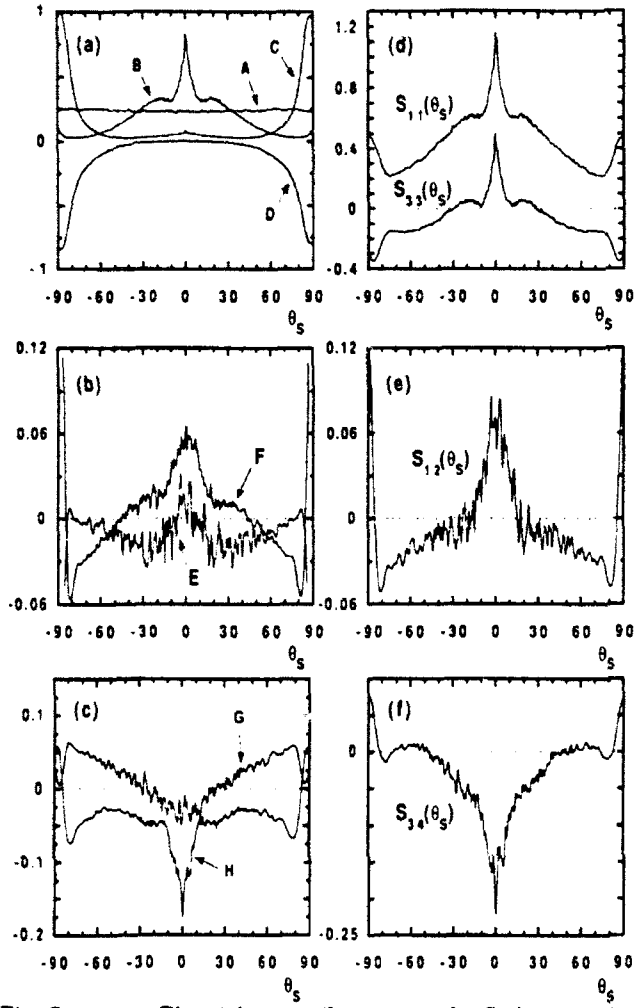

Fig. 7. (a)–(c) The eight contributions to the Stokes matrix elements computed with the single-, the double-, and the triple-scattering amplitudes for a one-dimensional, perfectly conducting rough surface at normal incidence. $\delta/a = 0.6$, $L/g = 4$, $a/\lambda = 3$, $g/\lambda = 20$; $N_s = 600$, $N_p = 4000$. **A**, $2C\langle|\Delta r_p^{(1)}(\theta_s)|^2\rangle$; **B**, $2C\langle|\Delta r_p^{(2)}(\theta_s)|^2\rangle$; **C**, $2C\langle|\Delta r_p^{(3)}(\theta_s)|^2\rangle$; **D**, $4C\Re e\langle\Delta r_p^{(1)}(\theta_s)\Delta r_p^{(3)*}(\theta_s)\rangle$; **E**, $4C\Re e\langle\Delta r_p^{(1)*}(\theta_s)\Delta r_p^{(2)}(\theta_s)\rangle$; **F**, $4C\Re e\langle\Delta r_p^{(2)}(\theta_s)\Delta r_p^{(3)*}(\theta_s)\rangle$; **G**, $4C\Im m\langle\Delta r_p^{(1)*}(\theta_s)\Delta r_p^{(2)}(\theta_s)\rangle$; **H**, $4C\Im m\langle\Delta r_p^{(2)}(\theta_s)\Delta r_p^{(3)*}(\theta_s)\rangle$.

and (42) as

$$I_-(\theta_s) \equiv 2C\{|r_p^{(1)}(\theta_s)|^2 + |r_p^{(3)}(\theta_s)|^2 + 2\,\Re e[r_p^{(1)}(\theta_s)r_p^{(3)*}(\theta_s)]\}, \quad (44)$$

$$I_+(\theta_s) \equiv 2C|r_p^{(2)}(\theta_s)|^2. \quad (45)$$

As was argued above, we observe that $I_-(\theta_s)$ contains the contributions that are due to paths including odd numbers of reflections, while processes containing even numbers of reflections contribute to $I_+(\theta_s)$. The off-diagonal elements of the Stokes matrix, however, contain only the cross terms between scattering amplitudes of scattering processes of different multiplicities.

The eight distinct terms contained in expressions (40)–(43), calculated from the incoherent part of the scattering amplitudes and averaged over an ensemble of $N_p = 4000$ surfaces with the same parameters as those used in Fig. 2, are shown in Figs. 7(a)–7(c). First, we may conclude that the first three terms of Eq. (38) all contribute significantly to the Stokes matrix. No enhanced backscattering peak is seen in the pure Kirchhoff approximation $2C\langle|\Delta r_p^{(1)}(\theta_s)|^2\rangle$, and most of the enhanced backscattering structure in the diagonal Stokes matrix elements arises from the term $2C\langle|\Delta r_p^{(2)}(\theta_s)|^2\rangle$, which describes pure double scattering. There is a small backscattering peak in the contributions from the pure triple-scattering processes $2C\langle|\Delta r_p^{(3)}(\theta_s)|^2\rangle$ to the diagonal elements of the matrix, as was seen in $I_-(\theta_s)$ in Fig. 5. The cross term $4C\,\Re e\langle\Delta r_p^{(1)}(\theta_s)\Delta r_p^{(3)*}(\theta_s)\rangle$ cancels part of the total power scattered at grazing scattering angles. The real and the imaginary parts of $4C\langle\Delta r_p^{(2)}(\theta_s)\Delta r_p^{(3)*}(\theta_s)\rangle$ are contributions to the off-diagonal elements that have well-defined peaks at $\theta_s = 0°$, but these peaks do not arise from the same origin as the backscattering peaks of the diagonal elements of the Stokes matrix.

The approximate Stokes matrix elements obtained by combining these results as described by expressions (40)–(43) are presented in Figs. 7(d)–7(f). Comparing the angular distribution of each of these elements with the distribution of the exact matrix element of Fig. 2, we observe that they differ simply by a scaling factor when $|\theta_s| < 70°$. Similar calculations performed with narrower beams were found to produce a better argeement between the exact and the approximate matrix elements. This behavior presumably results from the fact that the terms $2C|\Delta r_p^{(2)}(\theta_s)|^2$ and $2C|\Delta r_p^{(3)}(\theta_s)|^2$ are contributions to the scattered power diverging logarithmically with the surface length.[16] The inclusion of the contributions to the scattering amplitudes that are due to scattering processes of higher multiplicities cancels the contributions from scattering paths that are intercepted by the surface and restores unitarity. Similarly, the approximate matrix elements in Figs. 7(d)–7(f) will vanish at scattering angles $|\theta_s|$ close to 90° if all the scattering orders are included in the calculations. As was suggested in recent studies,[9,10] these multiple-scattering processes can be taken into account on average by including an incident and a scattering shadowing correction function in the Kirchhoff approximation for the scattered power and a propagation shadowing function in the calculation of the iterated source functions of Eq. (38). The calculations presented in Figs. 7(a)–7(d) were repeated with the use of a Gaussian propagation function $\exp[-(x_1 - x_1')^2/D^2]$ only, and the resulting matrix elements were found to be within 5% of the exact calculations for $D/a = 8$ and $|\theta_s| < 70°$. The significance of the propagation shadowing is also supported by the fact that the ratio of the total scattered power to the incident power is 1.167 in Fig. 7(d), while the inclusion of shadowing improves this to 1.093.

5. EXPERIMENTAL RESULTS

In this section we present experimental results to illustrate further the significance of the Stokes matrix elements and to make qualitative comparisons with the theoretical predictions of Section 3. Previous measurements with the surface discussed here at a different illumination wavelength have been reported[6]; however, for the wavelength used here the surface corresponds more closely to the perfectly conducting case.

The discussion of experimental procedures is brief; more detailed descriptions of the apparatus and procedures are available elsewhere.[6] Speckle-exposing tech-

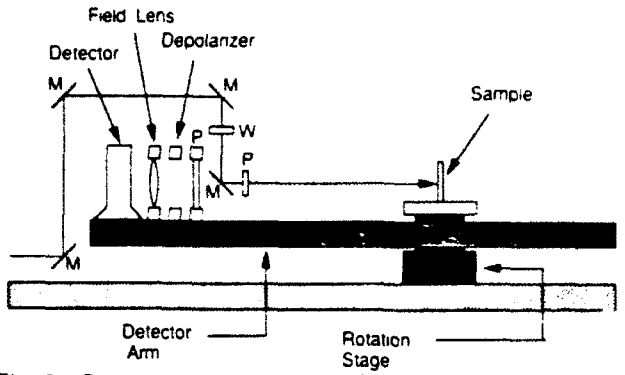

Fig. 8. Scattering instrument used in the measurements of rough surface scattering. The incident beam is brought over the detector by a series of mirrors and, after orientation of the polarization direction, is incident upon the rough surface. The detector arm may be moved out of the plane of the figure to measure the intensity at all the scattering angles. M denotes a mirror, P denotes a linear polarizer, and W denotes a half-wave plate.

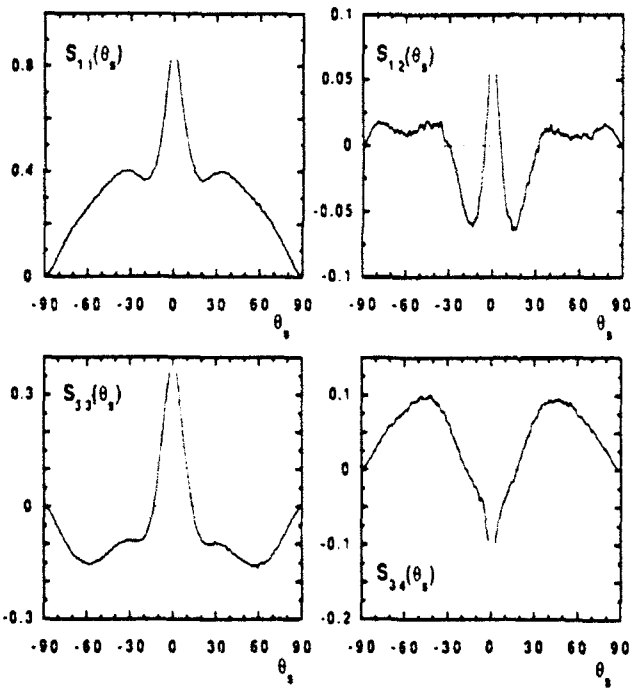

Fig. 9. Measured values of the four unique elements of the Stokes matrix. $S_{11}(\theta_s)$, $S_{12}(\theta_s)$, $S_{33}(\theta_s)$, and $S_{34}(\theta_s)$, for the one-dimensional surface at normal incidence.

niques[22] were employed to fabricate a rough surface in photoresist that was approximately one dimensional. This surface was then vacuum coated with gold, and subsequent scans with a surface profilometer revealed that it had nearly Gaussian statistics with standard deviation 1.95 μm and a Gaussian correlation function with 1/e width 3.57 μm.[6] The scattering properties of this surface were studied at the He–Ne laser wavelength λ = 3.392 μm. We then have δ/a = 0.55 and a = 1.05 λ, which is comparable to the case displayed in Figs. 4 and 5. We found that this surface did not produce a specular reflection; hence the Stokes matrix elements discussed below contain only incoherent contributions, as was found in Section 3. The real and the imaginary parts of the complex refractive index of gold at a nearby wavelength (3.351 μm) have been reported as n = 1.958 and k = 20.7, respectively.[23] The infrared wavelength was chosen in part because k is much larger than the values of common metals at visible wavelengths and thus is closer to the perfectly conducting case $k \to \infty$.

The geometry used in the scattering experiment is shown in Fig. 8. An incident beam illuminated a 20-mm-diameter area of the surface, and a photodiode InSb mounted upon an arm was scanned on an arc of radius 70 cm centered on the surface. The detector had a field lens of 24.0-mm diameter that served to reduce speckle noise, and in front of this lens was a quartz depolarizer.

The incident state was prepared in a +45° linearly polarized state by a titanium dioxide polarizer in the incident beam with extinction greater than 10^{-5}. This incident state was convenient because it produced the scattered Stokes vector of Eq. (34) containing all the unique Stokes matrix elements. The four scattered Stokes parameters were then measured with well-known procedures.[24] Specifically, a polarizer mounted in front of the detection unit determined the scattered powers passed with the transmission axis at 0° (p), 90° (s), +45° and −45°, and the first three Stokes parameters were determined from the appropriate sums and differences of these measurements. A quarter-wave plate was then mounted in front of the polarizer to produce sensitivity to right- and left-circular polarizations; the last Stokes parameter was found from the difference of these measurements. The data presented here were corrected only for losses in the quarter-wave plate; careful measurements revealed that any other corrections (such as for wave-plate retardation errors) were unnecessary.

The four unique Stokes matrix elements are shown in Fig. 9 for the case of normal incidence. First, the element $S_{11}(\theta_s)$ is the total scattered intensity for the +45° incident state; it clearly exhibits enhanced backscattering for angles roughly ±20° from the backscattering direction in the manner found in Fig. 4. The matrix element $S_{33}(\theta_s)$ is significantly positive in the backscattering region and then reaches a range of negative values; the general appearance as well as the height of maxima and minima is also similar to that in Fig. 4. The measurements also produce a small but experimentally significant curve for $S_{12}(\theta_s)$. In fact, the general form of the curve of $S_{12}(\theta_s)$ is strikingly similar to the theoretical results, although the scale of the experimental result is somewhat larger. The experimental result for $S_{34}(\theta_s)$ is negative for small θ_s, and then becomes positive for $|\theta_s|$ greater than approximately 17°, which is different from the theoretical result. Although it is not possible to determine the reason for this conclusively, the interpretation of $S_{34}(\theta_s)$ in previous work is dependent on the complex refractive index of real metals.[6] Hence this result for $S_{34}(\theta_s)$ may be a manifestation of the finite conductivity of gold at this wavelength; this is further suggested by the fact that, with the same surface, the magnitude of $S_{34}(\theta_s)$ was considerably larger for λ = 1.152 μm,[6] where the imaginary part of the refractive index of gold is less than one half of the value quoted above.[23]

It is also apparent that there are secondary maxima in the experimental result for $S_{11}(\theta_s)$ that are not present in the calculations. A related difference is also seen in

$S_{33}(\theta_s)$. Secondary maxima may be interpreted in terms of the fluctuations of multiple-scattering path lengths,[14] although it is not clear whether the differences are due to limitations in the theory or in the experiments.

Further results are presented in Figs. 10 and 11 for θ_0 = 10° and 30°, respectively. At θ_0 = 10°, there are similarities in $S_{11}(\theta_s)$ and $S_{34}(\theta_s)$ with the theoretical results of Fig. 5. There are still secondary maxima in these matrix elements that are strong in the measurements, the theory also shows a hint of secondary maximum to the right of the backscattering peak. Again $S_{12}(\theta_s)$ is of a form similar to that of the theory but is of larger magnitude, and $S_{34}(\theta_s)$ is quite different from the theoretical result. Lastly, the results for θ_0 = 30° indicate that the amount of backscattering structure present in $S_{11}(\theta_s)$ and $S_{12}(\theta_s)$ has reduced significantly, but otherwise all four matrix elements have remained significant.

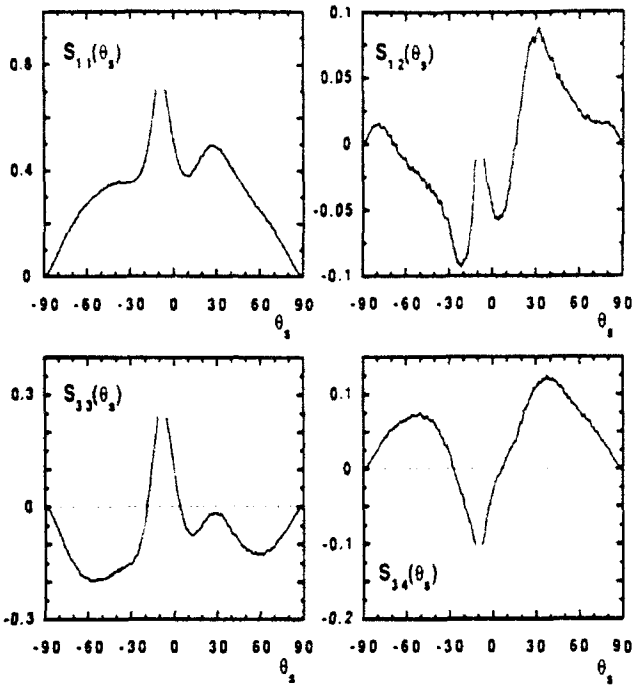

Fig. 10. Measured values of the four unique elements of the Stokes matrix, $S_{11}(\theta_s)$, $S_{12}(\theta_s)$, $S_{33}(\theta_s)$, and $S_{34}(\theta_s)$, for the one-dimensional surface; θ_0 = 10°.

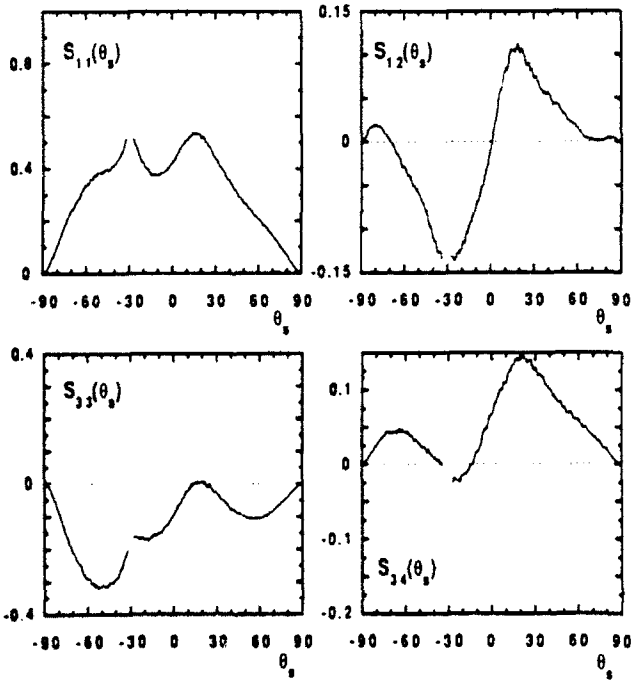

Fig. 11. Measured values of the four unique elements of the Stokes matrix, $S_{11}(\theta_s)$, $S_{12}(\theta_s)$, $S_{33}(\theta_s)$, and $S_{34}(\theta_s)$, for the one-dimensional surface; θ_0 = 30°.

We also note in passing that, for reasons discussed in more detail in Ref. 6, the data on any given figure are correctly scaled with respect to each other but that the vertical scale of each figure is chosen such that the total power contained in the *s*-scattering cross section $S_{11}(\theta_s) - S_{12}(\theta_s)$ is equal to unity. We may then determine the relative total powers contained in the *p* cross section $S_{11}(\theta_s) + S_{12}(\theta_s)$, which follow from the experimental results as 0.991, 0.991, and 0.959 for θ_0 = 0°, 10°, and 30°, respectively. These values are much closer to unity than those reported at a shorter wavelength and are close to the behavior of a perfect conductor.

6. CONCLUSIONS

We have presented results for the elements of the Stokes matrix of a one-dimensional, perfectly conducting rough surface calculated from an exact expression for the scattered field. The four unique elements of the Stokes matrix were found to be significant for a surface profile assumed to be a stationary, Gaussian stochastic process characterized by a Gaussian correlation function. In all the cases considered, the surface parameters and the incident wavelength were chosen such that enhanced backscattering was predicted in the two unique diagonal elements. The off-diagonal elements have complicated angular dependences, including extrema and sign changes. With the use of a method based on the iteration of the Kirchhoff approximation in the equations for the source functions, we showed that each term containing multiple-scattering amplitudes of even multiplicities contributes to the sum of the diagonal elements of the Stokes matrix, while each term containing multiple-scattering amplitudes of odd multiplicities contributes to their difference. The off-diagonal elements were shown to contain only contributions from cross terms between the scattering amplitudes of different multiplicities. In particular, for the surfaces considered here, enhanced backscattering is due mostly to pure double-scattering processes, as was apparent from the numerical calculations of each contribution to the diagonal elements. Similar calculations for the off-diagonal elements showed that the cross terms between single and double scattering and between double and triple scattering are the main contributions to these elements.

The experimental results with a characterized rough surface showed that the four distinct Stokes matrix elements were all significant. The results were largely similar to the theoretical results, although it was suggested that differences in one of the matrix elements could be attributed to the finite conductivity of the surface.

APPENDIX A: KIRCHHOFF ITERATES FOR DIRICHLET AND NEUMANN BOUNDARY CONDITIONS

In this appendix we derive the relationship [Eq. (39) of Section 4] between the scattering amplitudes computed through n iterations of the Kirchhoff approximation for s and p polarizations. We present this in the broader context of the scattering of scalar waves for Neumann and Dirichlet boundary conditions. For the one-dimensional surfaces of the present work these are equivalent to the s- and the p-polarized scattering problems, respectively.

A general result is established that relates the scattered fields computed from the source functions obtained through an iteration of the surface integral equation derived from the Helmoltz integral formula with Neumann and Dirichlet boundary conditions.[15,16] The physical system and the coordinate axes considered here are identical to the one described in Section 2, but we derive the results for the general case in which ζ depends on both x_1 and x_2. It is assumed that an incident scalar field $\psi(x_1, x_2, x_3 | \omega)_{\text{inc}}$ illuminates a finite section of the x_1x_2 plane. In the region $x_3 > \zeta(x_1, x_2)$, the scalar field $\psi(x_1, x_2, x_3 | \omega)$ is a solution of the Helmoltz equation

$$\left(\frac{\partial^2}{\partial x_1^2} + \frac{\partial^2}{\partial x_2^2} + \frac{\partial^2}{\partial x_3^2} + \frac{\omega^2}{c^2}\right)\psi(x_1, x_2, x_3 | \omega) = 0, \tag{A1}$$

where c is the velocity of the field and the time-dependent factor $\exp(-i\omega t)$ is omitted. Two boundary conditions are considered: the Dirichlet boundary condition

$$\psi_D(x_1, x_2, x_3 | \omega)|_{x_3 = \zeta(x_1, x_2)} = 0 \tag{A2}$$

and the Neumann boundary condition

$$\frac{\partial}{\partial n}\psi_N(x_1, x_2, x_3 | \omega)|_{x_3 = \zeta(x_1, x_2)} = 0, \tag{A3}$$

where

$$\frac{\partial}{\partial n} = \left\{1 + \left[\frac{\partial \zeta(x_1, x_2)}{\partial x_1}\right]^2 + \left[\frac{\partial \zeta(x_1, x_2)}{\partial x_2}\right]^2\right\}^{-1/2} \times \left[-\frac{\partial \zeta(x_1, x_2)}{\partial x_1}\frac{\partial}{\partial x_1} - \frac{\partial \zeta(x_1, x_2)}{\partial x_2}\frac{\partial}{\partial x_2} + \frac{\partial}{\partial x_3}\right] \tag{A4}$$

is the derivative along the normal to this interface at each point, directed from the perfect conductor to the vacuum. We also impose the condition that $\psi(x_1, x_2, x_3 | \omega)$ at $x_3 \to \infty$ consist of an incoming field and outgoing waves. The Green's function $G(x_1, x_2, x_3 | x_1', x_2', x_3')$ is a solution of

$$\left(\frac{\partial^2}{\partial x_1^2} + \frac{\partial^2}{\partial x_2^2} + \frac{\partial^2}{\partial x_3^2} + \frac{\omega^2}{c^2}\right)G(x_1, x_2, x_3 | x_1', x_2', x_3') = -4\pi\delta(x_1 - x_1')\delta(x_2 - x_2')\delta(x_3 - x_3') \tag{A5}$$

and satisfies an outgoing-wave boundary condition at $|\mathbf{x} - \mathbf{x}'| \to \infty$.

Applying Green's second integral theorem to a volume bounded by the rough surface and a hemispherical volume of infinite radius in the vacuum and imposing both kinds of boundary conditions, we may obtain two different extinction theorems. In the case of the Dirichlet boundary condition we have that

$$\Theta[x_3 - \zeta(\mathbf{X})]\psi_D(\mathbf{x}\ \omega) = \psi(\mathbf{x}\ \omega)_{\text{inc}} - \frac{1}{4\pi}\int_S ds' G(\mathbf{x}\ \mathbf{x}')\frac{\partial \psi_D(\mathbf{x}'\ \omega)}{\partial n'}, \tag{A6}$$

where $\Theta(x)$ is the Heaviside step function, $\mathbf{x}$ is the vector (x_1, x_2, x_3), $\mathbf{X}$ is the vector $(x_1, x_2, 0)$ and $\mathbf{x}'$ is the vector $[x_1', x_2', \zeta(x_1', x_2')]$ belonging to the reflecting surface. In what follows the primed coordinates ($\mathbf{x}'$ and $\mathbf{x}''$) are always assigned to vectors residing on the surface. In Eq. (A6) the source function $\partial\psi_D(\mathbf{x}'\ \omega)/\partial n'$ is the normal derivative of the total field evaluated at the surface. In the case of the Neumann boundary condition the extinction theorem is given by

$$\Theta[x_3 - \zeta(\mathbf{X})]\psi_N(\mathbf{x}\ \omega) = \psi(\mathbf{x}\ \omega)_{\text{inc}} + \frac{1}{4\pi}\int_S ds' \frac{\partial G(\mathbf{x}\ \mathbf{x}')}{\partial n'}\psi_N(\mathbf{x}'\ \omega). \tag{A7}$$

where the source function $\psi_N(\mathbf{x}'\ \omega)$ is the total field evaluated at the surface. The scattered field is determined by obtaining a surface integral equation for the source function for either boundary condition. To compute the source function $\psi_N(\mathbf{x}'\ \omega)$ we successively set $x_3 = \zeta(\mathbf{X}) + \epsilon$ ($\epsilon > 0$) and $x_3 = \zeta(\mathbf{X}) - \epsilon$ in Eq. (A7) and add the resulting equations; in the limit of $\epsilon \to 0^+$, there results

$$\psi_N(\mathbf{x}'\ \omega) = 2\psi(\mathbf{x}'\ \omega)_{\text{inc}} + \frac{2P}{4\pi}\int_S ds'' \frac{\partial G(\mathbf{x}'\ \mathbf{x}'')}{\partial n''}\psi_N(\mathbf{x}''\ \omega), \tag{A8}$$

in which it is understood that only the principal part (P) of the integral is kept. Similarly, if we set $x_3 = \zeta(\mathbf{X}) + \epsilon$ and $x_3 = \zeta(\mathbf{X}) - \epsilon$ in Eq. (A6) and add the normal derivatives of the resulting equations, the integral equation

$$\frac{\partial \psi_D(\mathbf{x}'\ \omega)}{\partial n'} = 2\frac{\partial \psi(\mathbf{x}'\ \omega)_{\text{inc}}}{\partial n'} - \frac{2P}{4\pi}\int_S ds'' \frac{\partial G(\mathbf{x}'\ \mathbf{x}'')}{\partial n'}\frac{\partial \psi_D(\mathbf{x}''\ \omega)}{\partial n''} \tag{A9}$$

for the source function $\partial\psi_D(\mathbf{x}'\ \omega)/\partial n'$ is obtained in the limit $\epsilon \to 0^+$.

Equations (A8) and (A9) are Fredholm integral equations of the second kind, and we write the solutions as Neumann–Liouville series as

$$\frac{\partial \psi_D(\mathbf{x}'\ \omega)}{\partial n'} = D^{(1)}(\mathbf{x}'\ \omega) + D^{(2)}(\mathbf{x}'\ \omega) + D^{(3)}(\mathbf{x}'\ \omega) + \cdots, \tag{A10}$$

where

$$D^{(1)}(\mathbf{x}'\ \omega) = 2\frac{\partial \psi(\mathbf{x}'\ \omega)_{\text{inc}}}{\partial n'}, \tag{A11}$$

$$D^{(m)}(\mathbf{x}'\ \omega) = -\frac{2P}{4\pi}\int_S ds'' \frac{\partial G(\mathbf{x}'\ \mathbf{x}'')}{\partial n'}D^{(m-1)}(\mathbf{x}''\ \omega), \quad m > 1; \tag{A12}$$

$$\psi_N(\mathbf{x}'\ \omega) = N^{(1)}(\mathbf{x}'\ \omega) + N^{(2)}(\mathbf{x}'\ \omega) + N^{(3)}(\mathbf{x}'\ \omega) + \cdots, \tag{A13}$$

where

$$N^{(1)}(\mathbf{x}' \mid \omega) = 2\psi(\mathbf{x}' \mid \omega)_{\text{inc}}, \tag{A14}$$

$$N^{(m)}(\mathbf{x}' \mid \omega) = \frac{2P}{4\pi} \int_S ds'' \frac{\partial G(\mathbf{x}' \mid \mathbf{x}'')}{\partial n''} N^{(m-1)}(\mathbf{x}'' \mid \omega), \qquad m > 1. \tag{A15}$$

When Eqs. (A10) and (A13) are substituted into Eqs. (A6) and (A7), respectively, the scattered fields may be expressed as the infinite sums

$$\psi_D(\mathbf{x} \mid \omega)_{\text{sc}} = \psi_D^{(1)}(\mathbf{x} \mid \omega)_{\text{sc}} + \psi_D^{(2)}(\mathbf{x} \mid \omega)_{\text{sc}} + \psi_D^{(3)}(\mathbf{x} \mid \omega)_{\text{sc}} + \ldots, \tag{A16}$$

where

$$\psi_D^{(m)}(\mathbf{x} \mid \omega)_{\text{sc}} = -\frac{1}{4\pi} \int_S ds' G(\mathbf{x} \mid \mathbf{x}') D(m)(\mathbf{x}' \mid \omega), \qquad m > 0; \tag{A17}$$

$$\psi_N(\mathbf{x} \mid \omega)_{\text{sc}} = \psi_N^{(1)}(\mathbf{x} \mid \omega)_{\text{sc}} + \psi_N^{(2)}(\mathbf{x} \mid \omega)_{\text{sc}} + \psi_N^{(3)}(\mathbf{x} \mid \omega)_{\text{sc}} + \ldots, \tag{A18}$$

where

$$\psi_N^{(m)}(\mathbf{x} \mid \omega)_{\text{sc}} = \frac{1}{4\pi} \int_S ds' \frac{\partial G(\mathbf{x} \mid \mathbf{x}')}{\partial n'} N^{(m)}(\mathbf{x}' \mid \omega), \qquad m > 0. \tag{A19}$$

Truncating the series of Eqs. (A16) and (A18) after the first term leads to the Kirchhoff approximation for the scattered fields in which only the single-scattering processes are taken into account. The term $\psi^{(m)}(\mathbf{x} \mid \omega)_{\text{sc}}$ describes the contribution to the scattered field that is due to the source function generated by m successive interactions of the scattered field with the surface. To support this physical interpretation, we rewrite Eqs. (A12) and (A15), respectively, as

$$D^{(m)}(\mathbf{x}' \mid \omega) = 2\frac{\partial \psi_D^{(m-1)}(\mathbf{x}' \mid \omega)_{\text{sc}}}{n'} - D^{(m-1)}(\mathbf{x}' \mid \omega), \tag{A20}$$

$$N^{(m)}(\mathbf{x}' \mid \omega) = 2\psi_D^{(m-1)}(\mathbf{x}' \mid \omega)_{\text{sc}} - N^{(m-1)}(\mathbf{x}' \mid \omega), \tag{A21}$$

by adding and subtracting the contribution to the integrals arising from the singularity of the kernels. These equations indicate that, for either boundary condition, the source function describing the mth-order scattering processes is identical to the source function computed in the Kirchhoff approximation from the field scattered $(m-1)$ times by the surface before being incident upon the surface, from which we must subtract the source function describing the $(m-1)$th-order scattering processes.

We now show that

$$\psi_D^{(m)}(\mathbf{x} \mid \omega)_{\text{sc}} = (-1)^m \psi_N^{(m)}(\mathbf{x} \mid \omega)_{\text{sc}}. \tag{A22}$$

The scattered fields computed within the Kirchhoff approximation $(m = 1)$ are

$$\psi_D^{(1)}(\mathbf{x} \mid \omega)_{\text{sc}} = -\frac{1}{4\pi} \int_S ds' G(\mathbf{x} \mid \mathbf{x}') 2\frac{\partial \psi(\mathbf{x}' \mid \omega)_{\text{inc}}}{\partial n'}, \tag{A23}$$

$$\psi_N^{(1)}(\mathbf{x} \mid \omega)_{\text{sc}} = \frac{1}{4\pi} \int_S ds' \frac{\partial G(\mathbf{x} \mid \mathbf{x}')}{\partial n'} 2\psi(\mathbf{x}' \mid \omega)_{\text{inc}}. \tag{A24}$$

The sum of these fields is then

$$\psi_D^{(1)}(\mathbf{x} \mid \omega)_{\text{sc}} + \psi_N^{(1)}(\mathbf{x} \mid \omega)_{\text{sc}} = \frac{-2}{4\pi} \int_S ds' \left[G(\mathbf{x} \mid \mathbf{x}') \frac{\partial \psi(\mathbf{x}' \mid \omega)_{\text{inc}}}{\partial n'} - \frac{\partial G(\mathbf{x} \mid \mathbf{x}')}{\partial n'} \psi(\mathbf{x}' \mid \omega)_{\text{inc}} \right]. \tag{A25}$$

Applying Green's second integral theorem to $\psi(\mathbf{x} \mid \omega)_{\text{sc}}$ and $G(\mathbf{x} \mid \mathbf{x}')$ in a volume bounded by the rough surface and a hemispherical surface of infinite radius in the upper half-space and using the radiation condition satisfied by the Green's function, we conclude that the integral in Eq. (A25) vanishes and that there is only a sign difference between the scattered fields computed within the Kirchhoff approximation for the Dirichlet and the Neumann boundary conditions. This simple result is well known.[24]

Assuming that Eq. (A22) holds for $(m-1)$ $(m > 1)$, we compute the contribution to the scattered field that is due to the mth-order scattering processes as

$$\psi_D^{(m)}(\mathbf{x} \mid \omega)_{\text{sc}} = -\frac{2}{4\pi} \int_S ds' G(\mathbf{x} \mid \mathbf{x}') \frac{\partial \psi_D^{(m-1)}(\mathbf{x}' \mid \omega)_{\text{sc}}}{\partial n'} - \psi_D^{(m-1)}(\mathbf{x} \mid \omega)_{\text{sc}}, \tag{A26}$$

$$\psi_N^{(m)}(\mathbf{x} \mid \omega)_{\text{sc}} = \frac{2}{4\pi} \int_S ds' \frac{\partial G(\mathbf{x} \mid \mathbf{x}')}{\partial n'} \psi_N^{(m-1)}(\mathbf{x}' \mid \omega)_{\text{sc}} - \psi_N^{(m-1)}(\mathbf{x} \mid \omega)_{\text{sc}}, \tag{A27}$$

where Eqs. (A20) and (A21) were substituted for the source functions in Eqs. (A17) and (A19). Using Eqs. (A26) and (A27) and the assumption of Eq. (A22) for $(m-1)$, we obtain

$$\psi_D^{(m)}(\mathbf{x} \mid \omega)_{\text{sc}} - (-1)^m \psi_N^{(m)}(\mathbf{x} \mid \omega)_{\text{sc}} = \frac{-2}{4\pi} \int_S ds' \times \left[G(\mathbf{x} \mid \mathbf{x}') \frac{\partial \psi_D^{(m-1)}(\mathbf{x}' \mid \omega)_{\text{sc}}}{\partial n'} - \frac{\partial G(\mathbf{x} \mid \mathbf{x}')}{\partial n'} \psi_D^{(m-1)}(\mathbf{x}' \mid \omega)_{\text{sc}} \right] - 2\psi_D^{(m-1)}(\mathbf{x} \mid \omega)_{\text{sc}}. \tag{A28}$$

Using Green's second integral theorem and the radiation condition on the functions $\psi_D^{(m-1)}(\mathbf{x} \mid \omega)_{\text{sc}}$ and $G(\mathbf{x} \mid \mathbf{x}')$, we see that the right-hand side of Eq. (A28) vanishes; thus the identity

$$\psi_D^{(m)}(\mathbf{x} \mid \omega)_{\text{sc}} = (-1)^m \psi_N^{(m)}(\mathbf{x} \mid \omega)_{\text{sc}} \tag{A29}$$

has been established for any scattering order m.

When the incident field and the surface profile are invariant under translation along a direction (x_2) of the mean surface, we apply Green's second integral theorem to a modified volume, and Eq. (A29) becomes

$\psi_D^{(m)}(x_2, x_1; \omega)_{\epsilon} = (-1)^m \psi_A^{(m)}(x_1, x_2; \omega)_{\epsilon}$. This result, applied in the far-field region to the angular spectra of scattered plane waves $r_p(\theta_s)$ and $r_s(\theta_s)$, is Eq. (39).

ACKNOWLEDGMENT

This research was supported by the U.S. Army Research Office.

REFERENCES

1. E. R. Méndez and K. A. O'Donnell, "Observation of depolarization and backscattering enhancement in light scattering from Gaussian random surfaces," Opt. Commun. **61**, 91–95 (1987).
2. K. A. O'Donnell and E. R. Méndez, "Experimental study of scattering from characterized random surfaces," J. Opt. Soc. Am. A **4**, 1194–1205 (1987).
3. M.-J. Kim, J. C. Dainty, A. T. Friberg, and A. J. Sant, "Experimental study of enhanced backscattering from one- and two-dimensional surfaces," J. Opt. Soc. Am. A **7**, 569–577 (1990).
4. A. J. Sant, J. C. Dainty, and M.-J. Kim, "Comparison of surface scattering between identical, randomly rough metal and dielectric diffusers," Opt. Lett. **14**, 1183–1185 (1989).
5. M. E. Knotts and K. A. O'Donnell, "Anomalous scattering from a perturbed grating," Opt. Lett. **15**, 1485–1487 (1990).
6. K. A. O'Donnell and M. E. Knotts, "The polarization dependence of scattering from one-dimensional rough surfaces," J. Opt. Soc. Am. A **8**, 1126–1131 (1991).
7. A. A. Maradudin, T. Michel, A. R. McGurn, and E. R. Méndez, "Enhanced backscattering of light from a random grating," Ann. Phys. **203**, 255–307 (1990).
8. Y.-Q. Jin and M. Lax, "Backscattering enhancement from a randomly rough surface," Phys. Rev. B **42**, 9819–9829 (1990).
9. A. Ishimaru and J. S. Chen, "Scattering from very rough metallic and dielectric surfaces: a theory based on the modified Kirchhoff approximation," Waves Random Media **1**, 21–34 (1991).
10. J. S. Chen and A. Ishimaru, "Numerical simulation of the second-order Kirchhoff approximation from very rough surfaces and a study of backscattering enhancement," J. Acoust. Soc. Am. **88**, 1846–1850 (1990).
11. M. Nieto-Vesperinas and J. M. Soto-Crespo, "Monte-Carlo simulations for scattering of electromagnetic waves from perfectly conductive random rough surfaces," Opt. Lett. **12**, 979–981 (1987).
12. J. M. Soto-Crespo and M. Nieto-Vesperinas, "Electromagnetic scattering from very rough random surfaces and deep reflection gratings," J. Opt. Soc. Am. A **6**, 367–384 (1989).
13. A. A. Maradudin, E. R. Méndez, and T. Michel, "Backscattering effects in the elastic scattering of *p*-polarized light from a large-amplitude random metallic grating," Opt. Lett. **14**, 151–153 (1989).
14. A. A. Maradudin, E. R. Méndez, and T. Michel, "Backscattering effects in the elastic scattering of *p*-polarized light from a large-amplitude random grating," in *Scattering in Volumes and Surfaces*, M. Nieto-Vesperinas and J. C. Dainty, eds. (North-Holland, Amsterdam, 1990), pp. 157–174.
15. W. C. Meecham, "On the use of the Kirchhoff approximation for the solution of reflection problems," J. Rat. Mech. Anal. **5**, 323–333 (1956).
16. E. G. Liszka and J. J. McCoy, "Scattering at a rough boundary—extension of the Kirchhoff approximation," J. Acoust. Soc. Am. **71**, 1093–1100 (1982).
17. E. Hecht, "Note on an operational definition of the Stokes parameters," Am. J. Phys. **38**, 1156–1158 (1970).
18. J. D. Jackson, *Classical Electrodynamics* (Wiley, New York, 1975), pp. 269–278.
19. M. Born and E. Wolf, *Principles of Optics*, 6th ed. (Pergamon, New York, 1980), p. 554.
20. H. C. van de Hulst, *Light Scattering by Small Particles* (Dover, New York, 1981).
21. E. I. Thorsos, "The validity of the Kirchhoff approximation for rough surface scattering using a Gaussian roughness spectrum," J. Acoust. Soc. Am. **83**, 78–92 (1988).
22. P. F. Gray, "A method of forming optical diffusers of simple known statistical properties," Opt. Acta **25**, 765–775 (1978).
23. E. D. Palik, ed., *Handbook of Optical Constants of Solids* (Academic, New York, 1985).
24. P. Beckmann and A. Spizzichino, *The Scattering of Electromagnetic Waves from Rough Surfaces* (Pergamon, New York, 1963), p. 24.

Angular correlation functions of amplitudes scattered from a one-dimensional, perfectly conducting rough surface

T. R. Michel and K. A. O'Donnell

School of Physics and Center for Optical Science and Engineering, Georgia Institute of Technology, Atlanta, Georgia 30332-0430

Received August 23, 1991; revised manuscript received February 3, 1992; accepted March 4, 1992

We study theoretically the angular dependence of the correlation functions of the scattering amplitudes occurring in the interaction of a beam of polarized light with a one-dimensional, perfectly conducting rough surface. For an ensemble of surface-profile functions that are realizations of a stationary stochastic process, a necessary condition for the exact scattering amplitudes to be correlated is established: the projection on the mean surface of the difference between the incident wave vectors must equal that of the scattered wave vectors. The exact expressions for the amplitudes of the scattered plane waves constituting the far field are derived from Green's second integral theorem. By numerical simulations, the dependence of these amplitude correlation functions on the angle of incidence and on the incident and the scattered polarization states is computed for Gaussian surfaces producing enhanced backscattering. Results are presented for the complex correlation functions of p- and s-polarized scattering amplitudes. However, it is argued that, for an incident field polarized at $+45°$, the single- and the multiple-scattering contributions to the amplitude correlation functions are clearly separated if the scattered field is resolved into $-45°$ and $+45°$ polarized plane waves. In this case the real part of the correlation function of the $-45°$ scattering amplitudes displays two peaks of large angular width. The maxima occur for angles of incidence at which the correlation between the $+45°$-polarized scattering amplitudes has sharp peaks of angular width approximately equal to λ/a, where the surface correlation length a may be interpreted as an estimate for the mean distance between successive scattering points on the surface. One of these maxima occurs when the correlated amplitudes are identical, and the other occurs when the role of the incoming and the outgoing directions is interchanged between the two scattering amplitudes, which are then related by the reciprocity condition. The coherent addition of the amplitudes arising from multiple-scattering processes and those of their time-reversed partners in directions close to the retroreflection direction is demonstrated in the calculations of the correlation functions.

1. INTRODUCTION

The consequences of multiple scattering in the interaction of waves with randomly rough surfaces have been of recent interest. The scattering of a beam of light from surfaces with strong surface slopes and height fluctuations comparable with the wavelength has been shown to exhibit enhanced backscattering.[1-6] Theoretical studies[7-10] have suggested that this enhancement results from the constructive interference of a multiple-scattering path with its time-reversed partner in directions close to the retroreflection direction where these two paths are correlated. The central quantities in these investigations have been the second moments of the scattered amplitudes, which may be introduced as the Stokes matrix elements of the scatterer.[6,11]

However, the existence of general correlations between scattering amplitudes for different incident and scattering angles has not to our knowledge been investigated, at least for randomly rough surfaces producing multiple scattering. Previous studies[12-15] considered the correlation of scattering amplitudes produced by two angularly displaced beams incident upon a randomly rough surface when single scattering dominates. The Kirchhoff approximation has been used in the case of the scattering from a one-dimensional rough surface on a perfect conductor to determine the condition involving the angles of incidence and of scattering for which correlations exist between scattering amplitudes. An analytic expression for this correlation function was derived by Pedersen[12] and by Léger *et al.*,[13,14] who also presented experimental measurements of this quantity in the case of scattering from two-dimensional, rough metal surfaces.

The correlations between scattering amplitudes were also considered more recently by Feng *et al.*[16] for the case of the transmission of waves through a disordered medium. One of the predicted correlations between transmitted amplitudes occurs if the incident and the scattering angles are related in a similar manner, as in the work of Léger *et al.* However, multiple scattering is accounted for in the mathematical treatment of Feng *et al.* through the use of a diffusion approximation. This correlation between multiply scattered waves, termed the memory effect, has also been investigated experimentally.[17] The effect was then predicted[18,19] and observed[20] in the reflection of waves from disordered media. Later, the introduction of time-reversal symmetry in the theory led to the prediction[21] of two distinct peaks in the amplitude correlation function of waves reflected from random media. The influence of the vector nature of optical waves on the amplitude correlation function for light transmitted or reflected by random media has also been studied.[22]

In this paper we study the angular correlation function of the scattering amplitudes in the interaction of a beam of polarized light with the one-dimensional, randomly rough surface of a perfect conductor. Previous investigations of these amplitude correlation functions[12-14] used a single-scattering approximation. In this study, however,

0740-3232/92/081374-11$05.00

exact scattering amplitudes are considered, and the correlations between the scattering amplitudes owing to multiple interactions are studied. Because polarization plays a significant role in the scattering from such surfaces,[6-11] the scattering amplitudes considered are generalized to include any incident and scattered polarization states. An exact expression for these amplitudes derived from Green's second integral theorem is used to find a necessary condition for these amplitudes to be correlated when the statistics of the rough surface are stationary. The exact formulation of the scattering problem is then used to determine by numerical simulations the dependence of the amplitude correlation function on the angle of incidence for various incident and scattered polarization states. Results are presented for surfaces assumed to be realizations of a stationary, Gaussian stochastic process with a Gaussian correlation function. The role of multiple scattering is analyzed by considering the correlations between polarized amplitudes that have been shown[11] to contain no contributions from pure single-scattering processes. Finally, we consider the physical significance of the amplitude correlation function, and its relationship to enhanced backscattering is discussed.

2. AMPLITUDE CORRELATION FUNCTIONS FOR ROUGH SURFACE SCATTERING

We first consider the polarization dependence of the scattered field; a more comprehensive discussion may be found in Ref. 11. The general conditions for the existence of correlations between scattering amplitudes are studied at the end of this section.

Consider the situation in which the half-space $x_3 < \zeta(x_1)$ is filled with a perfect conductor and is separated from the vacuum above it by a randomly rough surface of equation $x_3 = \zeta(x_1)$. The stochastic surface-profile function $\zeta(x_1)$ is assumed to be a stationary, zero-mean process having derivatives of arbitrary order. Further, the surface profile is one dimensional in the sense that ζ is independent of x_2.

A polarized light beam whose plane of incidence is the plane x_1x_3 perpendicular to the grooves of the surface illuminates the perfect conductor from the vacuum side. Such a beam may be expressed by a Gaussian angular spectrum of incoming plane waves and may be written as

$$\mathbf{E}(x_1, x_3 | \omega)_{\text{inc}} = \frac{\omega w}{2\sqrt{\pi}c} \int_{-\pi/2}^{\pi/2} d\theta \exp\left[-\left(\frac{\omega w}{2c}\right)^2 (\theta - \theta_i)^2\right] \times [E_p \hat{e}_p(\theta)_{\text{inc}} + E_s \hat{e}_s(\theta)_{\text{inc}}] \times \exp\left[i\frac{\omega}{c}(x_1 \sin\theta - x_3 \cos\theta)\right], \quad |\theta_i| < \frac{\pi}{2}, \tag{1}$$

where

$$\hat{e}_s(\theta)_{\text{inc}} = \hat{x}_2, \tag{2}$$

$$\hat{e}_p(\theta)_{\text{inc}} = -\hat{x}_1 \cos\theta - \hat{x}_3 \sin\theta, \tag{3}$$

c is the speed of light, and the time dependency $\exp(-i\omega t)$ is omitted. In the limit of $\omega w/2c \gg 1$, Eq. (1) describes a Gaussian beam propagating in the direction $(\hat{x}_1 \sin\theta_i - \hat{x}_3 \cos\theta_i)$ with transverse width $2w$ at the coordinate origin. The unit vector $\hat{e}_p(\theta)_{\text{inc}}$ $[\hat{e}_s(\theta)_{\text{inc}}]$ is in the direction of the electric field of a p- (s-) polarized plane wave with unit wave vector $(\hat{x}_1 \sin\theta - \hat{x}_3 \cos\theta)$. The complex amplitudes E_p and E_s determine the incident polarization state.

The scattered field may be determined by considering the incident field to be the sum of the p- and the s-polarized fields. It is well known[7] that the scattering of a p- (s-) polarized incident beam from a one-dimensional surface reduces to the scattering of a scalar field satisfying a Neumann (Dirichlet) boundary condition at the rough surface. Exact expressions derived from Green's second integral theorem may be used to calculate the scattered fields numerically. The p- and the s-polarized scattering amplitudes $r_p(\theta_s)$ and $r_s(\theta_s)$ (Ref. 7) that may then be obtained as solutions determine an exact expression for the scattered electric field in the far-field region $x_3 \to \infty$ as

$$\mathbf{E}(x_1, x_3 | \omega)_{\text{sc}} = \frac{i}{4\pi} \times \int_{-\pi/2}^{\pi/2} d\theta_s [E_p r_p(\theta_s) \hat{e}_p(\theta_s)_{\text{sc}} + E_s r_s(\theta_s) \hat{e}_s(\theta_s)_{\text{sc}}] \times \exp\left[i\frac{\omega}{c}(x_1 \sin\theta_s + x_3 \cos\theta_s)\right], \tag{4}$$

where

$$\hat{e}_s(\theta_s)_{\text{sc}} = \hat{x}_2, \tag{5}$$

$$\hat{e}_p(\theta_s)_{\text{sc}} = \hat{x}_1 \cos\theta_s - \hat{x}_3 \sin\theta_s. \tag{6}$$

The unit vector $\hat{e}_p(\theta_s)_{\text{sc}}$ $[\hat{e}_s(\theta_s)_{\text{sc}}]$ defines the direction of the electric-field vector of a p- (s-) polarized plane wave scattered in the direction $(\sin\theta_s \hat{x}_1 + \cos\theta_s \hat{x}_3)$.

Incident and scattered plane waves of arbitrary polarizations may be described if the following pairs of orthonormal vectors are introduced. These unit vectors[3] determine the linearly polarized states at $\pm 45°$ as

$$\hat{e}_+ = \frac{1}{\sqrt{2}}(\hat{e}_p + \hat{e}_s), \tag{7}$$

$$\hat{e}_- = \frac{1}{\sqrt{2}}(\hat{e}_p - \hat{e}_s), \tag{8}$$

and the right (R) and the left (L) circularly polarized states as

$$\hat{e}_R = \frac{1}{\sqrt{2}}(\hat{e}_p - i\hat{e}_s), \tag{9}$$

$$\hat{e}_L = \frac{1}{\sqrt{2}}(\hat{e}_p + i\hat{e}_s), \tag{10}$$

where $\hat{e}_\alpha$, $\alpha = p, s, +, -, R,$ or L, must be replaced by $\hat{e}_\alpha(\theta_i)_{\text{inc}}$ in the case of the incident field and by $\hat{e}_\alpha(\theta_s)_{\text{sc}}$ in the case of the scattered field. With these definitions, the projection of a field $\mathbf{E}(x_1, x_3 | \omega)$ onto $\hat{e}_\alpha$ is $\mathbf{E}_\alpha(x_1, x_3 | \omega) = [\hat{e}_\alpha^* \cdot \mathbf{E}(x_1, x_3 | \omega)]\hat{e}_\alpha$, and $\mathbf{E}(x_1, x_3 | \omega)$ may be decomposed as $\mathbf{E}(x_1, x_3 | \omega) = \mathbf{E}_\alpha(x_1, x_3 | \omega) + \mathbf{E}_\beta(x_1, x_3 | \omega)$, where $(\alpha, \beta) = (p, s), (+, -),$ or (R, L).

Next we consider some of the observable quantities associated with the far field. The total power incident upon the surface that is in the projection of the incident field $\mathbf{E}_\alpha(x_1, x_3 | \omega)_{\text{inc}}$ is denoted P_α. To obtain this total incident power, the magnitude of the third component of the time-

averaged Poynting vector of $\mathbf{E}_\alpha(x_1, x_3 | \omega)_{\text{inc}}$ is integrated on the portion of the plane $x_3 = 0$ where $0 < x_2 < L_2$, in which L_2 is an arbitrary length. This incident power is then given by $P_\alpha = \mathcal{P}_{\text{inc}} |\hat{e}_\alpha^* \cdot (E_p \hat{e}_p + E_s \hat{e}_s)|^2$, where $\mathcal{P}_{\text{inc}} \cong L_2 c\omega/(8\sqrt{2\pi})$ when $\omega w/2c \gg 1$, as shown in Ref. 7. Similarly, the scattered power per unit planar angle $P_\beta(\theta_s)_{\text{sc}}$ may be calculated from the field $\mathbf{E}_\beta(x_1, x_3 | \omega)_{\text{sc}}$ by considering the flux of the third component of its time-averaged Poynting vector through a plane $x_3 = h > \zeta(x_1)_{\max}$, $0 < x_2 < L_2$. The flux $P_\beta(\theta_s)_{\text{sc}}$ is then a measure of the scattered power per unit angle transmitted through a filter passing the field in the polarization state $\hat{e}_\beta(\theta_s)_{\text{sc}}$ and is given by

$$P_\beta(\theta_s)_{\text{sc}} = \frac{L_2 c^2}{64\pi^2 \omega} \times |\hat{e}_\beta(\theta_s)_{\text{sc}}^* \cdot [E_p r_p(\theta_s)\hat{e}_p(\theta_s)_{\text{sc}} + E_s r_s(\theta_s)\hat{e}_s(\theta_s)_{\text{sc}}]|^2. \quad (11)$$

In this study the polarization state of the incident field is always a pure state $\hat{e}_\alpha(\theta_i)_{\text{inc}}$ [$E_{p,s} = \hat{e}_{p,s}^* \cdot \hat{e}_\alpha$ in Eq. (1)]; a more general situation is discussed in Ref. 11. The intensity of the scattered light transmitted through a filter passing the field in the polarization state $\hat{e}_\beta(\theta_s)_{\text{sc}}$ may be obtained for such an incident field by normalizing $P_\beta(\theta_s)_{\text{sc}}$ by the total incident power $P_\alpha = \mathcal{P}_{\text{inc}}$. This ratio may be written as $|A(\theta_s, \beta | \theta_i, \alpha)|^2$, where the new scattering amplitude A is given by

$$A(\theta_s, \beta | \theta_i, \alpha) = \frac{c}{8\pi}\left(\frac{L_2}{\omega \mathcal{P}_{\text{inc}}}\right)^{1/2} [(\hat{e}_\beta^* \cdot \hat{e}_p)(\hat{e}_p^* \cdot \hat{e}_\alpha) r_p(\theta_s) + (\hat{e}_\beta^* \cdot \hat{e}_s)(\hat{e}_s^* \cdot \hat{e}_\alpha) r_s(\theta_s)]. \quad (12)$$

These amplitudes also determine other observable quantities of the far field.[14]

The scattering amplitudes are random quantities associated with the stochastic process $\zeta(x_1)$. Of primary interest in the present study is the dependence of the amplitude correlation functions of the scattered field on the angles of incidence and of scattering and on the incident and the scattered polarization states. A general result concerning the angular dependence of these correlations may be obtained for an ensemble of surface profiles assumed to be realizations of a stochastic process if it is assumed that the statistics of the surface are stationary. It is shown in Appendix A that the following relationship then holds for incident Gaussian beams with $\lambda/w \ll 1$ and fixed beam width w [Eq. (1)]:

$$\langle A(\theta_{s1}, \beta_1 | \theta_{i1}, \alpha_1) A^*(\theta_{s2}, \beta_2 | \theta_{i2}, \alpha_2)\rangle = \exp\left\{-\left(\frac{\omega w}{2c}\right)^2 \frac{[(\sin\theta_{i1} - \sin\theta_{s1}) - (\sin\theta_{i2} - \sin\theta_{s2})]^2}{\cos^2\theta_{i1} + \cos^2\theta_{i2}}\right\} \times \langle A(\theta_{s1}, \beta_1 | \theta_{i1}, \alpha_1) A^*(\tilde{\theta}_{s2}, \beta_2 | \theta_{i2}, \alpha_2)\rangle, \quad (13)$$

where $\tilde{\theta}_{s2}$ is the angle satisfying

$$\sin\theta_{i1} - \sin\theta_{s1} = \sin\theta_{i2} - \sin\tilde{\theta}_{s2} \quad (14)$$

and where α_i and β_j $(i, j = 1, 2)$ may be any of the polarization indices p, s, $+$, $-$, R, and L. Thus, according to Eq. (13), the condition

$$|(\sin\theta_{i1} - \sin\theta_{s1}) - (\sin\theta_{i2} - \sin\theta_{s2})| \leq \frac{\lambda(\cos^2\theta_{i1} + \cos^2\theta_{i2})^{1/2}}{\pi w} \quad (15)$$

must be fulfilled for the scattering amplitudes to be significantly correlated. In the limit of small angular widths of the speckles ($\sim\lambda/w$) this condition may be approximated by $\sin\theta_{i1} - \sin\theta_{s1} = \sin\theta_{i2} - \sin\theta_{s2}$.

In particular, Eq. (13) implies that if the angles of incidence are taken to be identical ($\theta_{i1} = \theta_{i2}$), as in the case when there is a single incident beam, a significant correlation may exist between the scattering amplitudes only when $\theta_{s2} = \theta_{s1} = \tilde{\theta}_{s2}$, and this correlation decays within the speckle width as θ_{s2} is moved away from θ_{s1}. Conversely, if θ_{s1} and θ_{s2} are taken to be equal, as occurs when scattering intensities are considered, the scattering amplitudes may be correlated only if the two directions of incidence have an angular separation smaller than the speckle width λ/w. However, in general, a scattered amplitude at θ_{s1} owing to the incident beam at θ_{i1} will be correlated most strongly with the amplitude owing to the beam incident at θ_{i2} only if $\theta_{s2} = \tilde{\theta}_{s2}$ as prescribed by Eq. (14). As θ_{s2} then deviates from $\tilde{\theta}_{s2}$, the decorrelation of the amplitudes follows the behavior described by Eq. (13). Hence in Eq. (13) the values of the correlation functions at $(\theta_{i1}, \theta_{i2}, \theta_{s1}, \theta_{s2})$ are determined by the functions of only three independent variables:

$$\Gamma_{\alpha_1\alpha_2\beta_1\beta_2}(\theta_{i1}, \theta_{i2}, \theta_{s1}) = \langle A(\theta_{s1}, \beta_1 | \theta_{i1}, \alpha_1) A^*(\tilde{\theta}_{s2}, \beta_2 | \theta_{i2}, \alpha_2)\rangle, \quad (16)$$

where $(\theta_{i1}, \theta_{i2}, \theta_{s1})$ determines $\tilde{\theta}_{s2}$ through Eq. (14).

The identity $\Gamma_{\alpha_1\alpha_2\beta_1\beta_2}(\theta_{i1}, \theta_{i2}, \theta_{s1}) = \Gamma_{\alpha_2\alpha_1\beta_2\beta_1}{}^*(\theta_{i2}, \theta_{i1}, \tilde{\theta}_{s2})$ follows from Eq. (16). If $(\alpha, \beta) = (p, s)$, $(+, -)$, or (R, L), Eq. (12) may be used to obtain the identities $\Gamma_{\alpha_1\alpha_2\beta_1\beta_2}(\theta_{i1}, \theta_{i2}, \theta_{s1}) = \Gamma_{\beta_1\alpha_2\alpha_1\beta_2}(\theta_{i1}, \theta_{i2}, \theta_{s1}) = \Gamma_{\alpha_1\beta_2\beta_1\alpha_2}(\theta_{i1}, \theta_{i2}, \theta_{s1}) = \Gamma_{\beta_1\beta_2\alpha_1\alpha_2}(\theta_{i1}, \theta_{i2}, \theta_{s1})$. In Appendix A the reciprocity condition[24] satisfied by the scattering amplitudes $r_{p,s}(\theta_s | \theta_i)$ for an incident plane wave is used to show that, for $\lambda/w \ll 1$, $(\cos^2\theta_{i1} + \cos^2\theta_{i2})^{1/2}\Gamma_{\alpha_1\alpha_2\beta_1\beta_2}(\theta_{i1}, \theta_{i2}, \theta_{s1}) = (\cos^2\theta_{i1} + \cos^2\tilde{\theta}_{s2})^{1/2}\Gamma_{\alpha_1\alpha_2\beta_1\beta_2}(\theta_{i1}, -\tilde{\theta}_{s2}, \theta_{s1})$ if the width of the Gaussian beam w is kept constant when different angles of incidence are considered. Finally, because the surface profiles $\zeta(x_1)$ and $\zeta(-x_1)$ are statistically identical, we may reflect the angles of incidence and of scattering in the surface normal, and it follows that $\Gamma_{\alpha_1\alpha_2\beta_1\beta_2}(\theta_{i1}, \theta_{i2}, \theta_{s1}) = \Gamma_{\alpha_1\alpha_2\beta_1\beta_2}(-\theta_{i1}, -\theta_{i2}, -\theta_{s1})$.

3. NUMERICAL RESULTS

The correlation function of the scattering amplitudes defined by Eq. (16) was calculated numerically as a function of the angle of incidence θ_{i2} and of the incident and the scattered polarization states $(\alpha_1, \alpha_2, \beta_1, \beta_2)$. The surface-profile function is assumed to be a stationary, Gaussian stochastic process characterized by the properties $\langle\zeta(x_1)\rangle = 0$ and $\langle\zeta(x_1)\zeta(x_1')\rangle = \delta^2 \exp[-(x_1 - x_1')^2/a^2]$, where δ^2 is the variance of $\zeta(x_1)$ and a is the transverse correlation length of the surface. Each realization of the surface profile $\zeta(x_1)$ was computed at $N_x = 400$ equally spaced abscissas, and for each of them the scattering amplitudes $r_p(\theta_s)$ and $r_s(\theta_s)$ were calculated as a function of the incident and the scattering angles by the method described in Ref. 7. The incident beam used in the computation may be obtained from Eq. (1) through an approximate integration that is valid in the limit $\omega w/2c \gg 1$. The analytic expressions for the incident beam and for the total inci-

dent power derived in this fashion have been described elsewhere[7]; these expressions are simpler to evaluate numerically and are sufficiently accurate. In all the calculations, the 1/e half-width of the incident beam w was kept constant when different angles of incidence were considered.

N_p independent realizations of the surface profile were used to calculate estimates for the amplitude correlation function. These estimates were obtained by arithmetically averaging the products of the scattering amplitudes $r_p(\theta_{s1})$ and $r_s(\theta_{s1})$ with the amplitudes $r_p(\theta_{s2})$ and $r_s(\theta_{s2})$ over the finite set of realizations ($N_p \geq 1000$). The correlation function $\Gamma_{\alpha_1\alpha_2\beta_1\beta_2}(\theta_{i1}, \theta_{i2}, \theta_{s1})$ contains contributions from the coherent and the incoherent parts of the random scattered amplitudes, $\langle r_\alpha(\theta_s)\rangle$ and $\Delta r_\alpha(\theta_s) = r_\alpha(\theta_s) - \langle r_\alpha(\theta_s)\rangle$, respectively ($\alpha = p, s$). In all the cases considered in this section the standard deviation of the surface height is large enough with respect to the wavelength to extinguish the mean scattering amplitudes, and the results presented contain only contributions from the incoherent part of the scattering amplitudes.

The length L of the surface was chosen such that the half-width of the intercept of the beam with the mean surface $w/\cos\theta_i$ was always several times smaller than L at the angles considered. The angle of incidence θ_i is measured counterclockwise from $\hat{x}_3$, and the scattering angle θ_s is measured clockwise from $\hat{x}_3$; all the angles in the figures are in degrees. The range of allowed angles θ_{i2} is determined by Eq. (14) and is given by the interval $[\arcsin(\sin\theta_{i1} - \sin\theta_{s1} - 1), \pi/2]$ if $\theta_{i1} > \theta_{s1}$ and by $[-\pi/2, \arcsin(\sin\theta_{i1} - \sin\theta_{s1} + 1)]$ if $\theta_{i1} < \theta_{s1}$. In the results presented here, this range was limited either by the lack of accuracy of the computation at shallow angles of incidence or by the amplitude correlation's being smaller than the statistical noise owing to the finite number of samples N_p. The calculated correlation functions verify the identity derived from the reciprocity condition (Section 2) to within the statistical noise. The total scattered power normalized by the incident power for a single surface realization of the surface profile is given by the integral over all scattering angles θ_s of $|A(\theta_s, \beta_1 | \theta_i, \alpha)|^2 + |A(\theta_s, \beta_2 | \theta_i, \alpha)|^2$, where $(\beta_1, \beta_2) = (p, s)$, $(+, -)$, or (R, L); this quantity was always between 0.99 and 1.0.

In Fig. 1 we present the results of the calculation of the amplitude correlation functions $\Gamma_{++\alpha\beta}(\theta_{i1}, \theta_{i2}, \theta_{s1})$ as a function of θ_{i2} for $(\alpha, \beta) = (p, p)$, (s, s), (p, s), and (s, p) and for $(\theta_{i1}, \theta_{s1}) = (-10°, 30°)$. The wavelength of the incident light is $\lambda = a/3$. The surface roughness is such that $\delta/a = 0.6$; the standard deviation of the surface slopes is then $\sqrt{2}\,\delta/a = 0.8485$. The four amplitude correlation functions are significant over an angular interval of ~45°. Two distinct peaks with their maxima at $\theta_{i2} = -30°$ and $\theta_{i2} = -10°$ are observed in the real part of each of the four complex correlation functions. The maxima occur for incident directions at which the two correlated scattering amplitudes either are identical ($\theta_{i2} = \theta_{i1} = -10°$, in which case the correlation is perfect) or are related through the reciprocity condition ($\theta_{i2} = -\theta_{s1} = -30°$). Γ_{++pp} and Γ_{++ss} have positive real parts and similar angular distributions; Γ_{++ps} and Γ_{++sp} are also similar but have negative real parts. The sign difference between these pairs of correlation functions may be interpreted if the Kirchhoff approximations[25] for the scattering amplitudes $r_p^{(1)}(\theta_s)$ and $r_s^{(1)}(\theta_s) = -r_p^{(1)}(\theta_s)$ are used in Eq. (16) instead of $r_p(\theta_s)$ and $r_s(\theta_s)$; the amplitude correlations calculated within this single-scattering approximation[26] would then be $\Gamma^{(1)}_{++pp} = \Gamma^{(1)}_{++ss} = -\Gamma^{(1)}_{++ps} = -\Gamma^{(1)}_{++sp}$. The sign difference between the correlation functions is then understood if it is assumed that there are large single-scattering contributions to these functions. The imaginary part of the correlation function is approximately an order of magnitude smaller than the real part in each case. The normalized intensities $\langle |A(\bar{\theta}_{s2}, \alpha | \theta_{i2}, +)|^2\rangle$ ($\alpha = p, s$) computed with the same realizations of the scattering amplitudes as the ones used in the calculation of the correlation function display a well-defined enhanced backscattering peak, as expected from this surface.[27] The retroreflection direction at which the enhancement is observed occurs when $\theta_{i2} = -\bar{\theta}_{s2} \cong -19.7°$, as obtained from Eq. (14), if θ_{i2} is set equal to $-\bar{\theta}_{s2}$. At this angle the real parts of the amplitude correlation functions have only minima.

The four correlation functions of Fig. 1 are the fundamental quantities from which one may obtain by linear combination any function $\Gamma_{\alpha_1\alpha_2\beta_1\beta_2}(\theta_{i1}, \theta_{i2}, \theta_{s1})$, according to Eqs. (12) and (16). The correlation functions Γ_{+---} and Γ_{+-+-} as computed from the results of Fig. 1 are shown in Fig. 2. The behaviors of these two correlation functions are very different. The real part of Γ_{+---} displays strong correlations between scattering amplitudes separated by as much as 50° and has maxima at $\theta_{i2} = -30°$ and $\theta_{i2} = -10°$. At each of these angles $\Re\,\Gamma_{+---}$ has a narrow peak whose full width at zero is ~10°. The two peaks are separated by a minimum around $\theta_{i2} = -20°$ where $\Re\,\Gamma_{+---}$ is negative. Minima at which the correlation

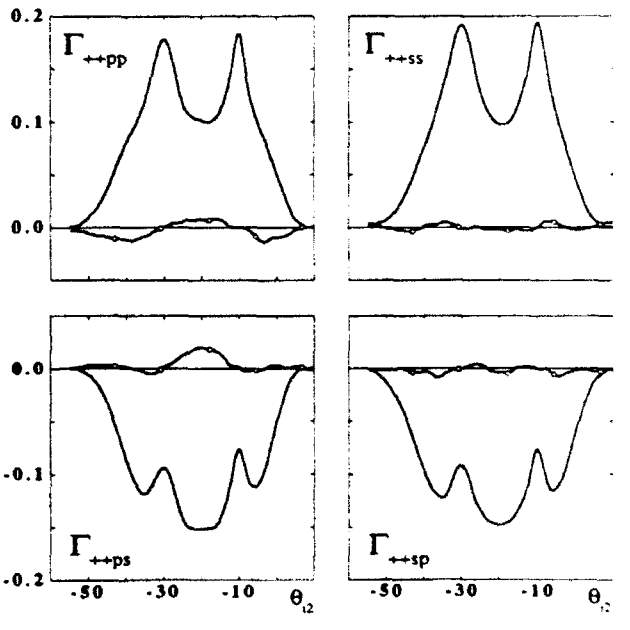

Fig. 1. Dependence of the real (solid curves) and the imaginary (curves with open circles) parts of the four complex amplitude correlation functions Γ_{++pp}, Γ_{++ss}, Γ_{++ps}, and Γ_{++sp} on θ_{i2} for $\theta_{i1} = -10°$ and $\theta_{s1} = 30°$. The one-dimensional profile of the randomly rough, perfectly conducting surface is characterized by $\delta/a = 0.6$. The wavelength of the incident light is $\lambda = a/3$, the half-width of the Gaussian beam is $w = 7\lambda$, and the length of the segment of surface considered is $L = 6w$. $N_s = 400$ discretization points were used, and the estimates of the correlation functions were obtained by averaging over an ensemble of $N_p = 2000$ independent surface realizations.

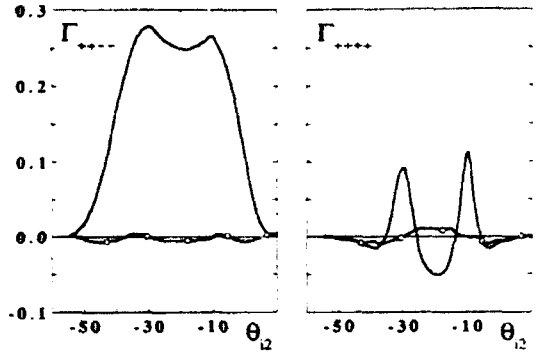

Fig. 2. Two complex amplitude correlation functions, Γ_{+---} and Γ_{+++-}, computed from the results of Fig. 1. The solid curves represent the real parts, and the curves marked with open circles represent the imaginary parts.

has a negative value are also present on both sides of the angular intervals containing the two peaks. As in Fig. 1, the imaginary parts of the correlation functions of Fig. 2 are small in comparison with the real parts.

These remarkable features may be attributed to single and multiple scattering in the following manner: Studies of the scattering behavior of similar surfaces have shown that the first- and the second-order Kirchhoff approximations for the scattering amplitudes may be used to compute mean intensities in reasonable agreement with the exact calculations.[27] The infinite series of Kirchhoff approximations[7,25] $r_{p,s}(\theta_s) = r^{(1)}_{p,s}(\theta_s) + r^{(2)}_{p,s}(\theta_s) + r^{(3)}_{p,s}(\theta_s) + \ldots$, where $r^{(n)}_{p,s}(\theta_s)$ $(n > 0)$ is the amplitude computed from the $(n-1)$th iteration of the surface integral equation for the source function, have been shown[11] to be related through $r^{(n)}_s(\theta_s) = (-1)^n r^{(n)}_p(\theta_s)$. The second-order Kirchhoff approximation for the amplitude correlation functions is then derived by keeping only the first two terms in the series for the scattering amplitudes and may be obtained from Eqs. (12) and (16) as

$$\Gamma_{+--+}(\theta_{i1},\theta_{i2},\theta_{s1}) \cong \left(\frac{c}{8\pi}\right)^2 \frac{L_2}{\omega \mathcal{P}_{\text{inc}}} \langle r_p^{(1)}(\theta_{s1}) r_p^{(1)*}(\theta_{s2})\rangle, \quad (17)$$

$$\Gamma_{++++}(\theta_{i1},\theta_{i2},\theta_{s1}) \cong \left(\frac{c}{8\pi}\right)^2 \frac{L_2}{\omega \mathcal{P}_{\text{inc}}} \langle r_p^{(2)}(\theta_{s1}) r_p^{(2)*}(\theta_{s2})\rangle. \quad (18)$$

The results of relations (17) and (18) suggest that, when single- and double-scattering processes are the dominant contributions to the scattering amplitudes, Γ_{+--+} and Γ_{++++} arise exclusively from pure single- and pure double-scattering processes, respectively. If higher-order processes are important, relations (17) and (18) may be generalized to show that Γ_{+--+} contains all the contributions of the form $\langle r_p^{(2n-1)}(\theta_{s1}) r_p^{(2n'-1)*}(\theta_{s2})\rangle$ and that Γ_{++++} contains all the terms of the form $\langle r_p^{(2n)}(\theta_{s1}) r_p^{(2n')*}(\theta_{s2})\rangle$.

The two correlation functions Γ_{++--} and Γ_{+--+}, according to the identity on the interchange of the polarization indices of Section 2, are needed to complete the description of the correlations of the amplitudes $A(\theta_s, \pm | \theta_i, \pm)$. However, in this case and in all the other cases discussed below, these functions were found to be more than an order of magnitude smaller than the functions Γ_{++++} and Γ_{+--+}, and the results were less significant given the level of fluctuations remaining after averaging over $N_p \sim 1000$ realizations. We thus surmise that most of the meaningful information is contained in Γ_{++++} and Γ_{+--+}, and in what follows we present further results for only these functions.

The dependence of the amplitude correlation functions on the surface correlation length a is illustrated in Fig. 3. the ratio δ/a is kept constant and is 0.6 as in Figs. 1 and 2. The angles $\theta_{i1} = 0°$ and $\theta_{s1} = 30°$ characterize one of the scattering amplitudes of the correlation function. The dependence of Γ_{++++} and Γ_{+--+} on θ_{i2} is shown in Fig. 3 for ratios a/λ equal to 1, 3, and 6. Correlations exist at large angles in the three cases. The real part of each correlation function has maxima at $\theta_{i2} = 0°$, where the two amplitudes in the correlation functions are identical, and at $\theta_{i2} = -30°$, where the reciprocity condition relates them. At those two angles $\Re e\, \Gamma_{++++}$ displays a sharp peak whose full widths at zero are 27°, 9°, and 5° when a/λ equals 1, 3, and 6, respectively. These widths have values close to the angular widths $\lambda/(2a)$. Minima at which $\Re e\, \Gamma_{++++} < 0$ are observed on both sides of each peak in the three right-hand panels, and their angular separation is close to λ/a. The correlation function $\Re e\, \Gamma_{+--+}$ has much broader peaks at $\theta_{i2} = 0°$ and $\theta_{i2} = -30°$ that overlap at intermediate angles; the widths of these peaks also decrease with an increasing ratio a/λ.

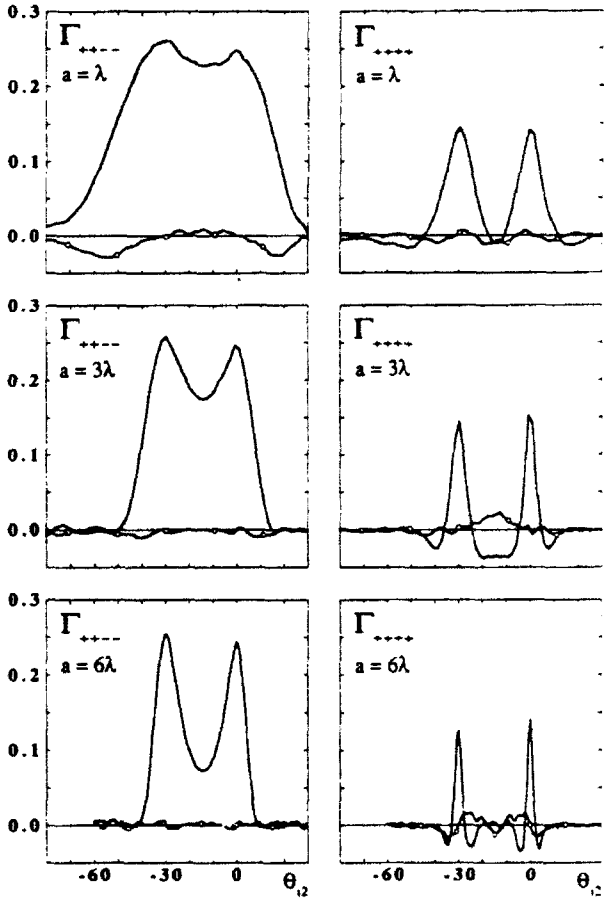

Fig. 3. Dependence of the two complex amplitude correlation functions Γ_{++++} and Γ_{+--+} on the transverse correlation length a of the surface profile. The values of the parameters kept constant are $\theta_{i1} = 0°$, $\theta_{s1} = 30°$, $\delta/a = 0.6$, and $N_s = 400$. Top row: $a = \lambda$, $w/\lambda = 7$, $L/w = 6$, $N_p = 1000$; middle row: $a/\lambda = 3$, $w/\lambda = 7$, $L/w = 6$, $N_p = 2300$; bottom row: $a/\lambda = 6$, $w/\lambda = 12$, $L/w = 4$, $N_p = 1400$. The solid curves represent the real parts, and the curves marked with open circles represent the imaginary parts.

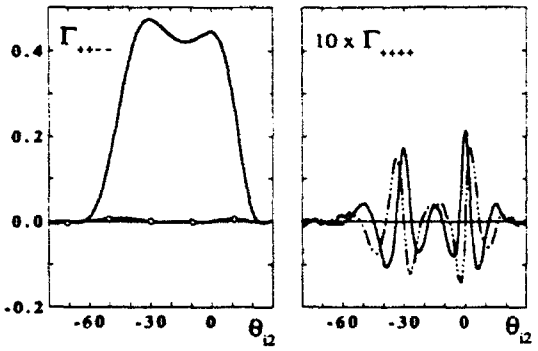

Fig. 4. Two complex amplitude correlation functions, Γ_{++++} and Γ_{++--}, for the same parameters as in Fig. 3 ($a/\lambda = 3$) but for $\delta/a = 0.3$ and $N_p = 1800$. The solid curves represent the real parts, the curve marked with open circles represents the imaginary part of Γ_{++--}, and the dotted-dashed curve represents the imaginary part of Γ_{++++}.

In Fig. 4 the incident wavelength is $\lambda = a/3$, and the surface is characterized by $\delta/a = 0.3$; the surface slopes are thus weaker than in the previous cases. As in Fig. 3, the angles $\theta_{i1} = 0°$ and $\theta_{s1} = 30°$ are kept constant, and the dependence on θ_{i2} is shown. The maximum value of $\Re e\ \Gamma_{++--}$ is seen to be approximately two times larger for $\delta/a = 0.3$ than for $\delta/a = 0.6$ (Fig. 3, $a/\lambda = 3$); the angular width of this function is also larger than in Fig. 3 when $a/\lambda = 3$. In contrast, the correlation function $\Re e\ \Gamma_{++++}$ is ten times smaller than in the previous case, and its dependence on θ_{i2} has changed. Sharp peaks at $\theta_{i2} = 0°$ and $\theta_{i2} = -30°$ are observed, but each peak has subsidiary maxima on both sides, the correlation function being negative at the intermediary minima. The widths of the main peaks are somewhat smaller than for $\delta/a = 0.6$. The imaginary part of this function has the same magnitude as the real part but has a zero when the real part has an extremum and vice versa.

We now consider the approach to the special case in which one of the correlated amplitudes is an amplitude of retroreflection ($\theta_{s1} = -\theta_{i1}$). Figure 5 shows the correlation functions Γ_{++++} and Γ_{++--} as a function of θ_{i2} for the same incident wavelength and surface characteristics as in Figs. 1–3 ($a/\lambda = 3$) and for $\theta_{s1} = 0$ but for angles of incidence increasingly close to the retroreflection direction: $\theta_{i1} = 15°$, 5°, and 0°, successively. When $\theta_{i1} = 15°$ the same qualitative features are observed in the two correlation functions as in Figs. 2 and 3. At $\theta_{i1} = 15°$ the two peaks of Γ_{++--} overlap, but the maximum values are only slightly larger than for larger angle of incidence (Fig. 3); the two peaks of Γ_{++++} are separated, and their maximum values are approximately the same as in Fig. 3. The values of the correlation at the minima on both sides of each peak decrease when θ_{i1} decreases. When the angle of incidence θ_{i1} is 5°, which is half the width at zero of the amplitude correlation function, the value of the maximum of the correlation function Γ_{++++} at $\theta_{i2} = \theta_{i1} = 5°$ is the averaged intensity scattered in the direction $\theta_s = 0°$ owing to an incident beam at $\theta_i = 5°$. This intensity is now somewhat larger than the intensity given at $\theta_i = 5°$ by Γ_{++--}. The minima on either side of the main peak are clearly observed. The imaginary part of Γ_{++++} also has two minima symmetrically located about the peak. The case in which one of the amplitudes in the correlation functions is the retroreflection amplitude ($\theta_{i1} = 0°$) is also shown in Fig. 5. The magnitude of the function $\Re e\ \Gamma_{++--}$ is approximately the same as for $\theta_{i1} = 15°$, or 5°. This shows that the single-scattering contributions to the retroreflection amplitude and their time-reversed partners are not distinct processes and do not have to be added in the amplitude of retroreflection. The two peaks observed in $\Re e\ \Gamma_{++++}$ when $\theta_{i1} = 15°$ coincide in this case. The maximum value of the peak at $\theta_{i2} = \theta_{i1} = 0°$ is 0.6, which is approximately three times its value at 15°. The minima in $\Re e\ \Gamma_{++++}$ occur at $\theta_{i2} = \pm 10°$, and the minima in $\Im m\ \Gamma_{++++}$ occur at $\theta_{i2} = \pm 15°$. In this sequence of figures the constructive interference of the contributions of multiple-scattering processes with those of their time-reversed processes is clearly observed about the retroreflection direction where these contributions are correlated.

We now examine whether the result of Fig. 5 at $\theta_{i1} = 0°$ exhibits the same dependence on the characteristics of the surface roughness as observed in Figs. 3 and 4. The effect of a/λ and of δ/a on the amplitude correlation functions $\Gamma_{++--}(\theta_{i1}, \theta_{i2}, -\theta_{i1})$ and $\Gamma_{++++}(\theta_{i1}, \theta_{i2}, -\theta_{i1})$ is thus considered in Figs. 6 and 7, respectively. In Fig. 6 the surfaces are characterized by large surface slopes ($\delta/a = 0.6$) and increasingly large correlation lengths: $a/\lambda = 1$, 3, and 6, as in Fig. 3. The retroreflection direction is the

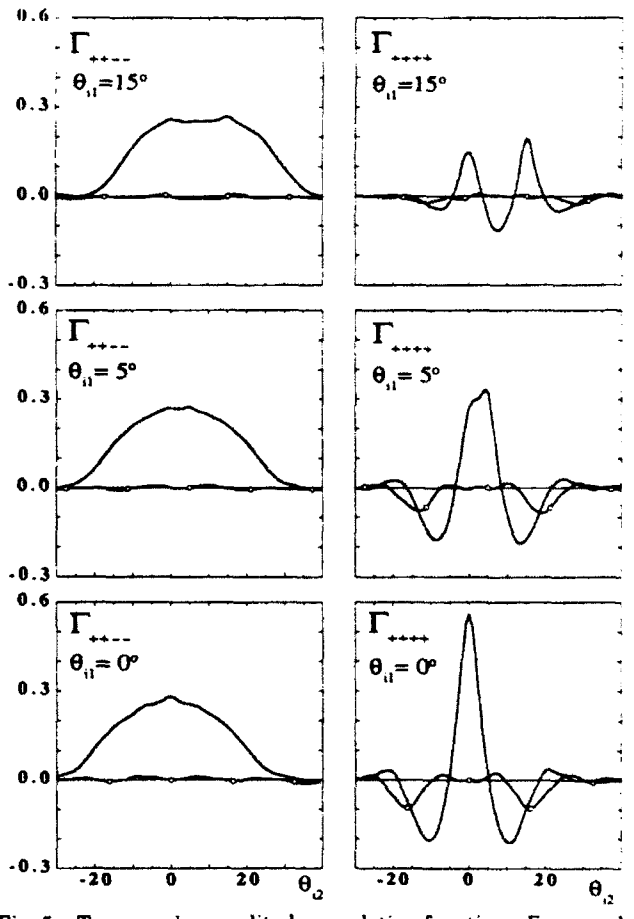

Fig. 5. Two complex amplitude correlation functions, Γ_{++--} and Γ_{++++}, for the same parameters as in Fig. 3; that is, $a/\lambda = 3$, $w/\lambda = 7$, and $L/w = 6$ but $\theta_{s1} = 0°$. Top row: $\theta_{i1} = 15°$, $N_p = 2000$; middle row: $\theta_{i1} = 5°$, $N_p = 2000$; bottom row: $\theta_{i1} = 0°$, $N_p = 1300$. The solid curves represent the real parts, and the curves marked with open circles represent the imaginary parts.

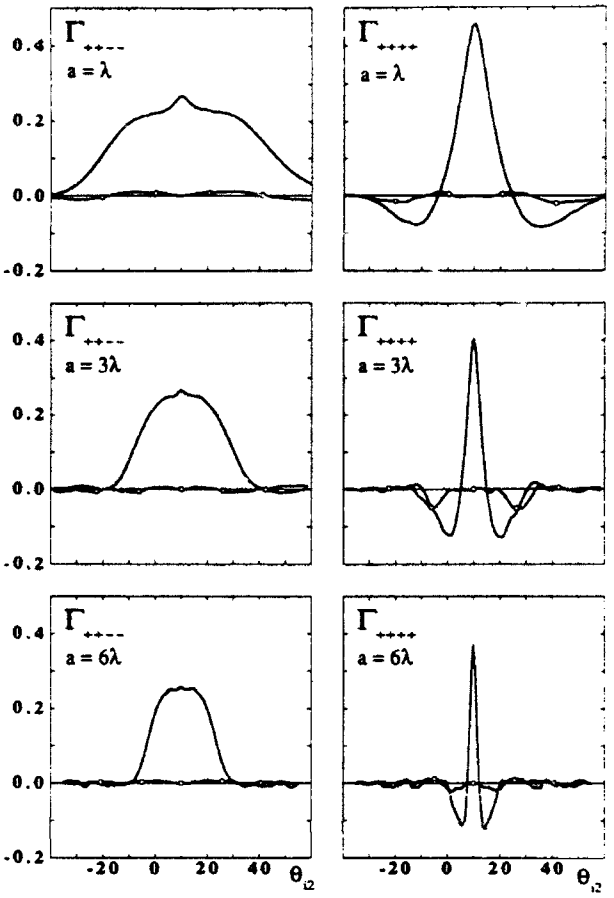

Fig. 6. Dependence of the two complex amplitude correlation functions Γ_{++++} and Γ_{+---} on the transverse correlation length a of the surface profile. The values of the parameters kept constant are $\theta_{i1} = -\theta_{s1} = 10°$, $\delta/a = 0.6$, and $N_x = 400$. Top row: $a = \lambda$, $w/\lambda = 7$, $L/w = 5$, $N_p = 2000$; middle row: $a/\lambda = 3$, $w/\lambda = 7$, $L/w = 5$, $N_p = 1300$; bottom row: $a/\lambda = 6$, $w/\lambda = 12$, $L/w = 4$, $N_p = 1800$. The solid curves represent the real parts, and the curves marked with open circles represent the imaginary parts.

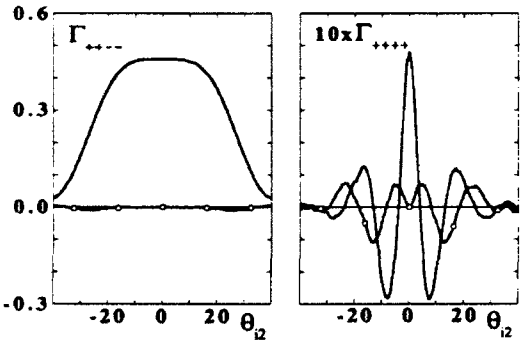

Fig. 7. Two complex amplitude correlation functions, Γ_{++++} and Γ_{+---}, for $a/\lambda = 3$ as in Fig. 5 ($\theta_{i1} = 0°$) but for $\delta/a = 0.3$ and $N_p = 1200$. The solid curves represent the real parts, and the curves marked with open circles represent the imaginary parts.

direction $\theta_{s1} = -\theta_{i1} = -10°$. The same qualitative behavior is observed in these cases as in Fig. 5 for $\theta_{i1} = 0°$, even though the angles of incidence and the parameters of the surface roughness are different. Correlations between scattering amplitudes over a large range of angles are observed in the two functions in all the cases. The width of the correlation functions decreases when the ratio a/λ increases. The magnitude of Γ_{+---} stays constant, and the function is almost purely real. The maximum value of Γ_{++++} decreases slowly when a/λ increases, but the most striking effect of this increasing ratio is the decrease in the width of the peak. Measured at the minima of the function on either side of the peak, these widths are 50°, 18°, and 8°, which are close to the diffraction width λ/a.

Figure 7 shows the case when $a/\lambda = 3$ and $\delta/a = 0.3$, as in Fig. 4, but for $\theta_{s1} = -\theta_{i1} = 0°$. The width of the real part of the function $\Re e\,\Gamma_{+---}$ as well as its maximum value are much larger than in the case of the rougher surface. The imaginary part of this function is indistinguishable from the statistical fluctuations present in the calculations. The correlation function Γ_{++++}, in contrast, has a much smaller magnitude than in Fig. 4, and its imaginary part is nearly as significant as its real part. As expected from the statistical symmetry of the surface, Γ_{++++} is, within the accuracy of the calculations, an even function of θ_{i2}. The distance between the adjacent maxima or minima of $\Re e\,\Gamma_{+---}$ is very close to λ/a.

4. DISCUSSION

In the limit of plane-wave illumination $w/\lambda \to \infty$, the necessary condition for scattering amplitudes to be correlated [Eq. (14)] is that the projection onto the mean surface of the difference of the incident wave vectors must equal that of the scattered wave vectors. This property of the amplitude correlation function is a consequence of the stationarity of the height statistics of the surface profile. An identical condition was derived previously within the Kirchhoff approximation.[12,14] In another context the existence of correlations among the scattering amplitudes produced by the reflection of light from a random volume scatterer[18] was also shown to occur under the condition of Eq. (14) if the statistics of the disorder are homogeneous. In the case of Gaussian beam illumination, the correlation of the amplitudes has been shown to decay within the speckle angular width when one of the angles is moved away from a value such that the condition of Eq. (14) is fulfilled. This behavior has been used here to reduce the number of independent angles determining the correlation functions to three.

In Section 3 the results of calculations of the correlations between the exact scattering amplitudes are presented. These correlations are reported as functions of one of the angles of incidence (θ_{i2}) and of the incident and the scattered polarization states. The real part of the correlation function of the scattering amplitudes $A(\theta_s, + \mid \theta_i, +)$, which are due exclusively to multiple-scattering processes, has two distinct peaks whose full widths measured between the adjacent minima are λ/a in all the cases considered. A maximum occurs either when the two amplitudes are identical ($\theta_{i2} = \theta_{i1}$) or when the roles of the outgoing and the incoming directions are interchanged between the two scattering amplitudes ($\theta_{i2} = -\theta_{s1}$), which are then related by the reciprocity condition. The height of a peak is given either by the mean intensity at $\theta_{i2} = \theta_{i1}$ or by this intensity multiplied by an angular factor derived from the reciprocity condition. The widths of the peaks in the correlation function of the scattering

amplitudes $A(\theta_s, +|\theta_i, +)$ may be qualitatively understood if the width of the function $\chi_{--}[\alpha(k_{s1}), \alpha(k_{s2}), |s|]$ of Eq. (A5) in Appendix A is estimated. χ_{--} is the correlation function of the stationary parts of $j_-(x_1)\exp[-i\alpha(k_{s1})x_1]$ and $j_-^*(x_1 + s)\exp[i\alpha(k_{s2})(x_1 + s)]$, where the source function $j_-(x_1) = j_p(x_1) + j_s(x_1)$ contains only multiple-scattering contributions. The multiple-scattering paths contributing significantly to the source functions give rise to sequences of correlated source elements on the surface. The average length of these sequences is given by the distance between the first and the last interaction points. As suggested in studies of enhanced backscattering,[27] for a surface with a Gaussian correlation function this distance may be approximated by the average groove width at $\zeta = 0$ that has been shown to be of the order of the transverse correlation length.[28] As a consequence the spatial extent of χ_{--} may be approximated by a, and from Eq. (A5) we conclude that the angular width around zero of the amplitude correlation function is of the order of λ/a, as observed in the numerical simulation results. The presence of well-defined peaks when the standard deviation of the surface slopes is 0.42 (Fig. 4) shows that multiple scattering occurs even though the magnitude of its contributions is an order of magnitude smaller than for slopes twice as large.

Two peaks have also been predicted[21] in the correlation functions of amplitudes reflected from a random volume scatterer and are known as the memory effect. The angular width of these peaks, calculated within a diffusion approximation, is given by the diffraction width produced by the transport mean free path. The analog of this mean free path in the surface scattering case considered here is thus the correlation length a, as has been suggested in studies of enhanced backscattering[27] from similar surfaces. The peak corresponding to pairs of scattering amplitudes related by the reciprocity condition, known as the time-reversed memory effect and obtained by imposing a reciprocity condition on the diffusion approximation in the volume scattering case, was obtained here directly from the exact scattering amplitudes, satisfying the reciprocity condition.

The correlation function of the scattering amplitudes $A(\theta_s, -|\theta_i, +)$ also has maxima at $\theta_{i2} = \theta_{i1}$ and $\theta_{i2} = -\theta_{s1}$, but these maxima are broader than the peaks in Γ_{++++}. The widths of these broad structures decrease when the ratio a/λ increases, if δ/a is kept constant. The scattering intensity given by the magnitude of the correlation function Γ_{++--} at the maximum $\theta_{i2} = \theta_{i1}$ increases, and the width of the maxima increases when the standard deviation of the slopes is decreased while a/λ is kept constant. The dependence of this correlation function on the roughness parameters is thus comparable with the results[12,14] obtained within the Kirchhoff approximation. This indicates that, of all the scattering processes participating in the scattering amplitude $A(\theta_s, -|\theta_i, +)$, the contributions from single-scattering processes are dominant for the surfaces considered here.

When the correlations of all the scattering amplitudes with an amplitude of retroreflection are considered, the two peaks of Γ_{++++} coincide. The height of the peak is found to be more than three times the height when the peaks do not overlap. This maximum value is the scattering intensity in the retroreflection direction, and similar enhancement factors were obser d in calculations[11] of this intensity. The angular width of the unique peak measured between the adjacent minima is again λ/a. In this case all the scattering paths that are participating incoherently in the scattering amplitude when θ_{i1} is different from $-\theta_{s1}$ are contributing coherently. If these scattering amplitudes are due exclusively to multiple interactions, the pairs of scattering processes related by the reciprocity condition consist of distinct processes interfering constructively. The magnitude of the peak occurring when $\theta_{i1} = -\theta_{s1}$ is thus enhanced owing to the constructive interference of these pairs of contributions, which are correlated. The width of the peak may be estimated as above, and thus the same width, of the order λ/a, may be obtained. The correlation Γ_{++--} does not change significantly when the direct- and the reciprocal-scattering amplitudes coincide. The single-scattering contributions do not differ from those of their time-reversed partners, and no addition of their contribution occurs in the retroreflection direction. The small enhancement observed in Fig. 6 at $\theta_{i2} = 10^\circ$ may then be interpreted as being due to pure triple-scattering contributions.

5. CONCLUSIONS

In this paper we have shown that single and multiple scattering play significant and distinct roles in the amplitude correlation function of waves scattered from randomly rough, perfectly conducting surfaces. The generalization of the scattering amplitudes to incident and scattered fields of arbitrary polarizations [Eq. (12)] was used to separate the single- and the multiple-scattering contributions to the amplitude correlation functions. In the study of mean scattered intensities for incident and scattered fields of arbitrary polarizations it has been shown that four unique real Stokes matrix elements are required[6,11]; for the general second-order amplitude correlation function, four complex quantities must be considered.

The calculation of the amplitude correlation functions from exact expressions for the scattered field by using a result of the stochastic Fourier-transform method developed by Brown[29,30] was shown to lead to an analytic expression valid for wide Gaussian beams ($\lambda/w \ll 1$) of constant width and for stationary surface statistics. A necessary condition for scattering amplitudes to be correlated was written for the incident and the scattering angles in the limit of small angular speckle widths: the projection on the mean surface of the difference of the incident wave vectors must equal that of the scattered wave vectors. The amplitude correlation functions have thus been found to be completely determined when three different angles are specified.

The simulation results for the dependence of the amplitude correlation functions on one of the angles of incidence have shown that strong correlations exist between the scattering amplitudes if the condition concerning the wave-vector projections is fulfilled, even when the incident or the scattering directions are separated by angles much larger than the angular width of the speckles. The calculations were performed in the case of a Gaussian surface with a Gaussian correlation function; various standard deviations of the surface heights and transverse correlation lengths were considered. When single-

scattering processes account for all the contributions to the scattering amplitudes, correlation functions of large angular width are expected, and they have been investigated theoretically and experimentally.[12-14] However, we have demonstrated the existence of strong correlations between scattering amplitudes that are due exclusively to multiple-scattering processes, and we have found that these correlation functions have a complex physical content.

The results of this paper show that when the scattering amplitudes are due exclusively to multiple-scattering processes the real part of the amplitude correlation function has two distinct peaks whose full widths measured between adjacent maxima are λ/a. A maximum occurs either when the two amplitudes are identical or when they are related by the reciprocity condition. In the reciprocal configuration the roles of the outgoing and the incoming directions are interchanged between the two scattering amplitudes. We have suggested that the angular width of the interval of angles of incidence over which direct or reciprocal scattering amplitudes are strongly correlated is inversely proportional to the characteristic distance separating the first and the last reflection of a multiple-scattering path on the surface. A good estimate of this mean free path for the surfaces considered here is the transverse correlation length a. Finally, we have clearly demonstrated the constructive interference of the direct- and the reciprocal multiple-scattering processes by calculating the amplitude correlation functions at angles of incidence and of scattering close to the retroreflection direction.

APPENDIX A: STATIONARY EXPRESSION FOR THE SOURCE FUNCTIONS

In this appendix we show how the expression of Eq. (13) for the correlation of scattering amplitudes characterized by arbitrary directions of incidence and scattering and arbitrary incident and scattered polarization states may be obtained from a result derived by Brown.[29,30] The only assumption necessary is that the rough surface profile must be a stationary random process.

For one-dimensional surfaces, the s- and the p-polarized electromagnetic scattering problems reduce to the scattering of a scalar field with Neumann and Dirichlet boundary conditions, respectively. The scalar field corresponding to the p- $[(E_p, E_s) = (1,0)]$ and the s- $[(E_p, E_s) = (0,1)]$ polarized incident electric fields in Eq. (1) is given by Eq. (1) itself, in which the quantity in square brackets must be replaced by unity.[7] Green's second integral theorem is then used to obtain the scattering amplitudes $r_s(\theta_s)$ and $r_p(\theta_s)$ in the form

$$r_\alpha(\theta_s) = \int_{-\infty}^{\infty} dx_1 \exp\left\{-i\frac{\omega}{c}[x_1 \sin\theta_s + \zeta(x_1)\cos\theta_s]\right\} j_\alpha(x_1), \quad \alpha = p, s. \tag{A1}$$

Expressions for the source functions $j_\alpha(x_1)$ may be found in Ref. 7.

The correlation of the scattering amplitudes at scattering angles θ_{s1} and θ_{s2} is first considered for plane waves incident at angles θ_{i1} and θ_{i2}, respectively. The incident scalar fields are then $\exp[ik_{i1}x_1 - i\alpha(k_{i1})x_3]$ and $\exp[ik_{i2}x_1 - i\alpha(k_{i2})x_3]$, where the component of the incident wave vector parallel to the mean surface is $k_i = (\omega/c)\sin\theta_i$ and $\alpha(k_i) = (\omega^2/c^2 - k_i^2)^{1/2}$. Similar notation is adopted for the components of the scattered wave vectors in this appendix. The correlation of the scattering amplitudes $r_\alpha(\theta_s|\theta_i)$ for incident plane waves then becomes $(\alpha, \beta = s, p)$

$$\langle r_\alpha(\theta_{s1}|\theta_{i1}) r_\beta^*(\theta_{s2}|\theta_{i2})\rangle = \int_{-\infty}^{\infty} dx_1 \int_{-\infty}^{\infty} dx_1' \times \exp[-i(k_{s1}x_1 - k_{s2}x_1')] \times \langle j_\alpha(x_1) j_\beta^*(x_1') \exp\{-i[\alpha(k_{s1})\zeta(x_1) - \alpha(k_{s2})\zeta(x_1')]\}\rangle. \tag{A2}$$

The statistical properties of the expression in angle brackets has been studied by Brown, using the stochastic Fourier-transform approach to rough surface scattering. The method also uses the exact expression for the scattered field derived from Green's second integral theorem. Equation (21) of Ref. 29 may be used to obtain the behavior under translation along the mean surface of the statistical moments of $j_\alpha(x_1)\exp[-i\alpha(k_s)\zeta(x_1)]$, with the key result that this random function may be written as the product of the incident field evaluated on the mean surface times a stationary random process. The quantity in angle brackets in Eq. (A2) may thus be expressed as

$$\langle j_\alpha(x_1) j_\beta^*(x_1') \exp\{-i[\alpha(k_{s1})\zeta(x_1) - \alpha(k_{s2})\zeta(x_1')]\}\rangle = \exp[i(k_{i1}x_1 - k_{i2}x_1')]\chi_{\alpha\beta}[\alpha(k_{s1}), \alpha(k_{s2}), |x_1 - x_1'|]. \tag{A3}$$

With this equation, the amplitude correlation in the case of the incoming plane wave of Eq. (A2) becomes

$$\langle r_\alpha(\theta_{s1}|\theta_{i1}) r_\beta^*(\theta_{s2}|\theta_{i2})\rangle = \delta[(k_{i1} - k_{s1}) - (k_{i2} - k_{s2})] C_{\alpha\beta}(k_{i1}, k_{i2}, k_{s1}), \tag{A4}$$

where

$$C_{\alpha\beta}(k_{i1}, k_{i2}, k_{s1}) = 2\pi \int_{-\infty}^{\infty} ds \exp[-is(k_{i1} - k_{s1})]\chi_{\alpha\beta}[\alpha(k_{s1}), \alpha(k_{s2}), s] \tag{A5}$$

and $C_{\alpha\beta}$ is taken to depend only on the independent wave vectors (k_{i1}, k_{i2}, k_{s1}), the wave vector k_{s2} being determined through the argument of the Dirac delta function $\delta(x)$. For surfaces with stationary statistics, a correlation between scattering amplitudes may thus exist only if the differences between the parallel components of the incident and the scattered wave vectors are equal for both scattering amplitudes $(k_{i1} - k_{s1} = k_{i2} - k_{s2})$ or, equivalently, if the changes in the parallel components of the incident and the scattered wave vectors are equal $(k_{i1} - k_{i2} = k_{s1} - k_{s2})$. This necessary condition is identical to that derived within the Kirchhoff approximation[12] and may be interpreted as the law giving the angular rotation of the speckle pattern when the angle of incidence is varied.[13]

Next we consider the case in which a Gaussian beam with a fixed transverse width w illuminates the surface. When the incident plane wave $\exp[ikx_1 - i\alpha(k)x_3]$ is multiplied by $\{\omega w/[2\sqrt{\pi}c\alpha(k_i)]\}\exp(-\{(\omega/c)w(k - k_i)/[2\alpha(k_i)]\}^2)$ and integrated over all k, the scalar field of Eq. (1) is obtained with a good accuracy.[7] The amplitude

correlation for Gaussian incident beams then becomes

$$\langle r_\alpha(\theta_{s1}) r_\beta^*(\theta_{s2})\rangle = \frac{1}{4\pi}\left(\frac{\omega w}{c}\right)^2 \frac{1}{\alpha(k_{i1})\alpha(k_{i2})} \times \int_{-\infty}^{\infty} dk_1 \int_{-\infty}^{\infty} dk_2 \exp\left[-\left(\frac{\omega w}{2c}\right)^2 \frac{(k_1 - k_{i1})^2}{\alpha^2(k_{i1})}\right] \times \exp\left[-\left(\frac{\omega w}{2c}\right)^2 \frac{(k_2 - k_{i2})^2}{\alpha^2(k_{i2})}\right] \times \delta[(k_1 - k_{s1}) - (k_2 - k_{s2})] C_{\alpha\beta}(k_1, k_2, k_{s1}). \quad \text{(A6)}$$

Next we assume that the correlation function is nearly constant over the angular width of the Gaussian spectrum $\lambda \cos\theta_i/w$. This is equivalent to the assumption that the angular width of the speckle is much smaller than the angular width of the correlation; the results of Section 3 justify this assumption. It follows that $C_{\alpha\beta}(k_{i1}, k_{i2}, k_{s1})$ may be factored out of the integral in Eq. (A6), which may then be performed exactly. The resulting approximation for the amplitude correlation function may be written as

$$\langle r_\alpha(\theta_{s1}) r_\beta^*(\theta_{s2})\rangle = \frac{\omega}{c}\frac{w}{2\sqrt{\pi}} \frac{\exp\{-(\omega w/2c)^2[(k_{i1} - k_{s1}) - (k_{i2} - k_{s2})]^2/[\alpha^2(k_{i1}) + \alpha^2(k_{i2})]\}}{[\alpha^2(k_{i1}) + \alpha^2(k_{i2})]^{1/2}} C_{\alpha\beta}(k_{i1}, k_{i2}, k_{s1}). \quad \text{(A7)}$$

In the limit as $\lambda \cos\theta_i/w \ll 1$, the necessary condition for scattering amplitudes to be correlated is still $k_{i1} - k_{s1} = k_{i2} - k_{s2}$, or $k_{i1} - k_{i2} = k_{s1} - k_{s2}$. Equation (A7) also indicates that

$$\langle r_\alpha(\theta_{s1}) r_\beta^*(\theta_{s2})\rangle = \exp\left\{-\left(\frac{\omega w}{2c}\right)^2 \times \frac{[(\sin\theta_{i1} - \sin\theta_{s1}) - (\sin\theta_{i2} - \sin\theta_{s2})]^2}{\cos^2\theta_{i1} + \cos^2\theta_{i2}}\right\} \times \langle r_\alpha(\theta_{s1}) r_\beta^*(\tilde{\theta}_{s2})\rangle, \quad \text{(A8)}$$

where

$$\sin\theta_{i1} - \sin\theta_{s1} = \sin\theta_{i2} - \sin\tilde{\theta}_{s2}. \quad \text{(A9)}$$

Finally, with Eq. (12) the correlation function of the polarized scattering amplitude in the case of incoming Gaussian beams with fixed width becomes

$$\langle A(\theta_{s1}, \beta_1 | \theta_{i1}, \alpha_1) A^*(\theta_{s2}, \beta_2 | \theta_{i2}, \alpha_2)\rangle = \exp\left\{-\left(\frac{\omega w}{2c}\right)^2 \frac{[(\sin\theta_{i1} - \sin\theta_{s1}) - (\sin\theta_{i2} - \sin\theta_{s2})]^2}{\cos^2\theta_{i1} + \cos^2\theta_{i2}}\right\} \times \langle A(\theta_{s1}, \beta_1 | \theta_{i1}, \alpha_1) A^*(\tilde{\theta}_{s2}, \beta_2 | \theta_{i2}, \alpha_2)\rangle, \quad \text{(A10)}$$

where α_i and β_j $(i, j = 1, 2)$ can be any one of the polarization indices p, s, $+$, $-$, R, and L.

The behavior of $\langle A(\theta_{s1}, \beta_1 | \theta_{i1}, \alpha_1) A^*(\theta_{s2}, \beta_2 | \theta_{i2}, \alpha_2)\rangle$ when the roles of the incoming and the outgoing directions are reversed in the second scattering amplitude is considered next. Under such a transformation, the scattering amplitude for an incident plane wave $r_\alpha(\theta_s | \theta_i)$ $(\alpha = p, s)$ remains invariant according to the reciprocity condition,[24] which is a consequence of time-reversal symmetry. However, this condition does not hold when the scattering amplitude concerns an incident Gaussian beam scattering into a plane wave of the angular spectrum. Nevertheless, we present here a consequence of the reciprocity condition that is used in Section 4. Starting with the reciprocity condition $r_\alpha(\theta_s | \theta_i) = r_\alpha(-\theta_i | -\theta_s)$, Eq. (A6) is used to compare $\langle r_\alpha(\theta_{s1} | \theta_{i1}) r_\beta^*(\theta_{s2} | \theta_{i2})\rangle$ with $\langle r_\alpha(\theta_{s1} | \theta_{i1}) r_\beta^*(-\theta_{i2} | -\theta_{s2})\rangle$. The identity $C_{\alpha\beta}(k_{i1}, k_{i2}, k_{s1}) = C_{\alpha\beta}(k_{i1}, -k_{s2}, k_{s1})$ is obtained, and Eqs. (12) and (A7) may be used to derive the identities

$$\begin{aligned}(\cos^2\theta_{i1} + \cos^2\theta_{i2})^{1/2}&\langle A(\theta_{s1}, \beta_1 | \theta_{i1}, \alpha_1) A^*(\theta_{s2}, \beta_2 | \theta_{i2}, \alpha_2)\rangle \\ &= (\cos^2\theta_{i1} + \cos^2\theta_{s2})^{1/2}\langle A(\theta_{s1}, \beta_1 | \theta_{i1}, \alpha_1) \\ &\quad \times A^*(-\theta_{i2}, \beta_2 | -\theta_{s2}, \alpha_2)\rangle \\ &= (\cos^2\theta_{s1} + \cos^2\theta_{i2})^{1/2}\langle A(-\theta_{i1}, \beta_1 | -\theta_{s1}, \alpha_1) \\ &\quad \times A^*(\theta_{s2}, \beta_2 | \theta_{i2}, \alpha_2)\rangle. \end{aligned} \quad \text{(A11)}$$

A manifestation of the reciprocity condition in the correlation of the scattering amplitudes for incoming Gaussian beams is thus established.

ACKNOWLEDGMENT

This research was supported by the U.S. Army Research Office.

REFERENCES AND NOTES

1. E. R. Méndez and K. A. O'Donnell, "Observation of depolarization and backscattering enhancement in light scattering from Gaussian random surfaces," Opt. Commun. **61**, 91–95 (1987).
2. K. A. O'Donnell and E. R. Méndez, "Experimental study of scattering from characterized random surfaces," J. Opt. Soc. Am. A **4**, 1194–1205 (1987).
3. M.-J. Kim, J. C. Dainty, A. T. Friberg, and A. J. Sant, "Experimental study of enhanced backscattering from one- and two-dimensional surfaces," J. Opt. Soc. Am. A **7**, 569–577 (1990).
4. A. J. Sant, J. C. Dainty, and M.-J. Kim, "Comparison of surface scattering between identical, randomly rough metal and dielectric diffusers," Opt. Lett. **14**, 1183–1185 (1989).
5. M. E. Knotts and K. A. O'Donnell, "Anomalous scattering from a perturbed grating," Opt. Lett. **15**, 1485–1487 (1990).
6. K. A. O'Donnell and M. E. Knotts, "The polarization dependence of scattering from one-dimensional rough surfaces," J. Opt. Soc. Am. A **8**, 1126–1131 (1991).
7. A. A. Maradudin, T. Michel, A. R. McGurn, and E. R. Méndez, "Enhanced backscattering of light from a random grating," Ann. Phys. (N.Y.) **203**, 255–307 (1990).
8. Ya-Qiu Jin and M. Lax, "Backscattering enhancement from a randomly rough surface," Phys. Rev. B **42**, 9819–9829 (1990).
9. P. Tran, A. A. Maradudin, and V. Celli, "Backscattering enhancement from a dielectric surface," J. Opt. Soc. Am. B **8**, 1526–1530 (1991).
10. A. Ishimaru and J. S. Chen, "Scattering from very rough metallic and dielectric surfaces: a theory based on the modified Kirchhoff approximation," Waves Random Media **1**, 21–34 (1991).
11. T. R. Michel, M. E. Knotts, and K. A. O'Donnell, "Stokes matrix of a one-dimensional perfectly conducting rough surface," J. Opt. Soc. Am. A **9**, 585–596 (1992).
12. H. M. Pedersen, "Second-order statistics of light diffracted from Gaussian rough surfaces with applications to the roughness dependence of speckles," Opt. Acta **22**, 523–535 (1975).
13. D. Léger, E. Mathieu, and J. C. Perrin, "Optical surface

roughness determination using speckle correlation techniques," Appl. Opt. **14**, 872–877 (1975).
14. D. Léger and J. C. Perrin, "Real-time measurement of surface roughness by correlation of speckle patterns," J. Opt. Soc. Am. **66**, 1210–1217 (1976).
15. There is a typographical error in Eq. (14) of Ref. 14: the correlation length T in the argument of the exponential should be squared.
16. S. Feng, C. Kane, P. A. Lee, and A. D. Stone, "Correlations and fluctuations of coherent wave propagation through disordered media," Phys. Rev. Lett. **61**, 834–837 (1988).
17. I. Freund and M. Rosenbluh, "Memory effect in propagation of optical waves through disordered media," Phys. Rev. Lett. **61**, 2328–2331 (1988).
18. L. Wang and S. Feng, "Correlations and fluctuations in reflection coefficients for coherent wave propagation in disordered scattering media," Phys. Rev. B **40**, 8284–8289 (1989).
19. R. Berkovits, M. Kaveh, and S. Feng, "Memory effect of waves in disordered systems: a real-space approach," Phys. Rev. B **40**, 737–740 (1989).
20. I. Freund, M. Rosenbluh, and R. Berkovits, "Geometric scaling of the optical memory effect i: coherent-wave propagation through random media," Phys. Rev. B **39**, 12403–12406 (1989).
21. R. Berkovits and M. Kaveh, "Time-reversed memory effects," Phys. Rev. B **41**, 2635–2638 (1990).
22. R. Berkovits and M. Kaveh, "The vector memory effect for waves," Europhys. Lett. **13**, 97–101 (1990).
23. J. D. Jackson, *Classical Electrodynamics* (Wiley, New York, 1975), pp. 269–278.
24. D. Maystre, O. Mata-Mendez, and A. Roger, "A new electromagnetic theory for scattering from shallow rough surfaces," Opt. Acta **30**, 1707–1723 (1983).
25. W. C. Meecham, "On the use of the Kirchhoff approximation for the solution of reflection problems," J. Rat. Mech. Anal. **5**, 323–333 (1956).
26. E. G. Liszka and J. J. McCoy, "Scattering at a rough boundary—extension of the Kirchhoff approximation," J. Acoust. Soc. Am. **71**, 1093–1100 (1982).
27. See, for example, A. A. Maradudin, E. R. Méndez, and T. Michel, "Backscattering effects in the elastic scattering of p-polarized light from a large-amplitude random grating," in *Scattering in Volumes and Surfaces*, M. Nieto-Vesperinas and J. C. Dainty, eds. (North-Holland, Amsterdam, 1990), pp. 157–174.
28. A. A. Maradudin and T. Michel, "The transverse correlation correlation length for randomly rough surfaces," J. Stat. Phys. **58**, 485–501 (1990).
29. G. S. Brown, "A stochastic Fourier transform approach to scattering from perfectly conducting randomly rough surfaces," IEEE Trans. Antennas Propag. **AP-30**, 1135–1143 (1982).
30. G. S. Brown, "Simplifications in the stochastic Fourier transform approach to random surface scattering," IEEE Trans. Antennas Propag. **AP-33**, 48–55 (1985).

Angular correlation functions of polarized intensities scattered from a one-dimensionally rough surface

M. E. Knotts, T. R. Michel, and K. A. O'Donnell

The School of Physics, Georgia Institute of Technology, Atlanta, Georgia 30332

Received January 30, 1992; accepted April 16, 1992; revised manuscript received May 8, 1992

Experimental results are presented for the angular correlation functions of far-field intensity scattered by a conducting, one-dimensionally rough surface that produces backscattering enhancement. A detailed study of the special case of equal incident and scattering angles is presented, in which it is found that the intensity correlation functions exhibit two distinct and equal maxima, both of which imply perfect correlation within experimental accuracies. One of these is an autocorrelation peak, and the second peak arises from the cross correlation between two distinct intensities related by a reciprocity condition. It is found that, if the rough surface is illuminated by a +45° polarization state, the angular correlation functions of scattered intensity polarized at −45° have broad structures that are interpreted as arising from single-scattering processes. The scattered intensity polarized at +45° has quite different correlation functions whose properties are attributed to multiple-scattering processes; this interpretation is based on generalizations of arguments presented in previous studies of backscattering enhancement. In support of these conclusions, rigorous theoretical results for the angular correlation functions of scattered amplitude are presented.

1. INTRODUCTION

The scattering of light by randomly rough surfaces has been of considerable recent interest. For conducting surfaces with steep slopes and roughness comparable with the illumination wavelength, backscattering enhancement has been observed in reflective scattering.[1,2] This phenomenon manifests itself as a well-defined peak in the retroreflection direction in the angular distribution of the scattered light. For a surface rough in one dimension, these peaks are apparent in the *p*- and *s*-polarized mean scattered intensities.[3–15] A more comprehensive description can be found in the Stokes matrix of the scatterer, which contains the second-order moments of the *p*- and *s*-polarized scattered amplitudes.[16,17] These effects have been interpreted as arising from the ensemble-averaged interference between multiple-scattering paths on the rough surface.

Although the most obvious consequence of multiple scattering has been backscattering enhancement, there may be equally significant effects on other fundamental quantities such as the correlation functions of scattered amplitude or intensity. These correlation functions have been of wide interest in studies of laser speckle phenomena,[18] in which single-scattering models have been applied to surface scattering. Nevertheless, the effect of multiple scattering on these basic quantities has not been widely addressed.

The far-field scattering properties of rough surfaces have been a central issue, so that it is of interest to investigate the angular correlation functions of the scattered light. We thus ask the fundamental questions: When will the amplitudes (or intensities) scattered into the far field for different incident and scattering angles be correlated with one another, and what form will these correlation functions take? Even assuming a reasonable statistical model of the surface roughness (such as a statistically stationary random process with well-behaved probability densities), rigorous answers to these questions appear to be quite difficult. In the context of speckle theory, previous studies of the angular correlation functions have been presented by Pedersen[19] and by Léger and Perrin,[20] who have applied the theoretical approach to surface scattering that is due to Beckmann and Spizzichino.[21] Although these authors derive relatively straightforward expressions for the angular correlation functions, the results are limited to single scattering because of the assumptions of the Beckmann theory.

In what follows, we present measurements of the angular correlation functions of the intensity scattered by a one-dimensionally rough surface that produces backscattering enhancement. We show experimentally that the far-field scattered intensity may be effectively perfectly correlated for quite different angles of illumination, as long as the two scattering angles involved satisfy a reciprocity condition. At other angles we find a smaller but generally nonzero correlation between the two intensities, if the four incident and scattering angles involved satisfy a condition discussed by Pedersen[19] and by Léger and Perrin.[20] Further, depending on the polarization component of the scattered field that is measured, it is shown that different forms of the intensity correlation functions are found. It is argued that intensity correlation functions consistent with either single or multiple scattering may be observed and that these correlation functions provide considerable insight into the scattering processes occurring on a rough surface.

We also note that the results presented here have counterparts in recent studies of the angular correlation functions of intensity scattered by disordered volume media. The intensity correlation functions have been investigated by using approximate theoretical approaches that incorporate multiple scattering,[22–24] and some experimental results have been presented.[25,26] In this field there are also theoretical studies of the consequences of reciprocity[27] and polarization[28] that parallel experimental results presented

0740-3232/92/101822-10$05.00

in this paper. Despite these similarities, the theoretical approaches as well as the form of the intensity correlation functions are quite different from those found in surface scattering.

Finally, it is important to note that a theoretical study of the angular correlation functions of amplitudes scattered from a perfectly conducting rough surface has recently been reported[29] that is highly relevant to the experimental results presented here. In particular, the significance of polarization, reciprocity, and multiple scattering in the correlation functions of amplitude is addressed theoretically in Ref. 29, much as discussions here consider the role of these phenomena in the experimental measurements. The correlation condition presented here [Eq. (3) in Section 2] and the effect of a finite illuminating beam are also investigated rigorously in Ref. 29. As is discussed here in Sections 3 and 5, the relation between the theoretical correlation functions of amplitude and the experimental ones of intensity is expressed quite simply by the Gaussian moment theorem.

2. DISCUSSION

As Fig. 1 shows, consider a one-dimensional rough surface illuminated by a wave incident at angle θ_i. Let $A_\alpha(\theta_i,\theta_s)$ represent the α-polarization component of the amplitude scattered to angle θ_s in the far field. The general angular correlation function of scattered amplitude may be written in the form

$$C_{\alpha\beta}(\theta_{i1},\theta_{s1},\theta_{i2},\theta_{s2}) = \langle A_\alpha(\theta_{i1},\theta_{s1})A_\beta^*(\theta_{i2},\theta_{s2})\rangle, \qquad (1)$$

where the angle brackets denote an average over an ensemble of surfaces. If α and β represent the p- and s-polarization components, these quantities reduce to the elements of the Stokes matrix in the special case $(\theta_{i1},\theta_{s1}) = (\theta_{i2},\theta_{s2})$,[16,17] so that Eq. (1) is clearly a more general moment of the scattered amplitudes.

The other properties of Eq. (1) are not immediately obvious, and it is important to determine for what other angles the scattered amplitudes may be significantly correlated. Some previous work may give insight into this question. Using scattering models that neglect polarization and assuming angles to be small, it has been shown in investigations of laser speckle[18] that, if $\theta_{i1} = \theta_{i2}$, a correlation exists in the scattered field when

$$|\theta_{s1} - \theta_{s2}| \le \lambda/w, \qquad (2)$$

where w is the illuminated width of the surface and λ is the wavelength. In more general analyses based on the Beckmann approach to surface scattering,[21] Pedersen[19] and also Léger and Perrin[20] have investigated moments of the form of Eq. (1). Pedersen's results, when applied to a one-dimensionally rough surface, imply that a correlation can be found only for angles satisfying

$$\sin(\theta_{i1}) - \sin(\theta_{s1}) = \sin(\theta_{i2}) - \sin(\theta_{s2}) \qquad (3)$$

and that a correlation will exist as long as this equality is not violated by more than λ/w. This result may thus be considered a generalization of relation (2) to arbitrary incident and scattering angles. Léger and Perrin[20] have used a similar approach and have calculated the amplitude correlation function in the large surface roughness limit. Although the results of Léger and Perrin are written explicitly for their case of interest (when changes in θ_i and θ_s are small), their results are applicable to general angles and are entirely consistent with Eq. (3).

There are a number of restrictive assumptions in the analyses of Ref. 19 and 20 that lead to Eq. (3). For example, the surface height statistics are assumed to be Gaussian, there is neglect of depolarization, and there are other assumptions associated with the Beckmann theory (for example, the neglect of multiple scattering and shadowing). However, in recent work based on completely rigorous theoretical methods, it has been shown that Eq. (3) is a necessary condition for a correlation to exist for a perfectly conducting rough surface.[29] Thus Eq. (3) has provided the choice of angles used in the experimental work of Section 4, even though, to the best of our knowledge, a proof of this correlation condition for a penetrable surface has not been presented in previous work. In any case, it is certainly true that, in the experiments described in Section 4, correlations (in the scattered intensities) were found only for angles obeying Eq. (3).

With the assumptions mentioned above, Léger and Perrin showed that, for angles satisfying Eq. (3), the amplitude correlation function takes on an exponential form that, at least in their cases of interest, is a smoothly decaying curve when plotted as a function of $(\theta_{i1} - \theta_{i2})$. The purpose of the present paper is to investigate analogous correlation functions when the surface causes multiple scattering and depolarization, which is a regime well beyond the limitations of the Beckmann theory.

3. EXPERIMENTAL PROCEDURE

Although it is possible to measure the angular correlation functions of the scattered amplitudes by using interferometric methods,[20] we have employed simpler means to measure the correlation functions of the fluctuations of scattered intensity. Of fundamental interest in such experiments is the quantity

$$\Gamma_{\alpha\beta}(\theta_{i1},\theta_{s1},\theta_{i2},\theta_{s2}) = \langle \Delta I_\alpha(\theta_{i1},\theta_{s1})\Delta I_\beta(\theta_{i2},\theta_{s2})\rangle, \qquad (4)$$

where ΔI_α denotes the fluctuations of the α-polarized intensity about the mean. If the illuminated area contains many correlation cells of the surface, it is commonly assumed that the Gaussian factorization theorem may be applied.[18,19] Applying this to the moment of Eq. (4) results in

$$\Gamma_{\alpha\beta}(\theta_{i1},\theta_{s1},\theta_{i2},\theta_{s2}) = |\langle A_\alpha(\theta_{i1},\theta_{s1})A_\beta^*(\theta_{i2},\theta_{s2})\rangle|^2, \qquad (5)$$

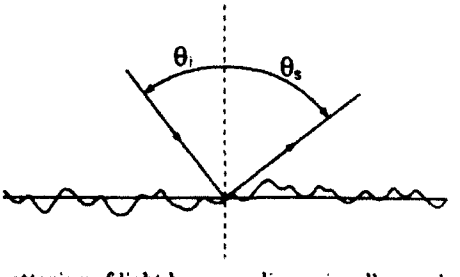

Fig. 1. Scattering of light by a one-dimensionally rough surface. The incident and scattering angles θ_i and θ_s are positive as shown.

so that the intensity correlation function is trivially related to that of the scattered amplitudes. In the experiments discussed below, we thus consider correlations between intensities for incident and scattering angles related through Eq. (3) because Eq. (5) then implies that these angles will produce the only significant correlation.

We have chosen to consider the correlation function of intensity such that one intensity corresponds to the symmetric situation $\theta_{i1} = \theta_{s1}$, which, from Eq. (3), implies that a correlation will be found only with other symmetric intensities with $\theta_{i2} = \theta_{s2}$. We have also employed polarization conditions that, for a highly conductive one-dimensional surface, isolate the single- and multiple-scattering contributions to the scattered intensity. It has been shown that, if the surface is illuminated with a +45° incident polarization state (equal p and s amplitudes), the mean scattered intensity with −45° polarization contains contributions from single scattering, while the mean intensity with +45° polarization contains contributions from double scattering.[16,17] Thus, to investigate the distinct effects of single and double scattering on the intensity correlation functions, we have chosen to measure

$$\Gamma_{++}(\theta_{i1},\theta_{i1},\theta_{i2},\theta_{i2}) = \langle \Delta I_{+}(\theta_{i1},\theta_{i1})\Delta I_{+}(\theta_{i2},\theta_{i2})\rangle, \quad (6)$$

$$\Gamma_{--}(\theta_{i1},\theta_{i1},\theta_{i2},\theta_{i2}) = \langle \Delta I_{-}(\theta_{i1},\theta_{i1})\Delta I_{-}(\theta_{i2},\theta_{i2})\rangle, \quad (7)$$

where the subscripts denote the ±45° detected polarization state and it is implicit that the +45° polarization state is incident.

The rough surface was strictly one dimensional and was fabricated in photoresist by using speckle-exposure techniques. A 50 mm × 50 mm glass plate was spin coated with three layers of Shipley 1375 photoresist. The prepared plate was exposed to laser speckle patterns from a He–Cd laser operating at 0.442-μm wavelength and then was developed in Shipley 355 developer. As has been discussed in more detail elsewhere,[2,30] exposure to a large number of independent speckle patterns leads to a surface with nearly Gaussian height statistics; further, the Gaussian beam of the laser produces a height correlation function of Gaussian form. After the surface was developed, it was coated with 145 nm of gold, and its roughness was measured with a Talystep profilometer with a small chisel-shaped diamond stylus. A total of 20 scans of independent parts of the surface were made, with each scan consisting of 8192 data points taken at 0.23-μm intervals. The surface height was found to have 1.73-μm standard deviation and a correlation function of nearly Gaussian form with $1/e$ half-width $a = 3.43$ μm. The histogram of surface heights also provided a reasonable fit of the desired Gaussian form (coefficient of skewness, −0.19; kurtosis, 2.90).

A simplified diagram of the scattering experiment is shown in Fig. 2. A laser beam from a Jodon HN-20 He–Ne laser of wavelength $\lambda = 1.152$ μm was reflected from a series of mirrors and was incident upon the rough surface; the plane of incidence was kept perpendicular to the surface groove direction. The beam was focused to a waist of $1/e$ intensity diameter $D = 230$ μm on the rough surface (as estimated from the measured rate of speckle decorrelation with transverse sample motion). Both the rough surface and a detector arm were mounted upon computer-controlled rotation stages that allowed the incident and scattering angles to be set as required. A polarizer in the incident beam produced a +45° polarized incident state, and the detector polarizer could be set to ±45° polarization positions.

A field lens imaged the surface onto the detector element so that all power passing through the lens aperture would be detected. In the lens aperture was a slit of 150-μm width and 2.0-mm vertical length. The narrow slit resolved the (effectively one-dimensional) speckles of the scattered field in the sense that, at the distance R of the field lens from the surface ($R = 700$ mm), the width of the slit was much smaller than the speckle size ($\lambda R/D \approx 3.5$ mm). The scattered light was detected by a cooled indium antimonide photodiode connected to a lock-in amplifier (Ithaco 3981), which served to reject ambient signals and other noise.

The correlation functions were determined by measuring a set of realizations of the intensity for a particular pair of incident and scattering angles, recording the data on a computer's hard disk, and later cross correlating this data set with analogous data taken for other incident and scattering angles. To achieve this, we first set the sample and detector stages to an initial pair of angles (θ_i, θ_s) and recorded the detected intensity. The sample was then moved by an amount Δx in a direction parallel to the surface roughness, and the corresponding new value of the scattered intensity was recorded. The stepping of the sample was repeated many times with the use of a computer-controlled linear translation stage, so that a finite ensemble of detected intensities was generated and then recorded on the computer disk. The incident and scattering angles were then changed to new values, the sample translator was reset to its starting coordinate, and the process was repeated. After this had been performed for all desired incident and scattering angles, the correlations between the sets of data were determined through direct computation.

The sample step size Δx that was used was 125 μm, which was found to provide an approximately 0.5 correlation coefficient between consecutive intensity measurements. The length of the surface that was used was limited by the range of the linear translator (26.5 mm), so that 212 intensities were generated for each pair of incident and scattering angles. Measurements of the inten-

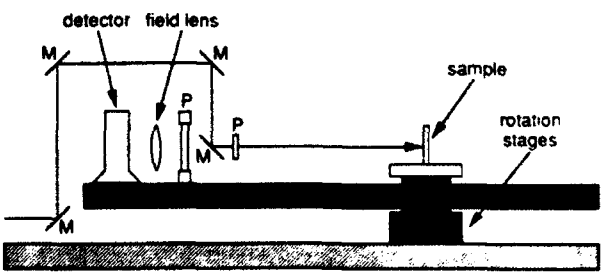

Fig. 2. Scattering experiment used to measure the angular correlation functions of intensity scattered from the rough surface. The incident beam was reflected by a series of mirrors (M's), passed through a polarizer (P) that produced a +45° polarization state, and was then incident upon the rough surface. One may rotate the surface about the vertical axis to determine the incident angle θ_i and rotate the detector arm out of the plane of the figure to determine the detected scattering angle θ_s. A slit of 150-μm width (not shown) was mounted immediately in front of the field lens.

sity I_- were performed for 82 pairs of angles (θ_i, θ_s) between $(-36°, -36°)$ and $(36°, 36°)$, and measurements of I_- were performed for 40 pairs of angles between $(-40°, -40°)$ and $(40°, 40°)$. The particular angles employed were chosen to provide adequate sampling of the correlation functions.

There were a number of critical practical concerns in this experiment. Considerable care was exercised in centering the incident beam upon the rotation axis of the sample stage as well as in aligning the plane of the rough surface with the sample rotation axis. Misadjustments of either of these parameters by as little as a few tens of micrometers would lead to an undesired decorrelation of the scattered intensity because different parts of the surface would be illuminated as the sample was rotated. Other crucial aspects of the experimental alignment were the angular orientation of the sample, determination of the polarization angles, and the adjustment of the detector's rotation stage with respect to the incident beam. After much effort was expended on such considerations, it was found that the system remained in alignment and that adjustments were not required during the extended experiment required to produce the results discussed in Section 4.

4. EXPERIMENTAL RESULTS

Before the correlation functions are presented, in Fig. 3 are shown the mean scattered intensities $\langle I_+(\theta_i, \theta_s)\rangle$ and $\langle I_-(\theta_i, \theta_s)\rangle$ obtained from averaging the data sets. There is a distinct backscattering structure in $\langle I_+(\theta_i, \theta_s)\rangle$ with secondary maxima at $\pm 7.0°$. The intensity $\langle I_-(\theta_i, \theta_s)\rangle$ does not exhibit such effects but instead has a weak maximum near 0° and then gradually rises to modest secondary maxima at $\pm 15.0°$. These data have been normalized in the sense that $I_\pm(\theta_i, \theta_s)\Delta\theta$ represents the polarized power scattered into a differential scattering angle $\Delta\theta$ for an incident power of unity. It is significant that this presentation of the mean scattered intensities is different from that of most previous work, where the intensities have been studied as a function of θ_s for a fixed value of θ_i.[1-17] Although we do not show these results here, the scattered intensities and Stokes matrix elements of this surface, when plotted in the usual fashion, qualitatively resemble those reported for a different surface.[16]

We first present the intensity correlation functions when one of the intensities corresponds to a relatively large incident angle. In Fig. 4 we show $\Gamma_{--}(\theta_{i1}, \theta_{i1}, \theta_{i2}, \theta_{i2})$ and $\Gamma_{+-}(\theta_{i1}, \theta_{i1}, \theta_{i2}, \theta_{i2})$ as a function of θ_{i2} for $\theta_{i1} = 25.0°$. It can be clearly seen that each curve has a pair of distinct maxima. The maximum at $\theta_{i2} = 25.0°$ obviously arises where an intensity is being correlated with itself. The other maximum falls where $I_\pm(25°, 25°)$ is correlated with $I_\pm(-25°, -25°)$, which corresponds to a reciprocal scattering configuration. The correlation coefficient of intensity ρ at $\theta_{i2} = 25.0°$ is obviously unity, while at $\theta_{i2} = -25.0°$ we find a strong recorrelation with $\rho = 0.91$ for both I_+ and I_-.

The peak at $\theta_{i2} = -25.0°$, as well as the overall symmetry of the correlation functions, is related to the reciprocity condition of scattering theory,[31] which follows from the time-reversal symmetry of Maxwell's equations. Reciprocity may be expressed as follows: if a scatterer is illuminated with a polarized plane wave and gives rise to a scattered amplitude at a point in the far field, this amplitude is identical to that obtained by exchanging the incident and scattered wave vectors.[32] Hence, for a given realization of a rough surface, the scattered amplitude for angles (θ_i, θ_s) is expected to be completely identical to that obtained for the angles $(-\theta_s, -\theta_i)$. Consequently one would expect not only the two distinct peaks in the intensity correlation functions of Fig. 4 but also the symmetry that is apparent throughout these results. Reciprocity also implies that even the residual statistical noise in the measured correlation functions should also be symmetric; this symmetry is evident in the small fluctuations that appear to be noise in Fig. 4.

The statement of reciprocity above does not strictly apply to the experimental situation. In the experiment the surface is illuminated not with a plane wave but with a beam, and we are detecting the scattered intensity integrated over the angular width of the detection slit rather than the intensity at a point in the far field. However, we may still surmise from our results that the symmetry of the experimental situation is entirely adequate to demonstrate the consequences of reciprocity in the near-perfect symmetry of Γ_{--} and Γ_{+-} in Fig. 4. We also attribute any small departures from perfect correlation between an intensity and its reciprocal counterpart as being due to residual alignment errors, although our results clearly demonstrate that these are small. In any case, the manifestation of reciprocity in the experimental results is remarkably consistent with fundamental considerations.

It is otherwise clear in Fig. 4 that the peaks in Γ_{--} are of ~7° full width (as measured at the half-maximum point), and there is nearly complete decorrelation of the

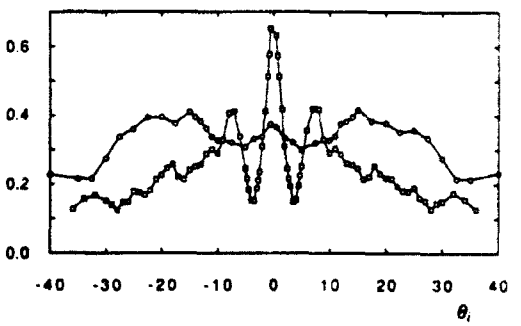

Fig. 3. Mean scattered intensities $\langle I_-(\theta_i, \theta_s)\rangle$ (circles) and $\langle I_+(\theta_i, \theta_s)\rangle$ (squares) obtained by direct averaging of the data.

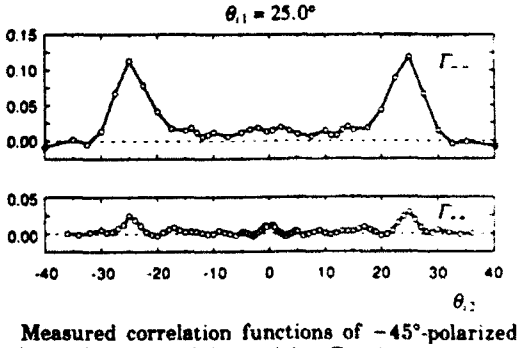

Fig. 4. Measured correlation functions of −45°-polarized and +45°-polarized scattered intensities $\Gamma_{--}(\theta_{i1}, \theta_{i1}, \theta_{i2}, \theta_{i2})$ and $\Gamma_{+-}(\theta_{i1}, \theta_{i1}, \theta_{i2}, \theta_{i2})$ for $\theta_{i1} = 25.0°$. The autocorrelation and reciprocal peaks are present at $\theta_{i2} = 25.0°$ and $\theta_{i2} = -25.0°$, respectively.

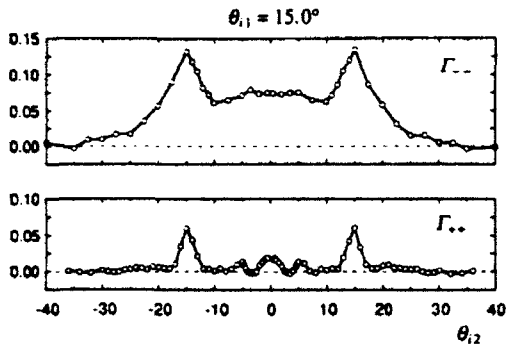

Fig. 5. Measured correlation functions of −45°-polarized and +45°-polarized scattered intensities $\Gamma_{--}(\theta_{i1},\theta_{i1},\theta_{i2},\theta_{i2})$ and $\Gamma_{++}(\theta_{i1},\theta_{i1},\theta_{i2},\theta_{i2})$ for $\theta_{i1} = 15.0°$. The autocorrelation and reciprocal peaks are present at $\theta_{i2} = 15.0°$ and $\theta_{i2} = -15.0°$, respectively, and some overlap may now be seen between the two peaks of Γ_{--}.

intensity for angles $|\theta_{i2}| < 15°$. The correlation function Γ_{++} has analogous behavior with smaller heights and angular widths. We believe that the small structure present in Γ_{++} near 0° is due to the noise in the measurements, which is significant there because $\langle I_+(\theta_{i2},\theta_{i2})\rangle$ is large in this region, although we cannot conclusively justify this in view of the noise levels present after 212 realizations of the scattered intensities. The normalization of the correlation functions in Fig. 4 (and in following figures) is such that the mean intensities are normalized as in Fig. 3, and the smaller height of the peaks in Γ_{++} then only implies that $\langle I_+(\theta_{i2},\theta_{i2})\rangle$ is smaller than $\langle I_-(\theta_{i2},\theta_{i2})\rangle$, which is apparent in Fig. 3.

Making use of the same sets of intensity data, we have studied the form of the intensity correlation functions as θ_{i1} decreases from 25.0° to nearly 0°, in which case the intensities are correlated with a backscattered intensity. In what follows, only the most significant results are shown. When θ_{i1} reaches 15.0° we have the result shown in Fig. 5. There are forward and reciprocal correlation peaks present in both correlation functions at $\theta_{i2} = \pm 15.0°$; the correlation coefficient ρ of the reciprocal peak is 0.99 and 0.98 for I_+ and I_-, respectively. The forward and reciprocal parts of Γ_{--} are no longer completely distinct as was found for Fig. 4, and this correlation function remains significantly nonzero near $\theta_{i2} = 0°$. The correlation function Γ_{++} has a greater height than in Fig. 4 but has remained fairly narrow (2.5° full width at half-maximum), and the two peaks present have remained distinct from each other.

With a further decrease in θ_{i1}, similar results are found until the two peaks in Γ_{++} approach each other. At first, one finds that Γ_{++} increases in size near $\theta_{i2} = 0°$ for $\theta_{i1} \cong 10.0°$, and this central region continues to grow until the situation at $\theta_{i1} = 7.0°$ is reached as shown in Fig. 6. It can be seen that Γ_{++} has the forward and reciprocal peaks present as in the earlier figures with their maxima at $\theta_{i2} = \pm 7.0°$. It is remarkable that at intermediate angles the intensities completely decorrelate at $\theta_{i2} = \pm 4.0°$ and then significantly recorrelate near $\theta_{i2} = 0°$. We find at the reciprocal point that the intensities I_+ have a correlation coefficient $\rho = 0.95$, although this rapidly falls to $\rho = -0.08$ at the minima at $\theta_{i2} = \pm 4.0°$, and then ρ rises to nearly 0.50 in the central region of the maximum near $\theta_{i2} = 0°$. It is significant that the maximum height of the central lobe occurs when $\theta_{i1} = 7.0°$, which is the location of a secondary maximum of $\langle I_-(\theta_{i1},\theta_{i1})\rangle$ in Fig. 3. The correlation function Γ_{--} does not exhibit such dramatic behavior, and the progressive merging of the forward and reciprocal parts of the correlation function is apparent, although the two peaks at $\theta_{i2} = 7.0°$ are still distinct.

We find that the central lobe of Γ_{++} is reduced in height with further decrease in θ_{i1} until it disappears at $\theta_{i1} = 3.5°$, which is the case shown in Fig. 7. There is a pair of small maxima in Γ_{++} at the forward and reciprocal positions. At the reciprocal point the correlation coefficient of I_+ is $\rho = 0.98$, although this rapidly falls to $\rho = 0.03$ at $\theta_{i2} = -2.0°$, and this coefficient remains essentially zero until the forward lobe of the intensity correlation function is encountered near $\theta_{i2} = 3.5°$. It is significant that the angle $\theta_{i1} = 3.5°$ is the location of a minimum of $\langle I_-(\theta_{i1},\theta_{i1})\rangle$ in Fig. 3. Although there are these dramatic differences in Γ_{++} compared with Γ_{++} in Fig. 6, the other correlation function Γ_{--} continues to show modest changes in Fig. 7. It can be seen that Γ_{--} again exhibits a broad form with peaks at the forward and reciprocal positions, although the shape of the curve is unusual in that there are minima appearing at $\theta_{i2} = \pm 10.0°$.

As θ_{i1} is reduced further, a central peak with secondary maxima reappears in Γ_{++}, and for small θ_{i1} this central maximum becomes extremely strong. In Fig. 8 is shown

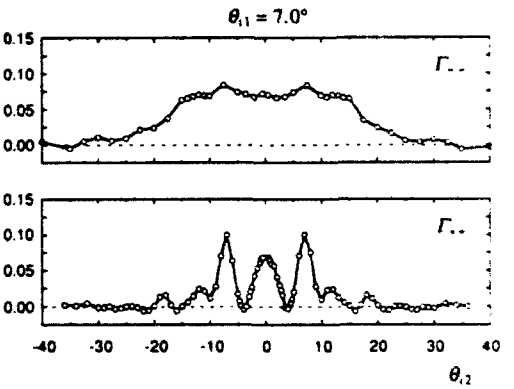

Fig. 6. Measured correlation functions of −45°-polarized and +45°-polarized scattered intensities $\Gamma_{--}(\theta_{i1},\theta_{i1},\theta_{i2},\theta_{i2})$ and $\Gamma_{++}(\theta_{i1},\theta_{i1},\theta_{i2},\theta_{i2})$ for $\theta_{i1} = 7.0°$, where there is significant interaction of the two peaks of Γ_{--}.

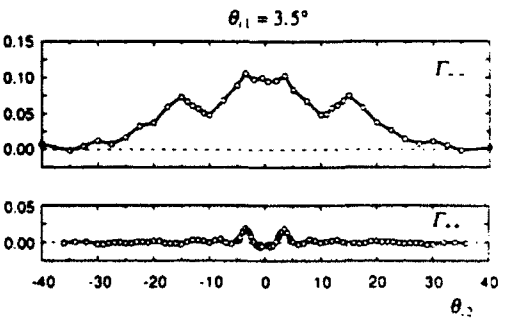

Fig. 7. Measured correlation functions of −45°-polarized and +45°-polarized scattered intensities $\Gamma_{--}(\theta_{i1},\theta_{i1},\theta_{i2},\theta_{i2})$ and $\Gamma_{++}(\theta_{i1},\theta_{i1},\theta_{i2},\theta_{i2})$ for $\theta_{i1} = 3.5°$. The central maximum present in Γ_{++} in Fig. 6 has completely disappeared, and only small autocorrelation and reciprocal peaks are present in Γ_{--}.

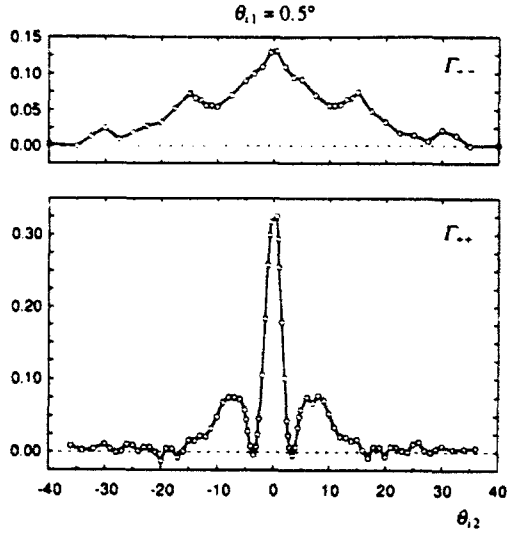

Fig. 8. Measured correlation functions of −45°-polarized and +45°-polarized scattered intensities $\Gamma_{--}(\theta_{i1},\theta_{i1},\theta_{i2},\theta_{i2})$ and $\Gamma_{-+}(\theta_{i1},\theta_{i1},\theta_{i2},\theta_{i2})$ for $\theta_{i1} = 0.5°$, which is the smallest useful angle in the experiment. On comparison with Fig. 7, Γ_{--} has completely changed form and exhibits a large central maximum, zeros at $\theta_{i2} = \pm 3.5°$, and significant recorrelation for larger $|\theta_{i2}|$.

the case $\theta_{i1} = 0.5°$, which is the smallest useful angle in the experiment before the final mirror in the incident beam in Fig. 2 obstructs the detector slit. There is again a remarkable change in the form of Γ_{--}, with a high central peak, a rapid fall effectively to zero at $\theta_{i2} = \pm 3.5°$, a recorrelation near $\theta_{i2} = \pm 8.0°$, and finally a more gradual decay for larger $|\theta_{i2}|$. The correlation coefficient of I_+ at the minima is found to be $\rho = -0.05$ at $\theta_{i2} = \pm 3.5°$, and this increases to approximately $\rho = 0.41$ at $\theta_{i2} = \pm 9.0°$. In contrast, the correlation function Γ_{-+} shows a modest change in form compared with Γ_{-+} in Fig. 7, and the nearly complete merging of the forward and reciprocal lobes seen in previous results is apparent.

At this point it is clear that the two intensities I_+ and I_- have completely different correlation functions, with the behavior of Γ_{--} being quite remarkable. To illustrate fully the properties of Γ_{--}, we show a three-dimensional plot of the experimental results in Fig. 9, where Γ_{++} is plotted as a function of θ_{i1} and θ_{i2}. The continuous change of form of Γ_{++} for θ_{i1} among the cases shown in Figs. 4–8 is made clear in Fig. 9. Along the line $\theta_{i2} = 0°$, the strong maximum at $\theta_{i1} = 0.5°$ can be seen to decay rapidly and disappear at $\theta_{i1} = 3.5°$, although this maximum reappears near $\theta_{i1} = 7.0°$, and then finally vanishes for large θ_{i1}. The secondary maxima at $\theta_{i2} = \pm 7.0°$ that are strong at $\theta_{i1} = 0.5°$ similarly vanish at $\theta_{i1} = 3.5°$ and return near $\theta_{i1} = 7.0°$. For θ_{i1} greater than ~10°, these secondary maxima are seen to evolve into the forward and reciprocal correlation peaks that are apparent along the lines $\theta_{i1} = \theta_{i2}$ and $\theta_{i1} = -\theta_{i2}$, respectively.

There are a number of general comments concerning the experiment that are appropriate. First, the average intensity contrast $\sigma_I/\langle I\rangle$ found in the experimental data was 0.92 for both I_+ and I_-. A contrast of unity is consistent with the Gaussian field assumption discussed in Section 3; the lower measured value may be attributed to the small effects of spatial integration of the detected intensity.[18] A significant related topic is the amount of statistical noise present in the measurements. This noise is directly related to the effective number of statistically independent intensity measurements used in the estimates of the correlation functions. More practically, it is then dependent on the length of the surface used in the experiment. As described in Section 3, this length was 26.5 mm because of the travel limit of a translation stage, although the statistically uniform region of the rough surface was only slightly larger than this. Hence the noise in our results is at the practical limit imposed by the severe difficulties encountered in the fabrication of photoresist surfaces with significantly larger uniform areas. From the higher-order moments of the detected intensities, we can also provide estimates of the signal-to-noise ratio of the measurements. We estimate the signal-to-noise ratio of the correlation functions of $I_\pm$ (as opposed to the correlation functions of $\Delta I_\pm$, which have zeros in places) to be 6.0, although this number varies by approximately ±1.0 throughout the correlation functions.

Although detailed data have been taken only for the symmetrical case $\theta_{i1} = \theta_{s1}$ and $\theta_{i2} = \theta_{s2}$, we have investigated asymmetrical cases. For example, we have confirmed experimental reciprocity for asymmetric conditions such as $(\theta_i, \theta_s) = (2.0°, 40.0°)$. We found that the reciprocal configuration generated a set of intensities that had a different mean but that was effectively perfectly correlated ($\rho > 0.9$) with the original one. We have also checked the correlation law of Eq. (3) for asymmetric intensities. Although we do not claim to have performed exhaustive tests of this correlation condition, statistically significant correlations have only been found for angles obeying Eq. (3), and other angles have not produced significant results.

5. DISCUSSION

In the experimental data discussed in Section 4, no statistically significant cross correlations between ΔI_+ and ΔI_- were found. This indicates that Γ_{++} and Γ_{--} are of principal importance for such a surface because the total scattered intensity for the +45° incident polarization state is

$$I = I_+ + I_-, \tag{8}$$

and the correlation function of ΔI may then be expressed

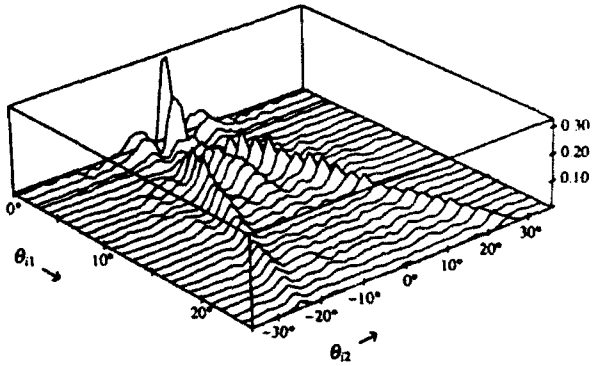

Fig. 9. Three-dimensional plot of the correlation function of +45°-polarized scattered intensity $\Gamma_{++}(\theta_{i1},\theta_{i1},\theta_{i2},\theta_{i2})$. The back face at the left is the result at $\theta_{i1} = 0.5°$ from Fig. 8, and the suppressed region at $\theta_{i1} = 3.5°$ is from Fig. 7. The evolution of the fringelike structures into the forward ($\theta_{i1} = \theta_{i2}$) and reciprocal ($\theta_{i1} = -\theta_{i2}$) parts of Γ_{++} is apparent for larger θ_{i1}.

as the sum of four terms. Two of these involve cross correlations of ΔI_+ and ΔI_- and are small, while the two significant terms are the correlation functions Γ_{++} and Γ_{--} of Section 4. The procedures used in Section 4 thus separate the two main parts of the correlation function of ΔI, presumably because they isolate the single- and double-scattering contributions to the total intensity.

It is also possible to interpret the different behavior of Γ_{++} and Γ_{--}. It has been found that Γ_{--} has broad forward and reciprocal lobes that progressively overlap one another as θ_{i1} approaches zero. To the extent that Γ_{--} is associated with single scattering, we may compare these observations with results for the angular correlation function of amplitudes predicted by the Beckmann theory, which predicts a perfect correlation between amplitudes at all angles of the symmetric case $(\theta_{i1}, \theta_{i2}) = (\theta_{s1}, \theta_{s2})$.[33] Thus the single-scattered amplitudes [and, from Eq. (5), the intensities] must decorrelate for subtle reasons that are beyond the mechanisms included in the Beckmann theory. For surfaces with steep slopes as in Section 4, a probable mechanism contributing to the decorrelation of ΔI_- is shadowing by the surface roughness,[34,35] which is a significant effect for angles where decorrelation is seen in Figs. 4–8.

The dramatic behavior observed in Γ_{++} in Figs. 4–9 may be interpreted as arising from multiple-scattering processes. While backscattering enhancement may be understood as coherent interference between multiple-scattering paths and their time-reversed partners on a rough surface, we believe that the properties of Γ_{++} may be attributed to coherent interference between two distinct sets of such paths for different incident and scattering angles. First, it is clear that, if the Gaussian factorization theorem is applied as discussed in Section 3, the behavior of Γ_{++} is associated with the more fundamental amplitude moment

$$C_{++}(\theta_i, \theta_s, \theta_i', \theta_s') = \langle A_+(\theta_i, \theta_s) A_+^*(\theta_i', \theta_s') \rangle. \tag{9}$$

The amplitude $A_+(\theta_i, \theta_s)$ contains contributions from the pair of scattering paths shown in Fig. 10(a), and $A_+(\theta_i', \theta_s')$ contains contributions from analogous paths but for different incident and scattering angles, as shown in Fig. 10(b). In the usual far-field approximation, the phase delay along the geometrical path $A \rightarrow B$ in Fig. 10(a) is given by

$$\phi_{AB} = \mathbf{k}_i \cdot \mathbf{r}_A - \mathbf{k}_s \cdot \mathbf{r}_B + k\Delta r, \tag{10}$$

where $\mathbf{k}_i$ and $\mathbf{k}_s$ are the incident and scattered wave vectors, $k = |\mathbf{k}_i| = |\mathbf{k}_s|$, $\mathbf{r}_A$ and $\mathbf{r}_B$ are vectors to points A and B, and

$$\Delta r = |\Delta \mathbf{r}| = |\mathbf{r}_A - \mathbf{r}_B|. \tag{11}$$

The phase delays for the other three paths of Fig. 10 are of a form analogous to Eq. (10). After inspection of the amplitude moment of Eq. (9), it is clear that there are four contributions to C_{++} that contain the phase differences $\Delta\phi_{AB,A'B'}$, $\Delta\phi_{AB,B'A'}$, $\Delta\phi_{BA,A'B'}$, $\Delta\phi_{BA,B'A'}$, where, for example, $\Delta\phi_{AB,B'A'}$ represents the phase difference between the paths $A \rightarrow B$ in Fig. 10(a) and $B \rightarrow A$ in Fig. 10(b). These follow from the four phases of the form of Eq. (10) as

$$\begin{aligned}
\Delta\phi_{AB,A'B'} &= \tfrac{1}{2}(\Delta\phi - \Delta\phi'), \\
\Delta\phi_{AB,B'A'} &= \tfrac{1}{2}(\Delta\phi + \Delta\phi'), \\
\Delta\phi_{BA,A'B'} &= -\tfrac{1}{2}(\Delta\phi + \Delta\phi'), \\
\Delta\phi_{BA,B'A'} &= -\tfrac{1}{2}(\Delta\phi - \Delta\phi'),
\end{aligned} \tag{12}$$

where

$$\Delta\phi = (\mathbf{k}_i + \mathbf{k}_s) \cdot \Delta\mathbf{r}, \tag{13a}$$

$$\Delta\phi' = (\mathbf{k}_i' + \mathbf{k}_s') \cdot \Delta\mathbf{r}, \tag{13b}$$

and an additive constant common to the four phase differences of Eqs. (12) has been omitted.

The quantities $\Delta\phi$ and $\Delta\phi'$ are the phase differences for the pairs of paths in Figs. 10(a) and 10(b), respectively. Following previous interpretations of backscattering enhancement from surfaces,[1,2,9,12,13,15] this implies that the mean intensity should be enhanced when $\Delta\phi = 0$, a depleted intensity may be seen at angles where $\Delta\phi = \pm\pi$, and some enhancement may return when $\Delta\phi = \pm 2\pi$, although the strength of the secondary maxima should be less because of the fluctuations in $\Delta\mathbf{r}$ occurring on a random surface. Such effects may be seen in $\langle I_+(\theta_i, \theta_i) \rangle$ in Fig. 3, and it is clear that the secondary maxima present are considerably weaker than the central one. In applying these arguments to the surface employed here, we find from the minima and maxima of $\langle I_+(\theta_i, \theta_i) \rangle$ in Fig. 3 that $\Delta\phi = \pm\pi$ for $\theta_i = \pm 3.5°$ and that $\Delta\phi = \pm 2\pi$ for $\theta_i = \pm 7.0°$.

These considerations provide considerable insight into the form of Γ_{++} that is apparent in Fig. 9. For example, the large maximum at $(\theta_{i1}, \theta_{i2}) = (0°, 0°)$ is where $\Delta\phi = \Delta\phi' = 0$, so that from Eqs. (12) the four contributions to C_{++} have identical phase angles $\{0, 0, 0, 0\}$. As expected, Γ_{++} is then extremely large for this pair of angles. At $(\theta_{i1}, \theta_{i2}) = (0°, \pm 7.0°)$ there are secondary maxima in Γ_{++}; here we have that $\Delta\phi = 0$ and $\Delta\phi' = \pm 2\pi$, and there is again coherent interference because the four phases of Eqs. (12) are $\{\mp\pi, \pm\pi, \mp\pi, \pm\pi\}$. Of course, averaging over fluctuations in $\Delta\mathbf{r}$ would give rise to a weaker maximum than at $(\theta_{i1}, \theta_{i2}) = (0, 0)$, which is consistent with Fig. 9. Related arguments may also be applied to the maxima of Γ_{++} near $(\theta_{i1}, \theta_{i2}) = (7.0°, \pm 7.0°)$. For example, at $(\theta_{i1}, \theta_{i2}) = (7.0°, 7.0°)$ we have the case $\Delta\phi = \Delta\phi' = 2\pi$, so that the

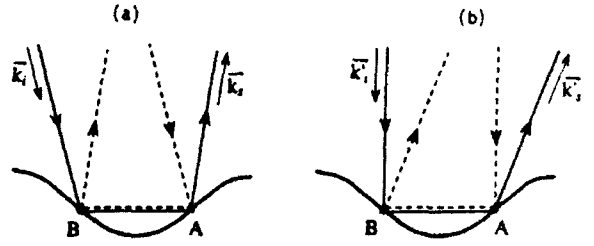

Fig. 10. Pairs of multiple-scattering paths occurring within a valley of a randomly rough surface: (a) a pair of paths for incident and scattered wave vectors $\mathbf{k}_i$ and $\mathbf{k}_s$; (b) the same pair but with incident and scattered wave vectors $\mathbf{k}_i'$ and $\mathbf{k}_s'$. The contributions to the correlation function of +45°-polarized scattered amplitudes arise from interference between the four distinct combinations of one path of (a) and one of (b).

phases of Eqs. (12) are $\{0, 2\pi, -2\pi, 0\}$ and there are again coherent effects. Including fluctuations in Δr, the net contribution to C_{+-} would be somewhat different from that found at $(\theta_{i1}, \theta_{i2}) = (0°, \pm 7.0°)$, and it can be seen that there are indeed differences in the peak height and shapes at these two locations in Fig. 9.

Further arguments may be applied to the four phases of Eqs. (12) to explain qualitatively the minima seen in Fig. 9, where either θ_{i1} or θ_{i2} is $\pm 3.5°$ and thus $\Delta\phi$ or $\Delta\phi'$ is $\pm\pi$, although detailed discussions are not presented here. We only note that the general condition at a reciprocal configuration follows from Eqs. (13) as $\Delta\phi = \Delta\phi'$, and four phases of Eqs. (12) are then $\{\Delta\phi, 0, 0, -\Delta\phi\}$. There is thus coherence between only two contributions to C_{+-}, but this is sufficient to produce the reciprocal structure present in Γ_{+-} throughout Fig. 9. It is interesting to note that there is enough residual constructive interference to produce the small but distinct reciprocal peak in Γ_{+-} in Fig. 7, where $(\theta_{i1}, \theta_{i2}) = (3.5°, -3.5°)$ and $\Delta\phi = \pi$.

These arguments are thus entirely adequate to enable us to appreciate the physical origin of the features seen in Γ_{+-}. It is naïve to consider the model presented too concretely, but it is to be expected that the mean length of Δr must be comparable with the correlation length of a Gaussian-correlated surface, and a modest range of statistical fluctuation must be present, considering the presence of the secondary maxima seen in Figs. 3 and 9. In any case, these arguments may be more rigorously understood as implying that the paths shown in Fig. 10 are the significant Feynman paths contributing to C_{+-} and Γ_{+-}.

Although a complete description of theoretical techniques is not appropriate here, we have carried out exact calculations of the amplitude correlation functions C_{+-} and C_{--}, using methods analogous to those used in previous studies of the mean scattered intensities.[3-5,8,11,15] We present only one such result here for a penetrable surface; more comprehensive calculations of C_{+-} and C_{--} for a perfectly conducting rough surface may be found elsewhere.[29] As in the experimental situation, the plane of incidence was perpendicular to the grooves of the surface; consequently the p- and s-polarized scattering problems could be solved independently. Expressions for the p- and s-polarized scattered amplitudes derived from Green's second integral theorem were numerically evaluated for a beam of finite width incident upon a realization of a one-dimensional, randomly rough metal surface. The $\pm 45°$-polarized scattered amplitudes were then computed from suitable combinations of the scattered p- and s-polarized amplitudes.

The wavelength of the incident beam was $\lambda = 1.152\ \mu$m, and the complex refractive index of gold near this wavelength has been reported as $(n + ik) = (0.312 + i7.93)$.[36] The impedance boundary condition method has been employed because it has been shown to provide an excellent approximation for surfaces of such high conductivity and with radii of curvature similar to the case of interest here.[37] The statistical properties of the surface profiles were comparable with those of the experimental surface. Each profile was a realization of a Gaussian stochastic process with a standard deviation of surface heights $\sigma = 1.5\ \lambda$; the height correlation function was Gaussian with a transverse correlation length $a = 3\lambda$. The ratio σ/a was thus sufficient to produce a significant amount of multiple scattering.[16,17]

The incident beam was of Gaussian form with transverse width $2w$; the ratio w/L, where L is the total length of the surface, was 4.5. First a realization of the surface profile was evaluated at $N_x = 400$ equally spaced points, the values of the incident and scattered field at the surface were then computed, and the corresponding realization of the scattered field was obtained as a function of the scattering angle. The number of points N_x used in the calculations was sufficient for us to obtain an accuracy of 1% in the scattered amplitudes. This procedure was repeated for 2000 realizations of the surface profile, and the realizations of the scattered field obtained in this fashion were used in the determination of the amplitude correlation functions C_{+-} and C_{--}.

In Fig. 11 are shown the results that were obtained for $C_{--}(\theta_{i1}, \theta_{s1}, \theta_{i2}, \theta_{s2})$ and $C_{+-}(\theta_{i1}, \theta_{s1}, \theta_{i2}, \theta_{s2})$ for the symmetric case $(\theta_{i1}, \theta_{i2}) = (\theta_{s1}, \theta_{s2})$ and for $\theta_{i1} = 0$. Both correlation functions contain significant real as well as imaginary parts. The real part of C_{--} exhibits a monotonically decreasing form that approaches zero near $\theta_{i2} = 30°$, and the imaginary part changes sign over the range of angles shown but remains small in magnitude. The correlation function C_{+-} is quite different in behavior. The real part of C_{+-} is large at first, but it rapidly passes through a zero at $\theta_{i2} = 4.5°$ and becomes significantly negative and then becomes slightly positive for $\theta_{i2} \geq 19°$. The imaginary part of C_{+-} is smaller in magnitude and oscillates over this range of angles, with the extrema of Im C_{--} occurring at nearly the same angles as the zeros of Re C_{--}.

The correlation function C_{--} presents a gradual and monotonic decorrelation that is presumably due to slowly varying angular effects, while C_{+-} shows an oscilla-

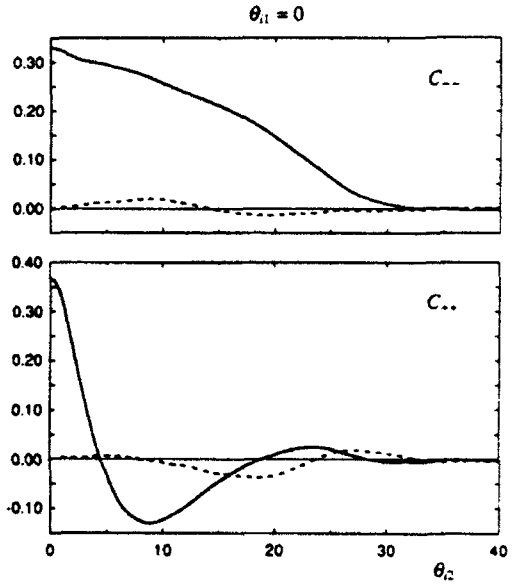

Fig. 11. Theoretical calculations of the correlation functions of scattered $-45°$-polarized and $+45°$-polarized scattered amplitudes $C_{--}(\theta_{i1}, \theta_{i1}, \theta_{i2}, \theta_{i2})$ and $C_{+-}(\theta_{i1}, \theta_{i1}, \theta_{i2}, \theta_{i2})$ for $\theta_{i1} = 0$ for a one-dimensionally rough conducting surface. The solid and dashed curves denote, respectively, the real and imaginary parts. The assumed surface statistics are those of a Gaussian process with a Gaussian correlation function [height standard deviation $\sigma = 1.5\lambda$, $1/e$ correlation half-width $a = 3\lambda$, complex refractive index $(n + ik) = (0.312 + i7.93)$]. These results may be compared with the experimental measurements of Γ_{--} and Γ_{+-} in Fig. 8.

tory behavior that strongly suggests the interference of multiple scattering paths on the rough surface. The negative region of Re C_{--} is consistent with the arguments above concerning C_{--} at a point where $\Delta\phi = 0$ and $\Delta\phi' = 2\pi$; the four phases of Eqs. (12) are then $\{-\pi, \pi, -\pi, \pi\}$, and one should indeed expect Re C_{--} to be significantly negative. Finally, on taking the modulus squared of the results of Fig. 11, one obtains results that are qualitatively similar to the experimental data of Fig. 8.

6. CONCLUSIONS

We have presented an experimental study of the angular correlation functions of far-field intensity scattered by a one-dimensionally rough surface. Statistically significant correlations of intensity have been found only for particular sets of incident and scattering angles. The general condition was that the difference of the sines of the incident and scattering angles must be constant, and a detailed study of the special case of equal incident and scattering angles has been undertaken. In this case it has been clearly demonstrated that the measured intensity correlation functions always exhibit two distinct and equal maxima corresponding to, within experimental accuracies, perfect correlation. One peak occurs where an intensity is correlated with itself, while the second corresponds to a correlation between two different intensities related by a reciprocity condition. As has been discussed, the reciprocal correlation peak is a direct manifestation of fundamental properties of Maxwell's equations, and its observation is a significant achievement when the experimental tolerances are considered.

The surface employed in the experiments was sufficiently rough to produce backscattering enhancement in the mean scattered intensities. To consider the distinct effects of single and double scattering, a +45° polarization state was incident upon the rough surface, and two differently polarized scattered intensities were considered. The correlation functions of the intensity polarized at −45° were found to have broad angular structures that have been attributed to single scattering. The intensity polarized at +45° was found to have entirely different correlation functions that have been attributed to multiple scattering. With intuitive models, it has been shown that the form of the correlation functions of +45°-polarized intensity may be qualitatively understood through generalizations of multiple-scattering arguments previously presented in the interpretation of backscattering enhancement. Theoretical calculations have been presented to provide a rigorous and clear confirmation of the nature of the angular correlation functions.

ACKNOWLEDGMENT

This research was supported by the U.S. Army Research Office.

REFERENCES

1. E. R. Méndez and K. A. O'Donnell, "Observation of depolarization and backscattering enhancement in light scattering from Gaussian random surfaces," Opt. Commun. **61**, 91–95 (1987).
2. K. A. O'Donnell and E. R. Méndez, "Experimental study of scattering from characterized random surfaces," J. Opt. Soc. Am. A **4**, 1194–1205 (1987).
3. A. A. Maradudin, E. R. Méndez, and T. Michel, "Backscattering effects in the elastic scattering of *p*-polarized light from a large-amplitude random metallic grating," Opt. Lett. **14**, 151–153 (1989).
4. T. Michel, A. A. Maradudin, and E. R. Méndez, "Enhanced backscattering of light from a non-Gaussian random metal surface," J. Opt. Soc. Am. B **6**, 2438–2446 (1989).
5. J. M. Soto-Crespo and M. Nieto-Vesperinas, "Electromagnetic scattering from very rough random surfaces and deep reflection gratings," J. Opt. Soc. Am. A **6**, 367–384 (1989).
6. A. J. Sant, J. C. Dainty, and M. J. Kim, "Comparison of surface scattering between identical, randomly rough metal and dielectric diffusers," Opt. Lett. **14**, 1183–1185 (1989).
7. M. J. Kim, J. C. Dainty, A. T. Friberg, and A. J. Sant, "Experimental study of enhanced backscattering from one- and two-dimensional random rough surfaces," J. Opt. Soc. Am. A **7**, 569–577 (1990).
8. M. Saillard and D. Maystre, "Scattering from metallic and dielectric rough surfaces," J. Opt. Soc. Am. A **7**, 982–990 (1990).
9. J. S. Chen and A. Ishimaru, "Numerical simulation of the second-order Kirchhoff approximation from very rough surfaces and a study of backscattering enhancement," J. Acoust. Soc. Am. **88**, 1846–1850 (1990).
10. M. E. Knotts and K. A. O'Donnell, "Anomalous scattering from a perturbed grating," Opt. Lett. **15**, 1485–1487 (1990).
11. J. A. Sanchez-Gil and M. Nieto-Vesperinas, "Light scattering from random rough dielectric surfaces," J. Opt. Soc. Am. A **8**, 1270–1286 (1991).
12. A. Ishimaru and J. S. Chen, "Scattering from very rough metallic and dielectric surfaces: a theory based on the modified Kirchhoff approximation," Waves Random Med. **1**, 21–34 (1991).
13. N. C. Bruce and J. C. Dainty, "Multiple scattering from rough dielectric and metal surfaces using the Kirchhoff approximation," J. Mod. Opt. **38**, 1471–1481 (1991).
14. A. Ishimaru, J. S. Chen, P. Phu, and K. Yoshitomi, "Numerical, analytical, and experimental studies of scattering from very rough surfaces and backscattering enhancement," Waves Random Med. **3**, S91–S107 (1991).
15. E. I. Thorsos and D. R. Jackson, "Studies of scattering theory using numerical methods," Waves Random Med. **3**, S165–S190 (1991).
16. K. A. O'Donnell and M. E. Knotts, "Polarization-dependence of scattering from one-dimensional rough surfaces," J. Opt. Soc. Am. A **8**, 1126–1131 (1991).
17. T. R. Michel, M. E. Knotts, and K. A. O'Donnell, "Stokes matrix of a one-dimensional perfectly conducting rough surface," J. Opt. Soc. Am. A **9**, 585–596 (1992).
18. See, for example, J. W. Goodman, "Statistical properties of laser speckle patterns," in *Laser Speckle and Related Phenomena*, J. C. Dainty, ed. (Springer-Verlag, Berlin, 1975), and references therein.
19. H. M. Pedersen, "Second-order statistics of light diffracted from Gaussian rough surfaces with applications to the roughness dependence of speckles," Opt. Acta **22**, 523–535 (1975).
20. D. Léger and J. C. Perrin, "Real-time measurement of surface roughness by correlation of speckle patterns," J. Opt. Soc. Am. **66**, 1210–1217 (1976).
21. P. Beckmann and A. Spizzichino, *The Scattering of Electromagnetic Waves from Rough Surfaces* (Pergamon, New York, 1963).
22. S. Feng, C. Kane, P. A. Lee, and A. D. Stone, "Correlations and fluctuations of coherent wave transmission through disordered media," Phys. Rev. Lett. **61**, 834–837 (1988).
23. R. Berkovits, M. Kaveh, and S. Feng, "Memory effect of waves in disordered systems: a real-space approach," Phys. Rev. B **40**, 737–740 (1989).
24. L. Wang and S. Feng, "Correlations and fluctuations in reflection coefficients for coherent wave propagation in disordered scattering media," Phys. Rev. B **40**, 8284–8289 (1989).
25. I. Freund, M. Rosenbluh, and S. Feng, "Memory effects in propagation of optical waves through disordered media," Phys. Rev. Lett. **61**, 2328–2331 (1988).

26. I. Freund, M. Rosenbluh, and R. Berkovits, "Geometrical scaling of the optical memory effect in coherent-wave propagation through random media," Phys. Rev. B **39**, 12,403–12,406 (1989).
27. R. Berkovits and M. Kaveh, "Time-reversed memory effects," Phys. Rev. B **41**, 2635–2638 (1990).
28. R. Berkovits and M. Kaveh, "The vector memory effect for waves," Europhys. Lett. **13**, 97–101 (1990).
29. T. R. Michel and K. A. O'Donnell, "Angular correlation functions of amplitudes scattered from a one-dimensional, perfectly conducting rough surface," J. Opt. Soc. Am. A **9**, 1374–1384 (1992).
30. P. F. Gray, "A method of forming optical diffusers of simple known statistical properties," Opt. Acta **25**, 765–775 (1978).
31. M. Nieto-Vesperinas, *Scattering and Diffraction in Physical Optics* (Wiley, New York, 1991).
32. D. S. Saxon, "Tensor scattering matrix for the electromagnetic field," Phys. Rev. **100**, 1771–1775 (1955).
33. See Eq. (17) of Ref. 20.
34. F. G. Bass and I. M. Fuks, *Wave Scattering from Statistically Rough Surfaces* (Pergamon, New York, 1979).
35. G. Brown, "The validity of shadowing corrections in rough surface scattering," Radio Sci. **19**, 1461–1468 (1984).
36. E. D. Palik, ed., *Handbook of Optical Constants of Solids* (Academic, New York, 1985).
37. R. Garcia-Molina, A. A. Maradudin, and T. A. Leskova, "The impedance boundary condition for a curved surface," Phys. Rep. **194**, 351–359 (1990).

Comparisons of theory and experiment in light scattering from a randomly rough surface

M. E. Knotts, T. R. Michel, and K. A. O'Donnell

The School of Physics, Georgia Institute of Technology, Atlanta, Georgia 30332

Received August 6, 1992; accepted November 16, 1992; revised manuscript received December 17, 1992

For a conducting surface with one-dimensional roughness, we compare experimental and theoretical results for the four unique elements of the Stokes-scattering matrix that provide a complete description of the diffusely scattered light. The rough surface has been fabricated with new techniques and is strictly one dimensional, and scattered intensities at infrared wavelengths show clear backscattering enhancement that arises from multiple scattering within surface corrugations. To obtain theoretical results for the Stokes matrix elements, we numerically apply an impedance boundary-condition method, appropriate for the roughness and the high conductivity of the experimental surface, to a statistical ensemble of rough surfaces. The experimental surface has been found to have nearly Gaussian first-order height statistics, and experimental measurements of the matrix elements are compared with theoretical results for a surface consistent with a Gaussian process. These comparisons suggest that there is more multiple scattering in the experimental data than is accounted for by the theoretical calculations. We attribute this observation to the properties of the second derivative of the experimental surface, which are found to be inconsistent with those of a Gaussian process. In further calculations that take account of the unusual properties of the experimental surface, excellent agreement of theoretical and experimental results is obtained.

1. INTRODUCTION

The scattering of electromagnetic waves by randomly rough surfaces has remained a challenging field of theoretical and experimental research. There have been a number of theoretical approaches to the problem of scattering by rough surfaces.[1-6] These approaches are sufficiently complex that, in the determination of physically measurable quantities, many assumptions are usually necessary. There has also been considerable experimental study of scattering from rough surfaces, though such research has also presented significant challenges. For example, it is usually difficult to determine the statistical properties of a rough surface,[7] and the experimental procedures necessary for characterization of the scattering properties may be complex.[8] Thus it is not surprising that critical comparisons of theory and experiment are generally quite difficult in rough-surface scattering.

The theoretical and experimental methods employed in surface scattering depend on the nature of the rough surface. For surfaces with roughness that is small compared with the illumination wavelength, experimental measurements of the angular distributions of scattered intensity have been compared with the results of perturbation theories.[9-15] In those studies significant differences have been seen in critical comparisons.[9-12] Better agreement has been obtained through the less satisfying procedure of adjusting theoretical results to fit data through assumptions for the statistical properties of the surface.[13-15] For rougher surfaces, where the Kirchhoff method may be applied, measurements of the angular scattering distributions of a rough surface have been compared with theoretical results.[16] Considerable care was taken in surface fabrication and characterization in Ref. 16, and good agreement was found with the Kirchhoff method for small angles of illumination.

Of more direct interest here is a rough conducting surface with strong slopes and correlation length comparable with the illumination wavelength. It has been observed that multiple scattering occurs under these conditions and that backscattering enhancement may be seen in the diffusely scattered intensity.[16,17] Considerable development of theoretical methods has been necessary to account for such effects. With the use of rigorous computational methods that average scattered intensities over a statistical ensemble of rough surfaces,[18] backscattering enhancement has been predicted for surfaces with one-dimensional roughness.[19-27] Others have predicted such effects from analytical extensions of the Kirchhoff method for surfaces that are rough in one[27,28] or two[29] dimensions.

In comparisons of theoretical and experimental results for rough surfaces that create backscattering enhancement, significant differences have remained. In particular, measurements of the p- and s-polarized intensities scattered from approximately one-dimensional rough surfaces have been found to be significantly different from the predictions of the numerical methods for a perfect conductor[30,31]; these differences have been most obvious for large incident or scattering angles. As discussed in Ref. 31, it is difficult to discern whether the disagreement is due to fundamental problems with theoretical methods or else arises from a number of possible experimental errors. Ishimaru *et al.*[27] have suggested that the differences could arise from a roughness spectrum of non-Gaussian form, though the optical surfaces had been believed to have Gaussian spectra.[30,31]

More recently, it has been appreciated that the properties of the light that is diffusely scattered by a one-

0740-3232/93/C50928-14$05.00

dimensional rough surface are not fully specified by the p- and s-polarized scattered intensities. Instead, they are specified by the Stokes-scattering matrix,[8] which has four unique elements in this case.[32,33] The additional information in the Stokes matrix elements is the cross correlation of the p and s amplitudes,[33] which may be determined from measurements of four additional polarized scattered intensities.[32] Through comparison[34] of theoretical results for a perfect conductor[33] with data for an approximately one-dimensional surface with similar statistics,[32,33] it becomes clear that significant differences also appear in these matrix elements. Some of these differences (particularly those in the matrix element s_{11}) are analogous to those reported in the p- and s-polarized intensities,[30,31] while previously unseen differences of significant magnitude are present in other matrix elements.

Thus, for rough surfaces that produce backscattering enhancement, there has been substantial development of both theoretical and experimental techiques, both of which should produce accurate results. Yet there is a clear lack of quantitative agreement, so the validity of both theoretical methods and experimental techniques must remain open to question. The resolution of this situation is clearly a highly significant issue. Hence, in the present paper, we discuss critical comparisons of theoretical and experimental results for a one-dimensional rough surface that produces backscattering enhancement. To provide a complete description of the diffusely scattered light, we employ the four unique elements of the Stokes-scattering matrix throughout these comparisons.

In order to isolate clearly the nature of possible disagreements, we have carefully chosen our theoretical and experimental techniques and parameters. We have conducted the experiments under conditions for which both the profilometric data and the scattering data should be reliable. Specifically, we consider measurements of the diffuse scattering from a strictly one-dimensional, metallic, rough surface that has nearly Gaussian first-order height statistics and a Gaussian height correlation function. The surface has structures that are large enough to be well resolved by a mechanical profilometer but are comparable with the infrared wavelengths used in the experiments. Furthermore, the surface has been fabricated with new techniques such that the scattered intensity remains strictly confined to the plane of incidence. This surface quality permits the absolute normalization of the measured intensities and of all elements of the Stokes-scattering matrix. The experimental techniques necessary for fabrication, characterization, and study of the scattering properties of the rough surface are discussed in Section 2.

We have also employed rigorous theoretical methods that are accurate for highly conductive rough surfaces with strong slopes. As in previous studies,[18-27] the scattered field derived from Green's second integral theorem has been evaluated numerically in the case of an illuminating beam of finite width. For the highly conductive case of interest here, difficulties arise in the numerical solution of the required integral equations by the method of moments.[35] We have avoided these difficulties through the use of an impedance boundary condition for curved surfaces,[36] which extends the range of validity of numerical methods developed in earlier research[19-27] to highly conducting surfaces. This method and the details of its numerical implementation are described in Section 3.

Because of the Gaussian first-order height statistics of the experimental surface, in Section 4 we compare experimental measurements with numerical calculations for a rough surface consistent with a Gaussian process, as has been done in previous studies.[30,31] Our comparisons of the Stokes matrix elements are good, but some differences remain, and in Section 5 we investigate the origin of these differences. We first demonstrate that the experimental rough surface has curvatures that are not consistent with those of a Gaussian process. The experimental scattering data are then compared with further numerical calculations that take account of these unusual properties of the experimental surface. Significant improvements are found in these comparisons, and in the conclusions of Section 6 we summarize our interpretation of the results.

2. EXPERIMENTAL TECHNIQUES

A. Surface Fabrication and Characterization

We first discuss the fabrication and the characterization of a strictly one-dimensional rough surface. Some aspects of our fabrication techniques are similar to those used in earlier studies.[30-33] In this procedure a 50 mm × 50 mm photoresist-coated glass plate was exposed to an anisotropic speckle pattern produced by a helium–cadmium laser of wavelength $\lambda = 0.442$ μm. In one direction this speckle pattern had fine structure (approximately 3-μm e^{-1} correlation width), but in the orthogonal direction it had broad structure (correlation width of a few millimeters). We have previously noted[32] that direct exposure of the photoresist to this speckle pattern, in the manner used previously,[30-33] does not necessarily produce a surface with strictly one-dimensional structure. Because of scattering from optical components in the exposing system and because of scattering in the photoresist itself, previous surfaces[32,33] had structures that were not entirely one-dimensional and therefore significantly affected the scattering properties of the surface.

We have eliminated the above problem partly through the use of low-scatter components and light baffles in the exposing system. During exposure we have also slowly and continuously moved the photoresist plate 25 mm in the direction of the large correlation scale of the exposing speckle pattern. This guaranteed that the time-averaged exposure of the photoresist plate was strictly one dimensional over the scanning length. Further, because a given point of the plate was exposed to a large number of correlation cells of intensity, the net exposure had nearly Gaussian statistics. On inspection of the processed plate, either visually or in an optical microscope, the resulting surface appeared to be completely constant over approximately 20 mm in the direction of motion. In the orthogonal direction a fine correlation scale was apparent with a uniformly rough region of length 40 mm.

A more meaningful measure of the quality of the fabricated surface is seen in its scattering characteristics. After the surface was coated with a thick layer (145 nm) of gold, the angular scattering distribution was examined with a visible laser source. As one would expect for a

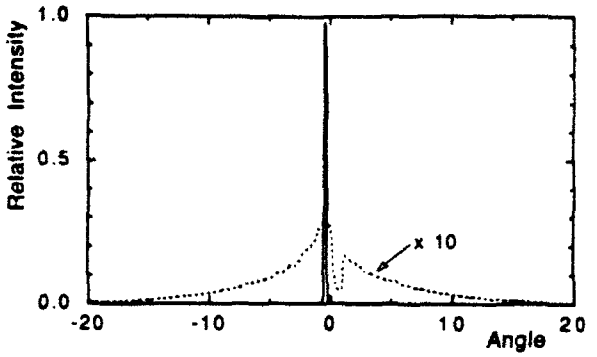

Fig. 1. Scans of the scattered intensity as a function of angle (degrees) in a direction orthogonal to the plane of incidence; $\theta_i \approx 0.5°$, incident wavelength $\lambda = 1.152$ μm. The dashed curve is the result for the approximately one-dimensional surface of Refs. 32 and 33 (multiplied by a factor of 10), and the solid curve is the result for the surface fabricated with the new techniques. The dashed curve is nearly symmetric, and the notch is due to obstruction by a mirror in the optical system.

one-dimensionally rough surface, a narrow line of one-dimensional speckles was observed in the far field of the surface. No significant deviations of scatter from the plane of incidence were seen. Figure 1 shows measurements of the intensity scattered in directions orthogonal to the plane of incidence at the wavelength $\lambda = 1.152$ μm. There is a narrow distribution of 0.3° width, which is comparable with the width of the detector aperture and demonstrates the effective confinement of scattering to the plane of incidence. Figure 1 also shows a similar measurement for the best surface that we fabricated using previous techniques, which exhibits (note the scale change) a broad distribution surrounding the plane of incidence. The new fabrication techniques thus represent a significant improvement over earlier methods.

To determine the statistical properties of the rough surface, we have employed a Talystep profilometer with a chisel-shaped stylus that is suitable for the characterization of one-dimensional roughness. In the direction of the surface roughness (i.e., the direction of the profilometer scan), the stylus had a 60° vertex angle and ended in a narrow blunt point of 0.4-μm width. In the orthogonal direction (that of the grooves of the rough surface), the stylus was of 2.0-μm width. The output signal of the profilometer was amplified and then digitized by an analog-to-digital converter connected to a personal computer. Twenty scans were made at uniformly spaced positions along the 40-mm rough dimension of the surface, with each scan consisting of 8192 height data taken along a 1.88-mm length. The data were corrected only for an unknown slope over the scan length by means of a least-squares fit to a linear function. Data were also calibrated to height standards and horizontal spacing standards, which ensured vertical and horizontal accuracy of ±2% and ±0.3%, respectively. Repeated scans of the same part of the surface were extremely reproducible; repeating a particular scan with a stylus tracking force higher than normal did not produce significant surface damage or distortion.

The correlation function and the histogram of surface heights were then determined directly from the sets of profilometric data. As we can see from Fig. 2, the correlation function provides a close fit to a Gaussian function. The standard deviation σ of surface height was found to be 1.73 μm, and the e^{-1} half-width a of the fitted correlation function was found to be 3.43 μm; these parameters were determined through a weighted least-squares fit of the measured spectrum. The histogram of surface heights is shown in Fig. 3 and provides a close fit to a Gaussian probability density. The higher-order moments of the height data yield a skewness of −0.190 and a kurtosis of 2.90, which are near the desired values of a Gaussian variate (0 and 3, respectively).

B. Experimental Procedures

As Fig. 4 shows, the surface was illuminated by a laser beam that was oriented so that the plane of incidence was perpendicular to the grooves of the rough surface. Under this condition the scattered light must remain in the plane of incidence, and thus one-dimensional distributions of intensity (scattered power per unit planar angle) are measurable quantities. Further, if the incident field is in a pure p or s polarization state, there will be no depolarization of the scattered light. It has been shown that this

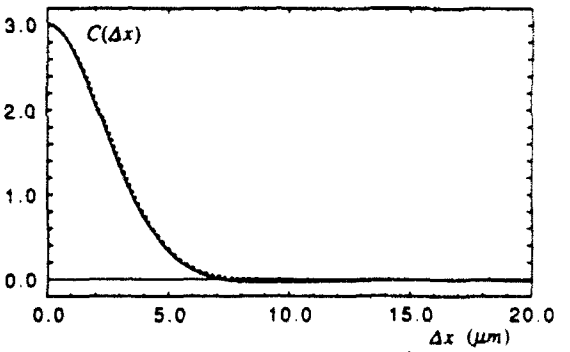

Fig. 2. Height correlation function $C(\Delta x) = \langle h(x)h(x + \Delta x)\rangle$ (solid curve) calculated from the measured rough-surface profile $h(x)$. The dashed curve is a comparison with a Gaussian correlation function with e^{-1} width $a = 3.43$ μm and height σ^2, where $\sigma = 1.73$ μm. The statistical errors (the standard deviations determined from the higher-order moments of the data) are 1.5% of σ^2 at $\Delta x = 0$, 1.3% at $\Delta x = 2.0$ μm, and 1.1% at $\Delta x = 20.0$ μm. The slightly negative foot of $C(\Delta x)$ is not statistically significant.

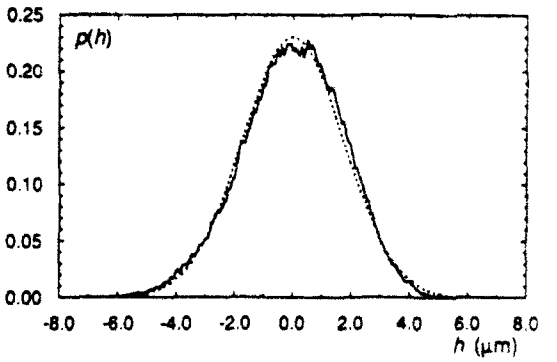

Fig. 3. Probability density of surface height, $p(h)$, calculated from the profilometry of the experimental rough surface (solid curve). The dashed curve is a comparison with a Gaussian probability density with standard deviation $\sigma = 1.73$ μm.

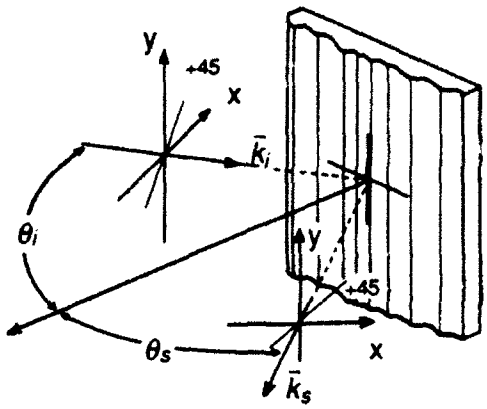

Fig. 4. Scattering of an incident wave by a surface with one-dimensional roughness. The direction of the incident beam is orthogonal to the groove direction.

polarization behavior implies that the Stokes vectors of the incident and scattered fields are related by a Stokes-scattering matrix **S** of the simplified form[32,33]

$$\mathbf{S} = \begin{bmatrix} s_{11} & s_{12} & 0 & 0 \\ s_{12} & s_{11} & 0 & 0 \\ 0 & 0 & s_{33} & s_{34} \\ 0 & 0 & -s_{34} & s_{33} \end{bmatrix}, \tag{1}$$

where all the matrix elements are implicitly functions of the incident and scattering angles. For an arbitrary incident polarization state the specification of the Stokes vector of the scattered field clearly requires the determination of the four unique matrix elements of **S**. The *p*- and *s*-polarized scattered intensities, as they have been studied previously,[19-28,30,31] are given by $s_{11} + s_{12}$ and $s_{11} - s_{12}$, respectively. The matrix elements s_{33} and s_{34} contain, respectively, the real and imaginary parts of the cross correlation of the *p*- and *s*-polarized scattered amplitudes.[32,33]

To measure the four unique elements of the Stokes-scattering matrix, we have employed procedures described elsewhere.[32,33] The surface was illuminated with an incident beam linearly polarized at +45°, as shown in Fig. 4. This incident state is represented by the Stokes vector

$$\mathbf{V}_- = \begin{bmatrix} 1 \\ 0 \\ 1 \\ 0 \end{bmatrix}, \tag{2}$$

where we assume that the incident field is of unit power. After multiplication of $\mathbf{V}_-$ by the matrix **S** of Eq. (1), the Stokes vector of the scattered light is obtained as

$$\mathbf{V}_{scat} = \begin{bmatrix} s_{11} \\ s_{12} \\ s_{33} \\ -s_{34} \end{bmatrix}, \tag{3}$$

and it is clear that $\mathbf{V}_{scat}$ contains all the unique elements of **S**.

The vector $\mathbf{V}_{scat}$ may be determined with standard procedures[37] through the measurement of six polarized intensities. Specifically, the four elements of $\mathbf{V}_{scat}$ follow from

$$s_{11} = I_p + I_s = I_- + I_- = I_R + I_L, \qquad s_{12} = I_p - I_s,$$
$$s_{33} = I_- - I_-, \qquad -s_{34} = I_R - I_L, \tag{4}$$

where I_p, I_s, I_-, and I_- denote the mean scattered intensities transmitted by a linear polarizer at 0° (*p*), 90° (*s*), +45°, and −45°, respectively. The intensities I_R and I_L are those transmitted by polarization components with sensitivity to right- and left-handed circular states, respectively; the necessary components are a quarter-wave plate followed by a properly oriented linear polarizer. The intensities and the matrix elements are formally defined through averages over a statistical ensemble of surfaces[32,33]; as we discuss below, the experiments determine these quantities partly through an average over a small range of scattering angles.

The details of the scattering experiment are shown in Fig. 5. The source was a Jodon HN-20 helium–neon laser of wavelength $\lambda = 1.152$ or 3.392 μm. A series of mirrors sent the vertically polarized laser beam over a detector and through a half-wave plate. The beam then reflected from a final mirror, passed through a polarizer, and was incident on the rough surface at angle θ_i. The half-wave plate permitted the incident polarization to be oriented predominantly at +45°; the polarizer that followed removed any residual ellipticity and produced a −45° polarization state with extinction stronger than 10^{-3}. The scattered light was detected as a function of scattering angle θ_s by a Cincinnati Electronics indium antimonide photodiode that was scanned on an arc of radius 70 cm centered on the surface. Suitable polarization components were mounted in front of the detector's field lens as required.

Because of the strict one-dimensional nature of the surface, an astigmatic illuminating wave was used in the experiment. In the plane in which the surface was rough, a slightly divergent wave illuminated a wide region of the surface to reduce speckle noise in the measured intensities.

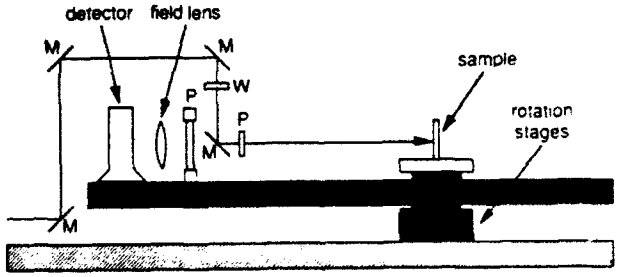

Fig. 5. Diagram of the scattering instrument used in the measurements of rough-surface scattering. The grooves of the rough surface are oriented in the vertical direction. The incident beam is brought over the detector and, after orientation of its polarization direction, is incident on the rough surface. The detector arm may be moved out of the plane of the figure for measurement of the intensity at all scattering angles. M denotes a mirror, P denotes a linear polarizer, and W denotes a half-wave plate.

In the orthogonal plane the illuminating wave converged on the detector aperture after reflection from the surface. This guaranteed that all the scattered power entered the detector aperture during measurement procedures, with the consequence that itwas possible to normalize data, as we discuss below. The illuminated region of the sample was approximately $w = 15.0$ mm along the surface roughness by 2.5 mm in the orthogonal direction.

The detector's field lens had a rectangular aperture that integrated the scattered intensity over an angle $\Delta\theta_{det} = 1.6°$ full width, which also served to reduce the speckle noise in the measurements. Nevertheless, each scan of intensity still contained a significant amount of reproducible speckle noise. To provide better averaging, we moved the surface in the direction of its roughness, made another angular scan of intensity, and repeated this procedure until all the rough surface had been illuminated. Six scans of each intensity were performed with a transverse sample motion of 5.0 mm between scans, such that the illumination remained within the 40.0-mm sample area. Then we averaged the six scans to provide the final measured intensity, and this process was carried out for each of the polarized intensities required by Eqs. (4).

The above procedures produce correct relative normalization of the four matrix elements. In a final procedure an accurate absolute normalization of all the matrix elements was performed through normalization of s_{11}. For the incident state $\mathbf{V}_-$, s_{11} is the first element of $\mathbf{V}_{scat}$ in Eq. (3) and thus represents the total scattered power per unit angle. To normalize s_{11}, we removed all the polarization components from the detector arm, removed the sample, and inserted an attenuating filter in the incident beam. The detector arm was rotated so that the incident beam was directly incident on the detector, and the incident power (apart from a proportionality constant) was determined. The attenuator was then removed, the sample was remounted, and an angular scan of the scattered intensity s_{11} was completed. By dividing these data by the constant determined from the detection of the incident beam, we achieved a correct absolute normalization of s_{11}. Finally, the incident power was again checked for reproducibility; a change of less than 0.5% was seen for all the results presented here. Thus results are normalized such that s_{11} represents the total scattered power per unit planar angle for an incident $+45°$ state of unit power. The accuracy of this normalization is dependent largely on the calibration of the attenuation filter, which we estimate to be accurate to better than $\pm 1\%$.

The results of the experiments are presented in Section 4, where they are compared directly with the results of the theoretical techniques discussed in Section 3.

3. THEORETICAL METHODS

In this section theoretical methods for the computation of the diffuse scattering properties of a randomly rough metal surface are presented, and in later sections the results of such calculations are discussed. The surface profile is one dimensional and is assumed to be a realization of a stationary stochastic process. As in the experimental situation of Section 2, the wavelength of the light is assumed to be comparable with the transverse correlation length of the surface, the slopes of the profile are permitted to take large values, and the metal is assumed to be highly conducting.

The computational method employed here is directly related to those employed in the study of the interaction of a monochromatic Gaussian beam with the one-dimensional, randomly rough surface of a dielectric or penetrable medium.[20-22,26] For the type of randomly rough metal surface considered here, this method has provided accurate theoretical results for the p- and s-polarized scattered intensities when the wavelength is in the visible part of the spectrum. In contrast, in the present paper we wish to describe completely any polarized scattered intensity, and the incident wavelength is in the infrared part of the spectrum. Our description of the polarization dependence of the scattering is similar to the method that has been described recently for the case of a perfectly conducting surface.[33] In this description the diffuse scattering properties of one-dimensional rough surfaces are completely determined by four unique Stokes matrix elements, which are the second-order moments of the p- and s-polarized scattered amplitudes.[32,33]

Comparisons[34] of experimental data for rough metal surfaces at infrared wavelengths with calculations that assume perfectly conducting surfaces have suggested[13] that the finite conductivity of the metal surfaces should be taken into account. The matrix elements that characterize surfaces of finite conductivity may be obtained by substitution of the exact expression for the scattered amplitudes of penetrable surfaces[23] in the general expressions for the Stokes matrix elements.[33] However, this approach fails at infrared wavelengths, where it is well known that the high conductivity of metals leads to numerical difficulties in the solution of the integral equation for the total field and its normal derivative on the surface.[35] In what follows we use an approximate method based on the impedance boundary condition for curved surfaces calculated by Garcia-Molina *et al.*[36] in order to obtain accurate estimates for the Stokes matrix elements of a highly conductive rough surface.

Consider the situation in which the half-space $x_3 < \zeta(x_1)$ is filled with a metal and is separated from the vacuum above it by a randomly rough surface of equation $x_3 = \zeta(x_1)$. The surface is assumed to be one dimensional in the sense that its height ζ is independent of x_2. The surface-profile function $\zeta(x_1)$ is described by a single-valued, zero-mean, stochastic process with continuous second derivatives. The metal is characterized by an isotropic, homogeneous, complex dielectric constant $\epsilon(\omega) = \epsilon_1(\omega) + i\epsilon_2(\omega)$. In the infrared portion of the spectrum the real part of the dielectric constant, $\epsilon_1(\omega)$, is taken to be negative and large in magnitude, so that $0 < \epsilon_2(\omega) \ll -\epsilon_1(\omega)$.

A polarized beam of finite width, whose plane of incidence is the plane x_1x_3 perpendicular to the grooves of the surface, illuminates the metal surface. The beam used in the calculations may be expressed as a Gaussian angular spectrum of incoming plane waves.[23] The half-width of the intercept of this beam with the mean surface is denoted by g and is kept constant when the angle of incidence θ_i is changed. The wavelength of the incident light is given by $\lambda = 2\pi c/\omega$, where c is the speed of light and

ω determines the value of the dielectric constant of the metal.[38]

In the scattering situations considered here, all the incident wave vectors are orthogonal to the grooves of the one-dimensional rough surface. Consequently, the Stokes-scattering matrix has the form given by Eq. (1), and the four unique matrix elements are the second-order moments of the p- and s-polarized scattered amplitudes.[32,33] In the case of dielectric surfaces, exact expressions for these scattered amplitudes have been obtained[23,26] through the use of Green's second integral theorem. These results are well known, but they will be outlined here to show how they may be used in an accurate and efficient way in numerical calculations that involve highly conductive surfaces. For each polarization the scattered amplitude may be expressed as an integral over two source functions, which are the values of the total field in the vacuum, $\psi_\alpha(\mathbf{x}')$, and its normal derivative $\partial\psi_\alpha(\mathbf{x}')/\partial n'$ evaluated on the surface. In what follows, the primed vectors $\mathbf{x}'$ and $\mathbf{x}''$ reside on the surface, and the vector $\mathbf{n}'$ ($n_3' > 0$) is normal to the surface. The two source functions satisfy the pair of coupled inhomogeneous integral equations

$$\psi_\alpha(\mathbf{x}') = 2\psi_\alpha(\mathbf{x}')_{\text{inc}} + \frac{P}{2\pi}\int_S ds''\left[\frac{\partial}{\partial n''}G_0(\mathbf{x}'|\mathbf{x}'')\right]\psi_\alpha(\mathbf{x}'') - \frac{1}{2\pi}\int_S ds'' G_0(\mathbf{x}'|\mathbf{x}'')\frac{\partial}{\partial n''}\psi_\alpha(\mathbf{x}''), \tag{5a}$$

$$0 = \psi_\alpha(\mathbf{x}') + \frac{P}{2\pi}\int_S ds''\left[\frac{\partial}{\partial n''}G_\epsilon(\mathbf{x}'|\mathbf{x}'')\right]\psi_\alpha(\mathbf{x}'') - \frac{\epsilon^\beta}{2\pi}\int_S ds'' G_\epsilon(\mathbf{x}'|\mathbf{x}'')\frac{\partial}{\partial n''}\psi_\alpha(\mathbf{x}''), \tag{5b}$$

where P indicates that only the principal part of the integrals is kept and where $(\alpha,\beta) = (p,1)$ or (α,β) $(s,0)$ for p or s polarization, respectively. The two Green's functions $G_0(\mathbf{x}|\mathbf{x}')$ and $G_\epsilon(\mathbf{x}|\mathbf{x}')$ are the solutions of the two-dimensional Helmholtz equations $(\nabla^2 + \omega^2/c^2)G_0(\mathbf{x}|\mathbf{x}') = -4\pi\delta(\mathbf{x}-\mathbf{x}')$ and $(\nabla^2 + \epsilon\omega^2/c^2)G_\epsilon(\mathbf{x}|\mathbf{x}') = -4\pi\delta(\mathbf{x}-\mathbf{x}')$, respectively, G_0 satisfies an outgoing wave condition at infinity, and G_ϵ vanishes at infinity. Using a point-matching method, several authors[20,23,24,26] have obtained accurate solutions of Eqs. (5) when the wavelength of the light incident on the surfaces is in the visible range. For highly conductive metals (i.e., gold at infrared wavelengths), a numerical difficulty arises[35]: the integration of the kernels of Eqs. (5) over each discretization interval may require many evaluations of the Green's function, since these kernels are sharply peaked at the origin. To overcome this problem, we note that the small width of G_ϵ and of $\partial G_\epsilon/\partial n''$ indicates that Eq. (5b) should be approximately equivalent to the imposition of a local linear relationship between the total field in the metal and its normal derivative evaluated on the surface. This relationship is called an impedance boundary condition, and an expansion of this boundary condition in powers of the skin depth $d = c/(\omega\sqrt{-\epsilon})$ has been calculated by Garcia-Molina *et al.*[36] in the case of a curved surface. When the boundary condition is used to eliminate one of the unknown source functions, the following equations are obtained:

$$\psi_\alpha(\mathbf{x}') = 2\psi_\alpha(\mathbf{x}')_{\text{inc}} + \frac{P}{2\pi}\int_S ds''\left[\frac{\partial}{\partial n''}G_0(\mathbf{x}'|\mathbf{x}'')\right]\psi_\alpha(\mathbf{x}'') - \frac{1}{2\pi}\int_S ds'' G_0(\mathbf{x}'|\mathbf{x}'')Z_\alpha(\mathbf{x}'')\psi_\alpha(\mathbf{x}''), \tag{6a}$$

$$\frac{\partial}{\partial n'}\psi_\alpha(\mathbf{x}') = Z_\alpha(\mathbf{x}')\psi_\alpha(\mathbf{x}'), \tag{6b}$$

$$Z_\alpha(\mathbf{x}') = \frac{1}{d\epsilon^\beta}\left(1 + \frac{d}{2}\frac{\zeta''(x_1')}{\{1+[\zeta'(x_1')]^2\}^{3/2}} - \frac{d^2}{8}\frac{[\zeta''(x_1')]^2}{\{1+[\zeta'(x_1')]^2\}^3}\right), \tag{6c}$$

where $Z_\alpha(\mathbf{x}')$ is the impedance boundary condition calculated in Ref. 36. The range of validity of this approximate integral equation is limited by the assumption made in the calculation of $Z_\alpha(\mathbf{x}')$. The exact boundary condition is linear but nonlocal, and the existence of a linear and local relationship between the source functions is an accurate approximation only if the skin depth d of the metal is much smaller than the incident wavelength λ.[36] Moreover, the terms neglected in the truncated series (6c) are small only if $d|\zeta''(x_1)| \ll 1$. Since both conditions will be fulfilled in the cases considered here, the boundary condition is sufficiently accurate. In addition, this approximation permitted highly efficient numerical calculation. The improvement is apparent if one considers that the elimination of one of the unknown source functions reduces by half the size of the linear system of equations that must be solved when a numerical solution of Eqs. (5) is calculated with the point-matching method. As a consequence, we used this method to obtain the numerical results presented in Sections 4 and 5.

4. COMPARISON OF RESULTS FOR A GAUSSIAN STATISTICAL MODEL

In this section the data from the experiment discussed in Section 2 are first compared with the results of the numerical methods that employ the surface impedance method described in Section 3. In the numerical results $N_s = 500$ discretization points spaced by $\lambda/12.5$ along the mean surface were used, the illuminated width was $g = 10\lambda$, and the surface length L was such that $L/g = 4.0$. We arrived at the value of N_s by increasing it until convergence in each Stokes matrix element was achieved, for a particular surface realization, to better than 1%. The values of the refractive index of gold were taken as $n + ik = 0.312 + i7.93$ and $1.96 + i20.7$ at $\lambda = 1.152$ and $3.392\ \mu$m, respectively, which are values reported at nearby wavelengths.[38] In all the numerical results of this section the surfaces employed were 4000 realizations of a Gaussian process with a correlation function of Gaussian form. The statistical parameters of the surface were $a = 3.43\ \mu$m and $\sigma = 1.73\ \mu$m, which were values determined from the profilometric measurements described in Subsection 2.A. In all figures the backscattering direction is given by $\theta_s = -\theta_i$.

We first present results for the wavelength $\lambda = 1.152\ \mu$m. Figure 6 shows the four unique elements of the Stokes-scattering matrix as a function of θ_s for $\theta_i = 0°$. First, s_{11}

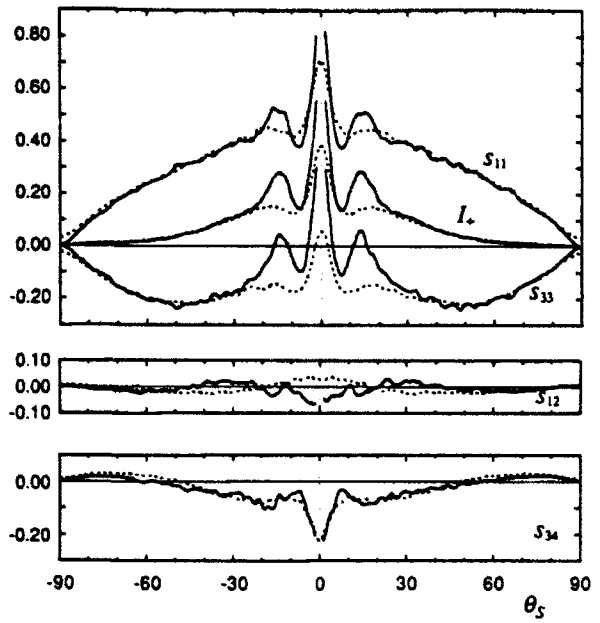

Fig. 6. For $\theta_i = 0°$ and $\lambda = 1.152$ μm, the unique matrix elements s_{11}, s_{12}, s_{33}, and s_{34} and the +45°-polarized intensity I_+. Experimental results (solid curves) are compared with numerical results (dashed curves; surface impedance method, surface roughness consistent with a Gaussian process).

and s_{12} are, respectively, the sum and the difference of the p- and s-polarized scattered intensities from Eqs. (4). For surfaces like the one discussed here, these intensities are generally large but similar, so that s_{11} resembles either intensity and s_{12} remains small in magnitude. Near $\theta_s = 0°$ in Fig. 6, it can be seen that s_{11} clearly exhibits backscattering enhancement with secondary maxima. The agreement of theory and experiment is excellent in s_{11} for $|\theta_s| \geq 20°$. For smaller $|\theta_s|$, there are significant differences and the experimental data present considerably stronger central and secondary maxima. Some differences are also apparent in s_{12}, although this matrix element remains small in both theoretical and experimental results.

The matrix element s_{33} in Fig. 6 has an unusual upward-turning shape with a positive central region that has been associated with multiple scattering in previous studies.[32,33] As we saw for s_{11}, the agreement of the theoretical and experimental results for s_{33} is excellent for high scattering angles, though the experimental results again exhibit a significantly stronger backscattering structure for $|\theta_s| < 25°$. The +45°-polarized scattered intensity I_+ is also shown in Fig. 6; this intensity is determined from the matrix elements as $(s_{11} + s_{33})/2$ from Eqs. (4). I_+ is of interest because it contains large contributions from double scattering, which one can see from either heuristic arguments[32] or rigorous arguments for a perfect conductor.[33] Thus I_+ contains strong backscattering enhancement, and, in the comparison, differences like those seen in s_{11} and s_{33} are apparent for small $|\theta_s|$.

The matrix element s_{34} in Fig. 6 is negative in the backscattering region, which implies from Eqs. (4) that the +45° incident state is, on average, scattered to right-handed elliptical states. This behavior may be interpreted as arising from the finite conductivity of the surface; that is, application of the Fresnel reflection coefficients two times (as in double scattering) to the +45° incident state produces a final state that has significant right-handed ellipticity.[32] The theoretical and experimental results for s_{34} provide the closest agreement in any of the matrix elements, particularly for small $|\theta_s|$.

For $\theta_i = 10°$ (Fig. 7) it can be seen that the backscattering enhancement has remained strong in s_{11} and that s_{33} still presents a peak in the backscattering direction. The intensity I_+ again shows backscattering enhancement but has become stronger for $\theta_s > -10°$, which indicates that the double scattering is preferentially distributed in the forward-scattering direction. In s_{11}, s_{33}, and I_+ the general shape of the theoretical results is similar to the experimental results, and for large $|\theta_s|$ the agreement remains quite good. However, there are again significant discrepancies in the heights of the structures related to backscattering enhancement, and the largest differences are now seen in the secondary maxima at $\theta_s \cong 5.0°$. As in Fig. 6, the small values of s_{12} show some differences and s_{34} provides relatively good agreement.

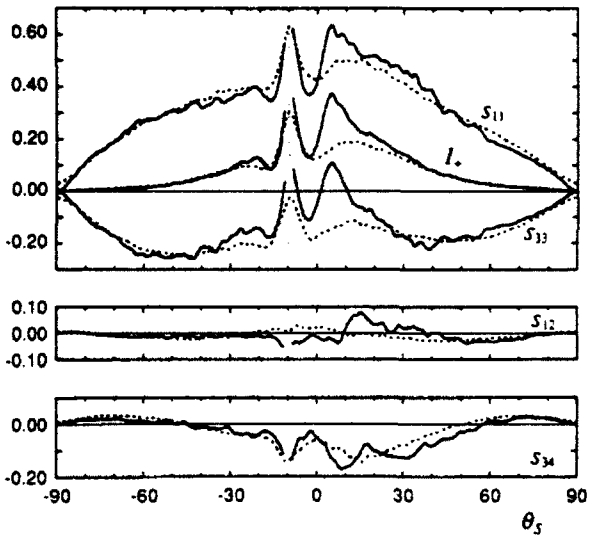

Fig. 7. Same as Fig. 6 but for $\theta_i = 10°$.

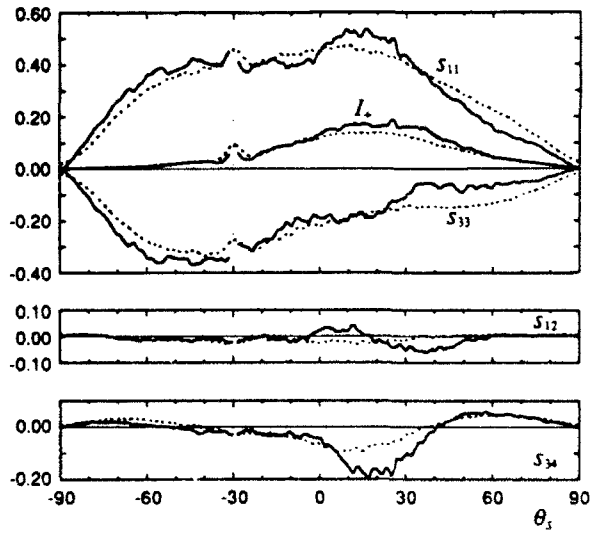

Fig. 8. Same as Fig. 6 but for $\theta_i = 30°$.

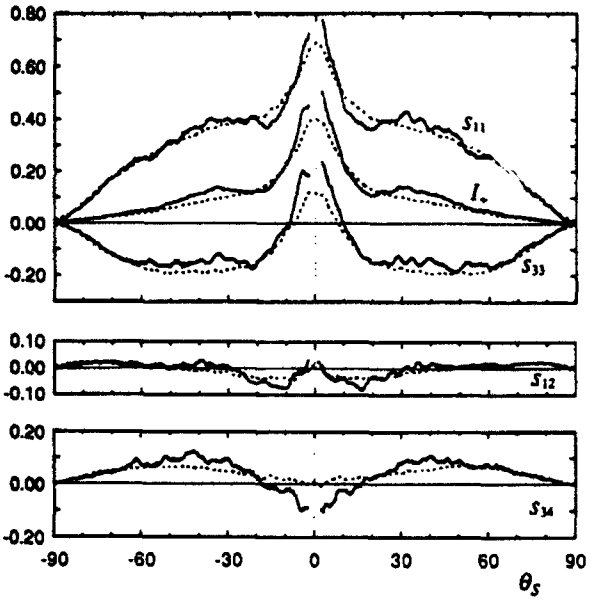

Fig. 9. For $\theta_i = 0°$ and $\lambda = 3.392$ μm, the unique matrix elements s_{11}, s_{12}, s_{33}, and s_{34} and the +45°-polarized intensity I_-. Experimental results (solid curves) are compared with numerical results (dashed curves; surface impedance method, surface roughness consistent with a Gaussian process).

In Fig. 8 the theoretical and experimental results for $\theta_i = 30°$ are shown, where it can be seen that most of the backscattering enhancement has disappeared in s_{11}, s_{33}, and I_-. The largest differences seen in the comparisons of these quantities are smaller than those in Figs. 6 and 7, but small differences are now distributed over a wider range of θ_s. In the negative region of s_{34} the experimental results show significantly smaller values of s_{34} for $10° < \theta_s < 40°$. The interpretation of the general shape of s_{34} is not entirely clear, though it suggests competition between contributions from single scattering ($s_{34} > 0$) and double scattering ($s_{34} < 0$). Again, s_{12} remains small in magnitude, and some differences are seen in the results.

We now present further comparisons for this rough surface at the longer wavelength ($\lambda = 3.392$ μm). These results are shown in Figs. 9, 10, and 11 for $\theta_i = 0°$, 10°, and 30°, respectively. As one would expect, the diffraction widths of structures related to backscattering enhancement have increased at the longer wavelength. For example, the full width of the enhancement peak in the experimental result for s_{11} is 35° in Fig. 9, but at the shorter wavelength in Fig. 6 this width is 14°. Generally, the theoretical and experimental results for s_{11}, s_{33}, and I_- show similar forms, though small differences are now apparent throughout a range of scattering angles. In Figs. 9 and 10 the experimental results for s_{11}, s_{33}, and I_- consistently exhibit somewhat stronger backscattering peaks, as had been found at the shorter wavelength in Figs. 6 and 7.

It is interesting that s_{12} has become more significant at the longer wavelength. In Fig. 9 the comparison of s_{12} is good, and in Figs. 10 and 11 the comparisons of s_{12} produce qualitative but not quantitative agreement. The shape of s_{34} in Figs. 9–11 has changed greatly at this wavelength, and the results have stronger positive regions than those seen in Figs. 6–8. We believe that the refractive index of gold, which shows a higher conductivity here than at the shorter wavelength, contributes to the change in shape of s_{34}. The comparisons show similar forms of s_{34} throughout Figs. 9–11, though the theoretical results are usually of smaller magnitude.

Throughout Figs. 6–11 the comparisons often show agreement in the shape of the matrix elements, though differences remain in many comparisons. The most significant differences seen in Figs. 6–11 involve structures related to backscattering enhancement, which are consistently stronger in the experimental results. We thus surmise that more multiple scattering occurs in the experiment than is accounted for by the theoretical calculations. Further, in the experimental measurements that have secondary maxima (as is often the case with I_-), these maxima are either relatively weak or even absent in the theoretical results. These differences are also clear in previous comparisons.[30,31,34]

It is significant that the differences noted in previous studies in the p- and s-polarized intensities[30,31] or in s_{11}

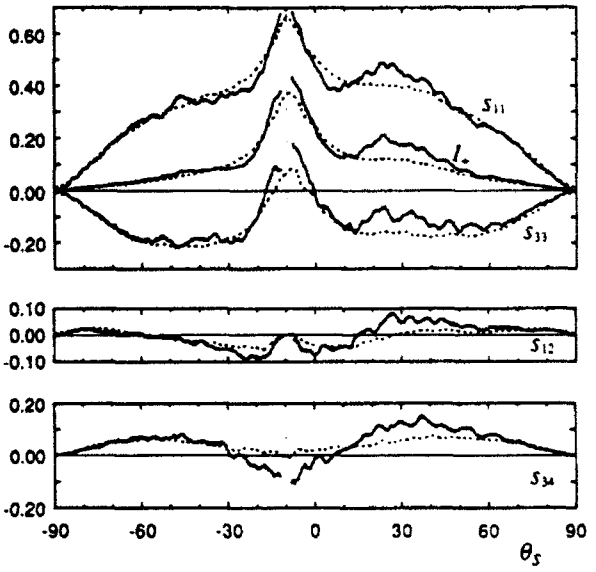

Fig. 10. Same as Fig. 9 but for $\theta_i = 10°$.

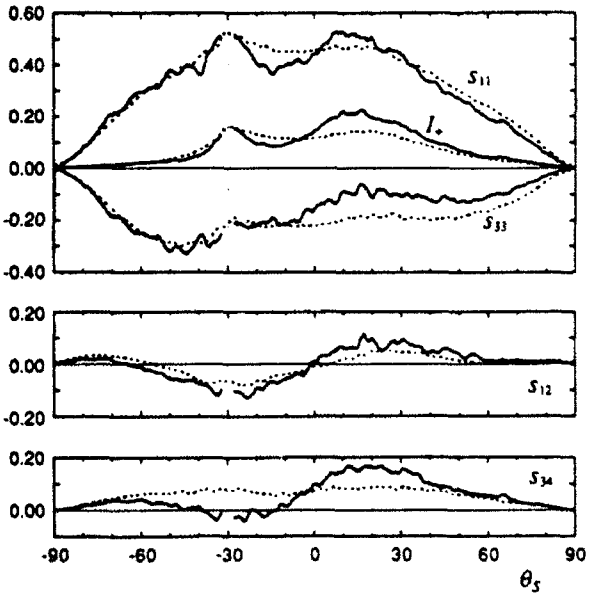

Fig. 11. Same as Fig. 9 but for $\theta_i = 30°$.

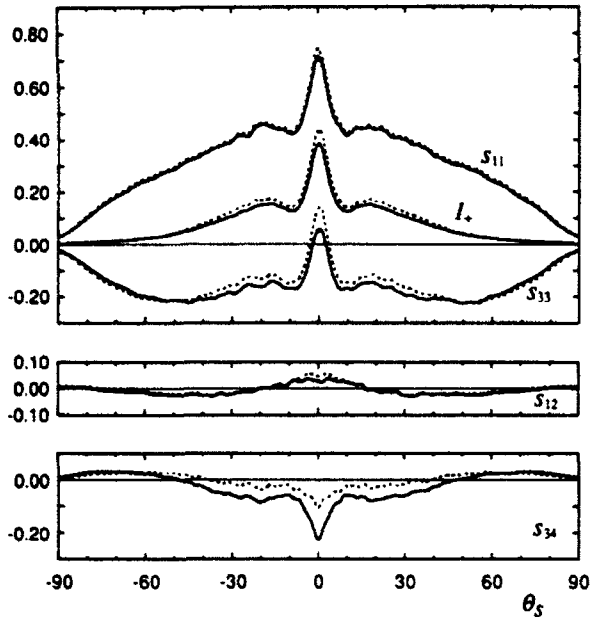

Fig. 12. For $\theta_i = 0°$ and $\lambda = 1.152$ μm, the unique matrix elements s_{11}, s_{12}, s_{33}, and s_{34} and the +45°-polarized intensity I_+. Numerical results that employ the surface impedance method (solid curves) are compared with results for the perfect conductor (dashed curves); the surface roughness is consistent with a Gaussian process.

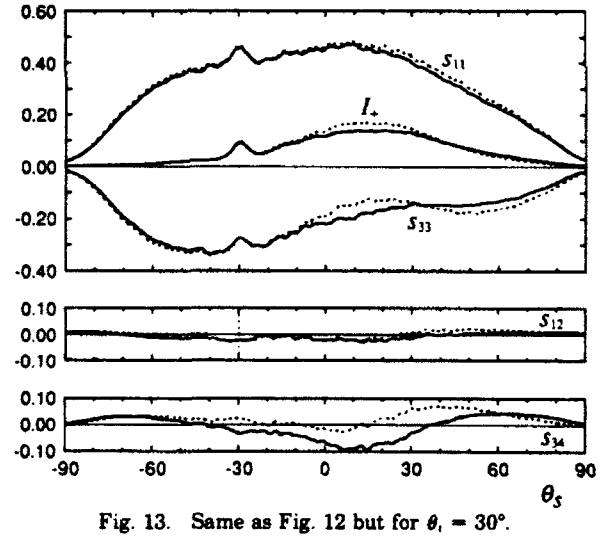

Fig. 13. Same as Fig. 12 but for $\theta_i = 30°$.

(Ref. 34) at high angles of incidence or scattering are not present in Figs. 6–11, where analogous differences would have been seen in s_{11}. We attribute the relatively good agreement at high angles to the strict one-dimensional character of the surface employed here. We also note that the experimental results of Figs. 6–11 contain more speckle noise than that seen in previous optical experiments with approximately one-dimensional surfaces.[30–33] We also attribute this increase to the quality of the experimental surface, which, as we discussed in Subsection 2.A, created speckles that were one dimensional. In previous experiments[32,33] the noise was considerably smaller because the speckles were effectively two dimensional; there the detector's circular field lens performed a two-dimensional rather than a one-dimensional average.

To demonstrate the necessity of employing the surface impedance method in the results of Figs. 6–11, we conclude this section by briefly comparing these theoretical results with analogous results for a perfectly conducting rough surface. The numerical methods for the perfect conductor applied here employ exact integral equations and are described in detail elsewhere.[33] The discretization and averaging parameters were identical to those quoted in the beginning of this section, and integration of the p- and s-polarized intensities always indicated that energy conservation was maintained to within 1%. Figures 12 and 13 show these comparisons at $\theta_i = 0°$ and 30°, respectively, for $\lambda = 1.152$ μm, while Figs. 14 and 15 show similar comparisons for $\lambda = 3.392$ μm. The results for s_{11}, s_{12}, s_{33}, and I_- for the perfect conductor are generally in close comparison with those of the penetrable surface. There are modest differences in these quantities at $\lambda = 1.152$ μm, while at $\lambda = 3.392$ μm (where the surface conductivity is higher) the comparisons are considerably

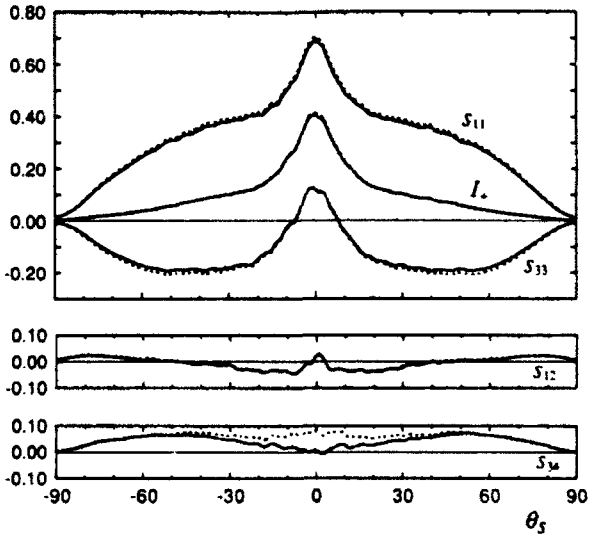

Fig. 14. For $\theta_i = 0°$ and $\lambda = 3.392$ μm, the unique matrix elements s_{11}, s_{12}, s_{33}, and s_{34} and the +45°-polarized intensity I_-. Numerical results that employ the surface impedance method (solid curves) are compared with results for the perfect conductor (dashed curves); the surface roughness is consistent with a Gaussian process.

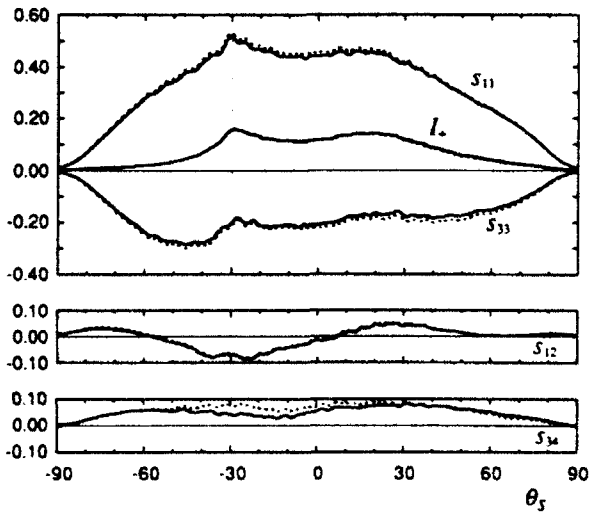

Fig. 15. Same as Fig. 14 but for $\theta_i = 30°$.

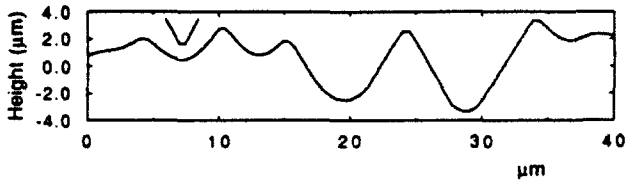

Fig. 16. Segment of one of the profilometer scans of the surface that illustrates the sharp peaks and the broad valleys of the experimental surface. The shape of the profilometer stylus employed is also indicated (60° wedge angle, 0.4-μm blunt tip).

closer. However, in any given figure the largest differences in the comparisons are consistently seen in the matrix element s_{34}. These differences are relatively large at $\lambda = 1.152$ μm, while in the more conductive case at $\lambda = 3.392$ μm they are smaller but still significant. Thus the form of s_{34} is strongly dependent on the finite conductivity in the cases shown here, while the other matrix elements have a weaker dependence. We conclude that the surface impedance method, which also produces results that are more consistent with the experimental data for s_{34} in Figs. 6–11, is entirely necessary for accurate results in the cases of interest here.

5. COMPARISON OF RESULTS FOR THE PROFILED SURFACE

It has been seen that the theoretical and experimental results of Figs. 6–11 of Section 4 provide reasonably good comparisons of the elements of the Stokes-scattering matrix. However, the differences that remain imply that more multiple scattering occurs in the experiment than is present in the theoretical results. The origin of this discrepancy is not immediately clear. As we have discussed in Section 3, the impedance boundary-condition method should be reliable for the surface of interest here, so we do not consider it to be a likely source of error. Considerable care has also been exercised in the scattering measurements, and thus we believe that the experimental results are accurate representations of the scattering properties of the surface. The measured statistical parameters σ and a of the experimental surface are of high accuracy (±0.75% statistical error and ±2.0% profilometer calibration error for σ, and estimated errors of a few percent in a); changes in σ and a of the size of the errors do not produce significant changes in the theoretical results.

On examination of this situation, we believe that there are unusual properties of the experimental surface that have a significant effect on its scattering properties. Figure 16 shows a selected segment of one of the profilometer scans of the surface. It can be seen that the peaks of the surface are often sharply curved, while the valleys tend to have a broader curvature. This behavior is usually much less obvious than it is in Fig. 16, but it is consistently present throughout the data. The sharp peaks and the broad valleys cannot be attributed to the width of the profilometer stylus, which would produce just the opposite effect, so we conclude that they are present in the surface itself.

It is clear from Fig. 3 that the first-order probability density of surface height is close to Gaussian form. However, this resemblance does not necessarily imply that the surface statistically conforms to a Gaussian process, as we assumed in the numerical results of Section 4. In fact, for a Gaussian process the peaks and the valleys of the surface must have a statistically identical appearance,[39] and we immediately conclude that the behavior seen in Fig. 16 is inconsistent with a Gaussian process. To study the deviations from Gaussian statistics, we could employ higher-order probability densities of height, but we have found it simpler to study the statistical properties of surface derivatives. In particular, we have compared the first-order probability densities of the first two surface derivatives with the Gaussian forms expected for a Gaussian random process.[40]

To achieve reliable estimates of the derivatives in the presence of digitization noise in the profilometer data, we computed the Fourier transform of each scan. Only the first 900 of the 4096 complex Fourier coefficients were kept because only noise was present in higher coefficients. On performing an inverse transform, we obtained a profile in which only noise had been effectively removed. With suitable linear or quadratic frequency weighting, inverse transformation of the 900 Fourier coefficients permitted reliable determination of the first two derivatives of the surface.

Figures 17 and 18 show the probability densities of the first and second derivatives, respectively, that have been

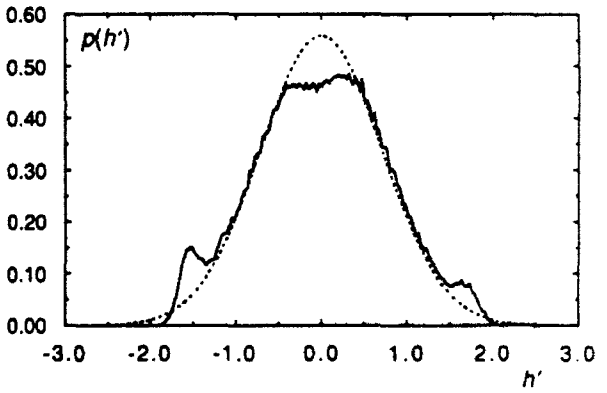

Fig. 17. Probability density of surface slope, $p(h')$, calculated from the profilometry of the experimental rough surface (solid curve). The dashed curve is a comparison with a Gaussian probability density (with root-mean-square slope $\sqrt{2}\,\sigma/a$, as would be expected for a height correlation function of Gaussian form).

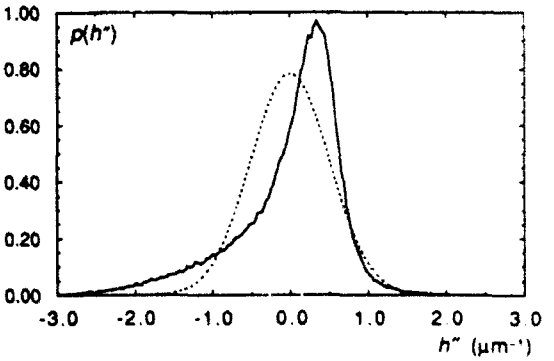

Fig. 18. Probability density of the second derivative of the surface, $p(h'')$, calculated from the profilometry of the experimental rough surface (solid curve). The dashed curve is a comparison with a Gaussian probability density (with root-mean-square second derivative $2\sqrt{3}\,\sigma/a^2$, as would be expected for a Gaussian height correlation function).

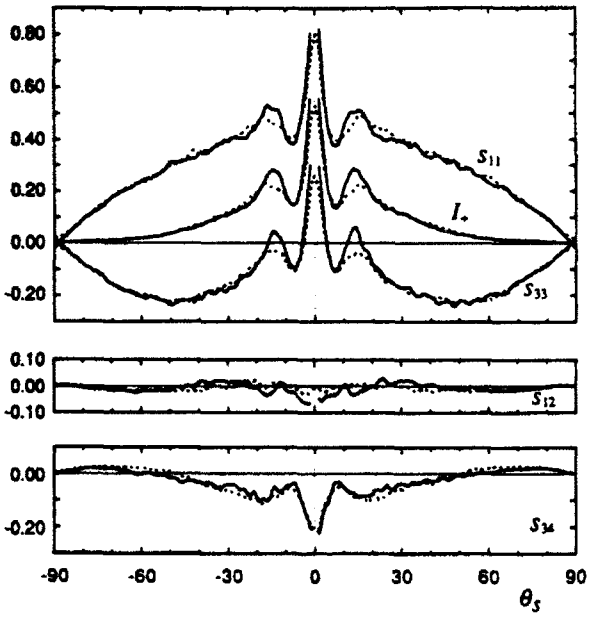

Fig. 19. For $\theta_i = 0°$ and $\lambda = 1.152$ μm, the unique matrix elements s_{11}, s_{12}, s_{33}, and s_{34} and the +45°-polarized intensity I_+. Experimental results (solid curves) are compared with numerical results (dashed curves; surface impedance method applied to profiled surface).

determined from the 20 profilometer scans. Both densities differ significantly from the Gaussian forms expected for a Gaussian process. The probability density of slope is flatter near the mean and presents small secondary maxima at −1.5 and 1.7. These secondary maxima fall near the maximum slope that is resolved with the 60° stylus described in Subsection 2.A. In particular, a steep side of the stylus touches the surface for slopes stronger than $\pm\tan 60° \cong \pm 1.7$; the maxima near these values in Fig. 17 appear to arise from surface slopes stronger than these critical values. In Fig. 18 the probability density of the second derivative is strongly left skewed in a manner consistent with Fig. 16. As discussed above, we attribute this behavior largely to the properties of the experimental surface rather than to stylus effects.

It is of obvious interest to determine the effect of these properties of the experimental surface on its scattering behavior. To apply the numerical techniques of Section 4, one would apparently need to find a statistical model completely consistent with the experimental surface. This problem has proven formidable, and we have instead taken a more direct approach. We have applied the numerical methods, using the impedance boundary condition, directly to the data obtained with the surface profilometer. In this procedure each profilometer scan was first filtered in frequency space, as discussed above, for the removal of digitization noise. We employed the surface impedance method to calculate the p and s scattered amplitudes for an illuminated width g near one end of the profilometer data. The illumination was then moved transversely by an amount Δx, and the process was repeated until the entire profilometer scan had been illuminated. We then averaged suitable products of the p and s amplitudes over all illuminated regions of the 20 profilometer scans to estimate the four elements of the Stokes-scattering matrix. The numerical parameters employed in the calculations were similar to those of Section 4, though it was necessary to make small changes to deal with the sampling interval of the profilometer data. In particular, we used $N_x = 600$ discretization points, the discretization interval $\lambda/10$, $g/\lambda = 12$ (at $\lambda = 1.152$ μm) or 8 (at $\lambda = 3.392$ μm), and the number of surface realizations of 3140 (at $\lambda = 1.152$ μm) or 1220 (at $\lambda = 3.392$ μm) owing to the fixed total length of the profilometer data.

We show the results of these calculations with the experimental data for $\lambda = 1.152$ μm in Figs. 19, 20, and 21 for $\theta_i = 0°$, 10°, and 30°, respectively. The comparisons here show substantial improvement over the analogous comparisons for the Gaussian model (Figs. 6–8). The heights of s_{11}, s_{33}, and I_- near the backscattering direction have increased in the theoretical results of Figs. 19 and 20, so we conclude that the amount of multiple scattering has increased. The secondary maxima in these theoretical results have also become more distinct and are now only slightly below those of the experimental results. At $\theta_i = 30°$ (Fig. 21) the comparisons of s_{11}, s_{33}, and I_- have also significantly improved. The comparisons of s_{34} are

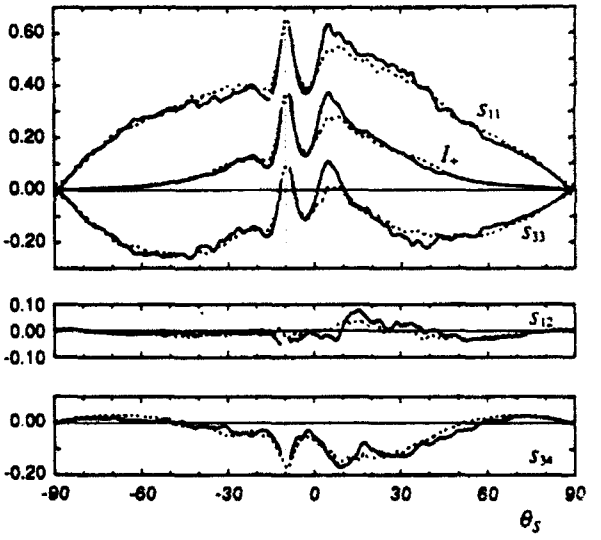

Fig. 20. Same as Fig. 19 but for $\theta_i = 10°$.

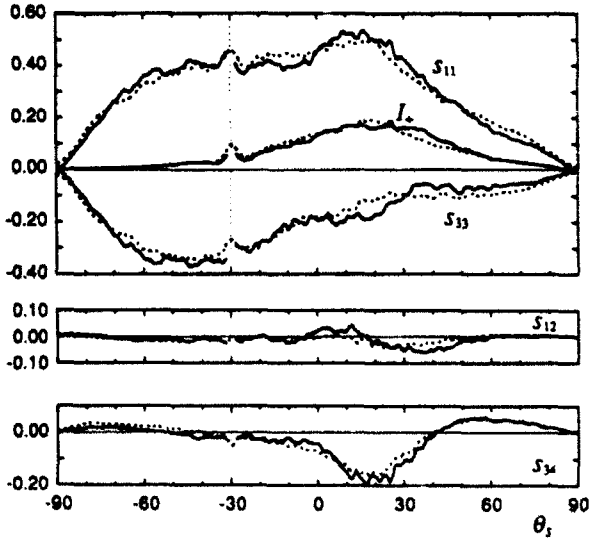

Fig. 21. Same as Fig. 19 but for $\theta_i = 30°$.

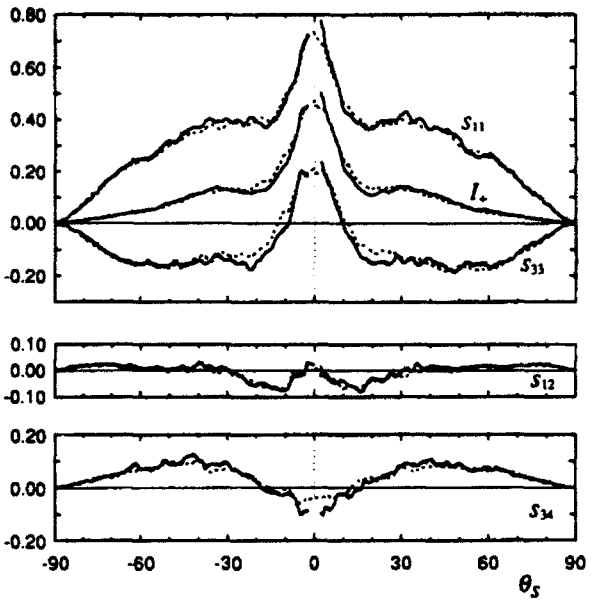

Fig. 22. For $\theta_i = 0°$ and $\lambda = 3.392$ μm, the unique matrix elements s_{11}, s_{12}, s_{33}, and s_{34} and the $+45°$-polarized intensity I_+. Experimental results (solid curves) are compared with numerical results (dashed curves; surface impedance method applied to profiled surface).

excellent not only at $\theta_i = 0°$ (as in Fig. 6) but also now at $\theta_i = 10°$ and even at $\theta_i = 30°$, where the negative part of s_{34} shows a close comparison. The theoretical results for s_{12} remain small but also show a more favorable comparison here than they do in Figs. 6–8.

Further comparisons are shown in Figs. 22, 23, and 24 for $\lambda = 3.392$ μm and $\theta_i = 0°$, 10°, and 30°, respectively. It can be seen that s_{11}, s_{33}, and I_- have again increased in the backscattering direction for $\theta_i = 0°$ and 10°, and generally excellent agreement is seen in these quantities for all the cases shown. The theoretical results for s_{12} are of larger magnitude in Figs. 22–24 than they are in Figs. 9–11 and now show favorable comparisons with the experimental results. The comparisons of s_{34} are also quite good in Figs. 22–24, and although small differences can sometimes be seen, they exhibit a clear and significant improvement over those of the Gaussian model. It is interesting to note that even the speckle noise in the theoretical and experimental results of Figs. 19–24 is of similar levels; this is because both results are based on the same total length of rough surface.

We conclude that the comparisons of this section are generally excellent and show a distinct improvement over those of Section 4. It follows that most of the differences seen in the comparisons of Section 4 arose from the inconsistency of the experimental surface with a Gaussian process. When the properties of the experimental surface are taken into account, as we have done in this section, excellent comparisons of the four elements of the Stokes-scattering matrix are made. This conclusion is significant, for the differences seen in the comparisons of Section 4 would have left doubts concerning the correctness of the theoretical and experimental methods that we have employed.

The increase in multiple scattering apparent in the theoretical results of this section is reasonable for the surface curvatures seen in Fig. 16. The bowl-shaped regions of the experimental surface would tend to create an abundance of multiple-scattering paths that are at the origin of backscattering enhancement.[16,17] On the other hand, a surface consistent with a Gaussian process would have statistically identical peaks and valleys, and the degree to which such multiple-scattering paths occur would be reduced.

We believe that our profilometry of the experimental surface is good, but we do not claim that it is perfect. For example, the slope statistics of Fig. 17 show clear effects of the width and the shape of the profilometer stylus. The small differences seen in the comparisons in this section (for example, in s_{11}, s_{33}, or I_- in Figs. 19 and 20) suggest that slightly more multiple scattering still occurs in the experiment, and small stylus effects could play a role in these differences. As we can see from the form of the stylus in Fig. 16, the surface itself should have even sharper peaks than those present in the profilometer data.

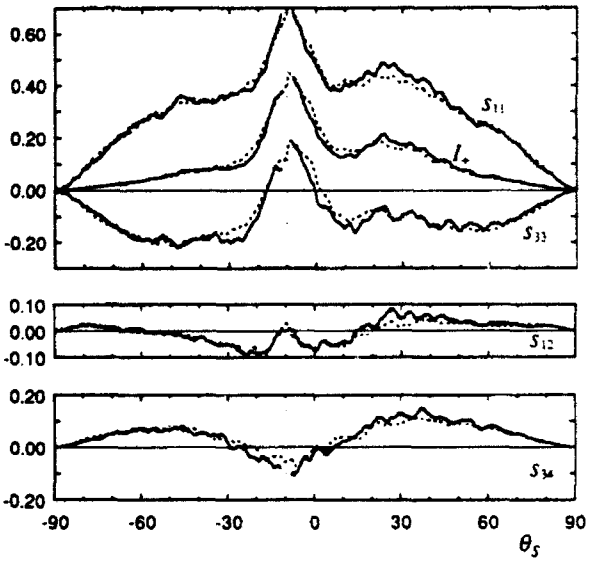

Fig. 23. Same as Fig. 22 but for $\theta_i = 10°$.

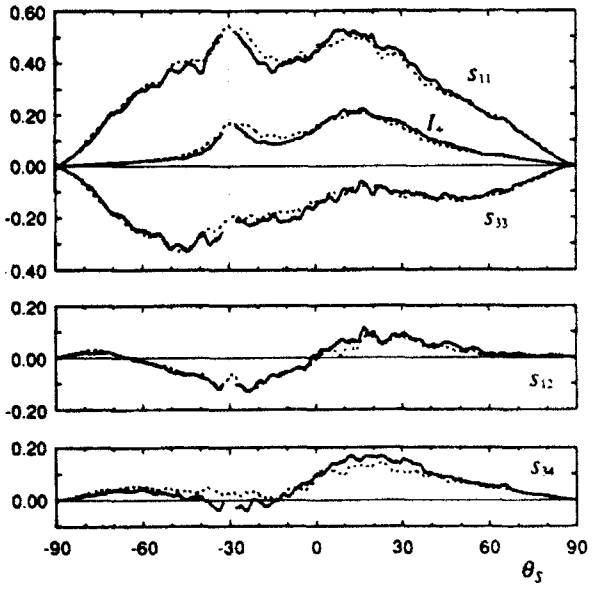

Fig. 24. Same as Fig. 22 but for $\theta_i = 30°$.

Table 1. Total Scattered Powers Contained in p, s, and +45° Polarization States

	p ($s_{11} + s_{12}$)	s ($s_{11} - s_{12}$)	+45° [($s_{11} + s_{33}$)/2]
Impedance Boundary Condition, Gaussian Model			
$\lambda = 1.152$ μm			
$\theta_i = 0°$	0.945	0.984	0.239
$\theta_i = 10°$	0.944	0.984	0.233
$\theta_i = 30°$	0.941	0.986	0.189
$\lambda = 3.392$ μm			
$\theta_i = 0°$	0.954	0.984	0.303
$\theta_i = 10°$	0.955	0.984	0.291
$\theta_i = 30°$	0.958	0.985	0.223
Impedance Boundary Condition, Profiled Surface			
$\lambda = 1.152$ μm			
$\theta_i = 0°$	0.947	0.989	0.286
$\theta_i = 10°$	0.945	0.989	0.275
$\theta_i = 30°$	0.945	0.991	0.220
$\lambda = 3.392$ μm			
$\theta_i = 0°$	0.952	0.987	0.355
$\theta_i = 10°$	0.953	0.987	0.340
$\theta_i = 30°$	0.957	0.988	0.256
Experimental Results			
$\lambda = 1.152$ μm			
$\theta_i = 0°$	0.943	0.991	0.300
$\theta_i = 10°$	0.947	0.987	0.279
$\theta_i = 30°$	0.937	0.992	0.207
$\lambda = 3.392$ μm			
$\theta_i = 0°$	0.975	0.989	0.350
$\theta_i = 10°$	0.974	0.980	0.334
$\theta_i = 30°$	0.965	0.971	0.250

which could lead to more multiple scattering than that found in the calculations of this section. However, the excellence of the comparisons of Figs. 19–24 clearly indicates that these effects would be quite small.

As we have discussed in Subsection 2.B, the quality of the experimental surface has permitted us to normalize scattering measurements from first principles. We thus conclude this section by presenting a comparison of experimental and theoretical results for the total powers contained in selected scattered intensities. Throughout the results shown in Table 1, it can be seen that the total p- and s-polarized diffuse reflectivities are all slightly less than unity and that there is consistently more absorption in p polarization. There is generally excellent agreement; only small differences are present in the experimental p reflectivity at $\lambda = 3.392$ μm, which shows 1–2% higher reflectivity than that of the numerical results. The numerical results for the profiled surface are in close agreement with the experimental results for the powers contained in I_-, while the numerical results for the Gaussian model produce significantly smaller powers.

6. CONCLUSIONS

In this paper we have compared in detail experimental and theoretical results for the light diffusely scattered from a surface that is rough in one dimension. This study, as presented here, has required considerably more than an exercise of established theoretical and experimental techniques. First, we have developed new experimental methods to fabricate a strictly one-dimensional rough surface with nearly Gaussian first-order height statistics. All four unique elements of the Stokes-scattering matrix were measured and normalized from first principles, and scattering behavior at high scattering angles has been seen to be more consistent with theoretical results. Second, we have developed new numerical methods based on an impedance boundary condition that are suitable for a highly, but not perfectly, conducting rough surface. For the cases discussed here, it has been made clear that this method is entirely necessary for accurate results, particularly for the matrix element s_{34}.

It has been found that the experimental measurements, when they are compared with the theoretical results for a rough surface consistent with a Gaussian process, produce favorable but by no means perfect comparisons. However, excellent agreement has been obtained in comparisons made with theoretical results for the profiled surface. We have surmised that this situation arises from properties of the experimental surface that differ from those of a Gaussian profile.

There are a number of points to be made concerning these observations. First, the excellent agreement obtained in Section 5 clearly indicates that the theoretical techniques and the experimental methods employed here, when they are applied with care, yield entirely consistent results for a rough surface that produces multiple scattering. For a problem as subtle and difficult as that of wave scattering from a randomly rough surface, this conclusion is significant and strong. Further, for the crucial purpose of testing experimental methods and theoretical techniques in this field, the lack of detailed consistency of the experimental surface with a Gaussian process is not significant. More precisely, we have satisfied the main goals of the Introduction concerning the accuracy of surface characterization, scattering measurements, and theoretical methods to the extent that excellent comparisons have been made. In drawing conclusions, we have not found it necessary to employ an experimental surface that conforms in all details to a Gaussian process or to find a statistical model consistent with a particular experimental surface.

Our results also demonstrate that relatively subtle statistical properties may play a significant role in the scattering behavior of a rough surface. In the case of interest here, we have seen a contribution of surface curvatures to the amount of multiple scattering. This statement is an oversimplification, which, although it is adequate for our arguments here, leads to a deeper question: What then are the statistical properties of a rough surface that have significant effects on its scattering behavior? This difficult question certainly warrants further investigation, though it is not easily addressed by the numerical methods employed here. In approximations such as the Kirchhoff method and perturbation methods, only low-order statistical properties of the surface appear in theoretical results, although one might expect that more rigorous results would depend significantly on probability densities of higher order.

Finally, despite the excellence of comparisons presented here, we do not intend to imply that scattering from rough

surfaces is, in any wide sense, a well-understood field. There are important regimes in which theoretical methods or experimental techniques still find formidable challenges and considerable progress remains to be made. For example, the numerical methods employed here would readily fail at high angles of incidence, and our methods of surface characterization would be completely inadequate for a surface with significantly smaller structures. Hence there remain many open questions in the scattering of waves from surfaces, but the good comparisons presented here provide one unusual and important instance in which there have been well-verified theoretical and experimental results in this field.

ACKNOWLEDGMENTS

This research was sponsored by the U.S. Army Research Office. K. A. O'Donnell is grateful to have been a visitor in the laboratory of A. Consortini of the University of Florence during the preparation of this manuscript.

REFERENCES AND NOTES

1. P. Beckmann and A. Spizzichino, *The Scattering of Electromagnetic Waves from Rough Surfaces* (Pergamon, New York, 1963).
2. F. G. Bass and I. M. Fuks, *Wave Scattering from Statistically Rough Surfaces* (Pergamon, New York, 1979).
3. G. S. Brown, "A comparison of approximate theories for scattering from random rough surfaces," Wave Motion **7**, 195–205 (1985).
4. J. A. DeSanto and G. S. Brown, "Analytical techniques for multiple scattering from rough surfaces," in *Progress in Optics*, E. Wolf, ed. (Elsevier, New York, 1986), Vol. 23.
5. J. A. Ogilvy, *Theory of Wave Scattering from Random Rough Surfaces* (Hilger, Bristol, UK, 1991).
6. M. Nieto-Vesperinas and J. C. Dainty, eds., *Scattering in Volumes and Surfaces* (North-Holland, Amsterdam, 1990).
7. J. M. Bennett and L. Mattsson, *Introduction to Surface Roughness and Scattering* (Optical Society of America, Washington, D.C., 1989).
8. W. S. Bickel and W. M. Bailey, "Stokes vectors, Mueller matrices, and polarized scattered light," Am. J. Phys. **53**, 468–478 (1985).
9. J. M. Elson and J. M. Bennett, "Relation between the angular dependence of scattering and the statistical properties of optical surfaces," J. Opt. Soc. Am. **69**, 31–48 (1979).
10. Y. Wang and W. L. Wolfe, "Scattering from microrough surfaces: comparison of theory and experiment," J. Opt. Soc. Am. **73**, 1596–1602 (1983).
11. Y. Wang and W. L. Wolfe, "Further comparisons between surface scattering theory and measurements," J. Opt. Soc. Am. A **1**, 783–784 (1984).
12. J. M. Bennett, H. H. Hurt, J. P. Rahn, J. M. Elson, K. H. Guenther, M. Rasigni, and F. Varnier, "Relation between optical scattering, microstructure and topography of thin silver films. 1: Optical scattering and topography," Appl. Opt. **24**, 2701–2711 (1985).
13. O. Hunderi and D. Beaglehole, "Study of the interaction of light with rough metal surfaces. II. Theory," Phys. Rev. B **2**, 321–329 (1970).
14. S. O. Sari, D. K. Cohen, and K. D. Scherkoske, "Study of surface plasma-wave reflectance and roughness-induced scattering in silver foils," Phys. Rev. B **21**, 2162–2174 (1980).
15. V. Celli, A. A. Maradudin, A. M. Marvin, and A. R. McGurn, "Some aspects of light scattering from a randomly rough metal surface," J. Opt. Soc. Am. A **2**, 2225–2239 (1985).
16. K. A. O'Donnell and E. R. Méndez, "Experimental study of scattering from characterized random surfaces," J. Opt. Soc. Am. A **4**, 1194–1205 (1987).
17. E. R. Méndez and K. A. O'Donnell, "Observation of depolarization and backscattering enhancement in light scattering from Gaussian random surfaces," Opt. Commun. **61**, 91–95 (1987).
18. E. I. Thorsos, "The validity of the Kirchhoff approximation for rough surface scattering using a Gaussian roughness spectrum," J. Acoust. Soc. Am. **83**, 78–92 (1988).
19. M. Nieto-Vesperinas and J. M. Soto-Crespo, "Monte Carlo simulations for scattering of electromagnetic waves from perfectly conductive random rough surfaces," Opt. Lett. **12**, 979–981 (1987).
20. A. A. Maradudin, E. R. Méndez, and T. Michel, "Backscattering effects in the elastic scattering of *p*-polarized light from a large-amplitude random metallic grating," Opt. Lett. **14**, 151–153 (1989).
21. T. Michel, A. A. Maradudin, and E. R. Méndez, "Enhanced backscattering of light from a non-Gaussian random metal surface," J. Opt. Soc. Am. B **6**, 2438–2446 (1989).
22. J. M. Soto-Crespo and M. Nieto-Vesperinas, "Electromagnetic scattering from very rough random surfaces and deep reflection gratings," J. Opt. Soc. Am. A **6**, 367–384 (1989).
23. A. A. Maradudin, T. Michel, A. R. McGurn, and E. R. Méndez, "Enhanced backscattering of light from a random grating," Ann. Phys. (N.Y.) **203**, 255–307 (1990).
24. M. Saillard and D. Maystre, "Scattering from metallic and dielectric rough surfaces," J. Opt. Soc. Am. A **7**, 982–990 (1990).
25. E. I. Thorsos and D. R. Jackson, "Studies of scattering theory using numerical methods," Waves Random Media **3**, S165–S190 (1991).
26. J. A. Sanchez-Gil and M. Nieto-Vesperinas, "Light scattering from random rough dielectric surfaces," J. Opt. Soc. Am. A **8**, 1270–1286 (1991).
27. A. Ishimaru, J. S. Chen, P. Phu, and K. Yoshitomi, "Numerical, analytical, and experimental studies of scattering from very rough surfaces and backscattering enhancement," Waves Random Media **3**, S91–S107 (1991).
28. A. Ishimaru and J. S. Chen, "Scattering from very rough surfaces based on the modified second-order Kirchhoff approximation with angular and propagation shadowing," J. Acoust. Soc. Am. **88**, 1877–1883 (1990).
29. Y. Q. Jin and M. Lax, "Backscattering enhancement from a randomly rough surface," Phys. Rev. B **42**, 9819–9829 (1990).
30. M. J. Kim, J. C. Dainty, A. T. Friberg, and A. J. Sant, "Experimental study of enhanced backscattering from one- and two-dimensional random rough surfaces," J. Opt. Soc. Am. A **7**, 569–577 (1990).
31. J. C. Dainty, N. C. Bruce, and A. J. Sant, "Measurements of light scattering by a characterized random rough surface," Waves Random Media **3**, S29–S39 (1991).
32. K. A. O'Donnell and M. E. Knotts, "Polarization-dependence of scattering from one-dimensional rough surfaces," J. Opt. Soc. Am. A **8**, 1126–1131 (1991).
33. T. R. Michel, M. E. Knotts, and K. A. O'Donnell, "Stokes matrix of a one-dimensional perfectly conducting rough surface," J. Opt. Soc. Am. A **9**, 585–596 (1992).
34. Compare Figs. 6 and 8 of Ref. 32 with Figs. 2 and 3 of Ref. 33; also compare Figs. 4 and 5 with Figs. 9 and 10 of Ref. 33.
35. D. Maystre, "Integral methods," in *Electromagnetic Theory of Gratings*, R. Petit, ed. (Springer-Verlag, Berlin, 1980).
36. R. Garcia-Molina, A. A. Maradudin, and T. A. Leskova, "The impedance boundary condition for a curved surface," Phys. Rep. **194**, 351–359 (1990).
37. M. Born and E. Wolf, *Principles of Optics* (Pergamon, Oxford, 1975).
38. E. D. Palik, *Handbook of Optical Constants of Solids* (Academic, New York, 1985).
39. More precisely, for a zero-mean Gaussian process $h(x)$, probability densities of arbitrary order are all invariant under the transformation $h(x) \rightarrow -h(x)$.
40. R. J. Adler, *The Geometry of Random Fields* (Wiley, New York, 1981).

Optics Communications 99 (1993) 1–6
North-Holland

OPTICS
COMMUNICATIONS

Backscattering enhancement from a conducting surface with isotropic roughness

M.E. Knotts and K.A. O'Donnell
The School of Physics, Georgia Institute of Technology, Atlanta, GA 30332, USA

Received 16 September 1992; revised manuscript received 27 January 1993

Measurements are presented of the angular distribution of scattered intensity associated with backscattering enhancement from a conducting surface with two-dimensional roughness. For a linearly polarized incident wave, the diffusely scattered intensity is found to be significantly polarization-dependent.

The scattering of light from randomly rough surfaces has been of considerable interest. For conducting surfaces with steep slopes and correlation length comparable to the illumination wavelength, backscattering enhancement has been noted in the reflected diffuse scattering [1,2]. Considerable effort has since been directed toward theoretical and experimental investigations of scattering by a surface with one-dimensional roughness, largely because this case is more directly addressed with theoretical methods. In the one-dimensional case, the scattering properties have been studied through the p- and s-polarized diffusely scattered intensities [3–5], or more completely with the four unique elements of the surface's Stokes scattering matrix [6,7]. The backscattering enhancement has been attributed to the coherence of multiple-scattering paths occurring within valleys of the rough surface.

Even though early observations of this type of backscattering enhancement were for a surface with two-dimensional roughness [1,2], there has been little subsequent work applied to this case [8–10]. This may be partly due to the difficulty of the theoretical methods necessary to approach a two-dimensional rough surface when multiple scattering is significant [8,9]. These theoretical approaches have required considerable simplifying assumptions and approximations (for example, assumptions in the development of the Kirchhoff method in ref. [8], and the discretization of integral equations for scalar waves in ref. [9]). Hence, controlled experiments with well-characterized rough surfaces could be expected to provide the most reliable data for the case of two-dimensional roughness.

Previous qualitative observations have noted a remarkable polarization-dependence of the backscattering enhancement of a two-dimensionally rough surface [1,2]. This is illustrated in fig. 1, which shows photographs of the co- and cross-polarized backscattering enhancement from a two-dimensional rough surface with gaussian height statistics and with a height correlation function of rotationally symmetry gaussian form. For the case of normal incidence, both scattered intensities contain a strong backscattering peak surrounded by an annular region where secondary minima and maxima are clearly visible at various field angles. There appears to be nearly four-fold symmetry about the backscattering direction in the results of fig. 1. However, the symmetry of the situation implies that only a pair of two-fold symmetries (left to right, and top to bottom in figs. 1A and 1B) must always be observed. The dark regions of the cross-polarized scattering are of somewhat higher contrast than those of the co-polarized scattering. These patterns remain fixed as the rough surface is rotated about its normal, which verified that these observations are connected to the polarization of the incident wave, rather than any lack of statistical isotropy of the rough surface. The two-dimensional features seen in fig. 1 have not been in-

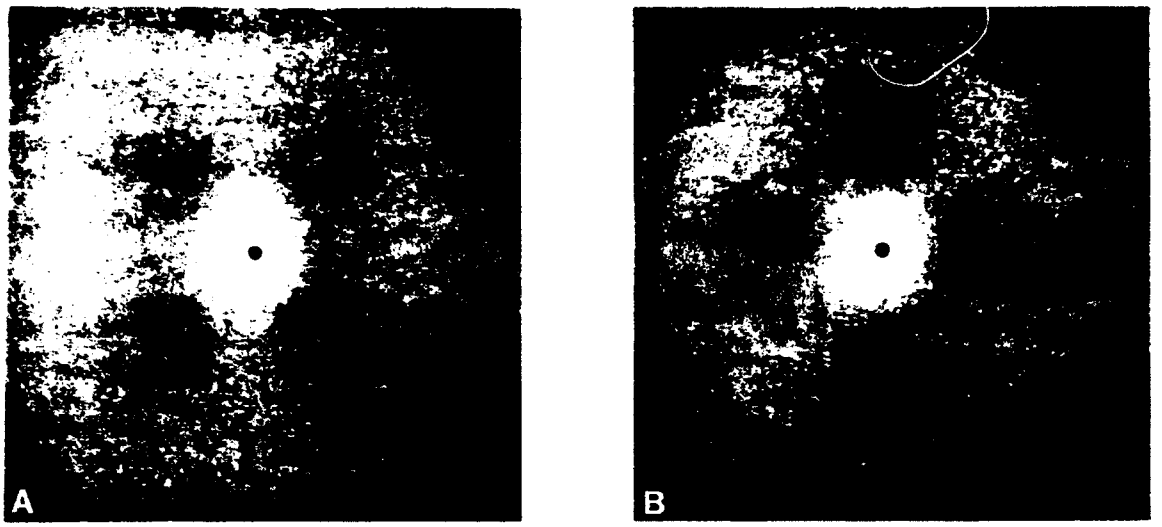

Fig. 1. Photographs of co-polarized (A) and cross-polarized (B) intensity scattered from a two-dimensional rough surface for normal incidence. The wavelength is 0.633 μm and the incident polarization is horizontal. The surface roughness has approximately gaussian height statistics with standard deviation $\sigma \approx 2\lambda$, and the height correlation function is of gaussian form with correlation length $a \approx 3\lambda$. The exact backscattering direction is denoted by the dark spot and the region shown is approximately $\pm 25^{\circ}$ wide.

vestigated in previous theoretical or experimental work, and previous results [1,2,8,10] correspond only to a one-dimensional section of the intensity of fig. 1A or 1B along a horizontal or vertical axis. The purpose of the present paper is thus to provide measurements of the two-dimensional nature of the backscattering enhancement under controlled experimental conditions.

The surface employed in fig. 1 (as well as those employed in previous experiments [1,2]) is difficult to characterize because of the fine structure of the surface roughness. To study the polarization-dependent scatter with a well-characterized surface, in the measurements to be discussed here we have increased the surface correlation length and illumination wavelength by a factor of approximately two. The rough surface was fabricated using techniques that have been described in more detail elsewhere [1,2]. A 50×50 mm^2 glass plate was first coated with three layers of Shipley 1375 photoresist. The plate was then exposed to a series of eight statistically independent speckle patterns from a HeCd laser of wavelength 0.442 μm. The central limit theorem thus implies that the net exposure was approximately a realization of a gaussian process. In the exposing plane, the speckle patterns were isotropic due to the rotational symmetry of the optical system that generated them; their correlation functions were of gaussian form due to the gaussian laser mode. The plate was developed in Shipley 355 developer and coated with a thick layer of gold using standard vacuum evaporation techniques. The processing produced an approximately linear response of the photoresist; this implies that the surface height should also have a correlation function of gaussian form.

The rough surface was characterized with a Talystep surface profilometer employing a diamond stylus of conical form with 60° full angle and with 0.5 μm tip radius. Eight scans of independent parts of the surface were made, with each scan consisting of 8192 data points taken along a 1.58 mm length. The scans were corrected only for an unknown slope over the scan length through a least-squares fit to a linear function. The histogram of surface height was found to provide a close approximation to a gaussian probability density with standard deviation $\sigma = 1.66$ μm (skewness $= -0.089$, kurtosis $= 2.84$); the height correlation function was found to be of nearly gaussian form with 1/e width $a = 3.75$ μm.

Figure 2 shows the definition of the polarization

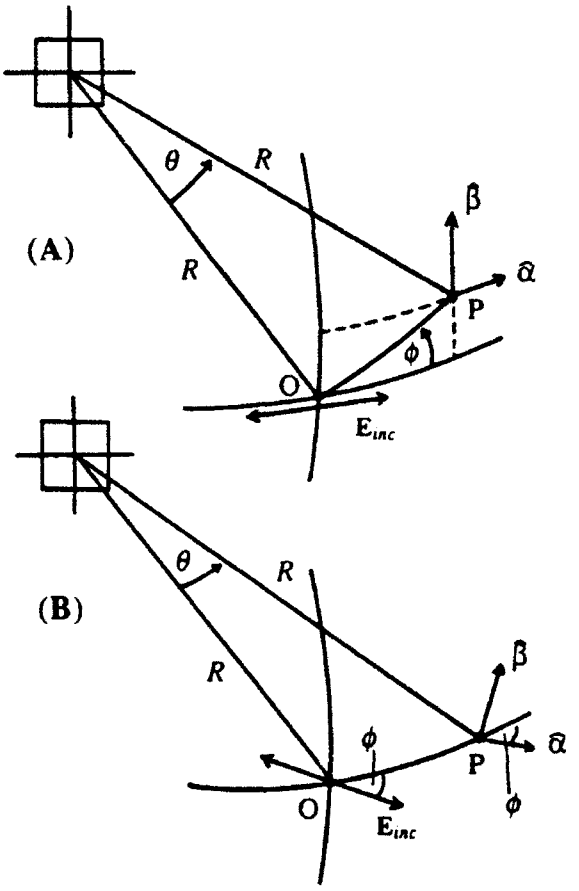

Fig. 2. Top: scattering of a horizontally polarized, normally incident wave by a two-dimensional rough surface into a direction (θ, ϕ). Bottom: the equivalent situation in which the incident and detected polarizations are rotated by ϕ, and the measurements are conducted at $(\theta, \phi) = (\theta, 0)$.

conditions employed in the scattering measurements presented here. As in fig. 1, the illuminating wave is assumed to be normally incident, linearly polarized, and, without loss of generality, to have horizontal polarization in fig. 2A. We consider the intensity scattered from the rough surface to a distant hemisphere of radius R. The point O determines the location of the incident wave on this hemisphere, and an arbitrary observation point P has coordinates (R, θ, ϕ) in the spherical coordinate system shown. The co-polarized intensity at P may then be defined as that polarized in the direction of the unit vector $\hat{\alpha}$, where $\hat{\alpha}$ is defined by parallel transport of the direction of the incident polarization along the arc OP, and the cross-polarized intensity may be defined as that polarized in the orthogonal direction along a second vector $\hat{\beta}$.

For the case of normal incidence, it is possible to effectively position a detector at the observation point P in a simpler manner. As can be seen in fig. 2B, if the incident polarization state, the detected polarization state, and the rough surface are all rotated by the angle ϕ, this is completely equivalent to the situation shown in fig. 2A. Of course, in the case of interest here the rough surface has isotropic roughness, and there is then no need to rotate it.

The experimental apparatus was similar to that described more completely elsewhere [6], with modifications to provide control of the direction of the incident polarization. The source was a Jodon HN-20 HeNe laser, which illuminated a 20 mm diameter of the rough surface. In the first results to be discussed here we employed the wavelength $\lambda = 1.152$ μm, so that $a/\lambda \approx 3$ as was the case in fig. 1. A half-wave plate allowed the incident polarization state to be rotated by the angle ϕ, and a polarizer that followed removed any residual ellipticity to produce a pure linear state with extinction better than 10^{-5}. Appropriate settings of a detector polarizer enabled the co- or cross-polarized scattered intensity to be measured. The detector was an indium antimonide photodiode mounted on an arm of length $R = 700$ mm. This arm was positioned by a computer-controlled rotation stage, so that the detector could be scanned rapidly and reproducibly. Data were taken for ϕ between 0° and 90° in steps of 5°, and for θ between −30° and 30° in steps of 0.25°. This range of angles comprises a complete set of measurements for a region of 30° radius surrounding the backscattering direction in fig. 2A; the results shown below were plotted by imposing the symmetry for $90° < \phi \leqslant 180°$ that follows from the isotropy of the surface roughness. A limited amount of data was taken for $90° < \phi \leqslant 180°$ that is not shown here but was adequate to demonstrate that the scattered intensities obeyed the necessary symmetries discussed earlier. In a final procedure, measurements of the incident power allowed the intensities to be normalized to scattered power per unit solid angle, for unit incident power.

The measured co- and cross-polarized scattered

intensities are shown in figs. 3 and 4, respectively, and compare favorably with the photographs of fig. 1. The data is plotted in figs. 3 and 4 such that the front half of the figures contains independent measurements. Both scattered intensities contain a distinct enhancement peak centered at $(\theta, \phi) = (0°, 0°)$ with an approximately $\pm 10°$ width. This peak is surrounded by an annular region for $|\theta|$ between 8° and 20° containing strongly polarization-dependent scatter with secondary minima and maxima. The co-polarized intensity has minima at $\phi = 45°$ and $\theta \approx \pm 12°$, maxima at $\phi = 90°$ and $\theta \approx \pm 14°$, and saddle-shaped regions at $\phi = 0°$ and $\theta \approx \pm 12°$. The cross-polarized intensity of fig. 4 has minima at $\theta \approx \pm 12°$ for $\phi = 0°$ and $\phi = 90°$ with stronger contrast than those of fig. 3, which is consistent with the observations of fig. 1. Beyond $|\theta| \approx 25°$, both the co-polarized and cross-polarized intensities remain significant, but they are no longer strongly dependent on the angle ϕ.

Figure 5 shows sections of the results of figs. 3 and 4 for $\phi = 0°$, 45°, and 90°, in addition to the total scattered intensity determined from the sum of the co- and cross-polarized intensities. The three curves of the co-polarized intensity show different forms, so that this intensity does not strictly have the four-fold symmetry that is suggested by fig. 1A. Instead, this intensity has only the pair of two-fold symmetries that are required by the symmetry of the experimental situation (that is, symmetry for

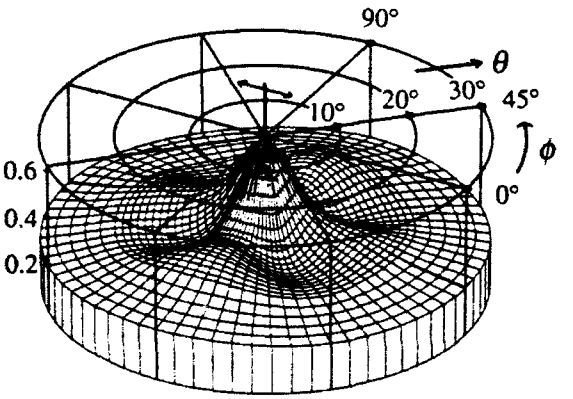

Fig. 3. The co-polarized scattering distribution from the rough surface as a function of the angles (θ, ϕ). The incident wavelength is $\lambda = 1.152$ μm, and the incident polarization direction is denoted by the arrow at the center of the figure.

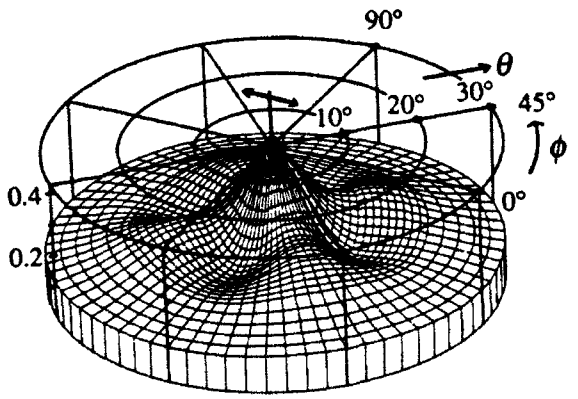

Fig. 4. The cross-polarized scattering distribution from the rough surface as a function of the angles (θ, ϕ). The incident wavelength is $\lambda = 1.152$ μm, and the incident polarization direction is denoted by the arrow at the center of the figure.

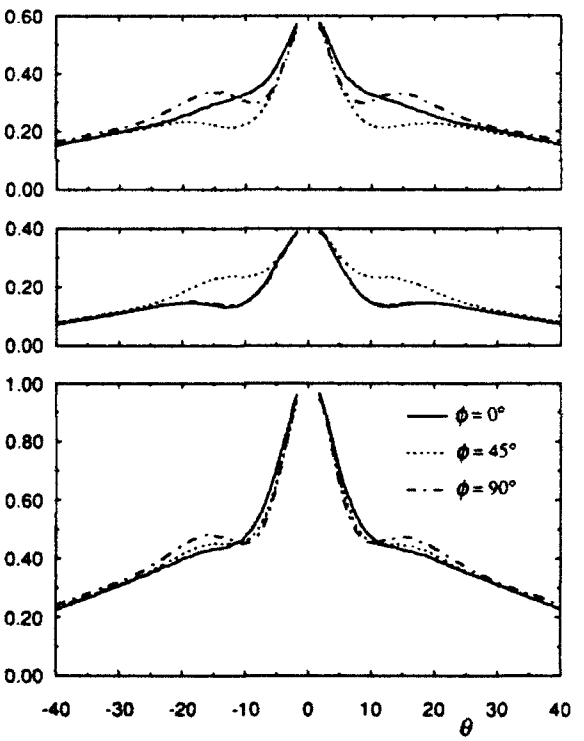

Fig. 5. The scattered intensities, for $\phi = 0°$, $\phi = 45°$, and $\phi = 90°$, as a function of the angle θ. Shown are the co-polarized intensity (top), the cross-polarized intensity (center), and the total scattered intensity (bottom). The illumination is normally incident and has wavelength $\lambda = 1.152$ μm.

$\phi \rightarrow (360° - \phi)$ and $\phi \rightarrow (180° - \phi)$). However, fig. 5 indicates that the form of the cross-polarized intensity is the same at $\phi = 0°$ and $\phi = 90°$. Thus, within the accuracy of our measurements, the cross-polarized intensity nearly satisfies a four-fold symmetry, even though this need not be the case. In the total scattered intensity in fig. 5, there are secondary maxima present at $\theta \approx \pm 16°$ for $\phi = 90°$, though these maxima are less distinct at $\phi = 45°$ and disappear at $\phi = 0°$. The total intensity has a weaker dependence on ϕ than is present in the co- or cross-polarized intensities.

For the case $a/\lambda \approx 3$, there is thus general consistency of the experimentally results of figs. 3–5 with the qualitative observations of fig. 1. However, under other conditions, this rough surface may have different scattering behavior. In particular, we have studied the scattering properties of this surface for $a/\lambda \approx 1$ by employing the 3.392 μm wavelength of our HeNe laser. In fig. 6 are shown the co-polarized, cross-polarized, and total scattered intensities for all θ and for $\phi = 0°$, 45°, and 90°. While the ϕ-dependence of these intensities was restricted to $|\theta| \leq 25°$ in fig. 5, in fig. 6 there is a significant ϕ-dependence for all values of $|\theta|$ to 90°. On comparison with fig. 5, the widths of enhancement peaks have increased, as is to be expected at the longer wavelength. The shapes of the co-polarized intensities have changed considerably at the longer wavelength, and there are now modest secondary maxima at $\theta \approx \pm 32°$ for $\phi = 0°$, while for $\phi = 45°$ and 90° this intensity has broader enhancement peaks without secondary maxima. The cross-polarized intensity shows nearly identical forms for $\phi = 0°$ and 90°, which was also noted in fig. 5, although the enhancement peaks are of smaller height in fig. 6. Finally, the total scattered intensity also has a lower enhancement peak than at $\lambda = 1.152$ μm, and the three curves show differences from one another that are larger than those of the corresponding curves of fig. 5. The forms of the total scattered intensity in fig. 6 generally resemble those of the co-polarized intensity.

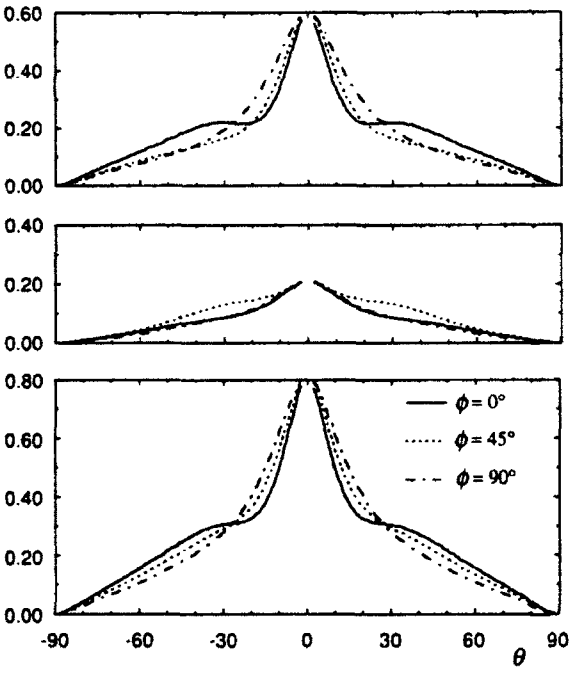

Fig. 6. The scattered intensities, for $\phi = 0°$, $\phi = 45°$, and $\phi = 90°$, as a function of the angle θ. Shown are the co-polarized intensity (top), the cross-polarized intensity (center), and the total scattered intensity (bottom). The illumination is normally incident and has wavelength $\lambda = 3.392$ μm.

The results presented in this paper thus demonstrate the detailed behavior of the co- and cross-polarized scattered intensities for a two-dimensional rough surface that creates backscattering enhancement. However, there is another way of interpreting these results for the case of normal incidence, which follows from fig. 2B. It is well-known that the polarization-dependence of the diffusely scattered light is determined by the 16 elements of the Stokes scattering matrix [6,7,11,12]. The elements of this matrix contain second-order moments of scattered amplitudes [11] and describe, for various incident polarization states, the scattered intensity measured with standard polarization components [12]. When $\phi = 0°$ and $\phi = 90°$ in fig. 2B, the incident polarization states are horizontal and vertical, and the co- and cross-polarized intensities may then be expressed in terms of the four elements in the upper left of this matrix [12]. When $\phi = 45°$ in fig. 2B, the incident state is at 45°, and other elements in the third row and third column of the Stokes scattering matrix contribute to the co- and cross-polarized scattered intensities [12]. These three values of ϕ are of primary importance, and at intermediate values the co- and cross-polarized intensities contain contributions from only the Stokes matrix elements men-

tioned above. From the point of view of fig. 2B, the polarization-dependence of the experimental results of figs. 3–6 thus demonstrate that the fundamental matrix elements cited above play a highly significant role in the scattering properties of this surface.

The form of the Stokes scattering matrix is dictated by the symmetries of the scattering configuration [11]. The symmetries present for a one-dimensional rough surface give rise to only four unique matrix elements [6,7], but the form of this matrix has not been investigated for a surface with isotropic roughness in two dimensions. We thus conclude that the results presented here also provide a clear indication that future theoretical and experimental research should address the Stokes scattering matrix of such a surface.

This research was sponsored by the U.S. Army Research Office.

References

[1] E.R. Méndez and K.A. O'Donnell, Optics Comm. 61 (1987) 91.

[2] K.A. O'Donnell and E.R. Méndez, J. Opt. Soc. Am. A 4 (1987) 1194.

[3] M. Nieto-Vesperinas and J.M. Soto-Crespo, Optics Lett. 12 (1987) 979.
J.M. Soto-Crespo and M. Nieto-Vesperinas, J. Opt. Soc. Am. A 6 (1989) 367.

[4] A.A. Maradudin, E.R. Méndez and T. Michel, Optics Lett. 14 (1989) 151.
A.A. Maradudin, T. Michel, A.R. McGurn and E.R. Méndez, Ann. Phys. 203 (1990) 255.

[5] M. Saillard and D. Maystre, J. Opt. Soc. Am. A 7 (1990) 982.

[6] K.A. O'Donnell and M.E. Knotts, J. Opt. Soc. Am. A 8 (1991) 1126.

[7] T.R. Michel, M.E. Knotts and K.A. O'Donnell, J. Opt. Soc. Am. A 9 (1992) 585.

[8] Y.Q. Jin and M. Lax, Phys. Rev. B 42 (1990) 9819.

[9] P. Tran and A.A. Maradudin, Phys. Rev. B 45 (1992) 3936.

[10] M.J. Kim, J.C. Dainty, A.T. Friberg and A.J. Sant, J. Opt. Soc. Am. A 7 (1990) 569.

[11] H.C. van de Hulst, Light scattering by small particles (Dover, New York, 1981).

[12] W.S. Bickel and W.M. Bailey, Am. J. Phys. 53 (1985) 468.

(Submitted to the Journal of the Optical Society of America, April '93)

Measurements of Light Scattering by a Series of Conducting Surfaces with One-Dimensional Roughness

M. E. Knotts and K. A. O'Donnell
The School of Physics
Georgia Institute of Technology
Atlanta, Georgia 30332
{Tel. (404) 894 - 8523}

April 23, 1993

Abstract

We present measurements of the polarization-dependence of the coherent and diffuse scatter from a set of conducting surfaces with strictly one-dimensional roughness. The surfaces have been fabricated with photoresist techniques and have been accurately characterized with stylus profilometry. The surface roughness varies by a factor of approximately seven throughout the series of surfaces, but all have height statistics that are close to Gaussian, and a correlation length that is nearly fixed and that is comparable to our illumination wavelengths. The polarization-dependence of the scattered intensity is fully specified by the four unique elements of the Stokes matrix, which are determined from six intensities measured with different polarization conditions. In studies of the coherent scatter we find large differences between the *p*- and *s*-polarized intensities, and we show that the relative phase of the *p* and *s* coherent amplitudes is strongly dependent on the surface roughness. In the case of diffuse scatter, we demonstrate the wide range of behavior exhibited by the scattered intensities and matrix elements. The rise of backscattering enhancement and associated polarization effects are seen with increasing surface roughness, and it is shown that surfaces with surprisingly modest slopes may produce backscattering enhancement. At high angles of incidence, large differences between the *p*- and *s*-polarized diffuse intensities are observed.

Applied Optics (in Press)

Effects of finite stylus width in surface contact profilometry

K. A. O'Donnell

A study of the effects of stylus width in the profilometry of a randomly rough surface is presented. An approximate solution for the path of a flat-tipped stylus on an arbitrary surface is expressed as a nonlinear function of the local surface height and its first two derivatives. This solution is then averaged to find the first two moments of the measured profile when the surface and its derivatives are jointly Gaussian variates. The measured surface variance is found to decrease with increasing stylus size in a manner consistent with computer simulations.

1. Introduction

The scattering of light by randomly rough surfaces has remained a field of highly active research. There have been many studies of the residual scatter from slightly rough surfaces,[1–3] while other researchers have considered the scattering of light by stronger surfaces where backscattering enhancement and unusual polarization effects may be observed.[4–6] In such research a significant problem has been the statistical characterization of the surfaces employed in experiments. Although there are a number of possible methods of surface profilometry,[7] mechanical profilometry with a small stylus has remained a relible (and often the preferred) means of characterizing a rough surface.

A fundamental limitation of the resolution achievable with mechanical profilometry is the finite width of the stylus. Styli are often of conical or shovel form with a sharp curvature on the profiling tip.[7,8] Others have employed a stylus with a blunt (but still quite small) tip, in which a pyramidal shape ends in a flat contacting area.[4–6,9] Micrographs of typical curved and blunt styluses may be seen in Refs. 8 and 9, respectively. Although realistic styluses may be submicrometer in size, they may not be sufficiently narrow to resolve the structures on the surface, even though these structures may play a significant role in the optical scattering experiments.

It is known that the effect of the stylus width is nonlinear in surface height, so that it is not generally possible to consider the profilometer output to be a convolution of the actual surface profile with an instrumental response. This nonlinearity has been noted through harmonic distortion in simulated scans of a sinusoidal profile,[10,11] while sum and difference frequencies can also be present in the simulated output for a surface composed of two sinusoids.[11] Furthermore, cusps can occur in the profilometer output when the contact point of the stylus changes position discontinuously while traversing a deep groove,[11–14] even though the surface itself may be differentiable.

Such observations indicate that, mathematically speaking, the profiling of a randomly rough surface is a subtle and difficult problem. In some previous research the maximum well-resolved spatial frequency of a stylus with a given radius of curvature was estimated.[2] Others have studied the effects of stylus width through numerical simulations of the profilometry of rough surfaces.[13,14] Whitehouse[15] has studied stylus effects for a model in which the stylus contacts the highest of three equally spaced points on the rough surface. A more realistic approach was taken by Church and Takacs,[12] who studied the measured surface spectral density for a curved stylus and predicted an increase in measured roughness with an increasing stylus tip radius.

In the present study we also discuss the effects of stylus width in contact profilometry. Our method of solution for the stylus path resembles that of Church and Takacs,[12] except that we consider the case of a one-dimensional stylus with a flat or blunt tip. This solution is expressed in terms of the local surface height and its first two derivatives and, as expected, in nonlinear in these quantities. We then determine

The author is with The School of Physics, Georgia Institute of Technology, Atlanta, Georgia 30332.

Received 4 May 1992.
0003-6935/93/000001-07$06.00/0.

the first two moments of a profiled random process that originally had jointly Gaussian statistics of the height and the first two derivatives. For the profilometry of a process with a Gaussian height correlation function, results are compared with computer simulations and show a physically reasonable reduction in the measured variance as the stylus width increases.

In passing, we also note that analogous nonlinear transformations of random processes have been of wide interest in previous work.[16,17] In particular, the effects of squaring, power-law transformations, and even clipping of random processes have been studied. As is shown here, the effects of stylus width provide another example of such a transformation, where the nonlinearities arise quite naturally in the calculation of the stylus path.

2. Determination of the Stylus Path

We first consider the trajectory of a one-dimensional stylus with a blunt tip of full width $2w$ that is following the contour of an arbitrary profile $h(x)$. This shape of the stylus is investigated here partly because it is mathematically convenient and the stylus path can be well approximated, as is seen below. Furthermore, results that are of general interest for any stylus (such as its nonlinear response to surface height and the effect on the measured roughness) one clearly demonstrated here for the blunt stylus, while showing these properties for other stylus shapes may be quite difficult. However, it is important to note that both the blunt stylus shape and the one-dimensionality of the problem posed here can correspond to realistic experimental situations. For example, recent research[4–6] employed a wedge-shaped chisel stylus with a blunt tip of submicrometer width to characterize surfaces with one-dimensional roughness. The wedge angle was sufficiently steep compared with surface slopes so that the contact point remained at the blunt tip, which is consistent with the case described here. In the particular applications of Refs. 4–6, a blunt stylus was chosen because it glides well on the gold-coated photoresist surfaces of interest, and a good resolution was obtained with a tip width considerably smaller than the correlation length of the surface.

As shown in Fig. 1, there are four ways in which such a stylus can contact the rough surface. If the slope of $h(x)$ is of large magnitude at the stylus location, either the right or left edge of the stylus will contact the surface as is shown in case (a) or (c) of Fig. 1. If a maximum of $h(x)$ falls within the stylus width, this maximum will be the contact point [case (d)]. Occasionally, both edges of the stylus will contact when the stylus is in a deep valley [case (b)]. Despite the simplicity of these four cases, the determination of the stylus path is still quite difficult unless approximations are made.

The path of the stylus may be considered to be that followed by an arbitrary reference point on the stylus.

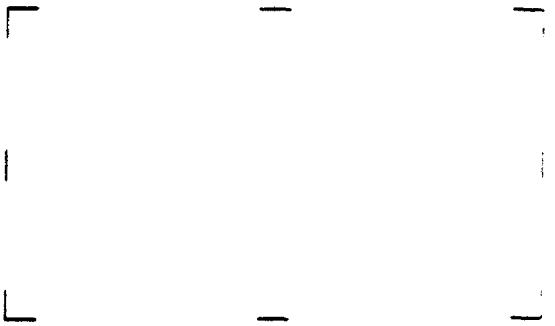

Fig. 1. Four possible configurations in scanning a stylus with a flat tip along a rough surface $h(x)$. The stylus is placed where h x has a negative slope (a), near a minimum of $h(x)$ so that both corners of the stylus contact (b), where $h(x)$ has a positive slope c and where a maximum in $h(x)$ falls within the stylus width (d). The full width of the blunt stylus tip is $2w$.

For simplicity, we then choose to study the path followed by the midpoint of the blunt face, and we consider the stylus to be centered on the point $x = x_0$. We assume that the random process $h(x)$ is twice differentiable and, near x_0, can be adequately approximated by the power series $f(\Delta x)$:

$$f(\Delta x) = h(x_0) + \Delta x \dot{h}(x_0) + \frac{\Delta x^2}{2} \ddot{h}(x_0), \qquad (1)$$

where $\Delta x = (x - x_0)$, and the single and double dots denote first and second derivatives, respectively. The approximating function $f(\Delta x)$ clearly reaches an extremum where its derivative is zero, which occurs at the point Δx_c where

$$\Delta x_c = -\frac{\dot{h}(x_0)}{\ddot{h}(x_0)}. \qquad (2)$$

This point is a minimum for $\ddot{h}(x_0) > 0$, while it is a maximum for $\ddot{h}(x_0) < 0$.

We first consider the case when $\dot{h}(x_0)$ is positive. If a maximum of $f(\Delta x)$ does not occur within the stylus width, we have case (c) of Fig. 1. The right edge of the stylus contacts the surface, and the height of the center of the stylus is given within our approximation of Eq. (1) by

$$s(x_0) = f(w) = h(x_0) + w\dot{h}(x_0) + \frac{w^2}{2} \ddot{h}(x_0). \qquad (3)$$

On the other hand, if there is a maximum occurring in $f(\Delta x)$ within the stylus width [that is, if $|\Delta x_c| < w$ and if $\ddot{h}(x_0) < 0$], this maximum will be the contact point and its height will determine the stylus height [see case (d) of Fig. 1]. Within the approximation of Eq. (1), the height of the center of the stylus $s(x_0)$ is then equal to $f(\Delta x)$ evaluated at the contact point as in

$$s(x_0) = f(\Delta x_c) = h(x_0) - \left[\frac{\dot{h}^2(x_0)}{2\ddot{h}(x_0)}\right] \qquad (4)$$

Fig. 2. Scanning a stylus with a flat tip along a realization of a Gaussian process with the slope standard deviation of unity. The curves represent the original Gaussian process (solid curves), the stylus path from Eq. (5) [dashed curve in (A)], and the exact path calculated numerically [dashed curve in (B)]. The case shown is $2w = 0.6\sigma$, where $2w$ is the full stylus width and σ is the surface correlation length. The tick marks on the horizontal axis are spaced by the correlation length σ.

if $|\Delta x_c| < w$ and $\ddot{h}(x_0) < 0$. Finally, a similar consideration of similar cases when $h(x_0)$ is negative permits the stylus position $s(x_0)$ to be written in the form

$$s(x_0) = h(x_0) - \left[\frac{\dot{h}^2(x_0)}{2\ddot{h}(x_0)}\right] \tag{5a}$$

if $|\dot{h}(x_0)| < w|\ddot{h}(x_0)|$ and $\ddot{h}(x_0) < 0$, and

$$s(x_0) = h(x_0) + w|\dot{h}(x_0)| + \frac{w^2}{2}\ddot{h}(x_0) \quad \text{otherwise,} \tag{5b}$$

where the condition of Eq. (4) has been written explicitly in Eq. (5a) with the help of Eq. (2). These results also apply to case (b) of Fig. 1 [when $\dot{h}(x_0) = 0$ and $\ddot{h}(x_0) > 0$]; Eq. (5b) then correctly implies that $s(x_0) = h(x_0) + (w^2/2)\ddot{h}(x_0)$. Within the parabolic surface approximation of Eq. (1), Eq. (5) is thus a complete solution for the profilometry of a surface $h(x)$ by a blunt stylus.

Equation (5) may be used to approximate the stylus path for an arbitrary deterministic surface or for a realization of a random surface. The nonlinear effects of the stylus width are immediately obvious in Eq. (5). The application of Eq. (5) to a realization of a Gaussian random process is shown in Fig. 2. One effect that can be clearly seen is that the stylus tends to broaden the maxima of the random process. This arises from Eq. (5a), which approximates a constant height of the stylus as long as a maximum of $h(x)$ falls within its width. A second pronounced effect is that the stylus often produces cusps in the valleys of the random process. A cusp occurs when the contact point of the stylus changes from one side of the stylus to the other; this arises from the term containing the modulus in Eq. (5b). Both the cusps present at minima and the broadening of maxima have been noted in previous research.[12-14]

3. First Two Moments of the Measured Profile

In this section the first two moments of $s(x)$ are determined through application of Eq. (5). Throughout this, it is assumed that the original process $h(x)$ is a statistically stationary and ergodic random process that is at least twice differentiable and, for the sake of convenience, is of zero mean. We first consider the completely general properties of the derivatives of such random processes. The second-order correlation function of $h(x)$ is defined as

$$C(\Delta x) = \langle h(x)h(x + \Delta x)\rangle, \tag{6}$$

where the angle brackets denote an ensemble average. The variance σ^2 of the random process $h(x)$ is $C(0)$. It is well known[18] that the derivative $\dot{h}(x)$ of the process $h(x)$ is of zero mean and has a variance of

$$\langle \dot{h}^2\rangle \equiv \dot{\sigma}^2 = -\ddot{C}(0) \tag{7}$$

and that $h(x)$ and $\dot{h}(x)$ are uncorrelated so that

$$\langle h\dot{h}\rangle = 0. \tag{8}$$

On applying these considerations to the random process $\dot{h}(x)$ and its derivative $\ddot{h}(x)$, we also have that

$$\langle \ddot{h}\rangle = 0, \tag{9}$$

$$\langle \ddot{h}^2\rangle \equiv \ddot{\sigma}^2 = C^{(4)}(0), \tag{10}$$

$$\langle \dot{h}\ddot{h}\rangle = 0, \tag{11}$$

where $C^{(4)}$ denotes the fourth derivative of $C(\Delta x)$. When we use methods directly analogous to those of Ref. 18, it is also straightforward to show that

$$\langle h\ddot{h}\rangle = -\dot{\sigma}^2. \tag{12}$$

Determination of the moments of the profiled process $s(x)$ also requires assumptions for the probability densities of $h(x)$ and its derivatives. Here we assume that the process $h(x)$ and its first two derivatives are jointly Gaussian variates. This is the case if $h(x)$ is a Gaussian process, for it is well known that any linear transformation (such as differentiation) of a set of Gaussian variates produces a set of such variates.[19] Because Gaussian variates are specified by their two lowest-order moments,[19] the moments given above completely specify the statistical properties of $h(x)$, $\dot{h}(x)$, and $\ddot{h}(x)$. Furthermore, for the Gaussian case, the correlations given by Eqs. (8), (11), and (12) then imply that

$$p(h, \dot{h}, \ddot{h}) = p(h, \ddot{h})p(\dot{h}), \tag{13}$$

where $p(\ )$ denotes the respective probability density.

To determine the mean of $s(x)$, care must be taken to average properly over different regions of probability space. In particular, the average of Eq. (5) may be written in the form

$$\langle s\rangle = \langle h\rangle + w\langle|\dot h|\rangle + \frac{w^2}{2}\langle\ddot h\rangle - w\langle|\dot h|\rangle_w - \frac{w^2}{2}\langle\ddot h\rangle w - \left\langle\frac{\dot h^2}{2\ddot h}\right\rangle_w, \tag{14}$$

where the angle brackets denote a statistical average over all values of the relevant variates, and $\langle\,\rangle w$ denotes an average in probability space only over the wedge $\ddot h < 0$ and $w\ddot h < \dot h < -w\ddot h$ as in

$$\langle f(h,\dot h,\ddot h)\rangle_w = \int_{-\infty}^{\infty} dh \int_{-\infty}^{0} d\ddot h \int_{w\ddot h}^{-w\ddot h} d\dot h f(h,\dot h,\ddot h)p(h,\dot h,\ddot h), \tag{15}$$

where $f(\,)$ is an arbitrary function. In particular, Eq. (14) follows by averaging Eq. (5b) over all the probability space, and to include the condition of Eq. (5a), by adding the second term of Eq. (5a) and subtracting the last two terms of Eq. (5b) averaged only where $\ddot h < 0$ and $w\ddot h < \dot h < -w\ddot h$. Now, of the first three terms of Eq. (14), only the second term is nonzero; direct integration over a Gaussian density yields

$$w\langle|\dot h|\rangle = \left(\frac{2}{\pi}\right)^{1/2} w\dot\sigma. \tag{16}$$

The last three terms of Eq. (14) may be evaluated by first carrying out the trivial integration over $\dot h$ in Eq. (15). The fourth term may then be written as

$$w\langle|\dot h|\rangle_w = \frac{w}{\pi\dot\sigma\ddot\sigma}\int_{-\infty}^{\infty} d\ddot h \exp\left(-\frac{\ddot h^2}{2\ddot\sigma^2}\right)\int_0^{-w\ddot h} d\dot h\dot h \times \exp\left(-\frac{\dot h^2}{2\dot\sigma^2}\right) \tag{17}$$

and evaluated in closed form as

$$w\langle|\dot h|\rangle_w = \frac{w\dot\sigma}{(2\pi)^{1/2}}\,1 - \frac{1}{[1+(w\ddot\sigma/\dot\sigma)^2]}. \tag{18}$$

The fifth term of Eq. (14) may be similarly expressed as

$$\frac{w^2}{2}\langle\ddot h\rangle_w = \frac{w^2}{2\pi\dot\sigma\ddot\sigma}\int_{-\infty}^{\infty} d\ddot h\ddot h \exp\left(-\frac{\ddot h^2}{2\ddot\sigma^2}\right)\int_0^{-w\ddot h} d\dot h \times \exp\left(-\frac{\dot h^2}{2\dot\sigma^2}\right). \tag{19}$$

Equation (19) may be evaluated by expanding the exponential in $\dot h$ in a power series, integrating term by term, and then integrating the resulting series over $\ddot h$[20], with the result that

$$\frac{w^2}{2}\langle\ddot h\rangle_w = -\frac{1}{2(2\pi)^{1/2}}\left(\frac{w^3\ddot\sigma^2}{\dot\sigma}\right)\sum_{n=0}^{\infty}\frac{(-1)^n(2n+1)!!}{n!(2n+1)2^n}\left(\frac{w\ddot\sigma}{\dot\sigma}\right)^{2n}. \tag{20}$$

A similar procedure may be applied to the last term of Eq. (14) [only the powers of $\ddot h$ and $\dot h$ arising in the integrals analogous to Eq. (19) are different] to obtain

$$\left\langle\frac{\dot h^2}{2\ddot h}\right\rangle_w = -\frac{1}{2(2\pi)^{1/2}}\left(\frac{w^3\ddot\sigma^2}{\dot\sigma}\right)\sum_{n=0}^{\infty}\frac{(-1)^n(2n+1)!!}{n!(2n+3)2^n}\left(\frac{w\ddot\sigma}{\dot\sigma}\right)^{2n}. \tag{21}$$

Finally, on substitution of Eqs. (16), (18), (20), and (21) into Eq. (14), we are able to sum the two series to obtain the reasonably simple result

$$\langle s\rangle = \frac{w\dot\sigma}{(2\pi)^{1/2}}\left(1 + \frac{1}{2}(1+\kappa^2)^{1/2} + \frac{1}{2\kappa}[\ln[(1+\kappa^2)+\kappa]\right), \tag{22}$$

where

$$\kappa = \left(\frac{w\ddot\sigma}{\dot\sigma}\right). \tag{23}$$

Determining the second moment of $s(x)$ requires techniques that are similar to averaging terms over regions of probability space, although there are more terms and the manipulations are thus more lengthy. We then briefly present the intermediate results rather than describing the details of the derivation. First, the square of Eq. (5) may be written in the form

$$\langle s^2\rangle = \langle T_1\rangle + \langle T_2\rangle_w, \tag{24}$$

where

$$\langle T_1\rangle = \langle h^2\rangle + w^2\langle\ddot h^2\rangle + \frac{w^4}{4}\langle\ddot h^2\rangle + 2w\langle h|\ddot h|\rangle + w^2\langle h\ddot h\rangle + w^3\langle|\dot h|\ddot h\rangle, \tag{25}$$

$$\langle T_2\rangle_w = -w^2\langle\dot h^2\rangle_w - \frac{w^4}{4}\langle\ddot h^2\rangle_w - 2w\langle h|\dot h|\rangle_w - w^2\langle h\dot h\rangle - w^3\langle|\dot h|\ddot h\rangle_w - \left\langle\frac{h\dot h^2}{\ddot h}\right\rangle_w + \left\langle\frac{\dot h^4}{4\ddot h^2}\right\rangle_w. \tag{26}$$

The fourth and sixth terms of Eq. (25) are zero because h and its derivatives are of zero mean. In the case of the fourth term, h and $\ddot h$ are statistically independent, the moment factorizes, and it is then zero; for the sixth term, a similar argument applied to $\dot h$ and $\ddot h$ shows the term to be zero. The remaining terms then follow directly from Eqs. (7–12) with the

result that

$$\langle T_1 \rangle = \sigma^2 + \frac{w^4}{4}\ddot{\sigma}^2. \quad (27)$$

Evaluation of the terms arising in Eq. (26) requires considerable more attention, and we only state the final results as follows:

$$w^2\langle \dot{h}^2 \rangle_w = \frac{2w^3\dot{\sigma}\ddot{\sigma}}{\pi}\kappa^2 \sum_{n=0}^{\infty} \frac{(-1)^n(n+1)}{(2n+3)}\kappa^{2n}, \quad (28)$$

$$\frac{w^4}{4}\langle \ddot{h}^2 \rangle_w = \frac{w^3\dot{\sigma}\ddot{\sigma}}{2\pi}\kappa^2 \sum_{n=0}^{\infty} \frac{(-1)^n(n+1)}{(2n+1)}\kappa^{2n}, \quad (29)$$

$$2w\langle h|\dot{h}|\rangle_w = \frac{2w^3\dot{\sigma}\ddot{\sigma}}{\pi}\frac{1}{1+\kappa^2}, \quad (30)$$

$$w^2\langle h\ddot{h}\rangle_w = -\frac{2w^3\dot{\sigma}\ddot{\sigma}}{\pi}\sum_{n=0}^{\infty} \frac{(-1)^n(n+1)}{(2n+1)}\kappa^{2n}, \quad (31)$$

$$w^3\langle |\dot{h}|\ddot{h}\rangle_w = -\frac{w^3\dot{\sigma}\ddot{\sigma}}{\pi}\frac{\kappa^2}{1+\kappa^2}, \quad (32)$$

$$\left\langle \frac{h\dot{h}^2}{\ddot{h}} \right\rangle_w = -\frac{2w^3\dot{\sigma}\ddot{\sigma}}{\pi}\sum_{n=0}^{\infty} \frac{(-1)^n(n+1)}{(2n+3)}\kappa^{2n}, \quad (33)$$

$$\left\langle \frac{\dot{h}^4}{4\ddot{h}^2} \right\rangle_w = \frac{w^3\dot{\sigma}\ddot{\sigma}}{2\pi}\kappa^2 \sum_{n=0}^{\infty} \frac{(-1)^n(n+1)}{(2n+5)}\kappa^{2n}. \quad (34)$$

Equations (28), (29), and (34) have been obtained with the same approach as used with Eq. (19); to derive Eqs. (30) and (32) the integral of Eq. (15) may be done exactly, while Eqs. (31) and (33) may be derived by integrating over h and $\dot{h}$ first in Eq. (15). On substitution of Eqs. (28–34) into Eq. (26) and then substitution of Eqs. (25) and (26) into Eq. (24), we obtain the second moment of $s(x)$ as

$$\langle s^2 \rangle = \delta^2 + \frac{w^4}{4}\ddot{\sigma}^2 + \frac{w^3\dot{\sigma}\ddot{\sigma}}{\pi} \times \left[\frac{\kappa^2-2}{\kappa^2+1} + \left(2 - \frac{\kappa^2}{2}\right)\sum_{n=0}^{\infty}\frac{(-1)^n(n+1)}{(2n+1)}\kappa^{2n} + 2(1-\kappa^2)\sum_{n=0}^{\infty}\frac{(-1)^n(n+1)}{(2n+3)}\kappa^{2n} + \frac{\kappa^2}{2}\sum_{n=0}^{\infty}\frac{(-1)^n(n+1)}{(2n+5)}\kappa^{2n}\right]. \quad (35)$$

Finally the series contained in Eq. (35) may be expressed in closed form in terms of analytic functions, with the relatively simple result

$$\langle s^2 \rangle = \sigma^2 + \frac{w^4}{4}\ddot{\sigma}^2 - \frac{w^3\dot{\sigma}\ddot{\sigma}}{4\pi\kappa^2} \times \left\{(1-3\kappa^2) - (1-\kappa^4)\left[\frac{\arctan(\kappa)}{\kappa}\right]\right\}. \quad (36)$$

Equations (22) and (36) thus comprise closed-form expressions for the first two moments of a Gaussian process profiled with a flat-tipped sylus of full width $2w$, within the locally parabolic approximation of Eq. (1).

3. Discussion

We now consider some of the consequences of the results derived in the section above. First, the mean of the profiled process of Eq. (22) is a positive quantity for all $w > 0$. This is quite reasonable, for, as seen in Fig. 2, the stylus path is expected never to fall below the level of $h(x)$, and the path coincides only with the process where a maximum of $h(x)$ lies at the stylus center. On expansion of Eq. (22) in powers of κ, we obtain the result

$$\langle s \rangle = \left(\frac{2}{\pi}\right)^{1/2} w\dot{\sigma}\left\{1 + \frac{\kappa^2}{12} - \frac{\kappa^4}{80} + \frac{\kappa^6}{224} - \cdots\right\}. \quad (37)$$

Equation (37) shows that the initial rise in the mean is linear in both w and $\dot{\sigma}$ and that surface curvatures become significant only through higher-order terms in κ.

It is also of interest to consider the variance of the random process $s(x)$. This follows from subtracting the square of Eq. (22) from Eq. (36), with the result that

$$\sigma_s^2 \equiv \langle s^2 \rangle - \langle s \rangle^2 = \sigma^2 - \frac{2\dot{\sigma}^2}{\pi}w^2 + \frac{2\dot{\sigma}\ddot{\sigma}}{3\pi}w^3 - \frac{(4-3\pi)\ddot{\sigma}^2}{12\pi}w^4 - \frac{\ddot{\sigma}^3}{5\pi\dot{\sigma}}w^5 + \cdots, \quad (38)$$

where, for purposes of interpretation, the variance has been expanded as a power series in w. It is clear from Eq. (38) that the lowest-order term is the variance of the original process $h(x)$ and that the next term is negative and of second order in both w and $\dot{\sigma}$. Hence there is in general an initial reduction in the measured variance of the random process resulting from the finite width of the stylus.

Further simplification of these results requires an assumed form of the correlation function $C(\Delta x)$ of $h(x)$. Here it is assumed to be of Gaussian form,

$$\langle h(x)h(x+\Delta x)\rangle = \sigma^2 \exp(-\Delta x^2/a^2), \quad (39)$$

and, on application of Eqs. (7) and (10), it is immediately found that

$$\dot{\sigma} = \sqrt{2}\sigma/a, \quad (40)$$

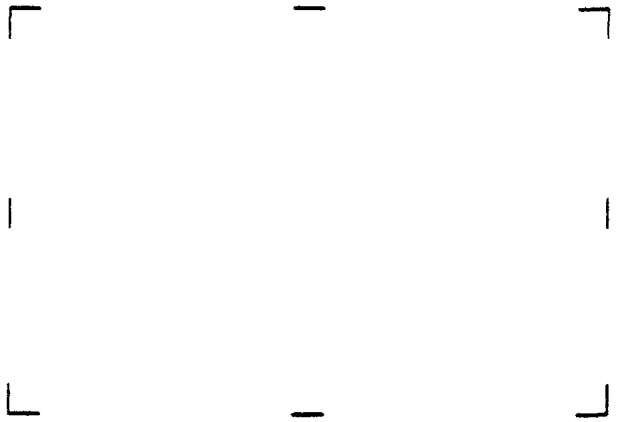

Fig. 3. Relative measured variance as a function of the stylus width for profilometry of a Gaussian process. The solid curve is from Eqs. (22) and (36), which is to be compared with the results from the numerical simulation of Eq. (5) (circles). Also shown are the fifth-order approximation of Eq. (42) (dashed curve) and results from numerical simulation of the exact stylus path (triangles).

$$\ddot{\sigma} = 2\sqrt{3}\sigma/a^2. \tag{41}$$

The variance of the profiled process $s(x)$ then follows from Eq. (38) as

$$\sigma_s^2 = \sigma^2\left[1 - \frac{4}{\pi}\left(\frac{w}{a}\right)^2 + \frac{4\sqrt{6}}{3\pi}\left(\frac{w}{a}\right)^3 - \frac{(4-3\pi)}{\pi}\left(\frac{w}{a}\right)^4 - \frac{12\sqrt{6}}{5\pi}\left(\frac{w}{a}\right)^5 + \cdots\right], \tag{42}$$

which demonstrates that the series generated is in fact a power series in the parameter (w/a).

To verify further the results derived in Section 2, we also made comparisons with computer simulations of the profilometry of a Gaussian process with a flat stylus. In this study, a large number of realizations of a Gaussian process with a Gaussian correlation function were generated. The stylus trajectory was then computed from Eq. (5) for each process, and the first two moments were then averaged over this ensemble.

These comparisons are shown in Fig. 3. It can be seen that the variance of the numerical simulations of Eq. (5) agrees well with the variance from the expressions derived here [Eqs. (22) and (36)], since both show a consistent decay as a function of w until $2w \approx a$. This decay is relatively slow, and a stylus width comparable with the correlation length produces only a modest reduction in the measured variance. However, this behavior is consistent with the stylus effects arising in Eq. (5). That is, as can be seen from Fig. 2, $s(x)$ has a shallower minima but broader maxima than $h(x)$. The former effect tends to reduce σ_s^2, while the latter tends to increase σ_s^2, so that the net effect is apparently only a slow decay in σ_s^2 as a function of w/a.

For larger w the numerical and exact analytical results employing Eq. (5) both show an increase in the measured variance. This is not entirely surprising, for the parabolic approximation of Eq. (1) should not be expected to hold for stylus widths greater than the correlation length. In fact in Fig. 2 a tendency can be seen for the approximation of Eq. (5a) to overshoot slightly the true stylus trajectory near maxima in $h(x)$; for larger w these effects significantly contribute to an overestimation of the measured variance.

Also shown in Fig. 3 is the variance of the stylus path determined by exact numerical calculation of the stylus trajectory in the computer simulations without approximation. It can be seen that we obtained excellent agreement with the results based on Eq. (5) until $2w \approx 0.8a$, while for larger w the exact results show the expected monotonic decrease in σ_s^2. The dashed curve in Fig. 3 is the fifth-order approximation of Eq. (42), which produces considerably better agreement with the exact numerical simulations. This convenient approximation may thus be employed until the full stylus width is approximately equal to the correlation length, with good numerical accuracy.

These results are of considerable practical interest, and, to illustrate this, we briefly note some practical consequences. In recent research[4,6] on characterization of a surface that was approximately a realization of a Gaussian process with correlation length $a = 3.57$ μm, a blunt stylus with $2w = 0.4$-μm nominal width was employed. From Eq. (42) it is then clear that the measured variance should be 0.996 times the actual variance. This indicates that the stylus width plays a small role in these measurements and that the experimental results represent the properties of the surface essentially without stylus effects. On the other hand, the stylus width cannot be reduced without limit because of surface damage, and if there are surface structures that are considerably smaller in a particular experiment, the variance predicted by the equations derived here will be considerably less than that of the actual surface.

4. Conclusions

It has been shown that it is possible to consider the effect of stylus width in the study of randomly rough surfaces with stylus profilometry. For the case of a stylus with a flat tip, an expression has been derived that provides a good approximation to the profilometer output for a realization of a rough surface as long as the stylus width is comparable with or less than the correlation length. This expression is based on a locally parabolic approximation and could be generalized to higher-order approximations, although dealing with such higher-order terms appears to be exceedingly difficult. The expression is nonlinear in the surface profile and its derivatives and produces cusps in deep valleys of the surface and maxima that are broader than those of the original random process.

Closed-form expressions have been derived for the first two moments of the profilometer output if the surface height and its first two derivatives obey

Gaussian statistics, which is the case for a Gaussian process. It has been shown that the mean should increase initially in a manner that is linear in stylus width, while the variance should slowly decrease with increasing stylus width. For the case of a profile with a Gaussian correlation function, good agreement of the derived results with exact results from computer simulations is obtained until the full stylus width is comparable with the correlation length.

This research was supported by the U. S. Army Research Office. The author is also grateful to have visited the laboratory of A. Consortini of the University of Florence during preparation of this paper.

References

1. E. L. Church, H. A. Jenkinson, and J. M. Zavada, "Relationship between surface scattering and microtopographic features," Opt. Eng. **18**, 125–136 (1979).
2. J. M. Elson and J. M. Bennett, "Relation between the angular dependence of scattering and the statistical properties of optical surfaces," J. Opt. Soc. Am. **69**, 31–48 (1979).
3. J. M. Bennett, H. H. Hurt, J. P. Rahn, J. M. Elson, K. H. Guenther, M. Rasigni, and F. Varnier, "Relation between optical scattering, microstructure and topography of thin silver films. 1: Optical scattering and topography," Appl. Opt. **24**, 2701–2711 (1985).
4. K. A. Do'Donnell and M. E. Knotts, "Polarization dependence of scattering from one-dimensional rough surfaces," J. Opt. Soc. Am. A **8**, 1126–1131 (1991).
5. J. C. Dainty, N. C. Bruce, and A. J. Sant, "Measurements of light scattering by a characterized rough surface," Waves Random Media **3**, S29–S39 (1991).
6. T. R. Michel, M. E. Knotts, and K. A. O'Donnell, "Stokes matrix of a one-dimensional perfectly conducting rough surface," J. Opt. Soc. Am. A **9**, 585–596 (1992).
7. J. M. Bennett and L. Mattsson, *Introduction to Surface Roughness and Scattering* (Optical Society of America, Washington, D.C., 1989).
8. J. M. Bennett and J. H. Dancy, "Stylus instrument for measuring statistical properties of smooth optical surfaces," Appl. Opt. **20**, 1785–1802 (1981).
9. D. J. Whitehouse and J. F. Archard, "The properties of random surfaces of significance in their contact," Proc. Soc. London Ser. A **316**, 97–121 (1970).
10. S. R. Wilson, G. A. Al-Jumaily, and J.R. McNeil, "Nonlinear characteristics of a stylus profilometer," in *Current Developments in Optical Engineering II*, R. E. Fischer and W. J. Smith, eds., Proc. Soc. Photo-Opt. Instrum. Eng. **818**, 10–12 (1987).
11. G. R. Al-Jumaily, S. R. Wilson, K. C. Jungling, J. R. McNeil, and J. M. Bennett, "Frequency response characteristics of a mechanical surface profilometer," Opt. Eng. **26**, 953–958 (1987).
12. E. L. Church and P. Z. Takacs, "Effects of non-vanishing tip size in mechanical profile measurements," in "*Optical Testing and Metrology III: Recent Advances in Industrial Optical Inspection*," C. P. Grover, ed., Proc. Soc. Photo-Opt. Instrum. Eng. **1332**, 504–514 (1991).
13. J. I. McCool, "Assessing the effect of stylus tip radius and flight on surface topography measurements," ASME J. Tribol. **106**, 202–210 (1984).
14. V. Radhakrishnan, "Effect of stylus radius on the roughness values measured with tracing stylus instruments," Wear **16**, 325–335 (1970).
15. D. J. Whitehouse, "Theoretical analysis of stylus integration," Ann. CIRP **23**, 181–182 (1974).
16. W. W. Harman, *Principles of the Statistical Theory of Communication* (McGraw-Hill, New York, 1963).
17. W. B. Davenport and W. L. Root, *An Introduction to the Theory of Random Signals and Noise* (McGraw-Hill, New York, 1958).
18. F. G. Bass and I. M. Fuks, *Wave Scattering from Statistically Rough Surfaces* (Pergamon, New York, 1979).
19. J. W. Goodman, *Statistical Optics* (Wiley, New York, 1985).
20. See Eq. (3.461.2) in I. S. Gradshteyn and I. M. Ryzhik, *Table of Integrals, Series, and Products* (Academic, New York, 1965).